Towards a glycobiological toolbox for the investigation of bacterial adhesion

Dissertation

in fulfillment of the requirements for the degree "Dr. rer. nat."

of the Faculty of Mathematics and Natural Sciences

at the Christiana Albertina University of Kiel

submitted by

Claudia Fessele

September 2016

First referee: Prof. Dr. Thisbe K. Lindhorst

Second referee: Prof. Dr. Axel J. Scheidig

Date of oral examination: 02.12.2016

Approved for publication: 02.12.2016

sgd., Dean

The present research work was prepared under supervision

of Prof. Dr. Thisbe K. Lindhorst

during the period from October 2012 to September 2016

at the Otto Diels Institute of Organic Chemistry

of the Christiana Albertina University Kiel.

I hereby confirm that apart from the advice by my supervisor this thesis is all my own work. It has not been submitted either partially or wholly as part of a doctoral degree to another examining body. Parts of thesis have been published.

C. Fessele, T.K. Lindhorst, Effect of Aminophenyl and Aminothiahexyl α-D-Glycosides of the *Manno-, Gluco-* and *Galacto*-Series on Type 1 Fimbriae-Mediated Bacterial Adhesion of *Escherichia coli, Biology*, **2013**, *2*, 1135-1149.

C. Fessele, S. Wachtler, V. Chandrasekaran, C. Stiller, T.K. Lindhorst, A. Krüger, Thiourea-bridged Nanodiamond Glycoconjugates as Inhibitors for Bacterial Adhesion, *Eur. J. Org. Chem.* **2015**, *25*, 5519-5525.

L. Möckl, C. Fessele, G. Despras, C. Bräuchle, T.K. Lindhorst, En route from artificial to natural: Evaluation of inhibitors of mannose-specific adhesion of *E. coli* under flow, *Biochim. Biophys. Acta*, **2016**, *1860*, 2031-2036.

This thesis has been prepared according to the Rules of Good Scientific Practice of the German Research Foundation.

Claudia Fessele

Abstract

Bacterial adhesion of pathogenic *Escherichia coli* triggers many diseases such as neonatal meningitis, gastroenteritis and urinary tract infections. The first initial adhesion step is mediated by carbohydrate specific lectins located at the tip of bacterial fimbriae. In uropathogenic *E. coli* the most common ones are type 1 and P fimbriae. Research interest is focused on the design and testing of new inhibitors against both of the lectins FimH and PapG. Additional to new inhibitors it is crucial to get a better understanding of the binding mechanism between lectins and carbohydrate as well as the influence of exterior ascendancies. Therefore three main topics were addressed: bacterial adhesion studies, examination of shear force influence and glyconanoparticles.

The influence of aglycones and variety of carbohydrate moiety was determined in bacterial adhesion inhibition assays with and without preincubation of the ligand with the type 1 fimbriated *E. coli.* Furthermore the surfaces in our assay studies were changed from artificial polystyrene to a natural cell surface of HMEC-1. For more variation with the assay surface, we introduced quartz glass to photochemically switch bacterial adhesion. For further developments to obtain a more biological setting in our assays, a flow system was established and bacterial adhesion was tested under flow.

For the examination of shear force influence two different projects were realized. Atomic force microscopy was used to determine binding strength between the FimH lectin and various carbohydrates. Therefore cantilever tips were functionalized with previous synthesized molecules and examined in AFM measurements with type 1 fimbriated *E. coli.* Interestingly, under the influence of shear force the lectin specificity for mannosides changes. To understand this change better a project to analyze the carbohydrate-lectin binding process in STD-NMR studies was designed. For this approach an amino acid exchange led to a free cysteine on FimH which can be chemically modified with a switchable carbohydrate moiety.

In the last topic two different glyconanoparticles were employed in bacterial adhesion. Glyconanodiamonds were fabricated with a thiourea-bridging method and their properties as inhibitor for bacterial adhesion in biofilm formation were proved. Additionally, magnetic PEG beads were functionalized with a synthesized Galα1,4Gal derivative and tested in bacterial adhesion studies with P fimbriated *E. coli.*

Zusammenfassung

Bakterielle Adhäsion pathogener *Escherichia coli*-Bakterien kann Krankheiten wie neonatale Meningitis, Gastroenteritis und Harnwegsinfektionen auslösen. Der erste Schritt der Adhäsion wird durch Kohlenhydrate-bindende Lektine, die sich an der Spitze von bakteriellen Fimbrien befinden, vermittelt. Zu den bekanntesten Fimbrien bei uropathogenen *E. coli*-Bakterien zählen Typ-1- und P-Fimbrien. Die aktuelle Forschung konzentriert sich auf die Entwicklung und das Testen von neuen Inhibitoren für die beiden Lektine FimH und PapG. Neben der Entwicklung neuer Inhibitoren ist es essentiell den Bindungsmechanismus von Lektinen und Kohlenhydraten besser zu verstehen und dabei auch äußere Einflüsse zu betrachten. Hierfür wurden drei Themengebiete bearbeitet: Bakterielle Adhäsionsstudien, Einfluss von Scherkräften und Glyconanopartikel.

In Adhäsions- und Inhibitionsassays mit und ohne Präinkubation des Inhibitors wurde der Einfluss des Aglycons und verschiedener Kohlenhydrate auf bakterielle Adhäsion untersucht. Weiterhin wurde die Oberfläche in bakteriellen Adhäsionsstudien von künstlichen zu natürlichen Zelloberflächen aus HMEC-1-Zellen variiert. Als weitere künstliche Oberfläche wurde Quartzglas verwendet um die bakterielle Adhäsion Typ-1-fimbriierter *E. coli* photochemisch zu schalten. Als nächster Schritt in der Entwicklung wurde ein Durchfluss-Assay etabliert um eine noch biologischere Umgebung für die Untersuchung bakterieller Adhäsion zu erhalten.

Um den Einfluss von Scherkräften zu untersuchen, wurden zwei verschiedene Projekte realisiert. Rasterkraftmikroskopie wurde verwendet um die Bindungsstärke zwischen dem Lektin FimH und verschiedenen Kohlenhydratliganden zu untersuchen. Hierfür wurden Cantilever-Spitzen mit zuvor synthetisierten Molekülen funktionalisiert und in Messungen mit Typ-1-fimbriierten *E. coli* verwendet. Interessanterweise ändert sich die Mannosespezifität des FimH unter dem Einfluss von Scherkräften. Um diese Veränderung besser verstehen zu können wurde ein weiteres Projekt bearbeitet. Hierbei wurde ein Aminosäurenaustausch an FimH vorgenommen um ein freies Cystein an der Proteinoberfläche zu erhalten. Diese FimH-Mutante kann nun mit einem photoschaltbaren Kohlenhydratmolekül reagieren, um später die Bindung zwischen Lektin und Ligand in STD-NMR-Messungen zu untersuchen.

Im letzten Themengebiet wurden zwei verschiedene Glyconanopartikel verwendet um bakterielle Adhäsion zu untersuchen. Per Thioharnstoffkupplung wurden Nanodiamanten mit Zuckermolekülen funktionalisiert und auf ihre inhibitorischen Eigenschaften in bakteriellen Adhäsionstests untersucht. Weiterhin wurden magnetische PEG-Partikel mit einem Galα1,4Gal-Molekül funktionalisiert und in Adhäsions- und Inhibitionsstudien mit P-fimbriierten *E. coli*-Bakterien verwendet.

A guide to this thesis

The research part of this thesis is divided into seven chapters. A general introduction to the research field of glycoscience is given in chapter 1. Chapter 2 describes the research objectives of this work. Additional to the general introduction at the beginning of every topic part (chapters 3, 4 and 5) there is an introduction which focuses on the respective theoretical background of the research in the corresponding chapter. Within every topic, different manuscripts and projects which depict all the research work and results of the performed studies. For every project or manuscript the molecule numbering starts with **1**. The obtained results are concluded in chapter 6. All supplementary information of the published manuscripts as well as all other experimental data are collected in chapter 7.

Contents

1 General Introduction

Interest in the glycosciences started long time ago with simple glycosides like fructose, sucrose and lactose and their attributes to fermentation and groceries production. Later the development of mammalian carbohydrates began with the research of diseases like *Diabetes mellitus*[1] as well as the identification of the ABO blood system.[2] Followed by various medical investigations, modern glycoscience today has evolved into areas from glycochemistry to glycobiology. It has gained broad importance within human and animal disease and biology areas. With the identification of the first lectin (ricin) in 1888 it has been recognized, that although simple monosaccharides differ only in their configuration, there is a huge difference in the binding affinity of lectins. Compared with other biomacromolecules like DNA and RNA, each built up by four different building blocks or proteins, composed of 20 different canonical amino acids, there is a huge variety in the building of glycans out of different monosaccharides.[3,4]

Parallel to the detection of lectins in animals, glycan binding proteins (GBPs) in influenza viruses were discovered.[5] With the identification of GBPs in various living organisms the need of new techniques and methods to identify glycans and understand the binding mechanism behind GBPs and carbohydrates are desperately needed. Development of analysis methods like mass spectrometry, NMR studies, fluorescent imaging and glycan array techniques led to further understanding.[6–10] Still it is a major challenge in the field of glycoscience to further improve and analyze the binding mechanism between glycans and the respective proteins which occur everywhere around us.

1.1 Glycan-binding proteins

The first glycan-binding proteins were discovered over 100 years ago in plants.[11] Until today there are no living organisms known in which no GBPs are found. It is possible to classify GBPs into two major subgroups - glycosaminoglycan-binding proteins and lectins.[10] In contrast to lectins, glycosaminoglycan-binding proteins lack similarities in sequence data or general structure but all recognize sulfated glycosaminoglycans like heparin or chondroitin sulfate. Antithrombin depicts the first and best known example for glycosaminoglycan-binding proteins. Discovered in 1916, its anticoagulant properties in the presence of heparin were detected in 1939.[12] The pentasaccharide heparin binds by hydrogen bonding of its sulfates and carboxylates to positively charged amino acids of antithrombin.[13–15]

However, the other major group of GBPs, the lectins, can be classified according to structure and sequence similarities in their carbohydrate recognition domains (CRD) which have apparently evolved from shared ancestral genes.[16–18] Nevertheless the variety of glycans recognized by members of one lectin family is quite large. Classification of lectins according to their structure homology

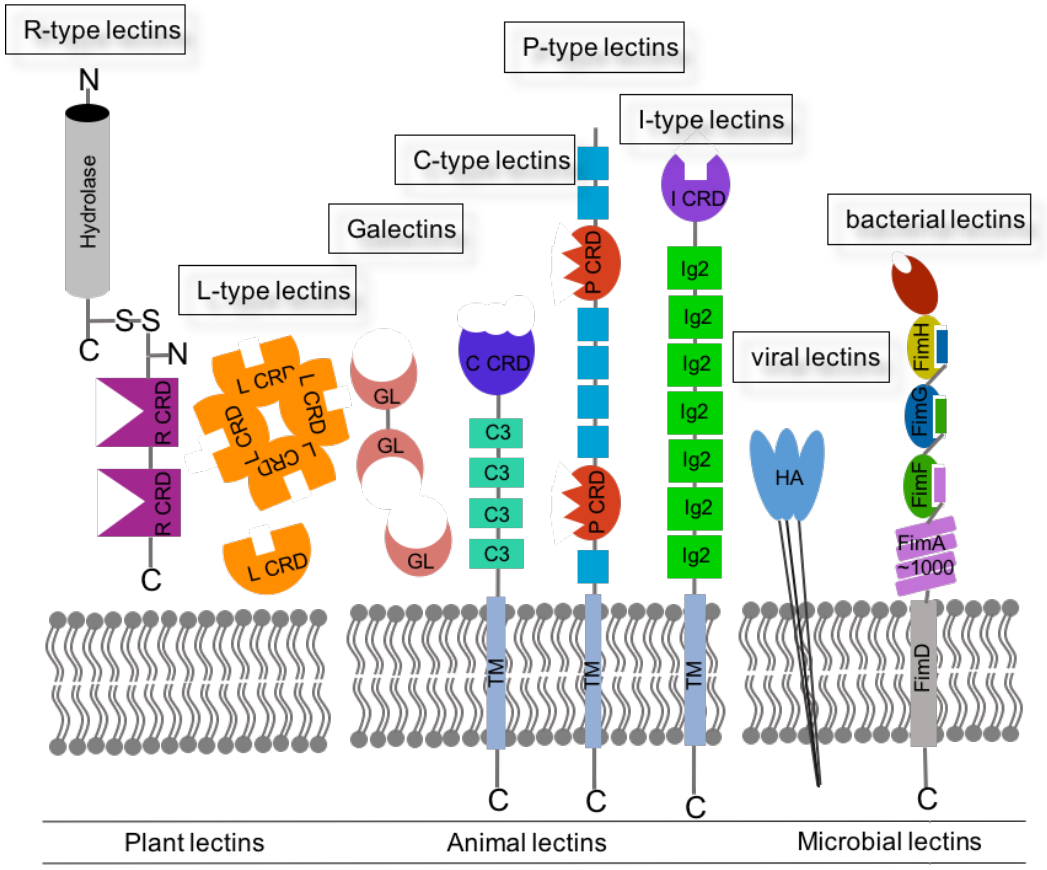

Figure 1.1.1: Schematic illustration of the major types of lectins in plants, animals and microbes according to their protein structure. All carbohydrate recognition domains are labelled according to their lectin type. Additional domains are: TM transmembrane region, C3 complement regulatory repeat, Ig2 immunoglobulin domain.

and evolutionary relatedness can be broadened respectively to their most related species like plants, animals and microbials. Figure 1.1.1 illustrates an example of the most common lectin types in plants, animals and microbes.

1.1.1 Plant lectins

R-type lectins are named after their first discovered lectin ricin recovered from *Ricinus communis* in 1888. It was found to agglutinate erythrocytes. In consequences of closely related sequences and structural homologies of the CRD various members of this lectin family could be identified. The highly toxic lectin ricin binds to β-linked Gal/GalNAc-containing glycans. After its transport into the cell and to the endoplasmatic reticulum (ER), the hydrolase domain is splitted of and blocks ribosome function and thus protein synthesis inside the cell. There are also other R-type lectins known which are not toxic and located in other species like bacteria or *Drosophila*.[11,19]

The most famous member of the L-type lectin family is Concanavalin A (ConA). Nevertheless the family is named after a lectin first identified in leguminose seed plants.[20,21] This family of lectins exhibit tertiary structures with four binding pockets. The monomer forms a structure called

"jelly-roll fold". These lectins are secreted in the cells as tetrameric structures (Fig. 1.1.1). The huge similarity within the L-type lectin family is due to remarkable homology in the primary amino acid sequence.[22]

1.1.2 Animal lectins

In animals a higher variety of lectin families occurs. The first identified lectins which are linked to human disease and glycoprotein biosynthesis are P-type lectins. They recognize mannose-6-phosphate which is located on the surface of newly synthesized lysosomal enzymes. After recognition of P-type lectins these enzymes are transported to the lysosomes inside the cell.[23]

The designation of C-type lectins is due to the fact that they are Ca^{2+}-dependent binding proteins. This dependency leads to huge structure homology in the amino acid sequence of the C-type lectins as well as in the secondary structure of their carbohydrate recognition domains. This large lectin family includes selectins, collectins, endocytic receptors and proteoglycans. Although they share huge structural homologies, they differ widely with regard to the types of glycans they recognize with high affinity. They play crucial roles as adhesins, signaling receptors in inflammation and in tumor immunity and virally infected cells.[24,25]

Similar to Ca^{2+}-dependent lectins, a group of thiol-dependent binding proteins was discovered in 1975.[26] Today, these lectins have been renamed from S-type lectins into galectins because not every lectin of this family requires a thiol function for the binding processes. Galectins in animals occur in mainly two major types (Fig. 1.1.1). There are prototypical galectins, which contain one CRD and tandem repeat galectins which consist of at least two CRDs connected via a peptide domain. Galectins are not membrane bound, recognize β-galactose-containing glycans and are important in biological processes such as apoptosis, T cell receptor activation, innate immunity and cancer.[27–29]

Another family of animal lectins are the I-type lectins which belong to the immunoglobulin superfamily. The best characterized group of this family are the sialic acid-binding immunoglobulin-type lectins (Siglecs) which can be divided into two major subgroups based on sequence homology or conservation within one mammal species. All siglecs are transmembrane proteins containing different amounts of Ig domains (Fig. 1.1.1). This important group of sialic acid-binding proteins is involved in the whole immune system, innate immunity as well as in acquired immune responses.[30–32]

1.1.3 Microbial lectins

Organisms like viruses, bacteria and protozoa possess a vast amount of microbial lectins, needed for cell attachment and tissue colonization, processes which finally lead to infection of pathogenic species.[10]

A well known example of a viral glycan-binding protein is hemagglutinin, which is located in the viral envelope of influenza.[33] The binding between this lectin and sialic acid-containing glycans on the cell surfaces of host cells is essential for uptake of the virus into the cell.[34] There are many more viruses, which use sialic acids for attachment processes, such as rotavirus and adenovirus.[35,36]

Bacterial adhesion to glycans is also mainly mediated by lectins. On the surface of bacteria, lectins appear mostly as part of fimbriae, located in the outer membrane of bacterial cells (Fig. 1.1.1).[37] One

of the best examined examples for these fimbriae are the type 1 and P fimbriae of *Escherichia coli*. Both types of fimbriae consist of various amounts of proteins with a lectin located at the tip of the fimbriae.[38,39] For further details on bacterial fimbriae and especially type 1 and P fimbriae see chapter 3.1.

1.2 Glycans

After these insights in the wide field of lectins, the next question concerns the way how all these different kinds of GBPs recognize specific glycan patterns or sometimes just a single carbohydrate out of the thousands surrounding animal cells. The glycocalyx on the outer membrane of cells

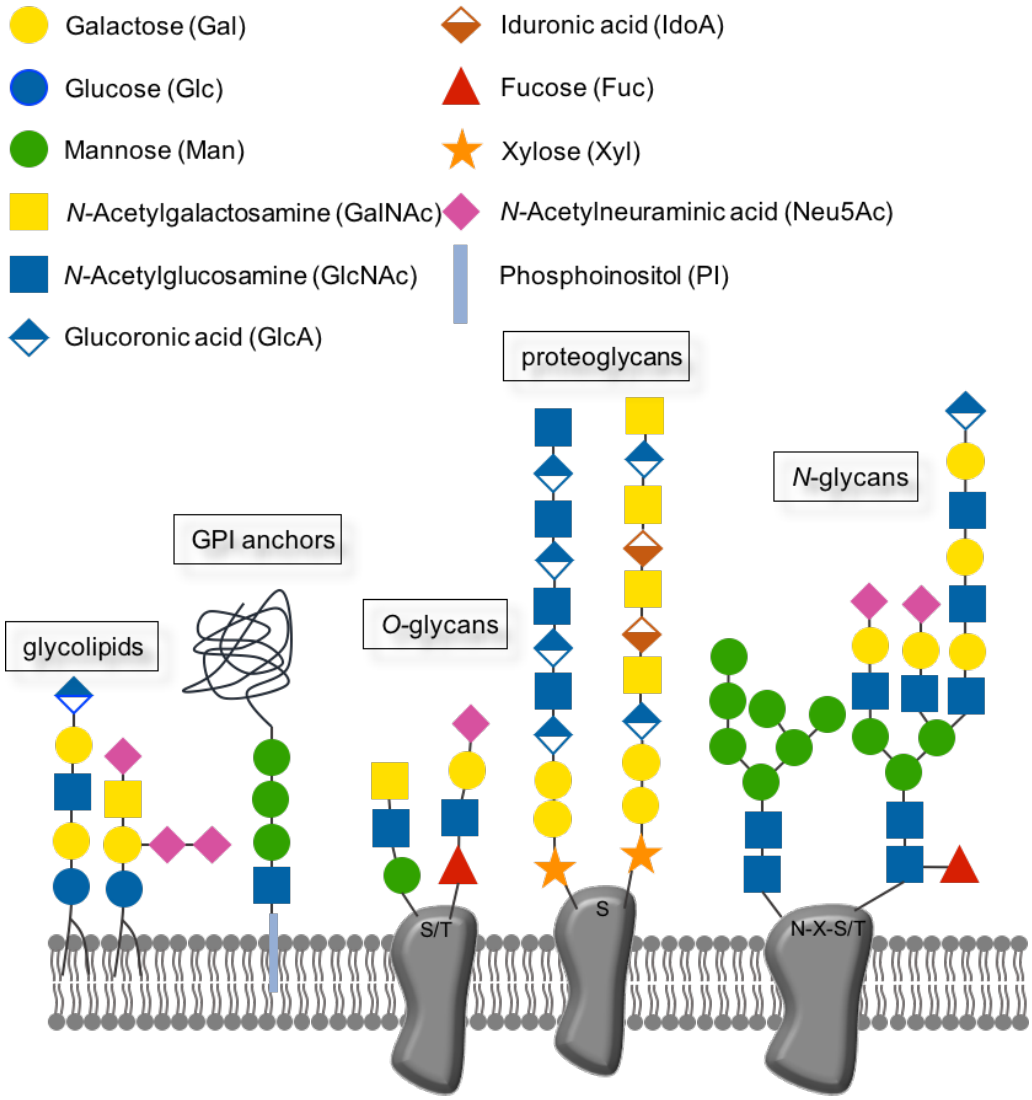

Figure 1.2.1: Overview of the most common glycans on cell surface.

is involved in almost all recognition and adhesion processes of the previous mentioned lectins. It consists of a variety of glycans depending on the age, healthiness and function of the cell.[40,41]

Figure 1.2.1 gives an overview of some glycan structures, most of them connected to lipids and proteins and therefore anchored in the cell membrane.[42]

Within the glycosylation machinery of a cell eight different glycosylation pathways exist, which lead to this huge variety of glycans. All of them require nucleotide sugars to be delivered to the endoplasmatic reticulum (ER) or Golgi apparatus where the glycan biosynthesis takes place. *N*-linked glycans consist of a highly conserved core of two GlcNAc moeities followed by three branched mannosides. The first GlcNAc is bound to an asparagine residue which emerges always in the same sequence: N-X-S/T, where X depicts a variable amino acid.[43] During the glycosylation process inside the ER, a 14 unit sugar precursor, consisting of the core and six additional mannosides as well as three glucosides is linked to dolichol. With an oligosaccharyltransferase (OST) the glycan is transferred to the asparagine often followed by a removal of the glucosides and by addition of other moieties like GlcNAc, Neu5Ac and Fuc. For *O*-linked glycosylation a linkage between a serine or threonine residue and GalNAc, Fuc, Xyl or Glc mediated by the respective transferases is required. This is followed by the addition of Gal, GlcNAc, Fuc or sialic acid to form further branched or linear glycans. On the contrary, glycosphingolipids are anchored in the membrane without any protein but through ceramides or phosphatidylinositol anchors.[10,44]

A major challenge in the field of the glycomics is derived from this huge variability of glycans as well as glycan-binding proteins. It is known that dysfunction in glycosylation pathways lead to severe diseases. This is equally important as the adhesion process of viruses and bacteria to the glycosylated cell surface. At this point, a better understanding of all these binding mechanisms between carbohydrates and lectins is urgently needed. Therefore new methods and techniques are required and these should be simple enough for everyday use and should be made available to every laboratory.

2 Objectives

Within the last decades the interest in bacterial adhesion and in its inhibition became more and more important due to the increased antibiotic resistance of bacteria. An example for bacterial infections are uropathogenic *E. coli* (UPEC). Every second woman suffers from bladder infection at least once a lifetime. The first initial contact between UPEC and the host is caused by fimbriae which are located on the outer membrane of the bacteria. The most common and known fimbriae of UPEC are type 1 and P fimbriae displaying a carbohydrate specific lectin (FimH and PapG). For further investigation it is of great interest to get a better understanding of the complete mechanism which occurs during bacterial adhesion. At that point this thesis initiates. The main objective was to design and investigate different techniques of carbohydrate-lectin interactions focused on both important lectins of UPEC FimH and PapG. Therefore three different parts were addressed: (i) bacterial adhesion studies, (ii) examination of shear force influence and (iii) glyconanoparticles (Fig. 2.0.1).

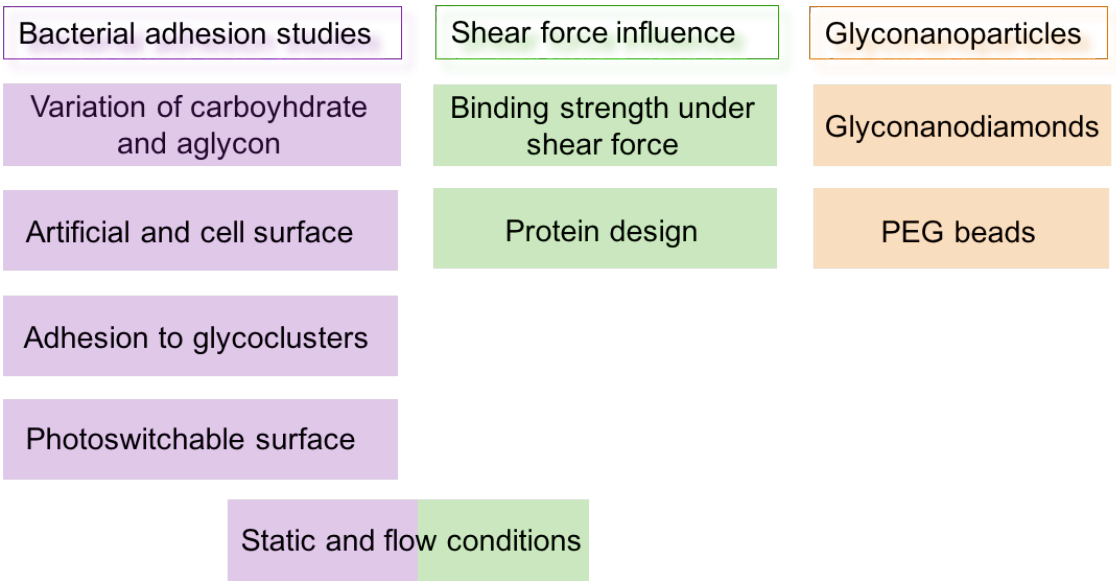

Figure 2.0.1: Overview of the three different main objectives with all methods and variations.

The first objective benefits from a bacterial adhesion assay which was introduced in the group earlier and allows fast identification and comparison of different ligands. Subsequently the influence of different aglycones at the anomeric position of carbohydrate ligands as well as the impact of order in this system were addressed. Also other open questions like the comparison between an artificial glycoarray and a cell surface, the adhesion to different stereoglycoclusters and the influence of the carbohydrate orientation on an artificial surface were considered. In addition bacterial adhesion to

carbohydrates under static and under flow conditions was compared. The influence of flow led to the second objective where the catch bond mechanism of the lectin FimH was under investigation with different biophysical and biochemical approaches. In the last objective, nanoparticles as tools to inhibit or analyze bacterial adhesion with type 1 and P fimbriated *E. coli* were used.

3 Bacterial adhesion studies

3.1 Introduction

3.1.1 Bacterial lectins

Adhesins are common in Gram-positive as well as in Gram-negative bacteria. Within the Gram-negative enterobacteria like *E. coli* or *Salmonellae* lectins are located on hairlike protein structures on the outer membrane of the bacteria known as fimbriae or pili.[45–47] Other types of fimbriae on the surface are flagella, used for the mobility, type III secretion systems (injectosomes) and pili which play different roles in bacteria.[48] Type IV pili are needed for movement, F pili for interbacterial DNA transfer and the different types of adhesive fimbriae are important for bacterial adhesion to cell surfaces. For all these adhesins various secretion systems exist. In Gram-positive bacteria it is mainly the sortase cell-wall anchoring system whereas in Gram-negative ones the type I, type III, type IV, type V secretion systems and the chaperone usher pathway become important.[49–53] Among the best characterized fimbriae of *E. coli* are the type 1 fimbriae, specific for mannose. They are secreted through the chaperone usher pathway (Fig. 3.1.1).[54–56] Other examples are the P fimbriae of *E. coli* which recognize Galα1-4Gal expressed by the neutral glycolipid globotriaosylceramide (Gb3), the S fimbriae of *E. coli,* specific for sialic acid containing receptors and type 1 fimbriae of *Salmonella.*[57–61]

3.1.2 The bacterial lectins FimH and PapG

P fimbriae as well as type 1 fimbriae are secreted through the chaperone usher pathway.[54] Both fimbriae are 1-2 μm long, around 7 nm thick and can be separated into a fimbrial shaft and a tip. The shaft is built up by about 1000 subunits of FimA or Pap which are ordered in a helical structure. In case of type 1 fimbriae, the fimbrial tip consists of two peripheral bound subunits, FimF and FimG.[39] At the tip of the fimbriae the lectin FimH is bound with its pili domain $FimH_P$ and its lectin domain $FimH_L$, where the CRD is located. The lectin FimH comprises of 279 aa and has a mass of 29 kD. Amino acids 1-156 form $FimH_L$ and $FimH_P$ is constructed of amino acids 157-279. Crystal structure analysis of the FimH with carbohydrate ligands identified different amino acids responsible for ligand complexation as well as one water molecule inside the binding pocket which is needed to improve the binding. All in all nine hydrogen bridge bonds between an α-D-mannoside and the amino acids F1, D47, D54, Q133, N135 and D140 are built. An α-anomeric aglycone sticks out of the carbohydrate recognition domain flanked by two tyrosines, Y48 and Y137.[62,63] Through ππ stacking between the tyrosine residues and the ligand, the binding affinity is improved.

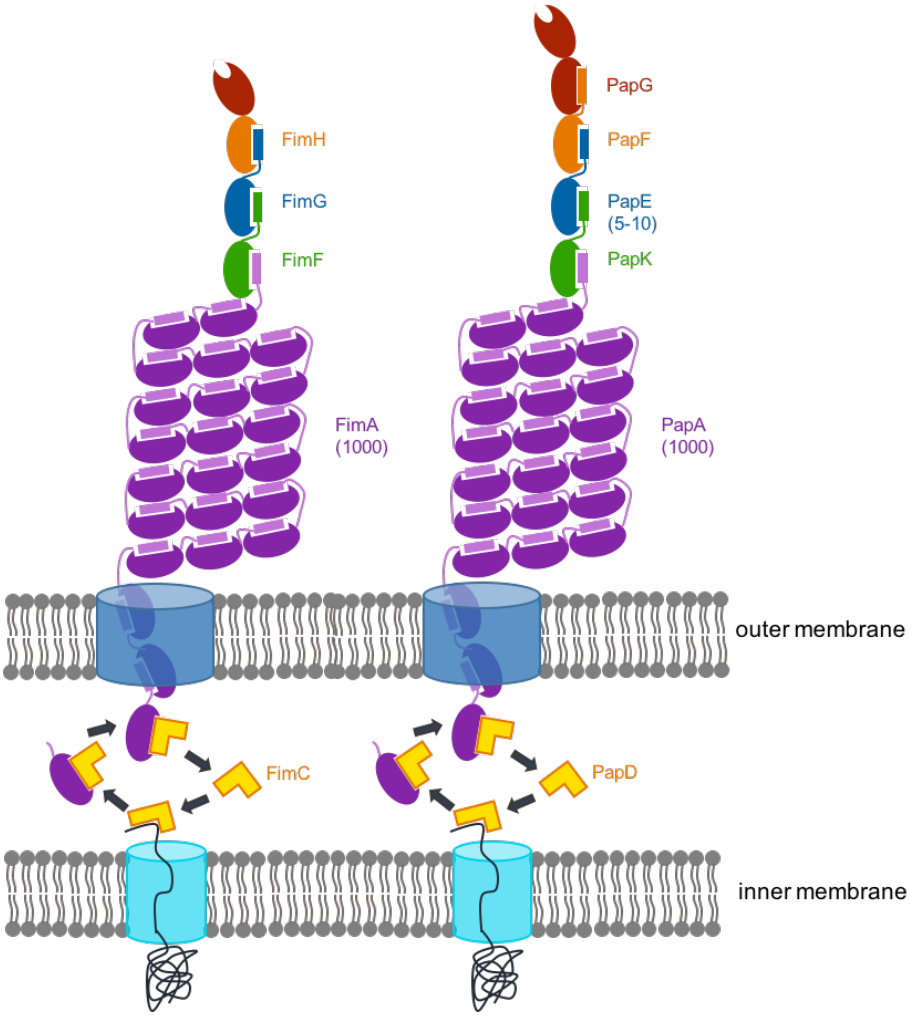

Figure 3.1.1: Structure of the type 1 and P fimbriae with all subunits.

Two prototypical crystal structures of the tyrosine gate are known, an open and a closed gate conformation (Fig. 3.1.2, PDB: 1KLF[64] and 1UWF[65]).

The P fimbriated tip consists of 5-10 domains of PapE surrounded by one PapK and PapF domain each.[58] The lectin PapG persists of 316 aa and similar to FimH there are two domains. A *N*-terminal receptor binding domain (with 196 aa) mostly β-sheet structures and a *C*-terminal pilin domain. Three different PapG alleles (I-III) exist and they bind with variable affinity to different isoreceptors which differ in carbohydrate residues among the common Galα1-4Gal core (Fig. 3.1.3).[66,67]

Every pili subunit has a similar structure: an unstructured *N*-terminus of 10-20 amino acids, followed by a core of six β sheet structures. Every subunit is directed into the periplasm through the Sec pathway. Inside the periplasm the chaperones FimC or PapD stabilize the subunit with donor strand complementation to protect the protein against aggregation and proteolytic cleavage. The chaperones lead the subunits to the transmembrane parts where the donor exchange mechanism takes place. The *N*-terminal end interacts with the previous subunit to complement the fimbrial structure (Fig. 3.1.1).[38,39,54]

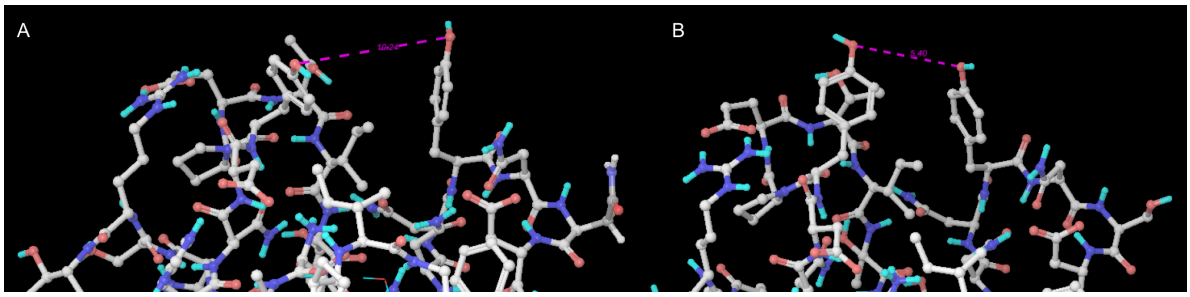

Figure 3.1.2: Tyrosine gate of the lectin FimH. (A) Open gate structure (1KLF), (B) closed gate structure (1UWF).

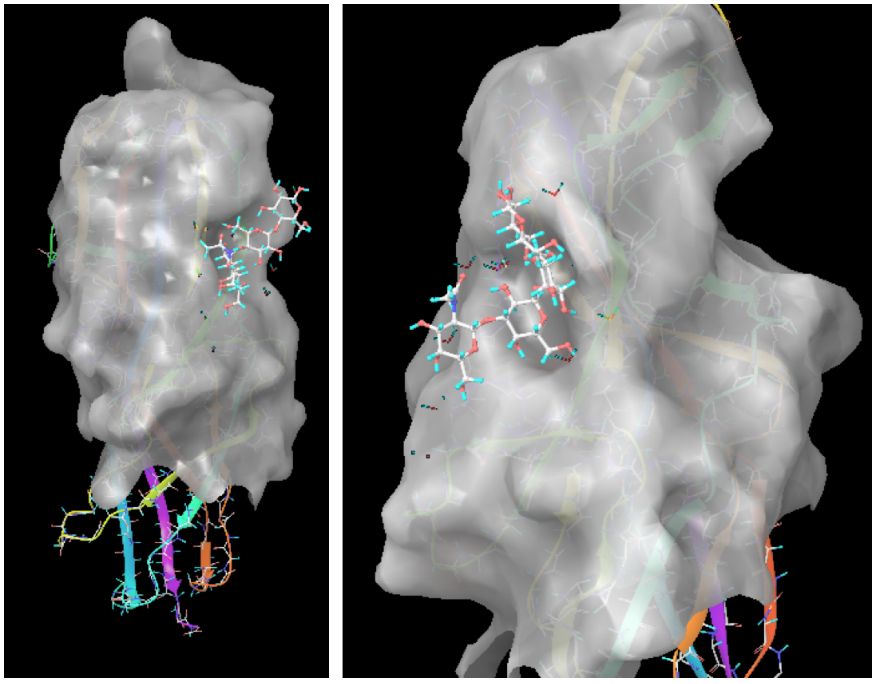

Figure 3.1.3: Crystal structure of the lectin PapGII bound to a Gb04 ligand (GalNAcβ1,3Galα1,4Galβ1,4Glc), PDB code 1J8R.[58]

3.1.3 Bacterial assay systems

Fimbriated bacteria are known to be more infective than their nonfimbriated counterparts. This is due to the bacterial lectins. In urinary or gastrointestinal tract infections they play a key role in the first contact between bacteria and host.[68,69] After this first initial contact, biofilm formation occurs which finally leads to the infection of the host organism.[70] Recently more and more bacteria exhibit antibiotic resistance.[71] Therefore, there is an increasing demand of other therapeutic compounds such as inhibitors of bacterial adhesion. To identify and investigate such compounds bacterial adhesion assays were introduced over the last few years. Various microarray-based techniques are used. They have the advantage of high-throughput screening but also the limitation that they are based on carbohydrate-lectin interactions instead of using the whole bacterial organism. However, in spite of this there is a huge benefit in high-throughput screening methods as plenty of compounds

can be tested simultaneously and small amounts are enough for testing. Then just the promising compounds can be investigated further.[72–74]

Test systems to analyze the interactions between whole bacteria and different carbohydrates are more limited. One common system is the use of erythrocytes to perform hemagglutination assays.[75] Another described method is ELISA (enzyme-linked immunosorbent assay) based.[76] In 2011 M. Hartmann *et al.* introduced an assay based on GFP-expressing *E. coli* which simplified the analysis of the binding properties as well as the inhibitor identification.[77] Further investigations with GFP-expressing bacteria led to the development of flow assays on epithelial cells[78,79] or the usage of magnetic PEG beads to analyze inhibitors of bacterial adhesion.[80] Taken together, the improvement of bacterial assay systems led to the identification of new inhibitors of bacterial adhesion.[81]

In the context of antibiotic multiresistant bacterial strains it is more and more important to improve the detection of carbohydrate driven antiadhesive molecules. For this purpose in the following part (3.2) of this thesis, the focus was layed on the influence of different aglycon moieties on the binding properties of the bacterial lectin FimH. To further elaborate this study the inhibition properties of different ligands within an assay system on a natural cell surface were investigated under static as well as under flow conditions (chapter 3.3). Furthermore glass surfaces were utilized for bacterial adhesion assays in two different ways. First a surface with photoswitchable azobenzene mannosides was tested to switch bacterial adhesion on a glass surface (chapter 3.4), and second prefunctionalized glass slides were used to immobilize synthetic compounds and determine the bacterial adhesion properties under flow conditions (chapter 3.5).

3.2 Effect of aminophenyl and aminothiahexyl α-glycosides of the *manno-*, *gluco-* and *galacto*-series on type 1 fimbriae-mediated bacterial adhesion of *Escherichia coli*

Bacterial adhesion studies with polystyrene surfaces have been performed since many years. In case of uropathogenic *E. coli* a main attention was focused on the interaction of type 1 fimbriae and α-D-mannoside ligands. This paper discusses the influences of different aglycone moieties compared with the variation of three different carbohydrate ligands. Additionally, the impact of ligand presentation, in solution or surface bound, was addressed.

The following manuscript has been published earlier: C. Fessele, T.K. Lindhorst, *Biology*, **2013**, *2*, 1135-1149.

DOI: 10.3390/biology2031135

I performed the experiments and the evaluation of the biological data and T.K. Lindhorst and I wrote the manuscript together.

3.2.1 Abstract

Adhesion of bacteria to the glycosylated surface of their target cells is typically mediated by fimbrial lectins, exposed on the bacterial surface. Among the best-investigated and most important fimbriae are type 1 fimbriae, for which α-D-mannopyranoside-specificity has been described. This carbohydrate specificity is mediated by the type 1 fimbrial lectin FimH. In this account, we have employed four different set-ups to assay type 1 fimbriae-mediated bacterial adhesion, including tailor-made glycoarrays. The focus of our study was on testing FimH specificity with regard to the aglycone part of a glycosidic ligand by testing a series of synthetic α-mannosides, as well as α-glucosides and α-galactosides. Unexpectedly, it was found that in solution all tested aminothiahexyl glycosides inhibit bacterial adhesion but that this effect is unspecific. Instead it is due to cytotoxicity of the respective glycosides at high mm concentrations.

3.2.2 Introduction

Escherichia coli is a widely distributed bacterial species that is responsible for many serious infections. Urogenital infections, for example, are caused by uropathogenic *E. coli* (UPEC). In order to infect their target cells, UPEC first have to accomplish adhesion to the glycosylated cell surface and establish colonization of the cell surface.[82,83] The bacterial adhesion process is facilitated by adhesive organelles, called fimbriae. The best-investigated fimbriae are type 1 fimbriae, which are hair-like, 1–2 μm long, and ~7 nm wide protein structures on the bacterial cell surface.[84,85] Type 1 fimbriae are widely expressed by *E. coli* and constitute important virulence factors of uropathogenic strains. They are used to mediate attachment to specific niches in the urinary tract.[86] Thus, type 1 fimbriae have a well-established role in urinary tract infections and in addition have been implicated in neonatal meningitis and Crohn's disease.[87,88] It has been shown that glycoproteins carrying one or more *N*-linked high-mannose type oligosaccharides serve as receptor molecules for

type 1 fimbriae. Early studies by Sharon and Ofek et al. have revealed the affinities of various oligosaccharides of different complexity.[37,89–92] From these studies it can be concluded that the presentation of α-D-mannosyl moieties, which varies in different oligosaccharides, is important for binding to type 1-fimbriated bacteria. This assumption is also supported by recent literature on carbohydrate binding of selectins.[93]

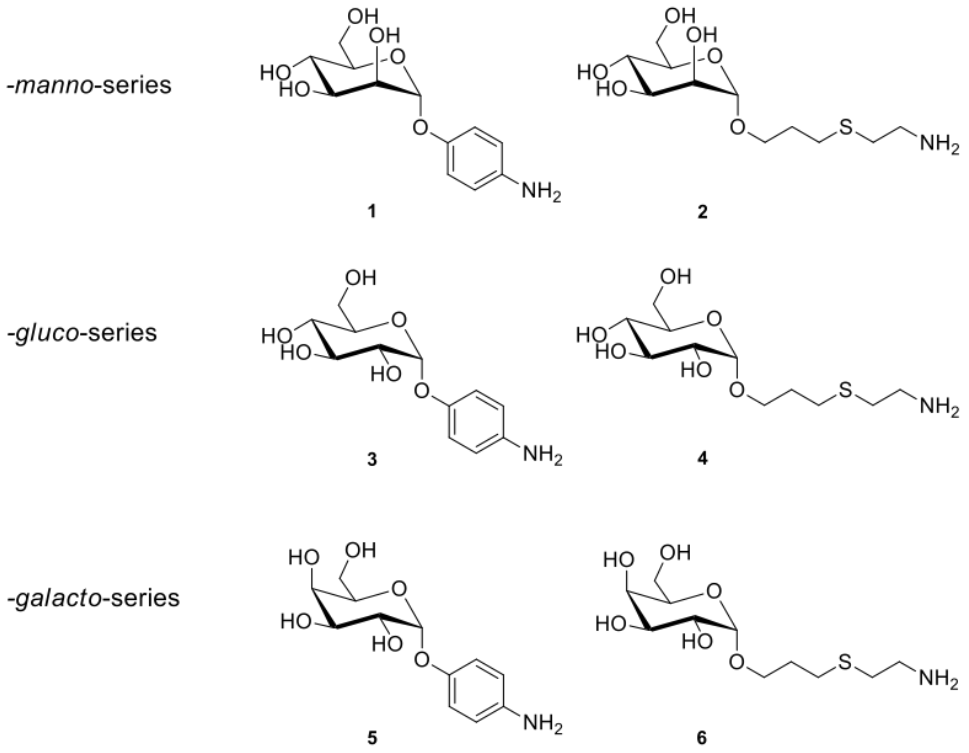

Figure 3.2.1: α-Glycosides of the manno-, gluco- and galacto-series, employed in the adhesion assays and for glycoarray fabrication. Nomenclature: 4-aminophenyl α-D-mannopyranoside (**1**, *p*APMan), 6-amino-4-thiahexyl α-D-mannopyranoside (**2**, ThiahexMan), 4-aminophenyl α-D-glucopyranoside (**3**, *p*APGlc), 6-amino-4-thiahexyl α-D-glucopyranoside (**4**, ThiahexGlc), 4-aminophenyl α-D-galactopyranoside (**5**, *p*APGal), 6-amino-4-thiahexyl α-D-galactopyranoside (**6**, ThiahexGal).

Additionally, many studies with type 1 fimbriated bacteria were performed using multivalent mannosides as carbohydrate ligands, such as glycodendrimers or neoglycoproteins.[75,94–103] In these cases, statistic multivalency can lead to high avidity of the respective ligands. More recently, type 1 fimbriae-mediated bacterial adhesion has been studied and inhibited employing an armada of various synthetic mannosides with differing non-carbohydrate aglycone moieties to achieve effective antagonists of FimH.[65,104–108] This work has been extensively reviewed.[81,109] Apparently, carbohydrate binding of type 1 fimbriae is mediated by the lectin FimH, which is located at the fimbrial tips.[38] FimH is a two-domain lectin with its pilin domain $FimH_P$ anchoring the lectin at the tip of the type 1 fimbrial shaft and its lectin domain, $FimH_L$, harboring the carbohydrate-binding site. X-ray analysis of FimH has shown that[63,64,110,111] exactly one α-D-mannosyl residue can be accommodated within the carbohydrate-binding pocket (β-glycosides do not fit into the binding site).

The aglycone moiety of a natural oligosaccharide exerts additional interactions at the periphery of the carbohydrate-binding site.[110] Likewise, non-natural aglycone portions can be used to increase the affinity of a synthetic α-D-mannoside according to computer docking and biological testing.[81,112] This approach has been promising in the context of an anti-adhesion therapy against urinary tract infections.[113–116] However, relatively recently, it has been found that FimH is a lectin that can function according to a catch bond mechanism.[117] Tensile forces, flow, or shear force, respectively, induce an allosteric switch, that also involves the carbohydrate-binding site, which is rearranged to a conformation, which binds α-D-mannosides more strongly.[118] Thus, FimH can be considered as an especially intriguing lectin, with the potential to structurally rearrange its carbohydrate-binding site. This has prompted us to revisit inhibition of type 1-fimbriated bacterial adhesion employing a collection of six synthetic α-glycopyranosides of the manno-, gluco-, and galacto-series, **1**–**6** (Figure 3.2.1). Many other mannose-specific lectins are known to display a carbohydrate specificity for monosaccharides other than mannose.[119] However, in the case of FimH and type 1-fimbriated bacteria, respectively, glycosides other than mannosides were typically used as negative controls.

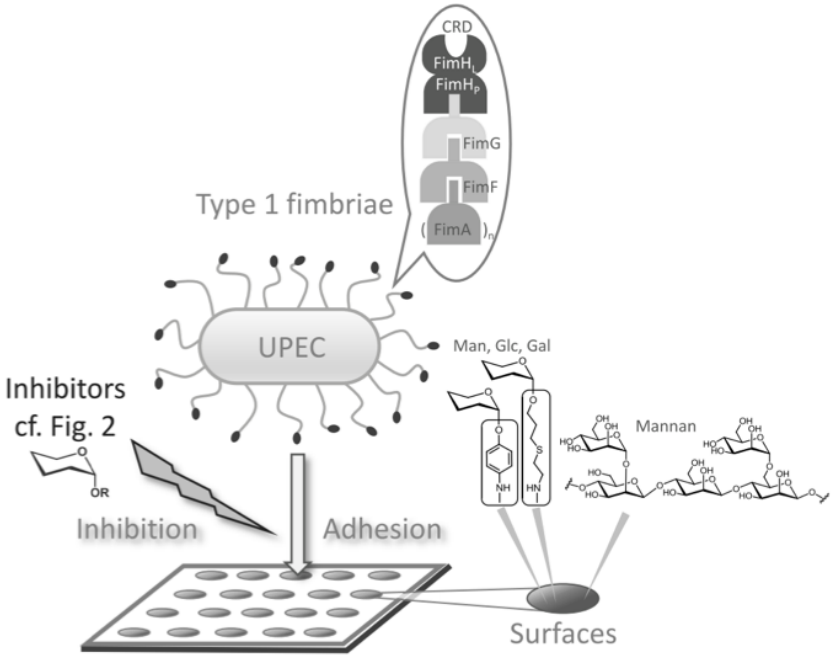

Figure 3.2.2: Type 1 fimbriae-mediated adhesion of uropathogenic *Escherichia coli* (UPEC) to a glycosylated surface is mediated by type 1 fimbriae. Type 1 fimbriae are rod-like adhesive organelles exposed by the bacteria, terminated by the lectin FimH for which a clear specificity for α-D-mannosides has been described. Here, it was tested if also glucosides and galactosides can also exert some inhibitory potency in this system. As glycosylated surfaces mannan-coated polystyrene microtiter plates were used on the one hand, and alternatively, tailor-made microtiter plate-based glycoarrays were employed, comprising α-mannoside, α-glucoside, and α-galactoside functionalization. A corresponding series of glycosides were tested as inhibitors of bacterial adhesion in solution.

Carbohydrate specificity of lectins is typically tested in solution or on polystyrene microtiter plates, which can be carbohydrate-decorated to allow type 1 fimbriae-mediated adhesion of *E. coli* (Figure 3.2.2). The potencies of inhibitors of this adhesion process are mostly obtained from inhibition curves and expressed in the form of IC_{50} values. In our study, four different assays were employed: (i) A binding assay with GFP-tagged *E. coli* to microtiter plate-based glycoarrays testing varied bacterial concentration and (ii) varied glycoarray density; (iii) an adhesion-inhibition assay to test the prepared series of synthetic α-glycosides as inhibitors of bacterial adhesion to a mannan-coated surface in solution, and (iv) a preincubation-inhibition-adhesion assay in which the bacteria are allowed to interact with the glycosides in solution before they are transferred to the microplates. This approach should allow us to test if in any set-up in altered carbohydrate specificity of type 1 fimbriae-mediated bacterial adhesion can be seen.

3.2.3 Results

3.2.3.1 Binding of GFP-tagged *E. coli* to glycoarrays on polystyrene microtiter plates

Glycoarrays have become valuable tools in glycobiology.[120–122] We, and others, have prepared glycoarrays on polystyrene microtiter plates to facilitate the study of cellular adhesion, including bacterial adhesion assays.[123–126] One of the classic approaches to study bacterial adhesion to carbohydrate surfaces is to employ mannan-coated microtiter plates. Mannan from *Saccharomyces cerevisiae* is a polydisperse polysaccharide that sticks to polystyrene surfaces by hydrophobic forces. It exposes α-D-mannosyl residues, which allow for attachment of type 1-fimbriated *E. coli* cells (Figure 3.2.2). However, when microtiter plates are functionalized using specific glycosides, the resulting glycoarray surfaces are more precisely defined than when mannan coating is employed. In addition, when synthetic glycosides are used for glycoarray fabrication, tailor-made surfaces can be designed to address specific questions of carbohydrate recognition and to test binding properties of lectins in great detail. The series of manno-, gluco- and galacto-configured α-D-glycosides we used carry aglycone portions modified with a terminal amino group (Figure 3.2.2). This allows us to chemically attach the respective glycoside to the surface of pre-activated polystyrene microtiter plates. Thus, glycosides **1**–**6** were individually immobilized onto the surface of microtiter plates using 10 mM concentrations in all cases. Following this, the fluorescent type 1-fimbriated *E. coli* bacteria were added in serial dilution to the resulting glycoarray-decorated plates. After washing of the plates bacterial adhesion was measured by readout of fluorescence intensity (Figure 3.2.3). Glycoarrays prepared from the phenyl mannosides **1** or the alkyl mannosides **2** led to effective adhesion of bacterial cells in a perfect concentration-dependent manner, as expected. However, the glycoarrays prepared from glycosides of the gluco- and galacto-series, respectively, were not suited to mediate type 1 fimbriae-mediated bacterial adhesion. Indeed, no bacterial adhesion was detected. As we were interested to assess, if the carbohydrate specificity of type 1 fimbriae-mediated bacterial adhesion is strictly limited to α-D-mannosides, we tested glycoarrays at higher sugar concentrations in the next step. Thus, glycoside solutions used for glycoarray fabrication were serially diluted starting with a comparatively high concentration (200 mM).

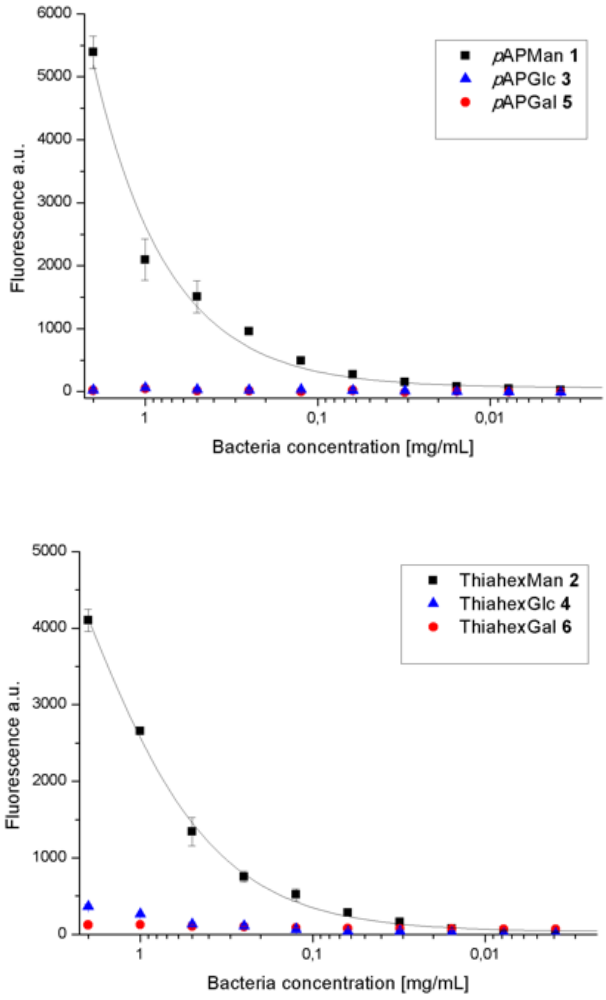

Figure 3.2.3: Bacterial binding to glycoarrays on microtiter plates with different bacteria concentrations. The depicted binding curves are representative examples from several (>3x) independent experiments. Error bars result from duplicate values on one plate.

On the other hand, a constant number of fluorescent *E. coli* cells were used in the adhesion experiments. Fluorescence read-out showed a plateau of maximal adhesion efficiency at "densely" functionalized plate surfaces and diminishing bacterial adhesion starting at lower glycoside concentrations when mannosides **1** or **2** were used for the functionalization of the microtiter plates (Figure 3.2.4). Again, glycoarrays prepared from glucosides (**3** or **4**) or galactosides (**5** or **6**), respectively, did not lead to an adhesive surface.

3.2.3.2 Adhesion-inhibition assay with GFP-tagged *E. coli*

In the next step of our study, all glycosides, which had been used before for glycoarray preparation (**1**–**6**), were now used as soluble inhibitors of type 1 fimbriae-mediated bacterial adhesion in solution.

It was important to test, if the effect of the putative FimH ligands in solution was different from their effect as immobilized ligands.

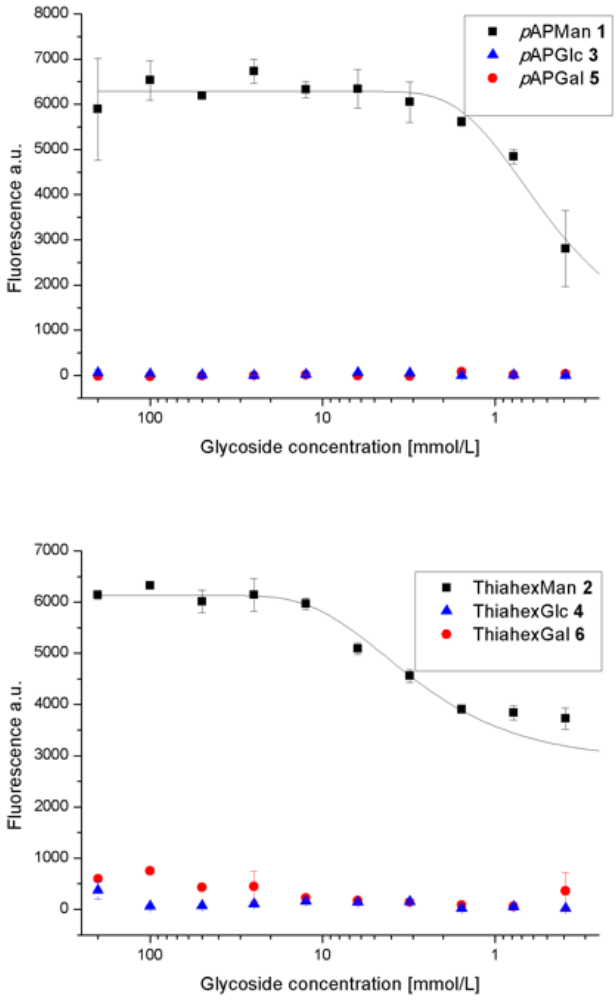

Figure 3.2.4: Bacterial binding to glycoarrays on microtiter plates. Various concentrations of glycosides were used for surface functionalization. The depicted binding curves are representative examples from several (>3x) independent experiments. Error bars result from duplicate values on one plate.

Hence, serial dilutions of inhibitor solutions were used to interfere with bacterial adhesion to mannan-coated microtiter plates. On each individual plate, we tested for methyl α-D-mannopyranoside (MeMan) to provide a universal reference inhibitor of type 1 fimbriae-mediated bacterial adhesion. Inhibition curves were determined for each tested inhibitor and IC_{50} values were deduced where possible. The IC_{50} value represents the inhibitor concentration at which 50 % of bacterial adhesion is prevented. As MeMan was always simultaneously tested, relative inhibitory potencies (RIP values) can be specified for all tested glycosides with respect to the IC_{50} obtained for MeMan, which was defined as reference inhibitor potency with IP=1. As expected, the two mannosides **1** and **2** gave the

best IC_{50} values in this assay. These results are in accordance with the literature.[81] Unexpectedly however, also the phenyl glucoside **3** showed an inhibitory potency, although it was smaller than that of MeMan (Figure 3.2.5 a).

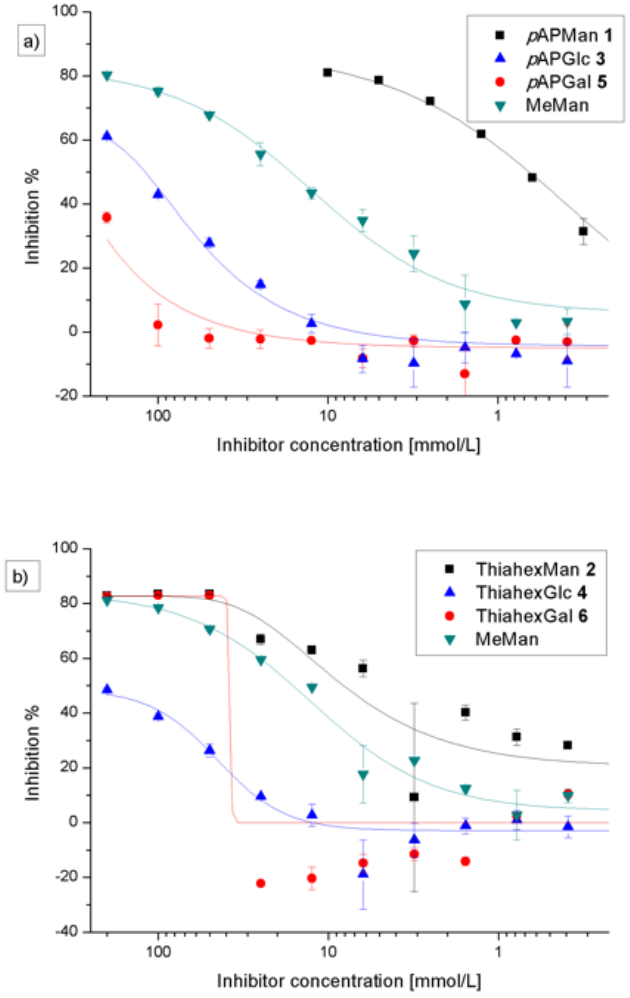

Figure 3.2.5: Inhibition curves obtained with the phenyl glycosides **1**, **3**, and **5** (a) and the alkyl glycosides **2**, **4**, and **6** (b) as inhibitors for type 1 fimbriae-mediated bacterial adhesion to mannan. The depicted inhibition curves are representative examples from several (>3x) independent experiments. The standard inhibitor MeMan was tested simultaneously on each plate. Error bars result from duplicate values on one plate.

Interestingly, the alkyl galactoside **6** showed an unexpected inhibitory effect when employed at concentrations greater than 25 mM. In the same concentration range, the alkyl glucoside **4** had a less pronounced effect (Figure 3.2.5 b). Strikingly, at concentrations <25 mM galactoside **6** had no effect on bacterial adhesion at all. The obtained "curve" cannot be considered a regular inhibition curve.

3.2.3.3 Preincubation-inhibition-adhesion assay with GFP-tagged *E. coli*

In the adhesion-inhibition assay (vide supra) a soluble inhibitor has to compete against a highly mannosylated (mannan-coated) surface for binding to the type 1 fimbrial lectin.

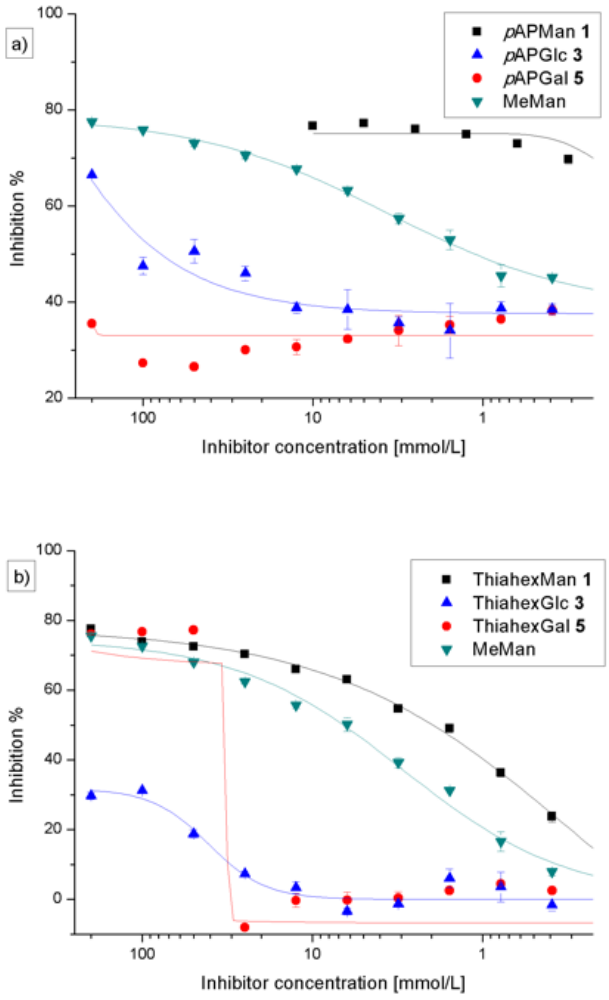

Figure 3.2.6: Preincubation-inhibition-adhesion assay with GFP-tagged *E. coli*: Inhibition of bacterial adhesion to mannan as obtained with the phenyl glycosides **1**, **3**, and **5** (a) and the alkyl glycosides **2**, **4**, and **6** (b) after preincubation with the bacteria. The depicted inhibition curves are representative examples from several (>3x) independent experiments. The standard inhibitor, MeMan, was tested on the same plate. Error bars result from duplicate values on one plate.

In contrast to this, in the preincubation-inhibition-adhesion assay[105], the uropathogenic *E. coli* were first incubated with the respective inhibitor under physiological conditions for 1 h. Only then, this suspension was transferred to the mannan-coated microtiter plate surface. In the adhesion-inhibition assay both ligands, mannan and the tested inhibitor, are presented to the bacteria at the same time. In contrast, preincubation of the bacteria with inhibitor solution can lead to saturation of the

lectin's carbohydrate binding sites prior to the adhesion experiment on the mannan-coated surface. Thus, in this assay bacterial binding to mannan is only possible if the fimbrial binding site is not effectively saturated with the inhibitor after preincubation.

However, bacterial adhesion after preincubation with the inhibitory glycosides led to very similar results as the adhesion-inhibition assay without preincubation (Figure 3.2.6, Table 3.2.1). The galactoside **6** showed a similar effect as seen before (Figure 3.2.5b). For a more detailed comparison, the testing results obtained in the adhesion-inhibition experiments without and with preincubation of bacteria are summarized in Table 3.2.1. Significant differences between the two assays can be seen mainly in the IC_{50} values for the mannosides **1** and **2**, as well as for the glucoside **3**. The glucoside **4** and the galactoside **5** could not effect 50 % inhibition of bacterial adhesion in both tests and, therefore, no IC_{50} values could be determined. Owing to the unusual curves obtained with galactoside **6**, no IC_{50} values were deduced in this case.

Table 3.2.1: Inhibition of type 1 fimbriae-mediated *E. coli* adhesion to mannan-coated microtiter plates. For IC_{50} and RIP values are averaged from mean values from three independent tests. # RIP values are relative inhibitory potencies based on the IC_{50} value measured for MeMan on the same plate.

	Adhesion-inhibition assay			**Preincubation-inhibition assay**		
Glycoside	IC_{50}[mM] (SD)	RIP# (SD)	total inhibition %	IC_{50}[mM] (SD)	RIP# (SD)	total inhibition %
1 *p*APMan	0.62 (0.21)	27.8 (1.65)	83	0.035 (0.02)	30.2 (7.8)	76
2 ThiahexMan	5.28 (2.47)	2.41 (0.37)	80	1.19 (0.79)	3.46 (0.12)	78
3 *p*APGlc	122 (1.99)	0.135 (0.01)	60	51.35 (27)	0.023 (0.01)	63
4 ThiahexGlc	-	-	45	-	-	46
5 *p*APGal	-	-	32	-	-	49
6 ThiahexGal	-	-	77	-	-	75

3.2.3.4 Bacterial growth tests

As a next step, it was important to analyze the effect of galactoside **6** on bacterial adhesion, and to assess whether it is due to specific inhibition of fimbriae-mediated binding or is caused by other processes. Thus, highly concentrated solutions of **6** were incubated with the bacteria and then bacterial growth was tested on agar plates. Visual inspection of the agar plates after one day clearly showed that solutions of galactoside **6** at concentrations >25 mM were cytotoxic for the bacteria. No bacterial growth was observed in repeated experiments. After this finding, all other glycosides we used were tested in the same assay and the results are summarized in Table 3.2.2. According to this test, none of the tested *p*-aminophenyl glycosides (**1**, **3**, **5**) are cytotoxic at high concentrations. However, all aminothiahexyl glycosides (**2**, **4**, **6**) were cytotoxic at high concentrations, the glucoside **4** at concentrations ≥100 mM, galactoside **6** at concentrations ≥50 mm, and, surprisingly, mannosides **2** inhibits bacterial growth even at a concentration of 25 mM.

Table 3.2.2: Bacterial growth was tested on agar plates after1 h of incubation with glycosides **1**–**6**, which were employed at the indicated concentrations. + Bacteria grow; − no bacterial growth could be seen by visual inspection; n.t. not tested.

	1 *p*APMan	**3** *p*APGlc	**5** *p*APGal	**2** ThiahexMan	**4** ThiahexGlc	**6** ThiahexGal
200 mM	+	+	+	-	-	-
100 mM	+	+	+	-	-	-
50 mM	+	+	+	-	+	-
25 mM	+	+	+	-	+	+
12.5 mM	n.t.	n.t.	n.t.	+	n.t.	n.t.

3.2.4 Discussion and conclusion

To test the carbohydrate specificity of the bacterial lectin FimH under different conditions, pairs of α-configured synthetic glycosides of the *manno*-, but also the *gluco*- and *galacto*-series (**1**–**6**) were investigated with type 1 fimbriae-mediated bacteria. Two different aglycone moieties were used, namely an aromatic *p*-aminophenyl unit and the 6-aminothiahexyl spacer (Figure 3.2.1). When these glycosides were used for glycoarray fabrication on polystyrene microtiter plates, a strict mannose specificity was seen in type 1 fimbriae-mediated bacterial adhesion (Figures 3.2.3and 3.2.4). The glucose-, as well as galactoside-decorated surfaces had no adhesive property in this adhesion system. However, when glucosides (**3** and **4**) and galactosides (**5** and **6**) were tested in solution as inhibitors of bacterial adhesion to a mannan surface, rather unexpectedly, an inhibitory effect was observed (Figures 3.2.5and 3.2.6). The α-glucosides **3** and **4** showed a concentration-dependent inhibitory potency in both tests, in the adhesion-inhibition assay as well as in the preincubation-inhibition-adhesion assay. However, in both cases the determined inhibitory potency was weaker than that of MeMan and of the mannosides **1** and **2**. The phenyl galactoside **5** had no inhibitory potency, but the inhibitory effect of the aminothiahexyl galactoside **6** was comparable to that of the respective mannosides **2** as well as MeMan at high concentrations of >25 mM. At lower concentrations, an abrupt decline occurred to basically zero inhibitory power and this result was obtained repeatedly in all experiments performed. To analyze the specificity of these effects, bacterial growth was tested after incubation with the employed glycosides at high concentrations (Table 3.2.2). In this assay we observed that all thiahexyl glycosides (**2**, **4**, and **6**) inhibit bacterial growth at high concentrations. Thus, the measured inhibitory effect could be shown to stem from toxicity rather than from carbohydrate-specific inhibition of adhesion. The question of why mannosides **2** shows the highest toxicity in this series cannot be answered at this stage, as *E. coli* bacteria have transporters for all three types of sugars, glucose, galactose, as well as mannose.[127] Recently, we have performed careful toxicity studies with various mannosides, which were designed as inhibitors of bacterial adhesion, and there little or no cytotoxicity was seen.[128] Interestingly, various biological effects have been reported for aminlothiaalkyl-modified organic compounds, including antimicrobial activity.[129–132] Our study has important implications for further utilization of aminothiahexyl glycosides, regardless whether they are used as specific inhibitors or as control compounds in solution. As the aminothiahexyl aglycone is especially easily accessed in synthetic organic chemistry using the "thiol-ene" reaction of cysteamine to allyl glycosides, respective compounds are quite popular.[133] It

has to be kept in mind that the aglycone part of a specific glycoside can not only alter its affinity to the bacterial lectin FimH but lead to unexpected toxicity such in in the case of mannosides **2**. On the other hand, when glycosides such as **2**, **4**, or **6** are used to decorate surfaces, the resulting glycoarrays exert no cytotoxicity, suggesting that cellular uptake is a prerequisite for the effect (cf. Figures 3.2.3 and 3.2.4). The effect of the assay set-up can be seen when data, which were obtained in the adhesion-inhibition assay are compared with those measured in the preincubation-inhibition-adhesion assay (Table 3.2.1). In the first case, a glycoside ligand has to compete for the carbohydrate binding sites of type 1-fimbriated *E. coli* with the highly mannosylated polysaccharide mannan. In contrast to this, in the preincubation assay the bacteria are initially exclusively presented to the glycoside ligand, and no competing compound is present in the first step of the assay. In accordance with these considerations, the IC_{50} of mannosides **1** is ~0.6 mM in the adhesion-inhibition assay, but 0.035 mM in the preincubation-inhibition-adhesion assay. An analogous observation was made with mannosides **2**. In addition, the IC_{50} of the glucoside **3** is ~120 mM in the first assay and ~50 in the second. At this end it remains unclear, whether conformational rearrangement of FimH can result in altered carbohydrate specificity. In the herein performed tests, a "relaxed" conformation of the FimH carbohydrate-binding site must be assumed. As a next step, we will perform adhesion studies under tensile force, based on the herein reported results. After allosteric activation of FimH according to the catch bond mechanism, carbohydrate specificity of FimH will be tested accordingly.

Acknowledgments

Financial support for this work came from "Fonds der Chemischen Industrie" (FCI) and is gratefully acknowledged.

Conflicts of interest

The authors declare no conflict of interest.

3.3 En route from artificial to natural: evaluation of inhibitors of mannose-specific adhesion of *E. coli* under flow

After the importance to find new compounds for the inhibition of bacterial adhesion has been discussed in the previous article in the following manuscript the attention is focused on the inhibition of bacteria after they had the opportunity to adhere to an endothelial cell surface compared under static and flow conditions.

The following manuscript has been published earlier: Leonhard Möckl[a,c], Claudia Fessele[b,c], Guillaume Despras[b], Christoph Bräuchle[a,*], Thisbe K. Lindhorst[b,*], *Biochim. Biophys. Acta*, **2016**, *1860*, 2031-2036. Reproduced with permission from Elsevier © 2016.

DOI: 10.1016/j.bbagen.2016.06.021

(a) Department of Physical Chemistry, Ludwig Maximilian University Munich, Butenandtstrasse 11, 81377 Munich, Germany, (b) Otto Diels Institute of Organic Chemistry, Christiana Albertina University of Kiel, Otto-Hahn-Platz 3-4, 24098 Kiel, Germany, (c) These authors contributed equally to this work.

G. Despras synthesized the trivalent cluster, I prepared the other molecules and performed the bacterial testing under static conditions. L. Möckl investigated bacterial adhesion under flow on cell surfaces. The manuscript was written by T.K. Lindhorst, C. Bräuchle, L. Möckl and myself.

3.3.1 Abstract

We investigated the properties of six *E. coli* adhesion inhibitors under static and under flow conditions. On mannan-covered model substrates and under static conditions, all inhibitors were able to almost completely abolish lectin-mediated *E. coli* adhesion. On a monolayer of living human microvascular endothelial cells (HMEC-1), the inhibitors reduced under static conditions adhesion as well, but a large fraction of bacteria still managed to adhere even at highest inhibitor concentrations. In contrast, under flow conditions *E. coli* did not exhibit any adhesion to HMEC-1 already at inhibitor concentrations where significant adhesion was detected under static conditions. This indicates that the presence of shear stress strongly affects inhibitor properties and must be taken into account when evaluating the potency of bacterial adhesion inhibitors.

3.3.2 Introduction

The adhesion of bacteria to surfaces is one of the key steps in processes where bacteria exhibit pathogenic effects. Examples include harmful triggering of cellular signaling cascades,[134] invasion of host cells,[135] or biofilm formation.[136] One of the most common infectious diseases caused by bacterial adhesion are urinary tract infections (UTI). It is estimated that every second woman and 5 % of the male population suffers from a UTI at least once in their lifetime. Uropathogenic *E. coli* (UPEC) are the primary reason for these infections.[137] The first contact between the eukaryotic cell and the bacterium, crucial for the subsequent development of the disease, is mediated by adhesive organelles anchored on the outer membrane and projecting from the surface of UPEC. These so-called fimbriae consist of various protein units with a lectin domain at the very end. One of the best

characterized fimbriae and among the most important virulent factors of *E. coli* are the type 1 fimbriae. Their associated lectin is FimH which is specific for α-D-mannosides. FimH is known to bind to high-mannose type oligosaccharides of the glycocalyx of eukaryotic cells. Multivalency of this specific protein-carbohydrate interaction leads to adhesion of bacterial cells.[138] To fight bacterial infections like UTI, antibiotics are commonly used. However, one of the main problems resulting from the widespread use of antibiotics is the appearance of resistant bacterial strains.[139] An alternative therapeutic strategy against bacterial infection is an anti adhesion therapy[102] in which carbohydrate inhibitors are employed to prevent bacterial adhesion. Numerous FimH antagonists have been developed for the inhibition of type 1 fimbriae-mediated bacterial adhesion.[65,77,140] Recently, bioisosters glycosides were shown to be promising drugs against UTI.[141] In spite of the unquestionable success of the anti adhesion approach, anti adhesion therapy has not yet led to general solutions against infectious diseases. The reason might be that it is still challenging to consider all different aspects of a complex natural environment in the development of anti adhesives. Typically inhibitors of bacterial adhesion are evaluated in a microtiter plate-based assay

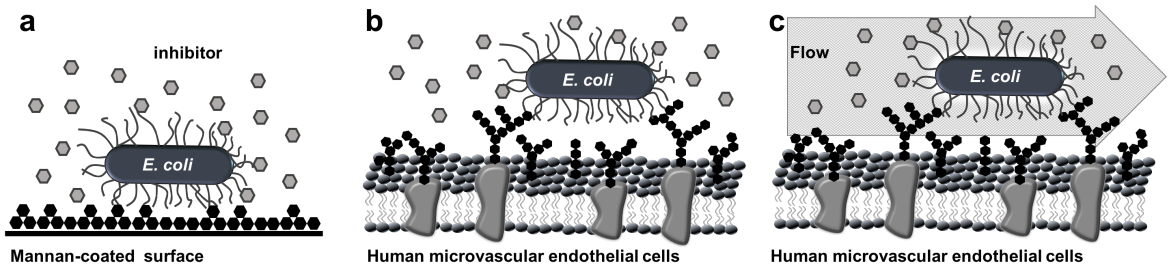

Figure 3.3.1: En route from artificial to natural: The mannose-specific fimbriae-mediated adhesion of bacterial cells to surfaces depends on the conditions. (A) Adhesion to artificial surfaces such as mannan-coated microtiter plates has been regularly used to evaluate the potency of sugar inhibitors under static conditions. (B) In bacterial adhesion to the glycosylated surface of human cells (HMEC-1) inhibitors compete with a more complex carbohydrate environment. (C) Under natural flow conditions, shear forces activate catch bonding of the bacterial lectins and thus, for inhibitors of bacterial adhesion different potencies might be found than under static conditions.

under static conditions (Fig. 3.3.1 A). However, a glycosylated microplate or any other artificial glycoarray cannot resemble the full complexity of a cell surface. Thus it is important to also test the potency of, here, FimH antagonists in cell-based assays (Fig. 3.3.1 B).[128] In addition, natural conditions of cell-cell interactions are characterized by flow and shear stress, respectively.[?] Flow is a critical parameter in bacterial adhesion as it has been described for the bacterial lectin FimH that it exerts so-called catch bonds under flow.[142] In catch bonding, FimH ligands are bound more tightly as a consequence of an allosteric process, in which FimH adopts a conformation of increased mannose affinity.[143–145] Bacterial adhesion under shear stress has been investigated since some time and recently the influence of shear stress on inhibition of bacterial adhesion attracts some interest.[144,146,147] Therefore, we commenced a study to compare the effect of FimH antagonists in an artificial environment, that is a microtiter plate-based adhesion inhibition assay, with a cell-based assay under physiological conditions (Fig. 3.3.1 B,C). As bacterial adhesion under physiological

conditions is almost never static, it is important to compare inhibition of bacterial adhesion under static conditions with testing under flow. An improved knowledge of inhibition of cell adhesion processes will eventually facilitate the development of new anti adhesive inhibitors. For our study, six α-D-mannosides with interesting properties as inhibitors of type 1 fimbriae-mediated adhesion of *E. coli* were selected (Fig. 3.3.2). Based on their IC_{50} values as inhibitors of bacterial adhesion to a mannan-coated polystyrene model surface (microplate), we were interested to measure their inhibitory potency in a more physiological environment by testing their ability to shut down *E. coli* adhesion on a monolayer of human microvascular endothelial cells, variant 1 (HMEC-1). In an important third step the static testing conditions were changed to flow conditions to investigate how the presence of shear stress affects the potency of the inhibitors to abolish *E. coli* adhesion.

3.3.3 Results and discussion

3.3.3.1 Selection and synthesis of inhibitors

Structures of the employed FimH antagonists are depicted in Fig. 3.3.2. Except for mannosides **2** they differ with regard to their aglycone. The aromatic moiety of *p*-aminophenyl mannosides **5** (PheMan) is known to improve FimH affinity based on ππ-stacking with the lectin's tyrosine residues Y48 and Y137, which are located at the entrance of the carbohydrate binding site of the lectin FimH.[148] The heptyl mannosides **3** (HeptylMan) and the octyl mannosides **4** (OctylMan) resembles examples of a series of potent alkyl mannosides.[65] In particular, octyl glycosides were shown to form glycomicelles in solution which might result in multivalency effects in inhibition of bacterial adhesion.[149] The trivalent mannosides **2** was introduced as multivalent FimH ligand. It was synthesized by glycosylation of tris(hydroxymethyl)-azidomethane **7** with benzoyl-protected thioglycoside **8**. and following deprotection with sodium methoxide. (see ESI Fig. 7.2.1).[150,151] The 6-amino-thiahexyl mannosides **6** (ThiahexMan) was recently shown to be toxic when applied in high concentrations (>12.5 mM).[152] Finally, the squaric acid derivative **1** (SAMan) completes the selection of tested mannosides. It has been reported to exceed the inhibitory potency of **1** by a factor of ~16 compared with *p*-nitrophenyl mannosides due to its affinity promoting aglycone.[105] All inhibitors, except the glycocluster **2**, were synthesized according to known procedures.[112,153–155] The obtained analytical data were in full accordance with those reported (cf. ESI Fig. 7.2.2-7.2.13).

3.3.3.2 Inhibition of *E. coli* adhesion to mannan surfaces under static conditions

All six mannosides under investigation, **1**-**6**, were tested in parallel using the well-known adhesion-inhibition assay.[77] Bacteria which express GFP where used to correlate the fluorescence intensity, recorded with a microplate reader, with the bacterial adhesion. In every assay, methyl αDmannoside (MeMan) was tested in parallel as reference inhibitor. From the obtained fluorescence data and the resulting sigmoidal inhibition curves (cf. ESI Fig. 7.2.14) we determined IC_{50} values and the corresponding RIP (relative inhibitory potency, based on MeMan). For all tested inhibitors, the RIP value was larger than 1 (Table 3.3.1). Thus, all tested inhibitors were more potent as inhibitors of type 1 fimbriae-mediated bacterial adhesion to mannosylated surfaces than the standard MeMan. The measured potencies are in accordance with reported data.[65,77,105,112,152] Anyway compared

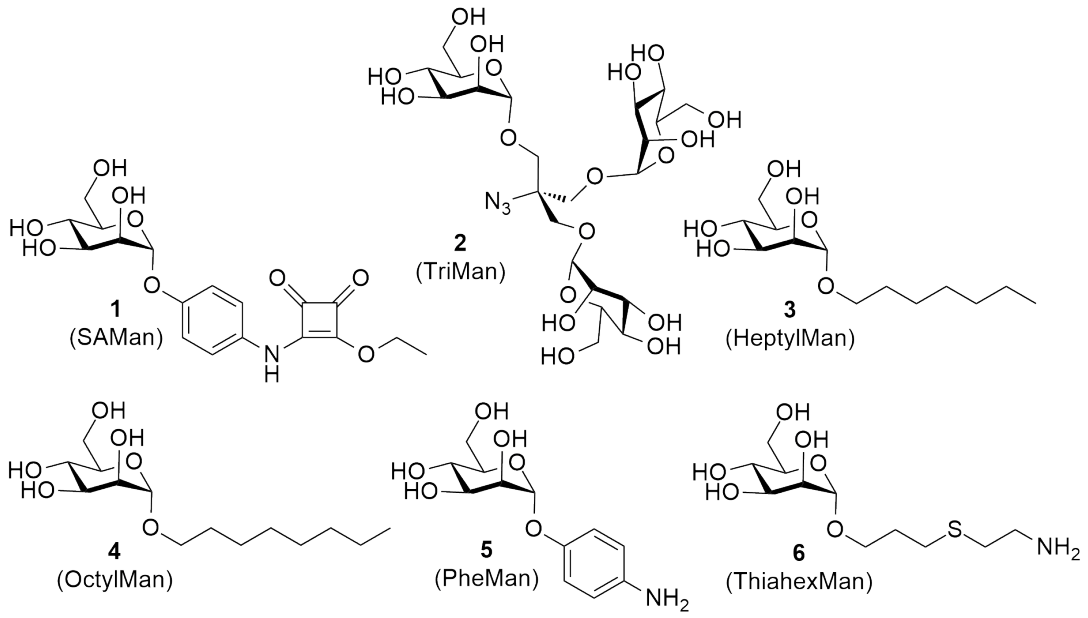

Figure 3.3.2: Structures of FimH ligands **1**-**6**, employed for inhibition of type 1 fimbriae-mediated bacterial adhesion.

with other reliable testing methods like hemagglutination assays or surface plasmon resonance, our assay showed similar inhibition properties for the investigated mannosides.[156,157] Due to the aromatic aglycone, mannosides **1** and **5** are almost 8000 and 25 times more potent inhibitors of type 1 fimbriae-mediated bacterial adhesion than MeMan. In particular the special potency of **1** has been reported and explained earlier.[112,150] ThiahexMan **6** is the weakest of the tested six.

Table 3.3.1: Inhibition of type 1 fimbriated *E. coli* adhesion to mannan-coated microtiter plates under static conditions. IC_{50} and RIP values are averaged from mean values from three independent tests. SD: standard deviation; RIP: relative inhibitory potency.

Inhibitor		IC_{50} [µM] (SD)	RIP (SD)	total inhibition [%]
1	SAMan	0.326 (0.75)	7850 (2.46)	96 % (0.025 mM)
2	TriMan	8.32 (0.71)	749 (2.3)	96 % (0.75 mM)
3	HeptMan	32.7 (1.8)	190 (2.1)	97 % (5 mM)
4	OctMan	124 (0.87)	62.7 (0.79)	98 % (5 mM)
5	*p*APMan	321 (0.23)	25.4 (0.02)	98 % (10 mM)
6	ThiahexMan	3120 (1.23)	2.1 (0.37)	84 % (100 mM)

At high concentrations this mannosides even showed an inhibitory potency weaker than MeMan. This could be explained by the fact that ThiahexMan, at high concentrations, is toxic to the bacteria cells, as published earlier.[152] Interestingly, OctMan (**4**) performs almost as good as the well-known inhibitor HeptMan **3**.[65] Mannoside **2** displays the second best potency to inhibit bacterial adhesion of *E. coli*. This is not unexpected as corresponding multivalency effects have been reported before with similar glycoclusters.[150] Here, they can be attributed the elevated local concentration of α-D-mannosyl ligands at the FimH carbohydrate binding site. Overall, the inhibitor potencies

decrease in the order of their numbering. All six mannosides could inhibit bacterial adhesion to mannan by almost 100 % at concentrations of 10 mM with the exception of ThiahexMan which leaves ~15 % of adhered bacteria unaffected even at a concentration 200 mM. Inhibition of *E. coli* adhesion to a mannan surface has shown once again, that mannosides **1-6** are antagonists of FimH.

3.3.3.3 Inhibition of *E. coli* adhesion to HMEC-1 under static conditions

Next, we went on to test the inhibitory power of mannosides **1-6** under more physiological conditions, i.e. using cells. Mannosides **1** and **5** were tested earlier as inhibitors of bacterial adhesion to the human colorectal cancer cell line HT-29 cells.[158] Here, we used immortalized human microvascular endothelial cells (HMEC-1) which are closer to the physiological situation. Hence, HMEC-1 were cultivated in 96-well plates and incubated with a suspension of *E. coli* in presence of the six inhibitors **1-6**. Each concentration for each inhibitor was tested in four independent wells. Inhibitor concentrations were chosen around the IC_{50}-value determined in the adhesion inhibition assays with mannan-coated microtiter plates. Thus **1-6** were employed 0.001-1 mM, 0.001-1 mM, 0.01-2 mM, 0.05-0.5 mM, 0.1-10 mM, and 0.5-20 mM. This time, bacterial adhesion was investigated using live cell fluorescence microscopy and the inhibitory potencies of the employed mannosides was determined by counting adhered bacteria after inhibition and washing (cf. ESI Fig. 7.2.15 for example images). As negative controls, two sets of cells were employed: on the one hand, untreated HMEC-1; and on the other hand, HMEC-1 treated with the highest DMSO concentration occurring in the experiments (2%). This was done because for live-cell experiments, inhibitor stock solutions in DMSO were prepared. For both sets of controls, bacterial adhesion was identical. We hence defined the ratio between cells treated with inhibitors and control cells as the relative adhesion. The results are shown in Fig. 3.3.3. From these results it can be seen that the relative inhibitory potencies of the six tested mannosides show similar ranking as in case of inhibition of *E. coli* adhesion to mannan. At the fourth tested concentration of 15 mM for **2**, it did not stay in solution when dissolved in cell medium, which is why the respective bar is not depicted here. As usual for experiments with live cells, error bars are relatively large, larger than those obtained with the mannan-coated polystyrene surface. Nevertheless, it can be clearly seen that the relative adhesion settles at a value of about 0.2 in all cases. This implies that adhesion is even at highest inhibitor concentrations not completely abolished. In any case, a 20 % fraction of bacteria compared to control cells remained adhering even when inhibitory mannosides much higher than the IC_{50}-values were applied. Since the residual bacterial adhesion is not dependent on the inhibitor concentration, it is reasonable to attribute this effect to interactions between bacterial surface structures the surface of HMEC-1. Considering that in the artificial environment of a microtiter plate unspecific, non-FimH dependent interactions are deliberately minimized, it is not astonishing that they play a much bigger role in the very complex setting of the cell surface.[159] Thorough washing of the samples in order to remove unspecifically adhered bacteria did not change the situation. Although we extensively rinsed the samples to remove residual bacterial adhesion, the fraction of remained bacteria stayed the same. We were interested to see if constant flow conditions would change the situation.

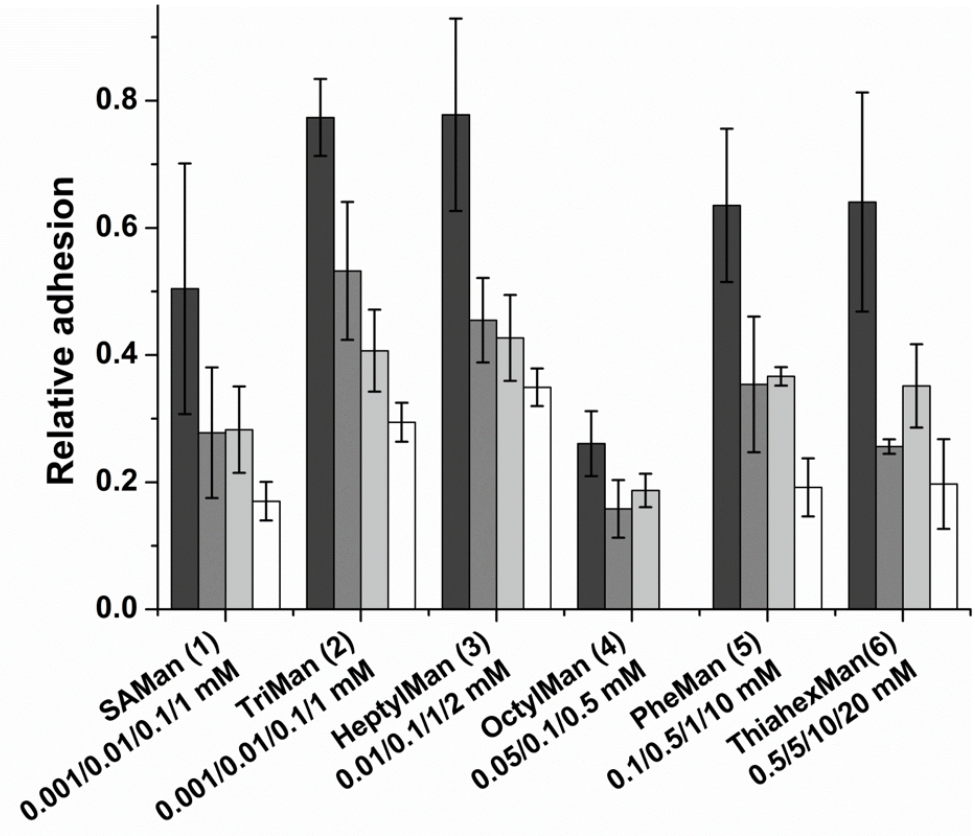

Figure 3.3.3: Adhesion of *E. coli* to HMEC-1 under static conditions. Vertical bars are colored from dark to light with rising inhibitor concentration. All six inhibitors are able to reduce adhesion of *E. coli* to HMEC-1. However, for none of the inhibitors the relative adhesion reaches zero. Relative adhesion remains constant at about 0.2. Errors are given as standard error of the mean (SEM). Each bar represents the mean of four independent wells.

3.3.3.4 Inhibition of *E. coli* adhesion to HMEC-1 under flow

Bacterial adhesion to eukaryotic cells under physiological conditions normally occurs under flow. We therefore moved to a flow-based setup where *E. coli* are streamed at a physiological shear rate of 1.5 dyn/cm^2 or 4.32 mL/min, typical for small blood vessels, continuously over HMEC-1 in presence or absence of inhibitors.[158]The shear stress created by urine flow in the urethra covers a wide range since it follows a bell-shape in normal urination. The value we use is comparable to the beginning and the end of urine flow.[160–162] Due to the characteristics of the flow setup, we had to investigate slightly higher inhibitor concentrations than under static conditions, however, the tested concentration ranges overlap in both cases. Bacterial adhesion was again followed via fluorescence microscopy. The increase of the recorded fluorescence signal, which was linear for our experiment times of several minutes, is a direct measure for the bacteria adhering over time: The more bacteria adhere, the faster the signal rises (cf. ESI Fig. 7.2.16 for example images). We evaluated this development by fitting a straight line to the obtained curves and calculated its slope, representing the adhesion rate for this condition. Analogous to the static condition, the relative

adhesion was defined as the ratio between the slope of treated cells and untreated cells. Of course, for the investigation of one inhibitor a single bacterial suspension was used where inhibitor solution was added to yield the respective concentrations in order to exclude any variations in adhesion due to different concentrations. Under these conditions, we expected unspecific adhesion to be reduced. The results are depicted in Fig. 3.3.4. The strong effect of shear stress on the effect of the inhibitors on bacterial adhesion is evident. For all investigated inhibitor concentrations, adhesion was almost completely abolished under shear stress (in this case, only the fluctuations in fluorescence is measured, which leads sometimes to a negative value for the relative adhesion: In this case, the fit curve exhibits a negative slope). This can be attributed to a significantly lower unspecific binding. Under the continuous force generated by the shear stress of 1.5 dyn/cm^2, bacteria are only able to adhere when they can form specific interactions between FimH and mannose groups on the cell surface. If they are blocked by an inhibitor, the unspecific interactions that are sufficient

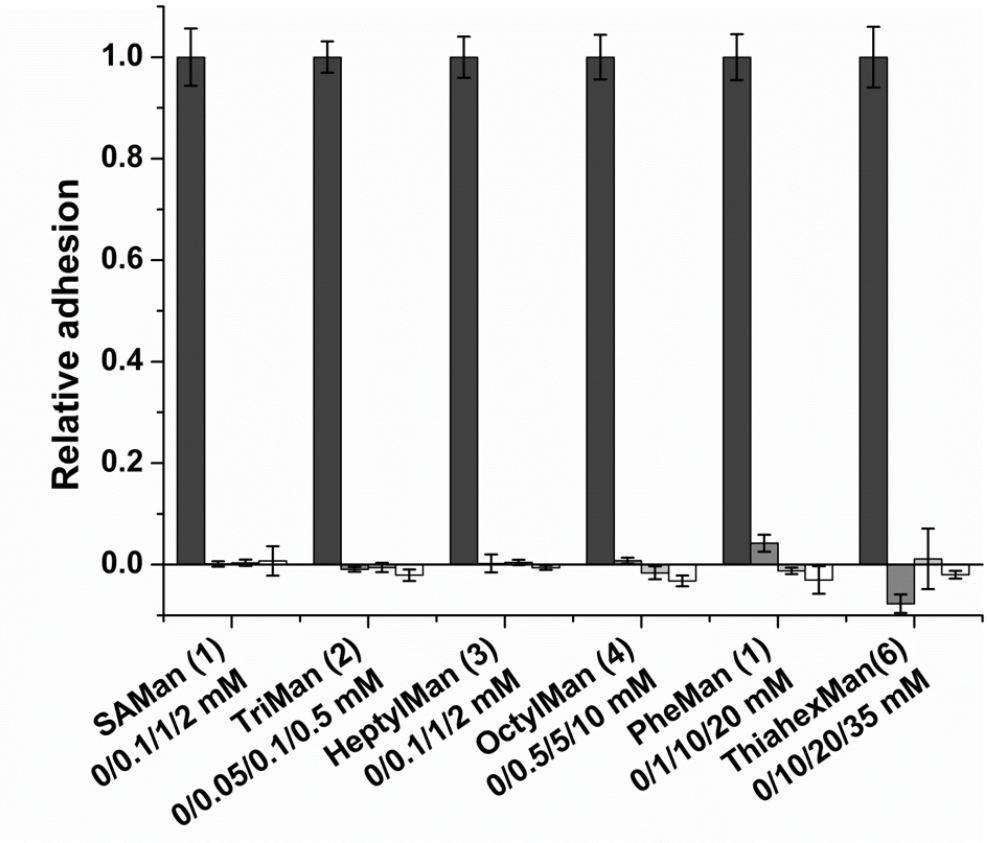

Figure 3.3.4: Adhesion of *E. coli* to HMEC-1 under flow conditions. For inhibitor concentrations that could not abolish bacterial adhesion under static conditions, adhesion was under flow close to zero and remained at this level also for the higher concentrations. It is clearly visible that the relative adhesion is close to zero for all six inhibitors already at these concentrations. Errors are given as the SEM of the fit.

to retain the bacteria on the cells under static conditions are not strong enough to prevent the bacteria from being washed away by the flow. We would like to point out that the shear stress we applied is low – in the body, much higher shear rates occur. An even stronger effect can be

expected when applying shear rates typical for e.g. arteries.[160,162] Hence, we could show that the potency of the six tested *E. coli* adhesion inhibitors is strongly affected by the presence of shear stress. Under static conditions and on a model substrate, inhibitors are able to abolish bacterial adhesion almost completely whereas they are only able to diminish adhesion on a monolayer of HMEC-1. A significant amount of *E. coli* is able to adhere to the cells even at very high inhibitor concentrations, presumably due to unspecific interactions. In contrast, the presence of shear stress strongly decreased unspecific adhesion. At inhibitor concentrations where significant adhesion was detected under static conditions, adhesion was shut down completely under flow conditions.

3.3.3.5 Conclusion

Taken together, our experiments highlight the complexity of the setting in which bacterial adhesion to human cells occurs. Considering the numerous therapeutic aspects of bacterial adhesion inhibition, our findings have consequences for the evaluation of inhibitor potencies. Meanwhile, FimH antagonists show promising effects in cystitis models,[141] but also the bacterial adhesin PapG, contributing to bacterial adhesion, has to be considered eventually.[140,163] Generally, according to our results, inhibitors of bacterial adhesion, assessed in simple microplate-based assays, should be further evaluated if they show promising inhibitory power. Their actual performance under physiological conditions is very likely to deviate from an idealized environment. To judge the in vivo-potency of anti adhesives and to elucidate the underlying adhesion mechanisms, it is crucial to investigate inhibitors of bacterial adhesion in a realistic setting. We hope that our experiments are a first step in this direction.

Acknowledgements

L.M. thanks the German National Academic Foundation and the Dr. Klaus Römer Foundation. C.B. and L.M. thank the excellence clusters Nanosystems Initiative Munich (NIM) and the Center for Integrated Protein Science Munich (CIPSM) as well as the Center for Nanoscience Munich (CeNS).

3.4 Azobenzene glycosides on glass: A tool to investigate photoswitchable cell adhesion

Instead of a natural cell surface, a photoswitchable glass surface was applied in the next part. It has been shown earlier in our group that it is possible to switch bacterial adhesion on gold surfaces.[164] Here we wanted to introduce quartz glass slides for photoswitching bacterial adhesion.

This manuscript has been prepared with the following contributors: A. Müller[a,b], C. Fessele[a,b], K. Kolbe, L. Daumlechner, T.K. Lindhorst[a]

(a) Otto Diels Institute of Organic Chemistry, Christiana Albertina University of Kiel, Otto-Hahn-Platz 3-4, 24098 Kiel, Germany, (b) This authors contributed equally to this work.

A. Müller performed the synthesis of the compounds as well as the functionalization of glass slides. A. Müller and myself performed the bacterial adhesion studies together. The manuscript was written by A. Müller and myself.

3.4.1 Abstract

We report about the fabrication of photoswitchable quartz glass surfaces to further investigate previous obtained results on photoswitching of bacterial adhesion on glyco-SAMs. The prepared slides are amenable to UV-vis absorption spectroscopy and thus switching behaviour of immobilized azobenzene glycosides could be determined. It was found that the photoresponsive glass surfaces fulfill all the requirements needed for bacterial adhesion studies such as fast and effective *E/Z* isomerization process with relatively thermally-stable *Z* form and almost no fatigue of the azobenzene switch after several switching cycles. Consequently, the prepared slides were utilized in bacterial adhesion studies and indeed irradiating of the surface resulted in switching of bacterial adhesion.

3.4.2 Introduction

Carbohydrate-lectin interactions are essential for health and disease of living organisms. Lectins are ubiquitous present in all kind of organisms.[69] In bacterial adhesion they play crucial roles in host infections and biofilm formation.[136,165] Especially uropathogenic *Escherichia coli* (UPEC) bacteria cause severe infections during first contact between lectins and the glycocalyx on the cell surface.[166] Among the best investigated lectin of UPEC is the αD-mannoside specific FimH which is located on the tip of type 1 fimbriae. These fimbriae are widely spread on the surface of *E. coli* and are well examined.[39,81] Still, due to the complexity and the disordered structure of the glycocalyx the molecular interactions between the lectin FimH and the respective carbohydrates are not yet fully understood.[18,167] Thus, it is of great interest to get a deeper insight into the biology and function of cell surface glycoconjugates and their interactions. It has been shown that not only the carbohydrate structure is crucial for specific carbohydrate-protein interactions but also spatial distribution and relative orientation of the carbohydrate ligands on the cell surface is at least equally important.[120–122,168–171] To probe carbohydrate-protein interactions and the specificity of carbohydrate ligands and their receptors, adhesive glycoarrays have become an important tool in the glycosciences.[172] Glycoarrays are all kinds of surfaces coated or functionalized with carbohydrates.

To further investigate the influence of spatial distribution and relative orientation of the carbohydrate ligand on the cell surface we have recently reported on the preparation of photoswitchable azobenzene glyco-SAMs on Au(111).[164,173] It was shown that bacterial adhesion to such surfaces was diminished by ~80 % in the *Z*-state of the SAM compared to the *E*-configured SAM. Thus, the adhesivity

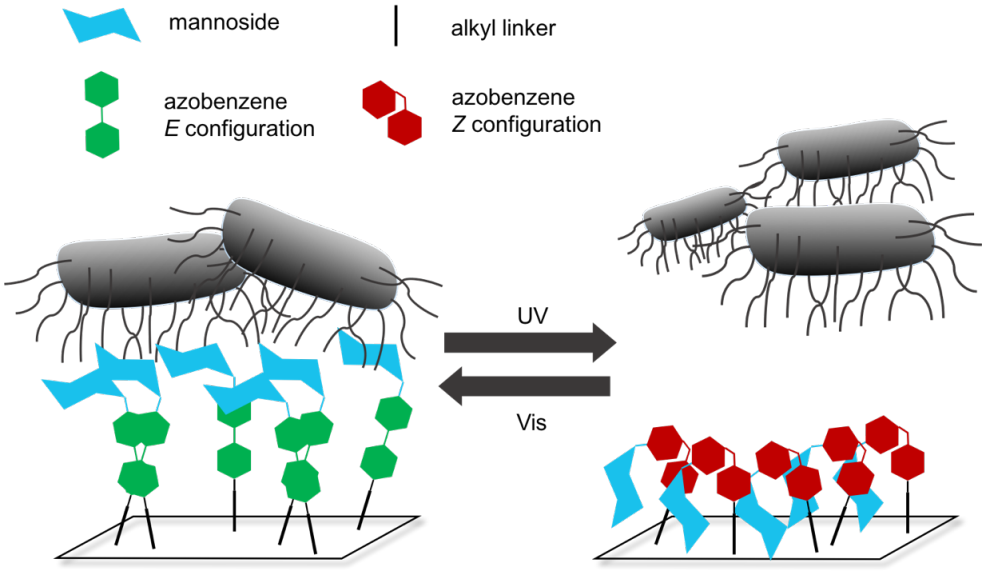

Figure 3.4.1: Switching of the azobenzene mannosides on the quartz glass surface determines bacterial adhesion.

of the fabricated surfaces indeed correlate with the configuration of the immobilized azobenzene glycoconjugate. While various azobenzene derivatives have been utilized as photoresponsive units to control numerous properties of designed surfaces,[174–178] our studies of switching carbohydrate-specific bacterial adhesion by reversible *E/Z*-isomerization of immobilized azobenzene glycosides on non-physiological surfaces or cell surface,[179] respectively is still unprecedented.

In order to investigate selective switching of the bacterial adhesivity in more detail, we describe herein the fabrication of glycosylated quartz glass surfaces (Figure 3.4.2). These have the advantage that the *E/Z* isomerization process of immobilized azobenzene derivatives can be easily monitored via UV-vis absorption spectroscopy. Besides that, fabricated quartz glass surfaces were tested in biological adhesion studies and adhesive properties of UPEC were determined upon *E/Z* isomerization. Our experimental approach is depicted in Figure 3.4.1: initially a silane functionalized azobenzene mannosides was immobilized on a quartz glass surface and in a subsequent step photochemical *E/Z* isomerization of the installed azobenzene moieties was achieved by irradiation with UV (365 nm) or blue light (440 nm), respectively. In a final step, bacterial adhesion was measured by readout of fluorescence intensity and additionally verified by fluorescence microscopy. For adhesion studies GFP-expressing type 1-fimbriated *E. coli* bacteria (PKL1162)[77] were used.

3.4.3 Preparation of photoswitchable glycosylated quartz glass surfaces

For the preparation of photoswitchable glycosylated quartz glass surfaces, a photoswitchable azobenzene derivative **6** was required (Figure 3.4.2). It incorporates in its structure an isothiocyanate-amine

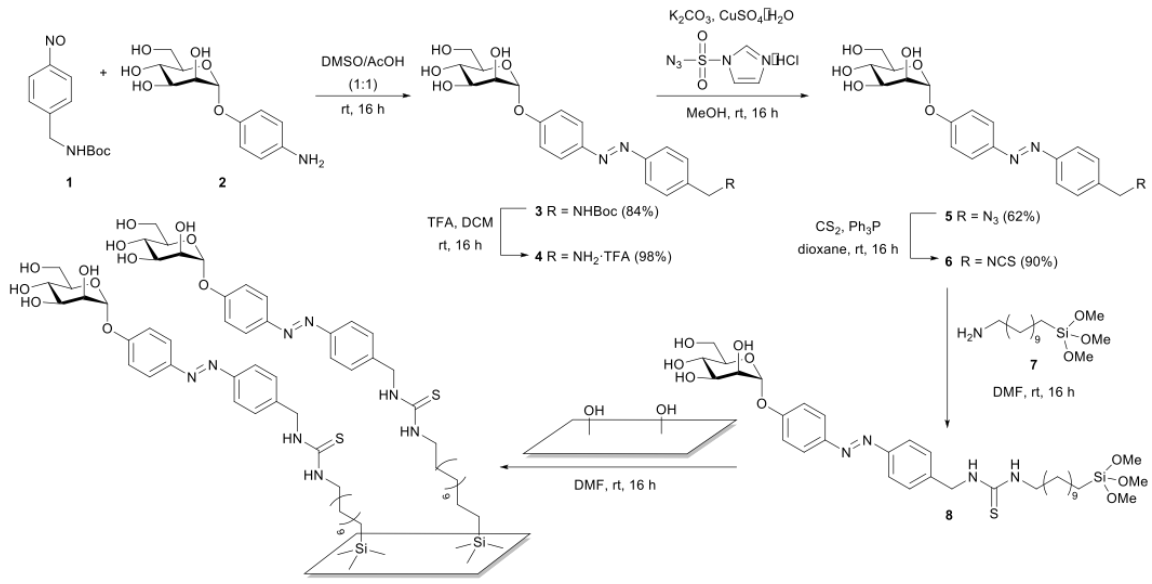

Scheme 3.4.2: Synthesis of the isothiocyanate functionalized azobenzene mannosides **6** and preparation of the photoswitchable quartz glass surface.

coupling with an amine functionalized silane **7** and a α-D-mannoside head group to effect type 1 fimbriae-mediated bacterial adhesion. Isothiocyanato azobenzene mannosides **6** was synthesized from the known *p*-aminophenyl mannoside **2**[77], which was initially subjected to a Mills condensation with the crude nitrososarene **1**[180], readily obtained from 4-(*N*-Boc-aminoethyl)aniline by reported methods,[180] in a dimethyl sulfoxide acetic acid mixture (1:1). The unsymmetrical azobenzene mannosides **3** was obtained in 84 % yield and subsequent cleavage of the Boc-protecting group with trifluoroacetic acid (TFA) furnished the tetraammonium salt **4** in nearly quantitate yield. Next, in a copper catalyzed diazotransfer reaction with the diazo donor imidazole-1-sulfonyl azide in methanol[181] the free amine **4** was converted in the corresponding azide **5** in 62 % yield. Following, under aza-Wittig reaction conditions with carbon disulfide and triphenylphosphine the desired isothiocyanate functionalized mannosides **6** was obtained in high yield. In a next step, mannosides **6** was utilized in an isothiocyanate-amine coupling reaction with silane **7** and led to the silane functionalized azobenzene derivative **8**. Silane **8** was then immediately immobilized on quartz slides, which were initially cleaned and activated with piranha solution.

Surface modification was monitored by UV-vis absorption spectroscopy. For quartz glass surfaces functionalized with silane **8**, the characteristic azobenzene absorption at 350 nm was observed and provides an evidence of successful surface functionalization. By applying sequential irradiation with UV (365 nm) and visible light (440 nm), $E \rightarrow Z$ isomerization of the immobilized mannoside **8** was achieved (Figure 3.4.3). The E/Z isomerization process was reversible over at least 3.5 switching cycles and almost no photobleaching was observed (Figure 3.4.4).

Moreover, the half-life for the Z isomer to revert to the E isomer of the immobilized azobenzene derivative **8** on the glass surface was found to be around 6 h. Furthermore, contact angle measurements were performed to provide an additional evidence of successful immobilization of azobenzene mannoside **8** on the quartz glass surface. Accordingly, the contact angle of the cleaned quartz surface

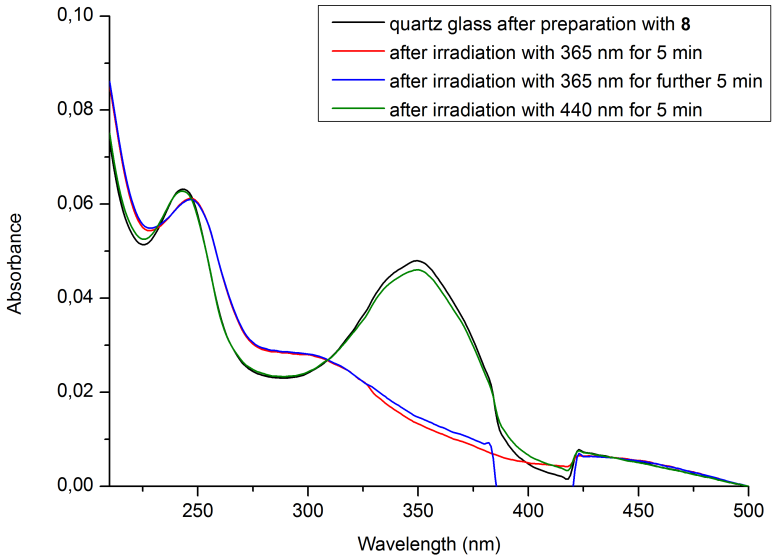

Figure 3.4.3: UV-vis spectra for monitoring the changes of absorption during the alternating irradiation at 365 nm and at 440 nm of the immobilized silane **8**.

was 27°, whereas upon functionalization with **8** the contact angle increased to 86° (cf Figure 7.3.2). Immobilized azobenzene mannosides **8** fulfills all the requirements needed for bacterial adhesion studies, i.e. a fast and effective *E/Z* isomerization process with relatively thermally-stable *Z* form and almost no fatigue of the azobenzene switch after several switching cycles.

3.4.4 Adhesion assay with GFP-expressing *E. coli* bacteria

Consequently, the functionalized glass slides were employed in bacterial adhesion studies with type 1 fimbriated *E. coli* (Figure 3.4.5).

Therefore we used a 96-well microarray format to obtain triplicate results of each slide. We exposed all glass slides in two switching cycles with 365 nm and 440 nm to receive *Z* and *E* configured mannosides on the glass surface. Afterwards all glass slides were incubated with type 1 fimbriated GFP-expressing *E. coli* bacteria. With our microarray system we were able to determine the adhered bacteria in a quantitate way. Our results show that we were able to diminish the bacterial adhesion to the glycosylated glass slides by switching from *E* to *Z* configuration significantly about 75 % which is in good accordance with earlier reported results.[164,179]

With switching the azobenzene mannosides back to *E* configuration we again obtained the start adhesion value *P* with stands for a not exposed glass slide. For further evidence of the different bacterial adhesion, fluorescence microscopy was performed. We prepared pictures of all configurations showed in Figure 7.3.4. Herein the same results than previous received could be seen. There are various bacteria adhered in *P* state and *E* configuration of the azobenzene mannosides whereas there is almost no adhesion in *Z* configuration.

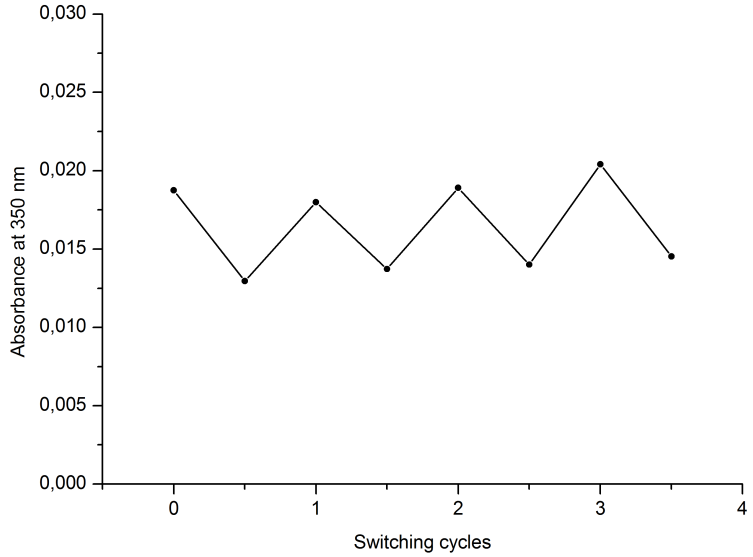

Figure 3.4.4: Multiple *E/Z* isomerization (alternating irradiation with light of λ = 365 nm (60 s, *E*→*Z*) and 435 nm (60 s, *Z*→*E*), respectively of immobilized mannoside **8**.

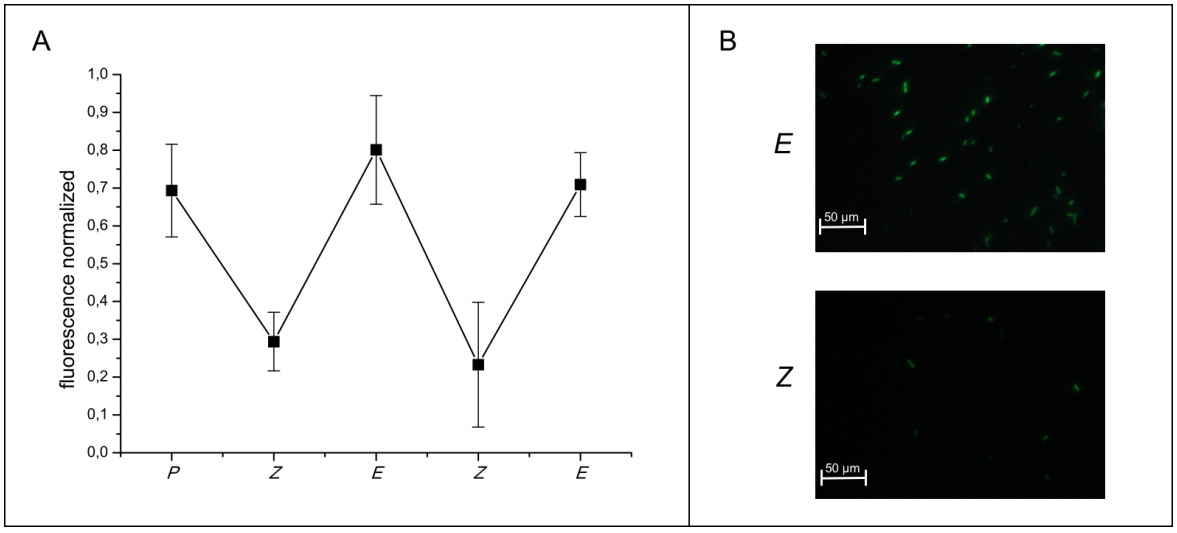

Figure 3.4.5: (A) Bacterial adhesion to *Z* and *E*-configured **8** on glass slides during two switching cycles between *E* and *Z* configuration of **8**. *P* depicts a not exposed glass slide. Error bars result from triplicate values. (B) Fluorescence microscopy of the adhered bacteria.

3.4.5 Conclusion

Conclusively, we were able to fabricate photoswitchable glycosylated quartz glass surfaces which were tested as adhesive surface for type 1 fimbriated UPEC. A straightforward synthesis leads to the NCS-functionalized azobenzene mannosides **8**, which could be successfully immobilized on a quartz glass surface. Direct UV-vis absorption spectroscopy as well as contact angle measurement demonstrated successful surface functionalization. Besides that photochromic properties of functionalized glass surfaces were determined. Due to effective *E/Z* isomerization and half-life times around 6 h the prepared surfaces could be utilized in bacterial adhesion studies. Irradiation of the quartz slides with two different wavelength (365 and 440 nm) resulted in switching of bacterial adhesion. The obtained findings are in accordance with earlier results, showing that the azobenzene configuration of the immobilized azobenzene mannoside **8** correlates with the adhesivity of the surface.

3.5 Biological effects of a small difference: glycocluster chirality

This chapter approaches different aspects of carbohydrate lectin-interactions: (i) multivalency, (ii) the influence of hetero- and homoglycoclusters, (iii) the stereochemistry of heteroglycoclusters and (iiii) the influence of flow on bacterial adhesion. In chapter 3.3 the influence of flow on bacterial adhesion to a surface was discussed. Additionally, in chapter 4.2 the influence flow on the catch bond mechanism of FimH was discussed by the implementation of atomic force microscopy. Herein a prefunctionalized glass slide was used to obtain a carbohydrate-covered surface which can be used in a flow assay system to study bacterial adhesion. The advantage of prefunctionalized glass slides is that a uniformly covered surfaces can be obtained. For further improvement of bacterial adhesion studies flow settings were combined with different glycoclusters.

This project was realized in cooperation with G. Despras, who performed the synthesis of all molecules. To realize this project the main biological part was to introduce and establish a system which is suitable for bacterial adhesion assays under flow conditions. The complete manuscript containing all synthetic details is in preparation. Herein my work, the establishment of a bacterial flow assay, and the biological results are reported and discussed.

3.5.1 Establishment of a flow assay for bacterial adhesions

3.5.1.1 Introduction

In biological surroundings flow always has a huge influence. Especially during the adhesion process of bacteria in a host system. Bacteria who want to adhere and effect the host systems need specialized mechanisms to achieve this.[37,55] Uropathogenic *E. coli* use their fimbriae with a lectin on top.[38,141] For the so called type 1 fimbriae a catch bond mechanism is reported. This mechanism takes effect under the influence of shear forces. If the lectin binds to a carbohydrate molecule under the influence of force the fimbrial tip changes its conformation. This leads to a extended fimbrial tip and thereby to a change in the carbohydrate binding domain.[79,117,158] Additional to the influence of flow on the binding process the influence of multivalency, hetero- and homoglycoclusters and the stereochemistry of the molecules are considered (Figure 3.5.1)

3.5.1.2 Results

For the establishment of a flow assay different points should be considered: (i) a surface which is easy to functionalize and suitable for detection of fluorescent *E. coli*, (ii) how to build a flow chamber with the previous functionalized surface and (iii) how to apply the flow. For the surface a previous functionalized glass slide with aldehyde silanes was chosen. This aldehyde can react with free amines on the aglycone of the compounds to obtain a covalent bond (Schiff base). The slide fitted perfectly in a microarray platform which allows an easy functionalization with less amount of synthesized compound. Furthermore, with the microarray platform a fluorescent readout can be done. A self sticking flow chamber allowed the preparation of six individual flow chambers on one glass slide (Fig 3.5.1). With luer connections syringes can be attached and by incorporating a syringe pump an equal and consistent flow can be applied. All synthesized and tested compounds

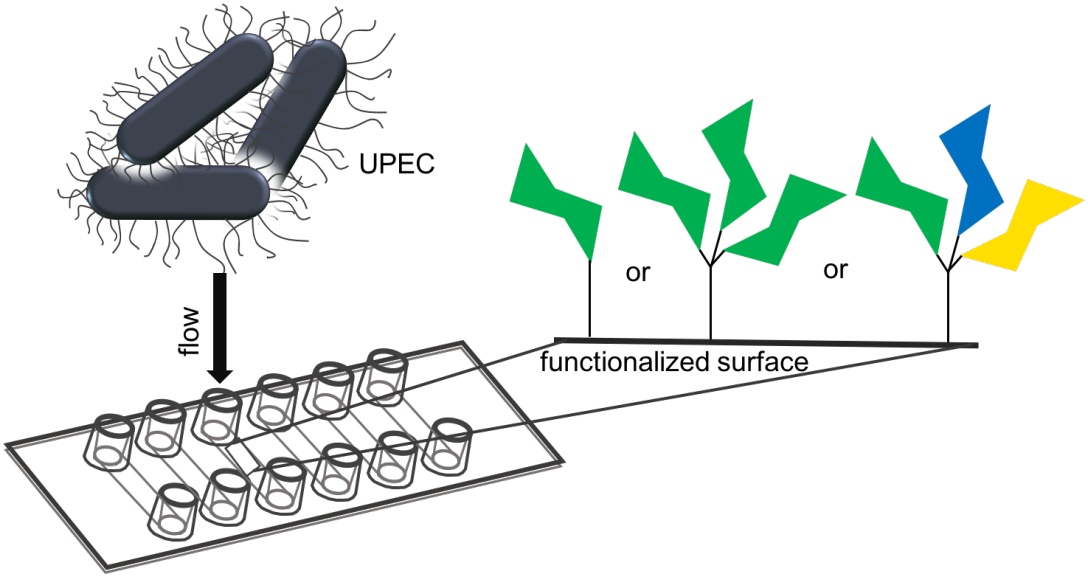

Figure 3.5.1: Schematic illustration of the flow assay with different carbohydrate functionalized surfaces (green: Man, blue: GlcNAc, yellow: Gal).

consist of a carbohydrate moiety on top, either a single or a trivalent glycoside. For the trivalent glycoside either three α-D-mannosides were used to obtain homoglycocluster **3** or one α-D-mannoside, one β-D-galactoside and one *N*-acetyl-β-D-glucosamine were used to obtain two stereoisomers of this heteroglycocluster (**1** and **2**). All different carbohydrates were prepared as monoglycosides (**4**, **5** and **6**). All compounds were connected via click reaction with a ethylene glycol linker with a free amine at the end (Fig. 3.5.2). Due to six flow chambers on one glass slide only two compounds can be compared with each other. All values were determined twice on one slide. A consistent flow of bacterial suspension was added to the prepared flow chambers and afterwards non-bound bacteria were washed away to detect only the adhered ones in the fluorescent readout. The results of the different comparison of the tested compounds are depicted in figure 3.5.3. The most surprising result shows a $\sim$ 4 times higher adhesion to stereoisomer **1** compared with stereoisomer **2** (cf. Fig. 3.5.3 A). Unfortunately until now we were not able to identify which stereoisomer dedicates to **1** and **2**. We are only aware that we have the two different stereoisomers. For the influence of heterogeneity a comparison of both stereoisomers (**1**, **2**) with the homoglycocluster **3** was made (cf. Fig. 3.5.3 B, C). Obviously the effect of heterogeneity is not as large as the effect of isomerism. The adhesion to the surface functionalized with **1** is $\sim$ 5 times higher than the adhesion to **3**. The other way round is the next result. There it can be seen that the adhesion to the stereoisomer **2**, which showed to be less adhesive than stereoisomer **1** displays also less adhesivity than homoglycocluster **3**. The multivalency influence leads to a higher bacterial adhesion to homoglycocluster **3** than to monomannoside **4** (cf. Fig. 3.5.3 D). This result is in good accordance with previous reported multivalency effects. In figure 3.5.3 E and F each of both stereoisomers (**1**, **2**) were matched with a mixture of the monoglycosides **4**, **5** and **6**. Both stereoisomers lead to a better bacterial adhesion than the surface functionalized with the mixture of monoglycosides.

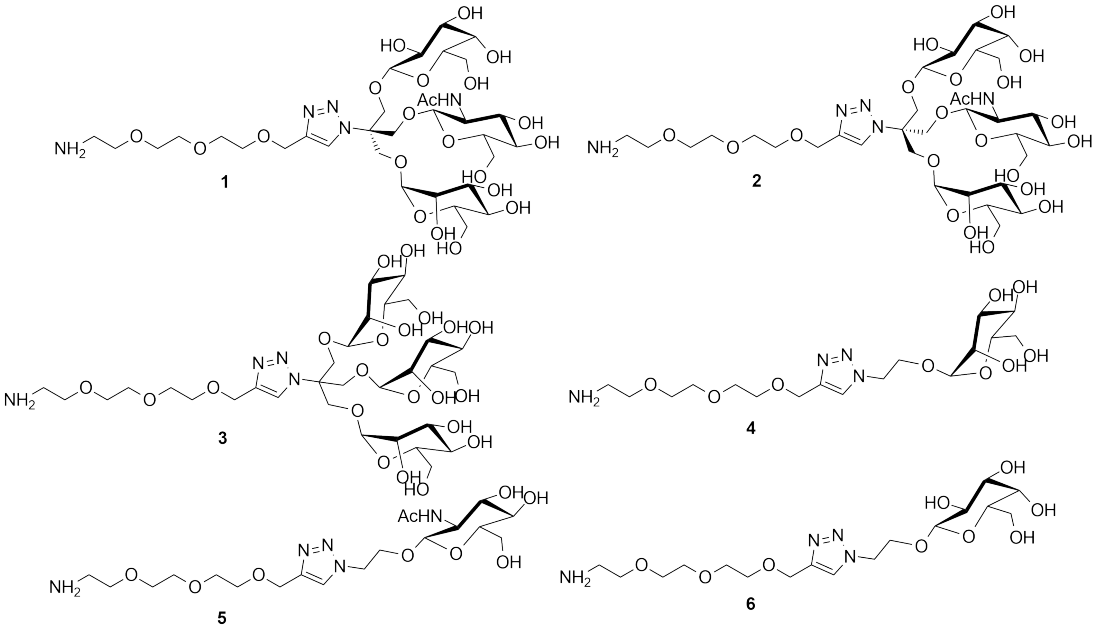

Figure 3.5.2: Overview of the different molecules used in the flow assay. The stereoisomers **1** and **2** can be interchanged. There is no exact identification possible.

The bacterial flow assay was established successfully and led to interesting new results regarding the influence of isomerism. It is necessary to follow up this new approach in bacterial adhesion studies. Up to now the multivalency effect was reported but not in comparison with heterogeneity and isomerism. Our results call for more investigations regarding this field. Therefor it is important to perform the experiments under flow since there was no difference in the adhesion properties when tested under static conditions.

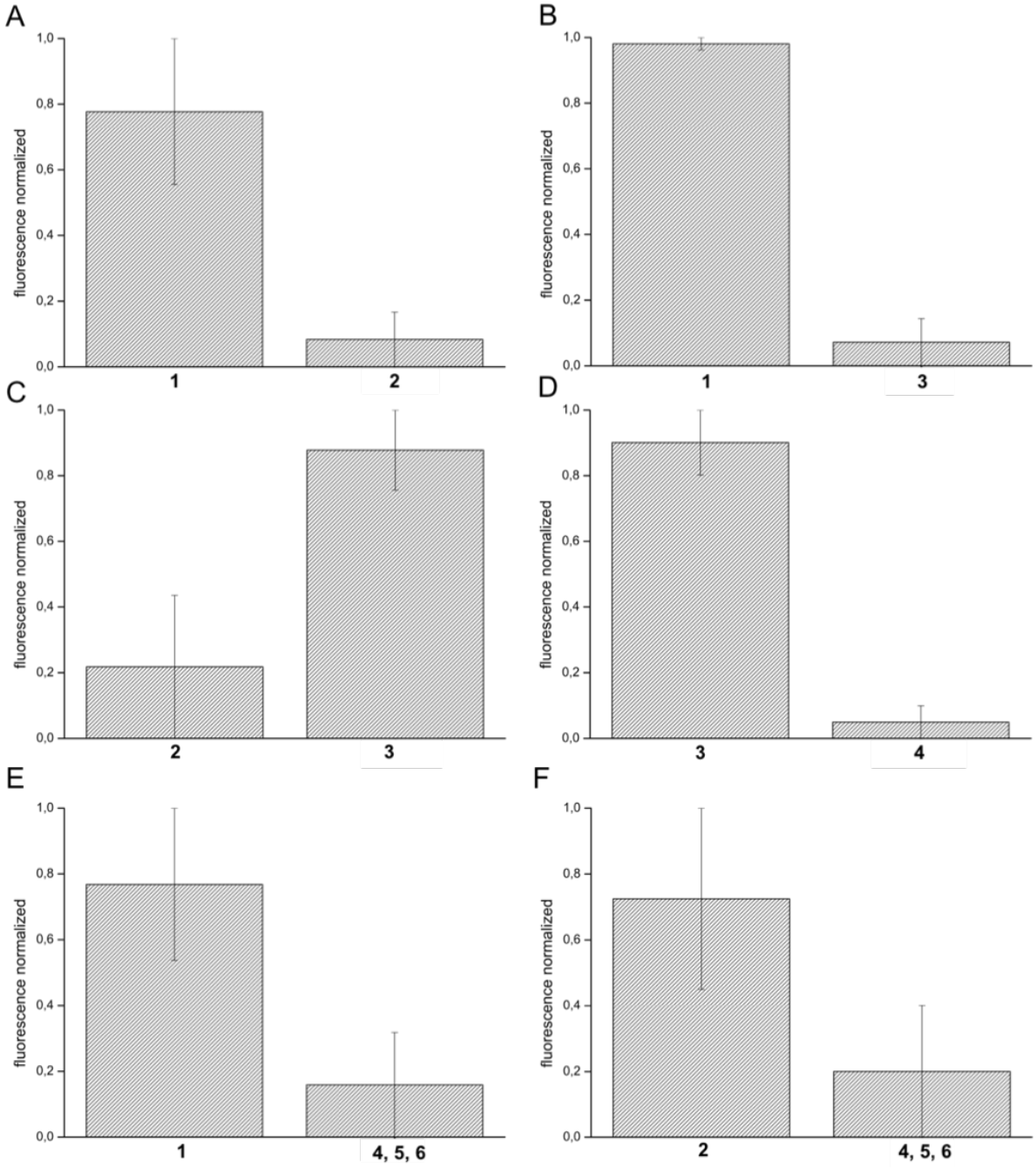

Figure 3.5.3: Results of the performed flow assay. On each glass slide two compounds were compared. (A) Adhesion difference between the two stereoisomers of the heteroglycocluster **1** and **2**. (B) Adhesion difference between heteroglycocluster **1** and the homoglycocluster **3**. (C) Adhesion difference between the heteroglycocluster **2** and the homoglycocluster **3**. (D) Adhesion difference between the homoglycocluster **3** and the monomannoside **4**. (E) Adhesion difference between the heteroglycocluster **1** and a 1:1:1 mixture of the monoglycosides **4**, **5**, and **6**. (F) Adhesion difference between the heteroglycocluster **2** and a 1:1:1 mixture of the monoglycosides **4**, **5**, and **6**. Error bars result from duplicate values on each glass slide. All experiments were replicated three times.

4 Examination of shear force influence

4.1 Introduction

4.1.1 Catch bond mechanism

Apart from influences like pH, temperature or carbohydrate structure, also mechanical shear forces can have a huge influence on carbohydrate-lectin interactions. There are two different binding events known, which can occur. Firstly, the so-called slip bond mechanism. In this case protein and carbohydrate detach faster when tensile force increases (Fig. 4.1.1).[182] In contrast, an attachment

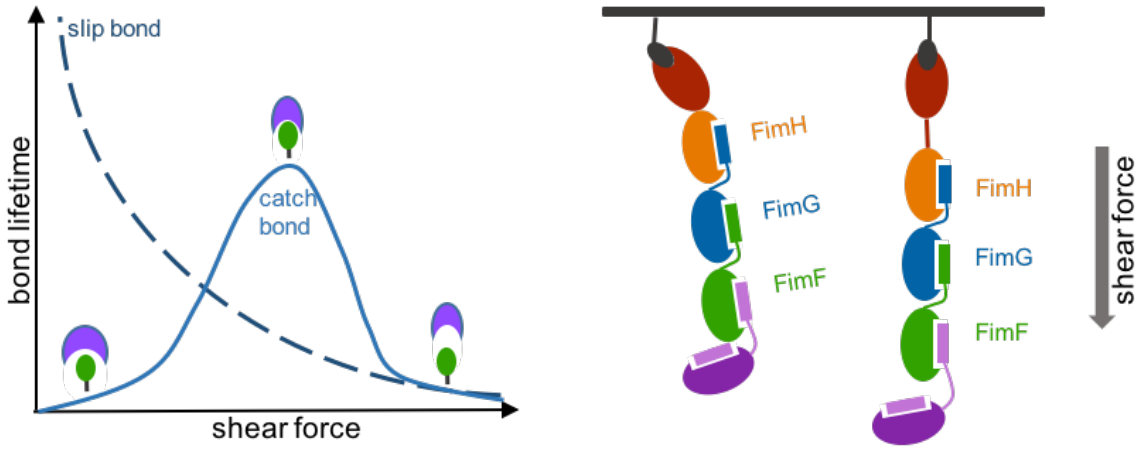

Figure 4.1.1: Schematic representation of the catch bond mechanism under the influence of shear force.

behavior called the catch bond mechanism is reported.[158] In this case the lifetime of the binding between carbohydrate and lectin increases under the influence of tensile force (Fig. 4.1.1). Catch bond mechanism can be found in various types of interactions within the vascular system like epithelial adhesion of cancer cells[183], leukocyte recruitment[184,185], or the interaction between T-cell receptors and peptide bound major histocompatibility complexes (MHC).[186,187] Furthermore it is known that the catch bond mechanism plays a major role in bacterial adhesion of uropathogenic *E. coli*.[188] Under the influence of shear force, the lectin domain of FimH is allosterically activated and due to this change, its conformation is altered from low affinity state to a high affinity structure (Fig. 4.1.1 and 4.1.2).[117,118,189] In addition to the change of the lectin domain the whole fimbrial tip conformation shifts. The main alteration occurs between the pilin and the lectin domain of the FimH. The protein elongates and the whole fimbrial tip increases in length by 22 %.[79]

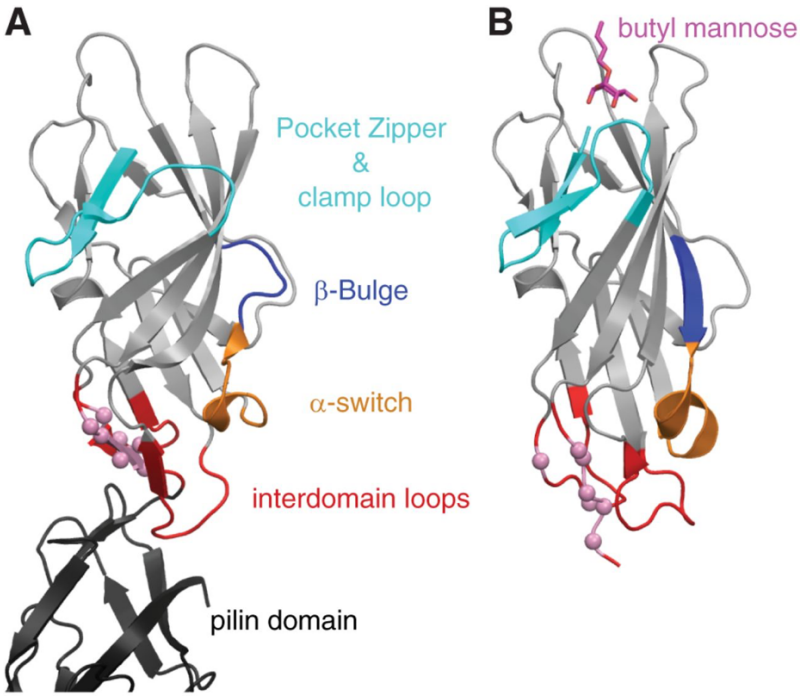

Figure 4.1.2: Crystal structures of the low affinity (PDB 3JWN) (A) and high affinity (PDB 1UWF) (B) lectin domains. Regions involved in the allosteric pathway are colored and labeled.[143]

4.1.2 Applied techniques

4.1.2.1 Atomic force microscopy

For the analysis of the catch bond mechanism different techniques can be applied. One method to analyze biological probes, which gained more interest over the last few years, is atomic force microscopy (AFM).[79,190,191] AFM measurements are based on a small probe, called cantilever, which interacts with a surface. For the detection a laser beam is installed which is reflected from the cantilever flat top to a position sensitive photodiode. Two different modes of measurement are possible. In the contact mode, the cantilever tip is placed on the surface of the probe and a three-dimensional surface measurement can be performed. A feedback loop to control the height of the tip above the surface maintains a constant laser position. Therefore, the AFM can generate an accurate topographic map of the surface features. The other way to use an AFM is to analyze single binding events. The tip approaches the surface when a repulsive force takes over and causes the tip to deflect from the surface. If a binding between the cantilever and the surface occurs single rupture events can be measured.[192,193]

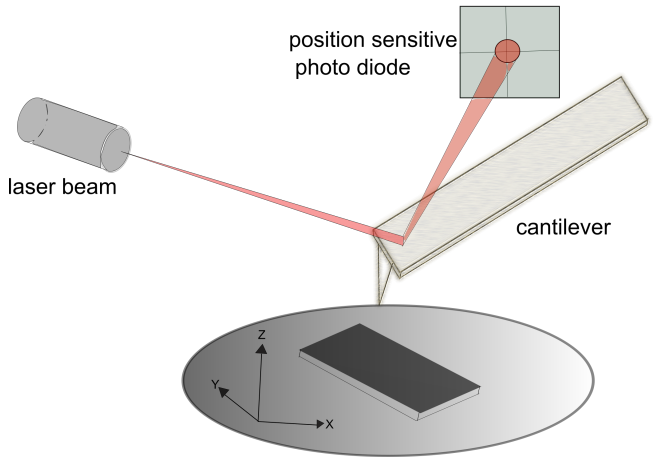

Figure 4.1.3: Schematic illustration of atomic force microscopy principle.

4.1.2.2 Molecular Modelling

Generally carbohydrate-lectin interactions are formed by relatively weak intermolecular forces like van der Waals interactions, hydrogen bonding and hydrophobic interactions. However the prediction of carbohydrate interactions are due to different factors like conformation especially of complex carbohydrate structures, linkage between single monosaccharides as well as anomeric positions. The implementation of molecular modelling enables the prediction of binding properties between carbohydrate ligands and the respective lectins. The concept allows the calculation of various carbohydrate conformations and their affinity to a receptor under the influence of water or other small molecules. Still it is just a calculation and not a measurable experiment. For that purpose other methods need to be applied. Among the best way to determine carbohydrate-lectin interactions is the combination of molecular modelling with another technique like surface plasmon resonance (SPR), isothermal titration calorimetry (ITC) or saturation transfer difference NMR (STD-NMR).

4.1.2.3 STD-NMR

Saturation transfer difference NMR is a technique to detect and characterize receptor ligand interactions in solution. In addition to the identification of interactions in solution, it also allows the determination of binding epitopes. To produce a STD-NMR spectrum the difference between on-resonance and off-resonance is measured. In an on-resonance measurement the protein sequences are irradiated with a radio frequency pulse train for a given (saturation) time. For the reference spectrum the off-resonance without protein saturation is detected. For the STD spectrum the on-resonance and off-resonance are subtracted and only the signals of the ligand which received saturation from the protein are recorded. With this technique a measurement of carbohydrate-lectin interaction is possible as well as the determination of the important functional groups of the ligand.

4.1.2.4 Chemical protein modifications

For further investigation of carbohydrate-lectin interactions, another technique which is advantageous to generate novel protein constructs is chemical protein modification. Various methods are known today either with natural or unnatural amino acid (UAA) modifications. Unnatural amino acids have the benefit that very site-selective modifications which can be addressed in a broader range than natural ones. Still there are limitations for the installation of UAAs and the available ligation chemistry which has to be performed in aqueous solution at moderate temperature and pH.[194,195] One of the best known examples for a bioorthogonal reaction is the Staudinger ligation, which involves the incorporation of an azido-modified unnatural amino acid. The azide reacts with triarylphosphine to generate a stable amide bond (Fig. 4.1.4 a).[196,197] A traceless variant of the reaction, where the amide bound is generated without residual phosphine oxide, has been reported (Fig. 4.1.4 b).[198,199] With the incorporation of azidohomoalanine and 4-azidophenylalanine the Staudinger ligation was applied for fluorogenic labelling[200], installation of photoswitches[201] and epitope mapping of G-protein-coupled receptors.[202–204] Other variants to react with unnatural

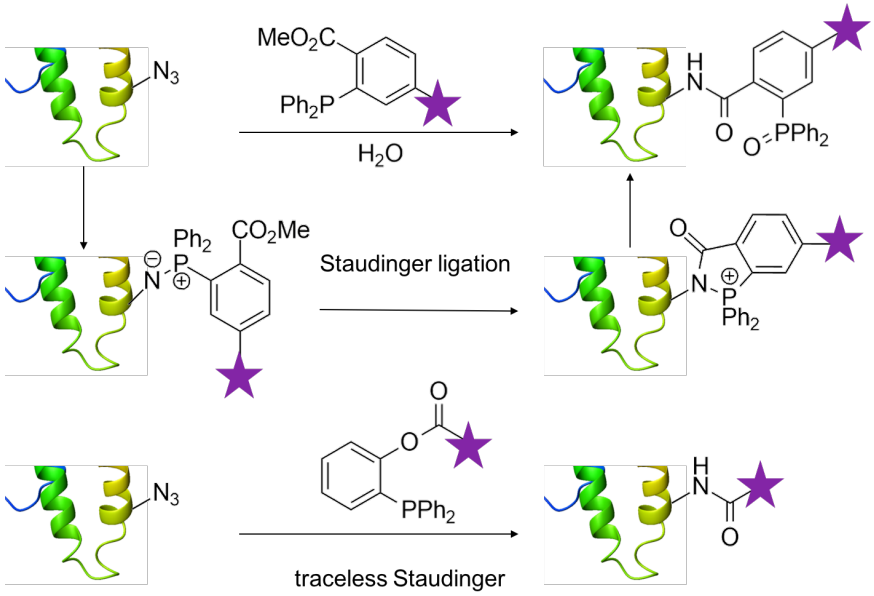

Figure 4.1.4: The Staudinger ligation. (a) A bio-orthogonal labelling of protein azides 55, (b) Traceless Staudinger variants involve loss of the phosphorus-containing prosthetic group 63.[194]

amino acids are for example Copper-promoted azide-alkyne cycloaddition (CuAAC), inverse-electron demand diels-alder (IEDDA) or 1,3-dipolar cycloaddition.[205–207]

However there is still an advantage in functionalization of natural amino acids. No specialized techniques are required. Amino acids like lysine and cysteine are nucleophilic and therefore a good choice for the introduction of a chemical functionalization. Mostly lysines are used for ligations when selectivity for the modification site is not important or multiple conjugations are important.[208,209] In contrast, if a more selective modification is of interest, cysteines display a unique reaction handle due to their low abundance (< 2 %) in proteins. With techniques like site-directed mutagenesis it is

possible to introduce a cysteine at a desired position within a protein.[210] Various selective reactions addressing the thiol group are reported. Electrophiles like halocarbonyls or maleimides are well known since a long time (Fig. 4.1.5 b,c).[211] Recently aminoethylating as well as transition metal-catalysed modifications were reported.[212] The first one resulted in thioether products which mimic lysines carrying posttranslational modifications like methylation or acteylation (Fig. 4.1.5 a).[213,214] Nevertheless, cysteine-based reactions are limited to *in vitro* applications due to free thiols in cells. Another method to functionalize cysteines is via the reaction with free thiols to form disulfide bonds (Fig. 4.1.5 e).[215]

This huge variety of possible reactions led to the utilization of cysteine as a good reaction partner for chemical modifications.

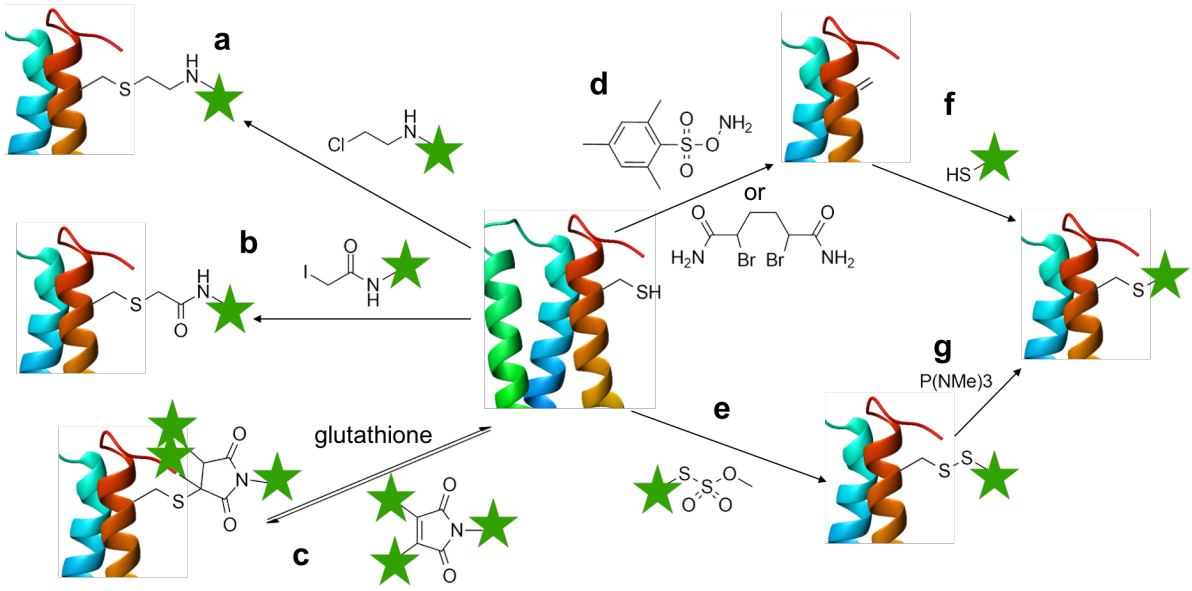

Figure 4.1.5: Chemical modifications at cysteine. (a) Aminoethylation[213] (b) iodoacetamides[211] (c) maleimides[216] (d) Dha formation[217] (e) disulfide formation[197] (f) reaction of Dha with thiols[218] and (g) desulfurization of disulfides.[194]

After all previously reported results with whole *E. coli* bacteria, the next step was now to get a deeper understanding of the adhesion process and the influence of the catch bond mechanism on carbohydrate binding. For this purpose two different projects were realized. First AFM measurements with carbohydrate-functionalized cantilevers were performed to get an impression of the strength of the binding between the lectin FimH and various carbohydrate molecules. In the second project FimH was mutated in order to attach a photoswitchable carbohydrate moiety. The interaction of the carbohydrate and the binding pocket of FimH should eventually be measured in STD-NMR experiments under the influence of shear force as exceeded by the switching moiety.

4.2 Applied tensile force determines lectin specificity

In chapter 3.3 and 3.5, the influence of flow on bacterial adhesion was discussed. In this project the main attention was drawn to the influence of flow or shear force on the binding properties of lectins and carbohydrates. In the first approach, AFM was used to measure the binding force between the lectin FimH and different ligands. Similar to chapter 3.2, we varied the used carbohydrate moieties as well as the aglycone. The synthesized molecules were used in bacterial adhesion assays, to functionalize the cantilever tips and finally in surface acoustic wave measurements.

This manuscript has been prepared with the following contributors: C. Fessele[a,c], M. Hartmann[a,c], C. Nehls[b], Th. K. Lindhorst[a], T. Gutsmann[b]

(a) Otto Diels Institute of Organic Chemistry, Christiana Albertina University of Kiel, Otto-Hahn-Platz 3-4, 24098 Kiel, Germany, (b) Research Center Borstel, Leibniz Center for Medicine and Biosciences, Division of Biophysics, Parkallee 10, 23845 Borstel, Germany, (c) These authors contributed equally to this work.

For this manuscript M. Hartmann started the project with first synthesis and AFM measurements, C. Nehls performed the SAW analysis, I expanded the project, added further synthetic compounds and further detailed AFM analysis. The manuscript was written by M. Hartmann, T.K. Lindhorst, T. Gutsmann and myself.

4.2.1 Abstract

Lectins are carbohydrate binding proteins, that are frequently reported to recognize their ligands with high specificity. We have performed binding studies with the α-D-mannoside-specific lectin FimH, abundant on the tips of bacterial type 1 fimbriae. Bacteria, e.g. *Escherichia coli*, need the fimbriae to adhere on surfaces. At static equilibrium conditions, compared to an α-D-glucoside and an α-D-galactosides, α-D-mannosides were recognized with high specificity. In contrast, in single binding force measurements utilizing atomic force microscopy we detected a loading rate dependent specificity shift. At higher loading rates higher forces were need to break the bond between FimH and the glucoside. Two effects are important: (i) FimH and the carbohydrates form catch bonds and (ii) the dissoziation rate as well as the transition state distance depends on the specific carbohydrate. The different transition state distance of the glucoside leads to the counterintuitive effect that despite a weak dissoziation rate higher force were needed to break the bond between the glucoside and FimH at high loading rates. This result was confirmed by surface acoustic wave measurements using high flow conditions. The loading rate dependent-specificity is a new aspect and have high impact on our understanding of bacterial infections.

4.2.2 Introduction

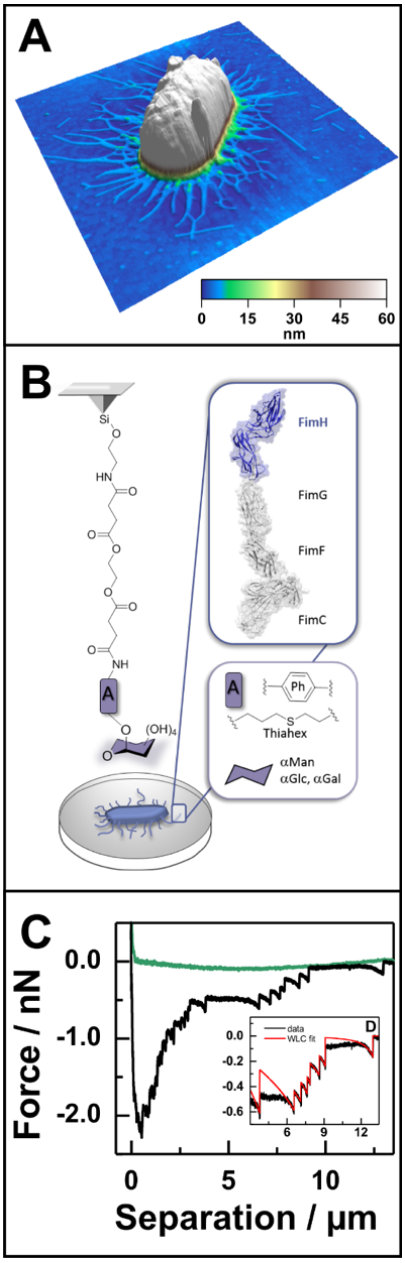

Figure 4.2.1: (A) AFM image of one *E. coli* cell on mica. (B) Schematic illustration of the force spectroscopic experiments. (C) Representative pulling curve. The tip was functionalized with PhαMan; pulling velocity 10 µm/s.

Nature has designed very specified systems to secure save flow of information. Intercellular communication for instance, requires highly specific interactions. Signal cascades are activated only upon binding of very specific motifs[219] and also cell-cell adhesion functions only under very defined conditions.[220] Lectins are a typical example for proteins with very high ligand specificity, too. Lectins by definition, bind carbohydrates without processing them and they do not have any immunological function.[37] Many pathogenic bacteria use lectins to recognize their target cell and firmly adhere to it. Such lectins that are part of adhesive organelles are referred to as adhesins.[221] In many cases, these adhesins are positioned on the distal tip of bacterial fimbriae, hair-like proteinaceous appendages on the outer bacterial surface. A well-investigated subclass of these, which is common in Enterobacteriaceae is called type 1 fimbriae. These fimbriae are composed of a helical convoluted thread of protein subunits all complementing each other with one β-sheet. The final subunit is FimH, a protein with lectin functionality.[63] For FimH, high specificity for α-D-mannosides has been reported for thirty years now,[81] a preference, which is biologically relevant, as their natural ligands are considered to be high-mannose-type oligosaccharides on eukaryotic cell.[110] Aromatic aglycone structures of the mannosides contribute to the FimH binding with strong ππ interactions to aromatic side chains in the entrance of the FimH binding site.[94] α-D-Glucosides are isomers to the respective mannosides, which are different in the configuration of one hydroxyl group. Affinity of FimH for glucosides was hardly ever reported and if so, it was found to be by 104-fold lower than the affinity to the corresponding mannosides.[94] In atomic force microscopy studies, Sokurenko, Thomas and co-workers could show,

that the FimH lectin domain constricts upon application of a tensile force.[118] This structural change tightens the carbohydrate binding site and thus increases binding force. Furthermore it could be shown, that the whole fimbrial shaft adapts to applied shear force to enhance the binding strength.[222] These changes in the quarternary structure of the Fim proteins even led to the description of FimH as mechanical force sensor.[79] Based on these interesting findings it was our aim to compare the affinity of FimH on type 1 fimbriae of *Escherichia coli* bacteria (cf. Fig. 4.2.1 B) to α-D-mannoside structures under differing dynamic conditions. The same set of measurements had to be performed with α-D-glucosides and α-D-galactosides. Furthermore, it was our aim to investigate the force of single carbohydrate-FimH interactions upon varying loading rates in single force measurements using atomic force microscopy.

4.2.3 Results and Discussion

Six different carbohydrate structures were designed to investigate different aspects of FimH binding. Two α-D-mannosides, two α-D-galactosides and two α-D-glucosides were prepared, one of which carried an aliphatic aglycone (ThiahexαMan, ThiahexαGal, ThiahexαGlc) and the other an aromatic aglycone (PhαMan, PhαGal, PhαGlc, cf Figure 7.5.1). This should allow for analyzing the effect of the aglycone properties on the strength of the FimH binding as well as the influence of the carbohydrate. With these synthetic FimH ligands, three different techniques were used to investigate the influence of pulling forces and velocity on the binding strength and specificity of FimH to the carbohydrates. In a bacterial adhesion inhibition assay[77] (BAI assay), type 1-fimbriated *E. coli* were incubated together with a respective carbohydrate in mannan-coated microtiter plates under no flow conditions in equilibrium. The relative inhibitory potency of the carbohydrates to inhibit binding of the *E. coli* bacteria to a mannan-coated surface compared to methyl α-D-mannopyranoside was measured. The results are summarized in table 4.2.1.

Table 4.2.1: Results of all performed analysis. BAI assay with the respective RIP values for all ligands.As well as k_{off} and x_B values and the critical velocity were no rupture events could be seen anymore. n.d. not detected

Ligand	Buffer	BAI Assay RIP	AFM k_{off}/ s^{-1}	AFM x_B/ nm	AFM crit. velocity
PhαGal	PBS	n.d.	$2.0 \pm 3.2\ 10^{-1}$	0.49 ± 0.09	10-50 nm/s
	PBS+DMSO	n.d.	-	-	-
PhαGlc	PBS	0.1	21.7 ± 13.5	0.22 ± 0.03	100-500 nm/s
	PBS+DMSO	0.03	4.4 ± 2.1	0.26 ± 0.02	100-500 nm/s
PhαMan	PBS	155.1	$1.4 \pm 4.3\ 10^{-4}$	0.77 ± 0.14	< 10 nm/s
	PBS+DMSO	16.6	$5.0 \pm 4.6\ 10^{-2}$	0.39 ± 0.04	10-50 nm/s
ThiahexαGal	PBS	n.d.	$6.7 \pm 17.0\ 10^{-4}$	0.69 ± 0.11	10-50 nm/s
	PBS+DMSO	n.d.	-	-	-
ThiahexαGlc	PBS	n.d.	$9.3 \pm 37.0\ 10^{-3}$	0.57 ± 0.18	10-50 nm/s
	PBS+DMSO	n.d.	-	-	-
ThiahexαMan	PBS	68.4	$3.0 \pm 4.3\ 10^{-3}$	0.84 ± 0.09	< 10 nm/s
	PBS+DMSO	6.3	$8.72 \pm 5.2\ 10^{-3}$	0.40 ± 0.2	50-100 nm/s

The strongest inhibitor was PhαMan. This finding was expected, as it is an α-D-mannoside carrying an aromatic aglycone. One order of magnitude less effective was ThiahexαMan and about four orders of magnitude less effective is PhαGlc. Whereas the other ligands, ThiahexαGlc, ThiahexαMan and PhαGal, showed no inhibition potency in the BAI assay. This result paralleled well with the earlier testings.[152] DMSO significantly reduced the inhibitory potency by a factor of 10. This has been tested only with the molecules which showed inhibition potency before. To analyze the influence of forces applied to the carbohydrate-FimH interaction, binding of *E. coli* to a carbohydrate-modified surface was measured by a surface acoustic wave (SAW) biosensor (cf Figure 7.5.3). The gold surface of the sensor was functionalized with three synthetic carbohydrates (PhαMan, PhαGlc and ThiahexαMan) showing a measurable RIP value (cf. table 4.2.1) and binding of *E. coli* to these chips under different flow stress was determined. Under all possible flow rates (minimum 12.5 µl/min) the bacteria showed the strongest binding to the PhαGlc-modified chip. Binding to PhαMan was stronger as compared to ThiahexαMan (cf Figure 7.5.3). These findings were in contrast to any adhesion assay, that has been performed with FimH so far. In both cases PhαMan showed a stronger binding to FimH than ThiahexαMan. However, in case of no force applied on the bond the mannosides bind stronger to FimH than the glucoside and in case of a relatively high force it is *vice versa*. To investigate this effect on the molecular level, single molecule force spectroscopy using atomic force microscopy was applied. This technique provides two major advantages: (i) individual bonds are examined and (ii) the possible pulling velocities span the most important range between the BAI assay, which was performed under static conditions in equilibrium and the SAW adhesion assay, in which strong shear force was applied. Therefore, *E. coli* bacteria were immobilized on a mannan-coated polystyrene petri dish and covered with PBS. Cantilevers were functionalized with the six different synthetic carbohydrates, respectively (Fig. 4.2.1 B) using a literature known protocol.[223] PEG-spacer were introduced between the cantilever surface and the carbohydrate (Fig. 4.2.1 B) to avoid artefacts and to make the ligand more easily accessible for the fimbrial adhesin. Single force curves with different pulling velocities (from 10 nm/s to 10 µm/s) were performed. A typical force curve using a PhαMan-functionalized cantilever is shown in figure 4.2.1 C. The black retrace shows a large overlap of unbinding events in the range of 5 µm apart from the surface. These events cannot be addressed to separate interactions. At the end of the curve single unbinding events can be identified. The stretching of the single fimbriae can be divided into three parts: (i) stretching of FimA leading to a plateau-region[224], (ii) stretching of the whole fimbriae which can be fitted by the worm-like-chain-(WLC-) model,[225] and (iii) breaking of the interaction between the carbohydrate and FimH. Before starting the experiments a force map of the adhered bacteria was depicted (cf Figure 4.2.2). With this orientation help the single rupture forces were determined and histograms generated (data not shown). The last and the second last rupture event showed no differences and therefore both were used for the analysis. A comparison of the three carbohydrate-functionalized cantilevers using a pulling velocity of 10 µm/s is shown in figure 4.2.3 A. The spring constants of the respective cantilever were comparable and thus also the loading rate. In figure 4.2.3 B the mean rupture forces are plotted against the loading rate. The plotted change in adhesion force upon loading for both α-D-mannosides increased with higher loading rates and both plots show the same slope. Type 1 fimbrial FimH showed a higher affinity for PhαMan than for ThiahexαMan at any loading rate. This linearity was expected and reflected the results from

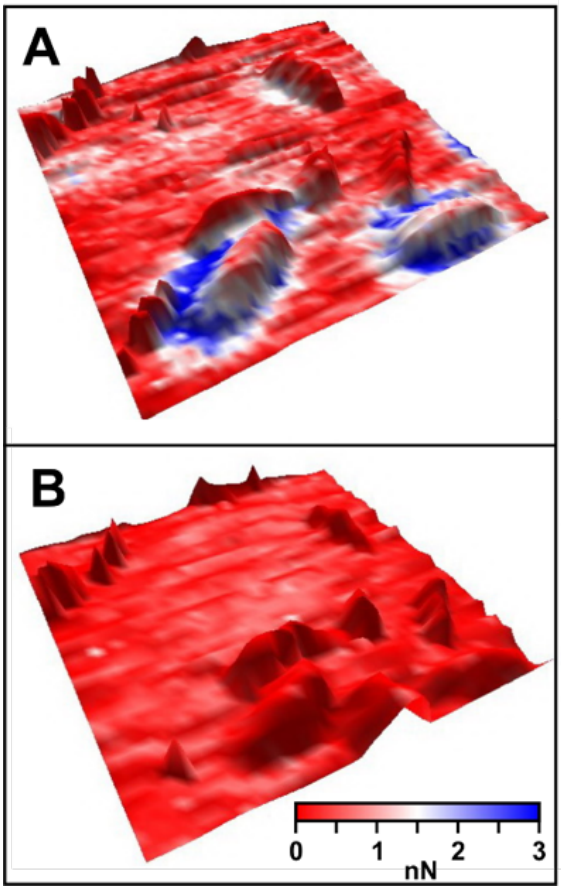

Figure 4.2.2: Force volume data of *E.coli* strain PKL1162 bacteria from spectroscopy using a PhαMan-functionalized cantilever. The height in the 3-dim images represent the height obtained from force curves and the color coding represents the adhesion force. (A) Experiment in PBS and (B) after addition of methyl α-D-mannoside (final concentration of 100 mM) at the same position. High adhesion could be observed around the bacteria with a mean distance of 1.6 µm perpendicular to the long axis of the bacteria. The binding could be blocked by methyl α-D-mannoside. The pulling velocity was 10 µm/s.

previous BAI assays. A totally different slope was detected for the α-D-glucoside, though. FimH binding to PhαGlc was even too low to be detected at low loading rates. This behavior was expected from the BAI assay under static conditions. However, Figure 4.2.3 B demonstrates that these binding properties changed dramatically at high loading rates. At 10 µm/s, FimH-PhαGlc binding was by far stronger than binding to the mannosides. At higher applied tensile force, the results from single binding force measurements supported the data obtained by the SAW adhesion assay. This loading rate-dependent change in binding specificity is a property, which has not been reported for lectins so far. The pull off force vs loading rate was fitted for each of the three carbohydrates by the Bell´s model (Fig. 4.2.3B) and the dissociation constant k_{off} and the transition state distance x_B were calculated and summarized in table 4.2.1. As a third parameter we determined the critical velocity at which no single rupture event between the fimbriae and the glucoside was observable. In case of the PhαGlc-functionalized cantilever it was between 100 nm/s and 500 nm/s. At 100 nm/s

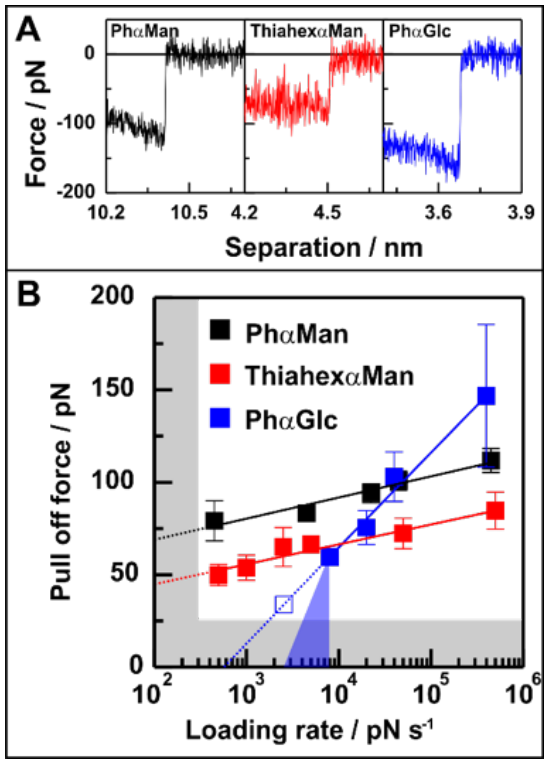

Figure 4.2.3: Comparison of the binding forces depending on the functionalization of the cantilever tip and the loading rate. The pull off forces were determined from single bond-rupture events. (A) The tips were functionalized with (a) ThiahexαMan, (b) PhαMan, and (c) PhαGlc. All three curves were taken with a pulling velocity of 10 µm/s and comparable cantilever spring constants. (B) The influence of the loading rate on the pull off forces was determined. From these curves the k_{off} and x_B were calculated. The data represent one experiment for each functionalization. The blue open square represents a fictive data point, which showed be measurable without the effect of catch-bond formation. The grey areas represent the areas in which the velocity and/or the force resolution were too low for proper data evaluation.

no rupture events could be observed in any of the pulling curves and at 500 nm/s the rupture events occurred in at least 10 % of the curves. At a velocity of 100 nm/s the signal-to-noise ratio was good enough to potentially observe single rupture events, thus, it is likely that a catch bond mechanism led to a discrepancy from the Bell model at lower loading rates. In case of ThiahexαMan and PhαMan no catch bond mechanism could be stated; however, the critical velocity can be below the resolution limit. In case of the presence of DMSO in the buffer for all three carbohydrates a critical velocity could be observed. A comparison of the dissociation rate k_{off} and the relative inhibitory potency RIP as depicted in figure 4.2.4, showed a log decrease of k_{off} with increasing RIP. The transition state distance x_B showed a sigmoidal increase with increasing RIP. Both types of values fit into these schemes in the absence as well as in the presence of DMSO. Both values k_{off} and x_B describe the profile of the energy landscape of the binding/unbinding between the three tested carbohydrates and FimH. The different values for x_B on the one hand side for PhαGlc (0.18 nm) and on the other hand side for ThiahexαMan (0.87 nm) and PhαMan (0.82 nm) explain the different pull off forces

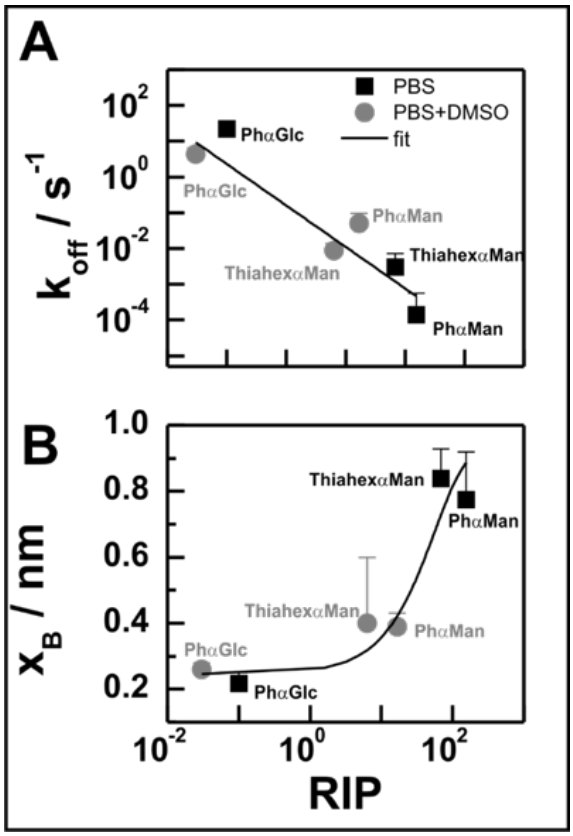

Figure 4.2.4: Correlation of data obtained from the inhibition assay and from the force spectroscopic experiments. The determined dissociation rate k_{off} decrease exponentially with increasing RIP-values (A) and the transition state distance x_B increases sigmoidal with increasing RIP-values (B).

needed at different loading rate and with that the carbohydrate-specific dependence of the binding strength on the loading rate. We have presented measurements of the binding of mannoside-specific type 1-fimbriated *E. coli* to different α-D-mannosides, α-D-galactosides and α-D-glucoside using three different methods: a bacterial adhesion inhibition assay, single force measurements using atomic force microscopy, and an SAW-biosensor adhesion assay. The three approaches complimented each other in terms of applied shear force during binding detection. The BAI assay is performed under static conditions, whereas in the SAW adhesion assay strong shear force acts on the interaction partners. In the AFM measurements, applied tensile force could be tuned in a way, that the gap between the other two techniques was filled. We could detect an increase in binding affinity with increasing shear force for all three carbohydrates. For the mannosides a FimH affinity could be increased by introduction of an aromatic aglycone structure, and effect, which had been expected based on previous experiments. The binding of FimH to a glucoside depends more strongly on the loading rate. Whereas for low loading rates no binding event could be detected, at high loading, binding forces at an average of 150 pN were detected – exceeding twice the binding strength of FimH to ThiahexαMan. To the best of our knowledge, this is the first time that a shear force-dependent shift in ligand specificity is reported for a lectin.

4.3 Protein engineering of the bacterial lectin FimH

The second approach for the examination of the catch bond mechanism is a protein engineering approach to functionalize the lectin with a switchable carbohydrate moiety and study the carbohydrate binding mechanism in STD-NMR experiments. To achieve this goal, an experimental setup was designed consisting of the following parts: (i) a modified lectin with a functionality for easy chemical ligation, (ii) a photoswitchable carbohydrate derivative to simulate shear force, (iii) STD-NMR studies to examine the interactions between the carbohydrate moiety and the lectin(Figure 4.3.1).

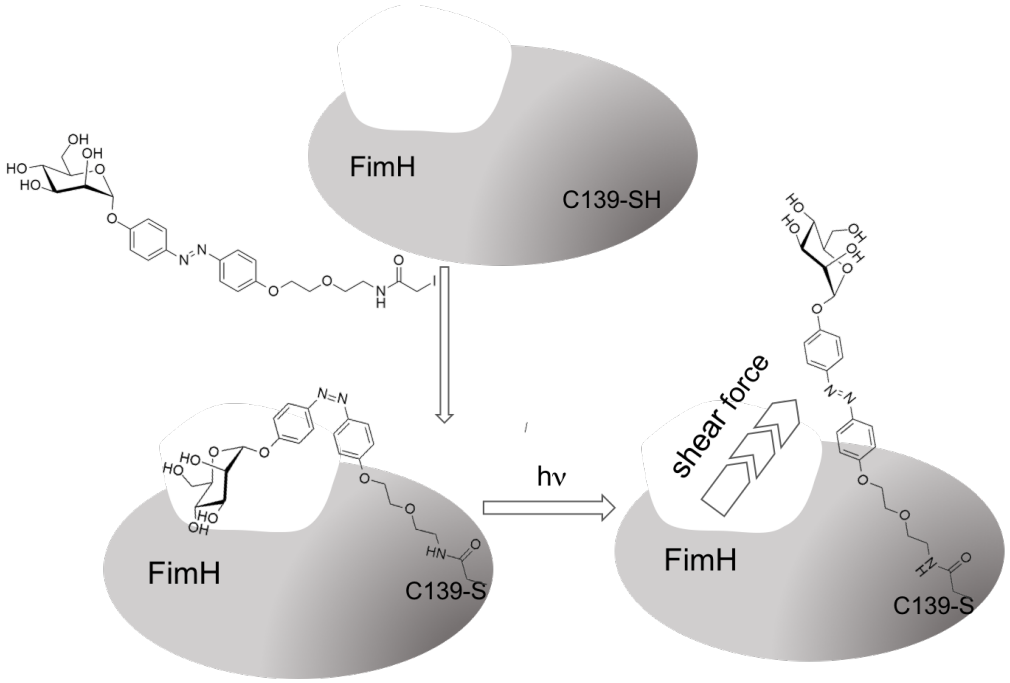

Figure 4.3.1: Schematic illustration of the designed experiment.

I started the project, performed the protein engineering part and performed a proof of principle study for functionalization of the lectin mutant. The synthesis part will be eventually further investigated in our group, as well as STD-NMR studies.

4.3.1 Results

The molecular binding mechanism between a lectin and its carbohydrate ligand is not conclusively understood. Still there are questions about the influence of the carbohydrate itself, the aglycone and additional external influences like flow. Herein we designed an experimental set up to determine all these influences for the bacterial lectin FimH which is reported to bind specific α-D-mannosides even though the results depicted in chapter 4.2 display interesting new results. Furthermore the lectin FimH is often examined regarding its catch bond mechanism. Owing these facts we wanted to further investigate the binding mechanism of FimH. Therefore we designed an experimental setup existing of different parts. The first part is the lectin itself. We planned to identify one amino acid which can be exchanged via site-directed mutagenesis with a cysteine to obtain an easily addressable

thiol group on the protein surface. For this approach we used molecular docking of the ligands with different linker lengths. After identifying the suited amino acid, a site-directed mutagenesis was performed to introduce a cysteine at this site. After successful mutagenesis, the ability to functionalize the protein was proven with a thiol-reactive maleimide dye. Related projects with a glutamate receptor led to successful switching of the azobenzene moiety and therefore regulation of the receptor.[226] These steps pave the way for this ongoing project (Fig. 4.3.1). An available benefit is the use of different dyes to obtain different fluorescent proteins without harming the carbohydrate binding pocket.

4.3.1.1 Docking studies

All docking studies were performed with Schrodinger Maestro software. Two known crystal structures of the lectin FimH were used (PDB: 1KLF, 1UWF).[64,65] Figure 4.3.2 depicts the ligands designed for this project. They consist of a α-D-mannoside connected to an azobenzene photoswitching moiety. Via an oligoethylene glycol linker of different length, the iodoacteamido function was introduced at the end of the molecule. The iodoacetamido function reacts via an alkylation with the free thiol of

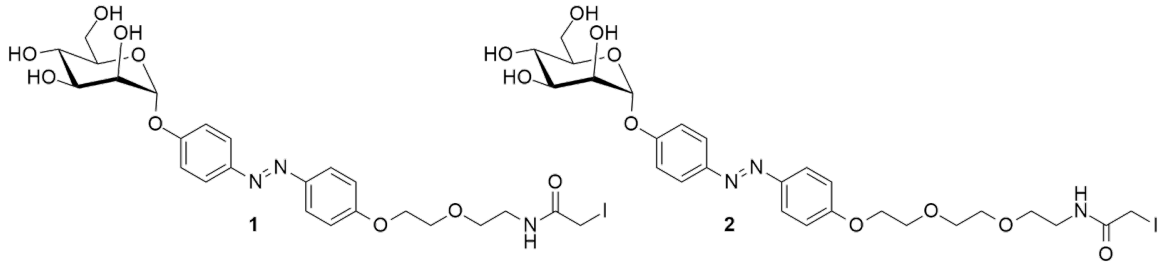

Figure 4.3.2: Designed ligands for the NMR studies with FimH.

the cysteine.[227] With these ligands, the docking analysis to identify the exchangeable amino acid were performed. The best docking results obtained with ligand **1** and **2** compared with the

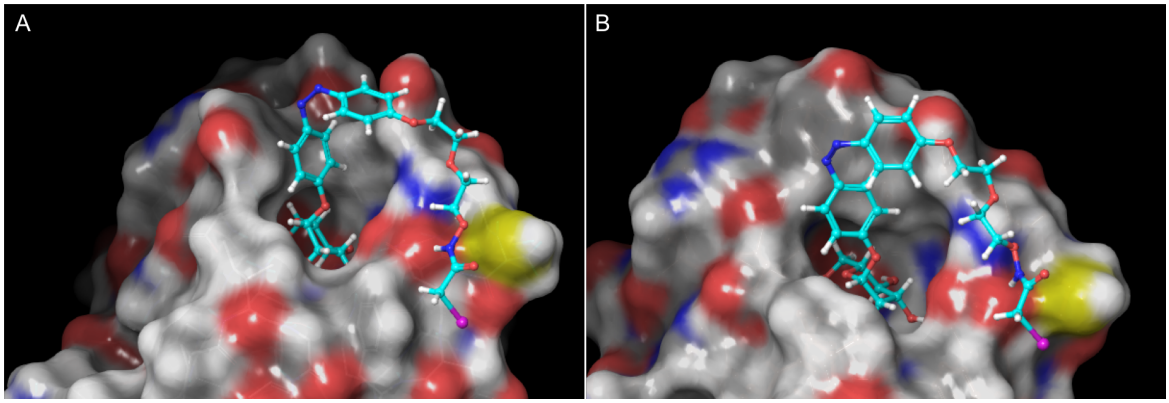

Figure 4.3.3: Results of the docking studies with the ligand **1**. (A) Docking of the *open gate* structure of FimH(1KLF[64]). (B) Docking of the *closed gate* structure of FimH (1UWF[65]). S139 was identified as exchangeable amino acid and the cysteine residue in this position is depicted in yellow.

Table 4.3.1: Docking results of both FimH structures with the ligands **1** and **2**.

	ligand **1**	ligand **2**	MeMan
1KLF (*open gate)*	-11.098	-11.098	-8.231
1UWF (*closed gate*)	-10.119	-10.535	-8.501

standard inhibitor methyl α-D-mannoside are depicted in Table 4.3.1. The more negative a docking score is, the better is the binding affinity. Both ligands displayed a better binding affinity than MeMan and the difference between the cysteine and the iodoacetamido function is less than 5 Å and therefore serine 139 is suited for the amino acid exchange. In addition asparagine 136 appears to be suitable for mutagenesis (cf Fig. 7.6.1).

4.3.1.2 Protein engineering

After the identification of S139 and N136 as suitable exchangeable amino acids, a site-directed mutagenesis[228] was performed with the plasmid pPKL241 and the new plasmid transformed in *E. coli* SG13009. The successful exchange was proven with DNA sequencing (Figure 7.6.2). The protein was expressed, purified and obtained as white lyophilisate (Fig. **4.3.4)**. For the SDS PAGE,

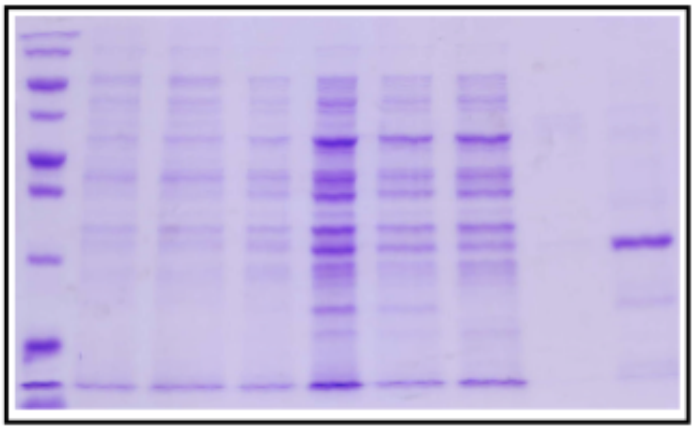

Figure 4.3.4: SDS PAGE of expression and purification of the modified FimH. Left: broad range marker, right: protein after purification.

a broad range protein ladder was used and it can be clearly seen that at the end of the purification procedure one single protein is left with ∼ 20 kDa (right band) which is the size of the truncated FimH. Subsequently the labelling of the free cysteine 139 was tested. A Texas red maleimide dye was used and an additional SDS PAGE performed (Fig. 4.3.5) The protein functionalized with fluorescent dye is visible in the coomassie stained SDS PAGE as well as under fluorescence.

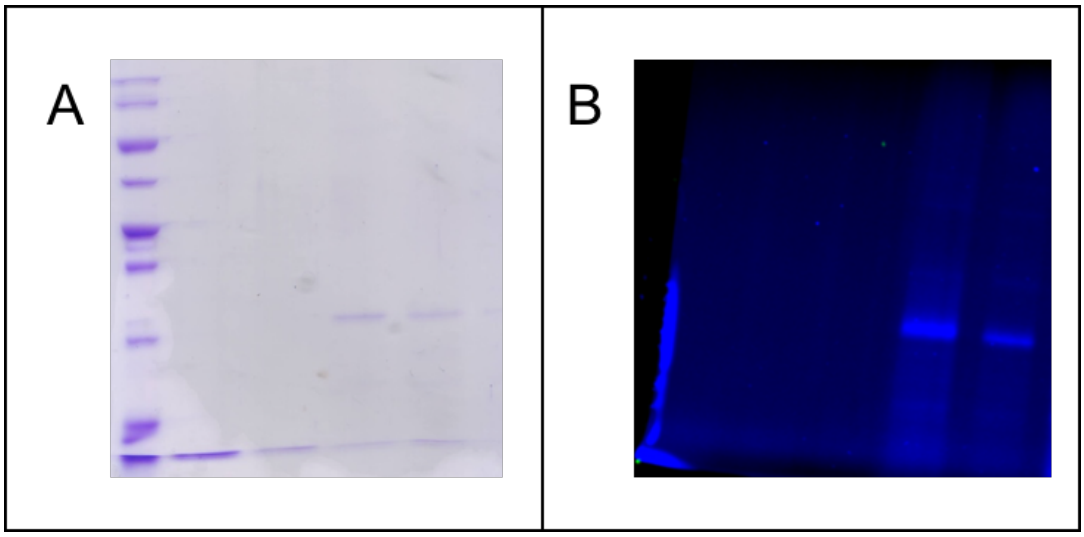

Figure 4.3.5: SDS PAGE of the modified lectin with a fluorescent dye. (A) Coomassie staining. (B) Fluorescent image.

4.3.1.3 Conclusion

Herein a method for the functionalization of the lectin FimH was shown. After the successful site-directed mutagenesis, the protein can be expressed and purified as often as needed. Different functionalities of FimH are possible based on ligation chemistry with the free thiol on the protein surface without harming the carbohydrate binding pocket or effecting compromised adhesive properties. The synthesis of the azobenzene glycosides for ligation is ongoing and when finished, the STD-NMR measurements will follow.

5 Glyconanoparticles

5.1 Introduction

Although the understanding of microbial pathogenesis was improved over the last decades, there are still remaining tasks within this field. Due to multiresistant bacterial strains, the need of new antibacterial compounds is higher than ever. Additionally to antibacterial properties, an interest in better understanding interactions between bacteria and cell surfaces as well as processes like biofilm formation exists. Within the last few years the importance of nanoparticles (NPs) increased within this research field.[229–233] Nanoparticles can be highly variable according to their production and functionalization and mainly due to their core materials. There are various representatives known, such as nanoparticles made of gold, silver, silver oxide, titanium dioxide or copper oxide.[234–236] Many of these have received great attention for their antimicrobial properties.[234,237] The next step to improve their antimicrobial activity and to decrease the cytotoxicity was the introduction of carbohydrate-covered nanoparticles (see Fig. 5.1.1).

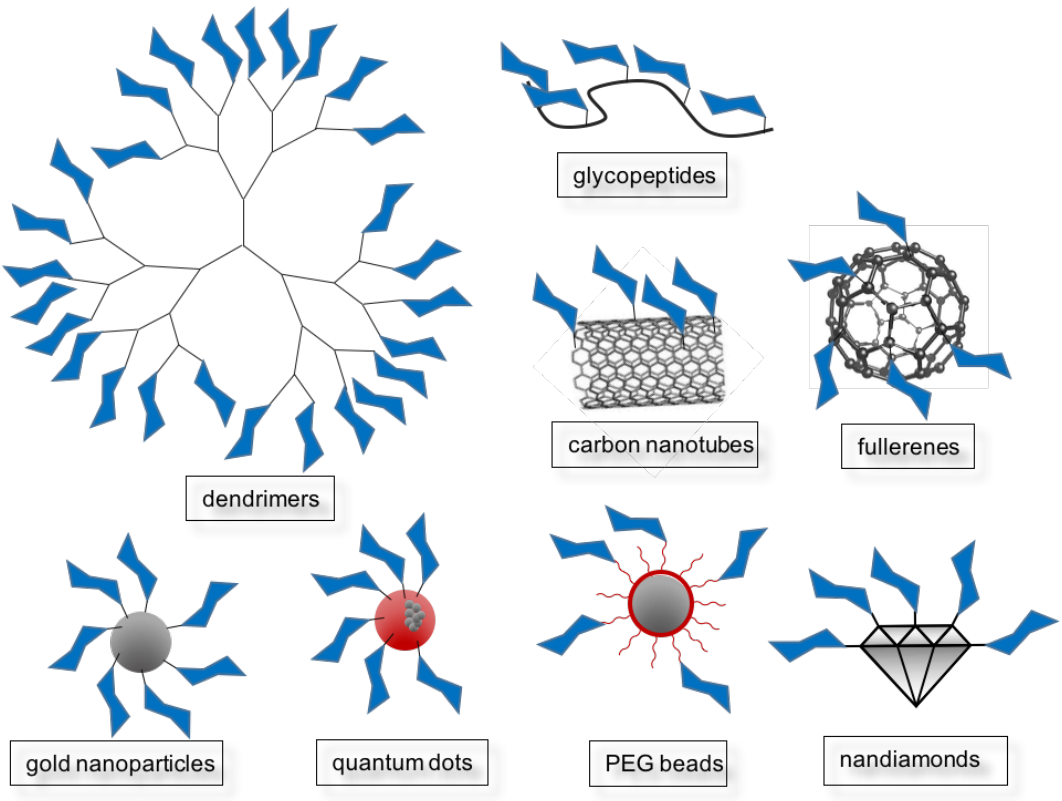

Figure 5.1.1: Schematic illustration of glyconanoparticles.

Different carbohydrate molecules can be immobilized on the nanoparticle surface. These compounds can be used as antimicrobial NPs as well as a surface for the investigation of glycan-lectin interactions, e.g. hemagglutination.[238] Various influences of the displayed carbohydrates on these interactions like multivalency, surface loading and influence of the chemical linkage can be examined. Glycosylated nanoparticles can be employed to study and evaluate carbohydrate–carbohydrate and carbohydrate–protein interactions as well as they serve as potential tools in antiadhesive therapy, for cell–cell adhesion studies and prevention of pathogen invasion.[239–242]

Gold glycoconjugates are among the first known glyconanoparticles (GNPs). They can be easily achieved through thiolated glycans and due to the physical properties of gold it is possible to detect them spectroscopically.[243] Additionally, also silver nanoparticle as well as silver-modified carbon nanotubes were reported and their biological activity documented.[244] Compared with these and other inorganic core nanoparticles like quantum dots,[245,246]which are based on Pd or Cd, there are also several nanoparticles based on organic structures. Fullerenes and carbon-based nanotubes were investigated as glycan scaffolds due to their stable surface functionalization properties as well as good solubility in aqueous solvents.[247,248] However, peptides and dendrimers can also be regarded as glyconanoparticles. Dendrimers, as well as cyclodextrins or branched oligo- and polysaccharides are well known. Like glycopeptides, they are advantageous for their solubility in aqueous solvents and their biological compatibility.[249–252]

Lately also carbohydrate-functionalized nanodiamonds have been added to the field of GNPs to investigate carbohydrate-protein interactions. Therefore, different synthetic approaches for the functionalizations have been discussed.[238,253,254] Recently, glycosylated magnetic PEG beads were introduced as a practical and fast method to detect carbohydrate-binding bacteria. Therefore, synthetic biotinylated carbohydrate ligands were immobilized on PEG beads with a streptavidin-conjugated surface. Due to the magnetic core of FeO_2, an easy extraction is possible.[255]

Here, glyconanodiamonds, which were obtained by thiourea-bridging, were reported. Their examination in bacterial adhesion as well as the introduction of Galα1,4Gal-functionalized magnetic PEG beads to determine P fimbriae-mediated bacterial adhesion is discussed. For this approach, additional molecular cloning work to obtain a GFP-expressing *E. coli,* solely equipped with P fimbriae, was performed.

5.2 Thiourea-bridged nanodiamond glycoconjugates as inhibitors of bacterial adhesion

Glyconanodiamonds have been used for the study of bacterial adhesion earlier. Within this approach a new technique to obtain glyconanodiamonds was introduced as well as the examination of their bacterial adhesion properties.

This manuscript has been published earlier: C. Fessele[a], S. Wachtler[b], V. Chandrasekaran[a], C. Stiller[b], T.K. Lindhorst[a], A. Krüger[b], *Eur. J. Org. Chem.* **2015**, *25*, 5519-5525.

(a) Otto Diels Institute of Organic Chemistry, Christiana Albertina University of Kiel, Otto-Hahn-Platz 3-4, 24098 Kiel, Germany, (b) Institute for Organic Chemistry, Würzburg University, Am Hubland, 97047 Würzburg, Germany.

DOI: 10.1002/ejoc.201500532

V. Chandrasekaran prepared the molecules, S. Wachtler and C. Stiller prepared the nanodiamond particles and I performed the biological testing and interpretation of the biological data. The manuscript was written by T.K. Lindhorst, A. Krueger and myself.

5.2.1 Abstract

The study of bacterial adhesion is of high importance for the understanding of infection processes as well as for the development of anti adhesives. Here we have investigated new nanodiamond glycoconjugates to inhibit adhesion of type 1 fimbriated *E. coli* bacteria. For conjugation of saccharides and nanodiamond, thiourea-bridging was employed, a method that has not been used before in nanodiamond derivatization. Amino-prefunctionalized diamond nanoparticles were prepared employing aromatic diazonium salts and reacted with different isothiocyanato-functionalized mannose derivatives. The resulting glyconanodiamonds were characterized and then tested in bacterial binding. They are recognized by the bacterial protein FimH according to the structure-activity relationships known for this lectin. Thus, owing to the particular properties of nanodiamond, a valuable material is introduced with the potential to control bacterial adhesion and colonization in a favorable way.

5.2.2 Introduction

Nanoparticles are versatile tools for the investigation of biological processes such as cell-cell interactions or encounter of chemicals with cells and organisms.[175,256] Several reports on the use of e.g. gold and polyethylene glycol nanoparticles for such purposes have been published.[257–259] An especially interesting material for biological and biomedical applications is nanodiamond (ND).[260,261] This material exhibits a range of very attractive properties such as low toxicity and biocompatibility, chemical inertness, small particle size and flexible surface chemistry.[262–268] Several studies on saccharide-functionalized nanodiamond particles have shown that glyconanodiamond (GND) can be used to specifically detect pathogens and to produce anti adhesive surfaces.[238,253,254] The

properties of GND are largely determined by their carbohydrate functionalization. For immobilization of biomolecules onto nanodiamond, several conjugation methods have been reported. These include conventional peptide coupling[269,270], click reaction of azides and alkynes[271–273] and benzoquinone-mediated nucleophilic displacement.[274–276] In our own work on GND preparation, we have prefunctionalized detonation ND for carbohydrate conjugation employing a Diels-Alder cycloaddition reaction.[238] However, this approach is only viable for diamond with surface-bonds, generated, i.e., by a thermal annealing. Therefore, here we introduce thiourea-bridging as alternative ligation method that allows the conjugation of saccharides (as well as other compounds) and easily accessible amino-functionalized ND (Figure 5.2.1). Thiourea-bridging leads to stable conjugates, is facile, 100 % atom efficient, and not producing any side products (which are sometimes difficult to remove). Moreover it does not require toxic reagents (such as copper salts).

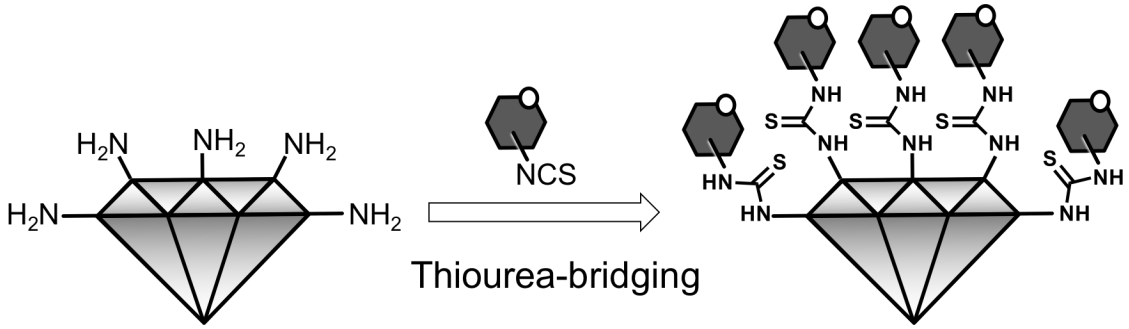

Figure 5.2.1: Thiourea-bridging is a new approach to glyconanodiamonds (GND) utilizing amino-prefunctionalized nanodiamonds (ND) and NCS-functionalized carbohydrate derivatives.

Thus, novel detonation nanodiamond glycoconjugates were obtained and were tested in bacterial binding experiments. Type 1 fimbriated *E. coli* cells were used as a relevant model system for bacterial adhesion. Type 1 fimbriae are common adhesive organelles that project from the surface of uropathogenic *E. coli* (UPEC) and are terminated by the lectin FimH.[39] FimH displays a specificity for α-D-mannosides[81], and consequently isothiocyanato-functionalized α-D-configured mannose derivatives were employed for thiourea-bridging.

5.2.3 Results and Discussion

Three different mannose derivatives were chosen to make GND by thiourea-bridging. The 6-NCS-functionalized α-D-mannoside **1**[277,278], the α-D-mannosyl isothiocyanate **2**[279], and the *p*-isothiocyanatophenyl mannosides **3**[280] (Figure 5.2.2). All three isothiocyanates are literature-known. Mannoside **1** was derived from the respective azide precursor by an aza-Wittig type reaction employing triphenyl phosphine and carbon disulfide, mannosyl isothiocyanate **2** was synthesized from the peracetylated precursor using trimethylsilyl isothiocyanate (TMS-SCN)[281], and the isothiocyanate **3** finally, was obtained from the respective *p*-aminophenyl mannosides using thiophosgene. This selection of sugar isothiocyanates is based on the perception that the bacterial lectin FimH does not allow modification of the α-D-mannosidic glycon moiety for mannosides binding. Hence, mannosides

1 is expected to serve as negative control in FimH-mediated binding assays because its 6-OH group is deleted. Mannosides **2** and **3**, on the other hand, are expected to be recognized by FimH, but with different affinity. Due to two tyrosine residues at the entrance of the FimH carbohydrate binding site, mannosides **3** is a better ligand for FimH than mannosyl isothiocyanate **2** because it forms π-π stacking interactions with the FimH 'tyrosine gate'[63]. All three NCS-functionalized mannosides derivatives were ligated to ND in their *O*-acetylated forms and deprotection was performed after ND conjugation.

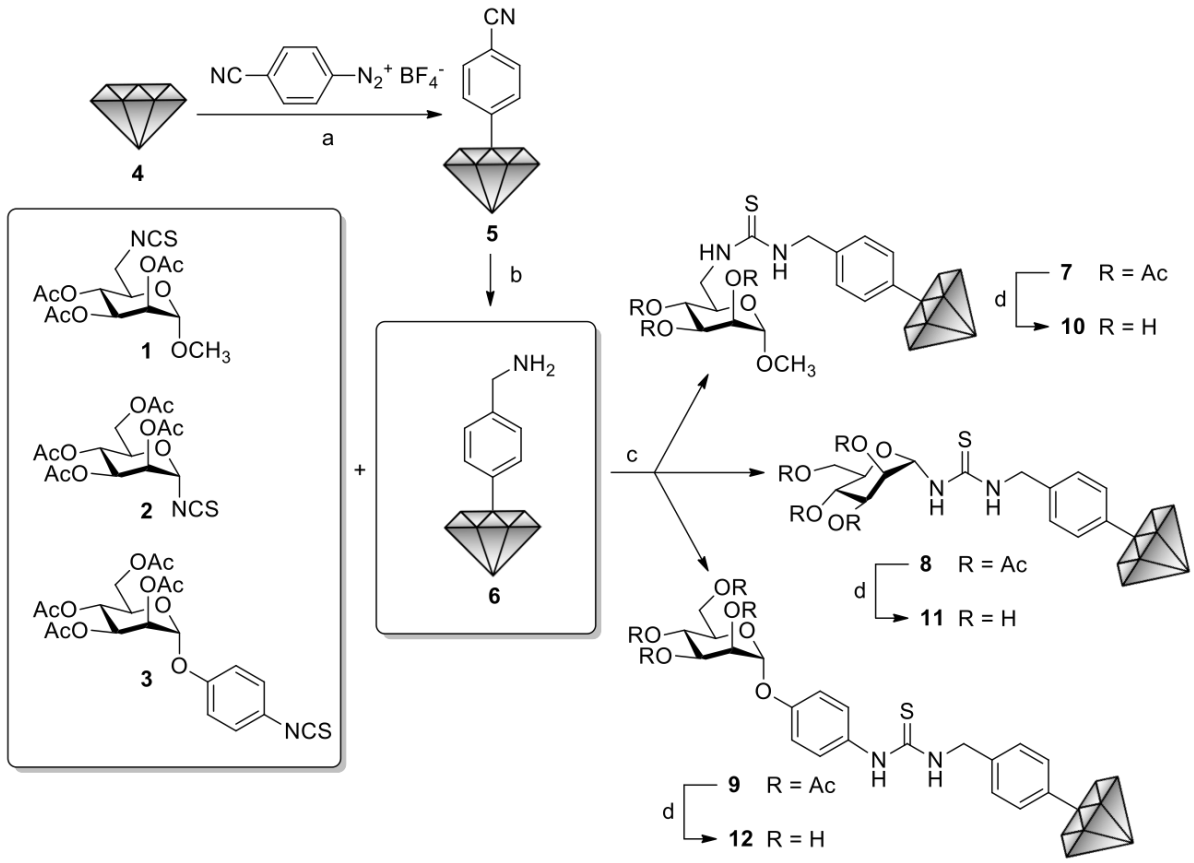

Scheme 5.2.2: Synthesis of GND **11-13** by thiourea-bridging. NCS-functionalized mannose derivatives **1-3** were synthesized according to the literature.[29-31] Reagents and conditions: a) sonification in H_2O, 75 min; b) 1 M borane-tetrahydrofurane complex, THF, 80 °C; 72 h; c) isothiocyanato-functionalized mannose derivatives **1**, **2**, or **3**, respectively, DIPEA, CH_2Cl_2, 0→RT, 90 h; d) NaOMe, MeOH, RT, 18 h.

In addition to sugar isothiocyanates, amino-functionalized nanodiamonds are needed to make thiourea-bridged GND. For this, a linker strategy was applied in this work that relies on the reaction of aromatic diazonium salts with the diamond surface (e.g. with OH groups, C=O groups as well as occasional π-bonds).[282] This technique allows a flexible and coupling reagent-free functionalization of the diamond surface with aromatic moieties. Previously, we have used this approach to enable azide-alkyne click-type conjugation of ND with bioactive compounds.[273] Here, we targeted an aminobenzyl functionalization instead of a clickable terminal group in order to

enable eventual thiourea-bridging (and also other grafting steps such as peptide coupling). Thus, for fabrication of the amino-prefunctionalized ND **7**, milled[283] detonation nanodiamond **4** was coupled with 4-cyanobenzenediazonium tetrafluoroborate **5**,[282] that was obtained by diazotization of 4-aminobenzonitrile in a Sandmeyer reaction as published previously[284] (Figure 5.2.2). This leads to nanodiamond **6** carrying 4-cyanophenyl groups. The presence of the aromatic nitrile groups is evidenced by the signals at 2229 and 864 cm^{-1} in the IR spectrum (Figure 5.2.3 A).

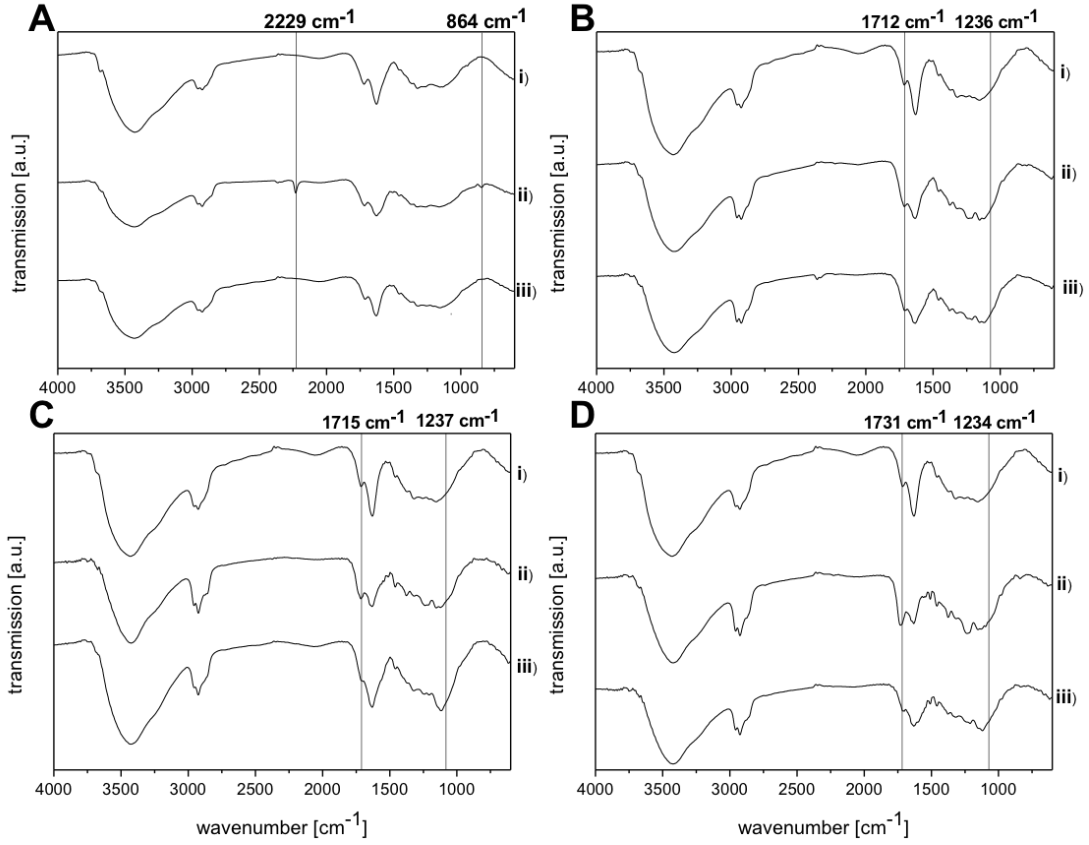

Figure 5.2.3: Comparison of infrared spectra of GND. (A) IR spectra of i) pristine ND **4**, ii) nitrile-functionalized intermediate ND **6** and iii) amino-prefunctionalized ND **7**. (B) IR spectra of i) amino-prefunctionalized ND **7**, ii) peracetylated GND **9** and iii) deprotected GND **12**. (C) IR spectra of i) amino-prefunctionalized ND **7**, ii) peracetylated GND **8** and iii) deprotected GND **11**. (D) IR spectra of i) amino-prefunctionalized ND **7**, ii) peracetylated GND **10** and iii) deprotected GND **13**. All spectra were measured using dried KBr pellets and a home-built vacuum IR cell. The lines A, B, C, D show the nitrile signal (A), the peak for 1,4-disubstituted aromatic rings (B, also present in panels b-d, but omitted for clarity), the carbonyl peak (C) and a peak for thiourea moieties.

In the next step the nitrile groups in ND **6** are reduced using a borane-tetrahydrofurane complex solution. Again, the successful conversion to **7** can be validated with IR analysis where the disappearance of the nitrile signal is seen (Figure 5.2.3A). The primary amino groups on ND **7** are also detectable by a modified Kaiser test (cf. ESI, Figure 7.7.1).[285] Next, the amino-prefunctionalized

ND **7** was conjugated with NCS-functionalized saccharides **1-3** by thiourea-bridging furnishing the acetyl-protected GNDs **8-10**. The use of peracetylated mannosides **1-3** enabled the clean coupling avoiding any concurrent reactions that would involve free saccharide OH groups. Finally, deprotection according to Zemplén[286] using sodium methanolate in methanol led to the unprotected mannose-decorated nanodiamond conjugates **11-13** (Figure 5.2.2). The IR spectra of the protected as well as unprotected GND are depicted in Figure 5.2.3 and compared to ND **7** in each case. As can be seen from Figure 5.2.3b-d the intensity of the carbonyl IR signal around 1720 cm^{-1} is reduced after the removal of the acetyl groups. The residual peak stems from the diamond surface itself as shown in the spectra i) of the starting ND **7** in Figure 5.2.3a. Due to strong water adsorption an increase in OH signal intensity cannot be observed. The presence of the thiourea moieties is evidenced by the signals around 1230 cm^{-1} both in protected and free glyconanodiamonds. The course of ND functionalization was also characterized by thermoanalytical determination of surface loading and measurement of particle sizes by dynamic light scattering (Table 5.2.1; for thermogravimetric profiles see ESI, Figure **7.7.4)**. The cyano-functionalized ND **6** has a surface loading of 0.12 mmol g^{-1}, whereas, for the amino-functionalized ND **7** it was determined as 0.09 mmol g^{-1}. The slightly reduced surface loading in **7** might be due to the possible cleavage of aromatic groups from the ND surface, that are bound through ether moieties. The surface loading for the *O*-acetylated GNDs **8-10** is in the range of 0.06-0.09 mmol g^{-1}. This proves the efficiency of thiourea-bridging. The somewhat reduced loading for the conjugation in case of mannosides **1** compared to **2** and **3** can be explained by the different orientation of the saccharide towards the surface; this might hamper the coupling process. On the other hand, the observed particle size as determined by dynamic light scattering does not change upon conjugation with the saccharide derivatives. Zeta potentials also remain in the high positive range which is an indicator for the good colloidal stabilization of the prepared GND in aqueous dispersion.

Table 5.2.1: Analytical data of glyconanodiamonds (GND).

	4	**6**	**7**	**8**	**9**	**10**	**11**	**12**	**13**
Surface loading value [mmol g^{-1}][a]	[b]	0.12	0.09	0.06	0.08	0.09	0.07	0.06	0.09
Particle size value [nm][c]	7	57	34	41	31	44	44	61	44
Zeta potential (pH = 7) [mV]	53.0	36.1	47.7	49.0	49.8	46.8	44.5	46.8	41.6

[a]determined by thermoanalysis; [b]initial material, no surface loading present; [c]the value represents 50 % of the volume distribution measured by DLS, i.e. 50 % of the sample volume consists of particles with a size smaller than the reported value.

For comparison of the prepared GND in their interaction with type 1 fimbriated *E. coli*, a standard microtiterplate based assay is not suited.[77] This is, because the GND particles form various aggregates with the bacterial cells that do not allow a quantitative analysis. Thus, a sandwich-type assay was used that is based on a method previously introduced by HARTMANN et.al.[238] In this assay, two bacterial strains are employed to allow testing of bacterial binding to a GND monolayer. The testing procedure starts with a mannan-coated polystyrene surface (Figure 5.2.4 A) and mannose-specific binding of the non-fluorescent *E. coli* strain PKL4. This forms the so-called "capture layer" to assemble a GND layer in the next step (Figure 5.2.4 B). Thus, the bottom face of the investigated GND is blocked and the remaining upper side of the particles ready to

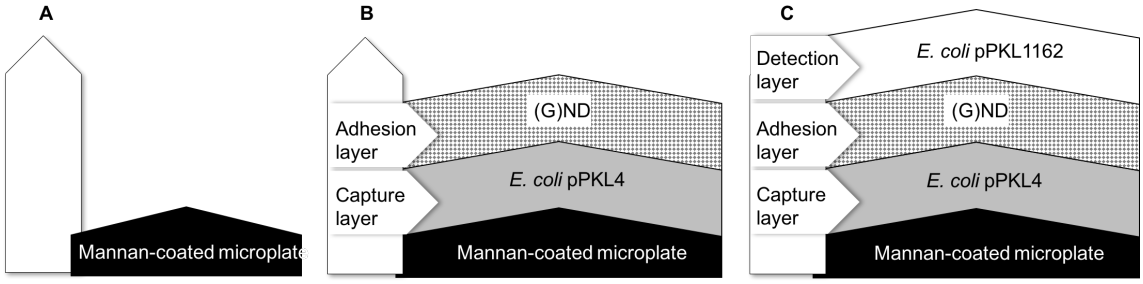

Figure 5.2.4: A sandwich assay involving two mannose-specific bacterial strains is necessary to measure bacterial binding to mannosylated ND. (A) Black polystyrene microtiter plates are coated with the polysaccharide mannan to bind non fluorescent *E. coli* PKL4; (B) *E. coli* PKL4 form the so-called 'capture layer' for GND, and GND in turn form the actual adhesion layer for the specific binding experiment; (C) bacterial binding to GND can then be determined using fluorescent *E. coli* PKL1162 and thus measured fluorescence intensity correlates with the adhesiveness of the respective saccharide-conjugated ND.

function as "adhesion layer" for binding of a second bacterial strain PKL1162, that is fluorescent (Figure 5.2.4 C). This way, the individual adhesiveness of the tested GND particles can be directly correlated with the fluorescence intensity that is read-out. GND particles were applied in serial dilutions and compared to ND **7** without sugar conjugation, which was tested on the same microplate. The resulting adhesion curves are depicted in Figure 5.2.5, where the given concentrations are calculated based on the sugar loading of the tested particles (rather than on their weight). It can be seen that all three prepared GND, **11**, **12**, and **13**, mediate binding to type 1 fimbriated *E. coli*. The (*p*-thioureidophenyl α-D-mannoside)-conjugated GND **13** is clearly more adhesive than the (α-D-mannosyl-thioureido)-conjugated ND **12** (Figure 5.2.5 B and C). This finding was expected with respect to the known FimH affinities of the corresponding sugar derivatives **2** and **3**. However, also GND **11** shows some adhesiveness (Figure 5.2.5 A) in spite of the fact, that mannosides **1** was conjugated via the 6-position of the sugar ring, which would be required for successful recognition by FimH.[81] Thus, this result has to be attributed to unspecific binding. Indeed, when GND **11** and GND **12** were assayed on the same microplate and compared, it was seen that GND **12** exhibits clearly stronger binding to type 1 fimbriated bacteria than GND **11**, as expected (cf. Figure 7.7.3). Nevertheless, also the pristine ND **4** as well as the 4-aminophenyl pre-functionalized nanodiamond **7** mediate bacterial binding, ND **7** being more adhesive than ND **4** (cf. Figure 7.7.2). Such unspecific adhesion is due to hydrophilic interactions of ND and bacterial cells and has been observed before.[238] At the bottom line, the sandwich assay with thiourea-bridged GND has confirmed mannose-specific binding of this new material to bacterial cells. The observed adhesiveness of the prepared GND corresponds to the expected affinities of mannose derivatives **1**-**3** for the bacterial lectin FimH that mediates binding.[81]

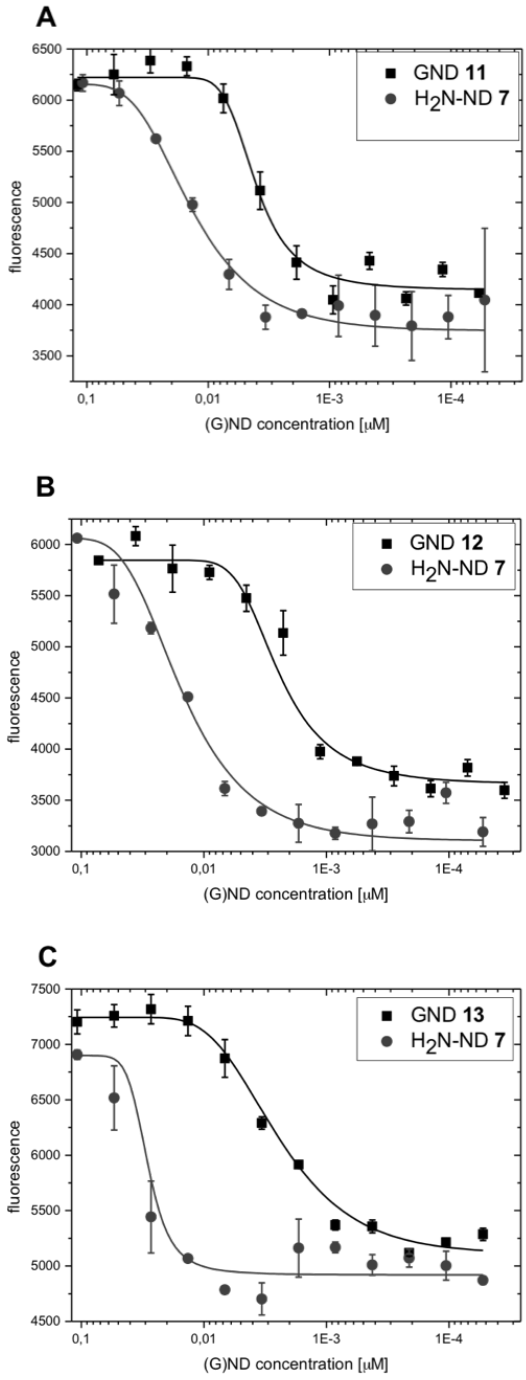

Figure 5.2.5: Bacterial adhesion to (glyco)nanodiamonds **11**-**13** as measured with the described sandwich assay (cf. Figure 5.2.4). Given concentrations are based on surface loading. (A) Bacterial adhesion to (methyl α-D-mannoside-6-thioureido)-conjugated ND **11** in comparison to amino-prefunctionalized ND **7**; (B) bacterial adhesion to (α-D-mannosyl-thioureido)-conjugated ND **12** in comparison to amino-prefunctionalized ND **7**; (C) bacterial adhesion to (*p*-thioureidophenyl α-D-mannoside)-conjugated ND **13** in comparison to amino-prefunctionalized ND **7**. Error bars are standard deviations from triplicate values on one plate.

5.2.4 Conclusion

In summary, we have shown a novel conjugation method for the grafting of saccharides or other biologically relevant molecules onto nanodiamond without the use of toxic reagents or the formation of problematic side products. This thiourea-bridging enables the efficient immobilization of saccharides onto amino-prefunctionalized nanodiamond. The resulting saccharide-nanodiamond conjugates show selective binding of type 1 fimbriated *E. coli*. The observed selectivities and efficiencies of bacterial binding prove that the immobilization of the saccharides onto the diamond surface does not hamper their proper interaction with bacterial cells. Thus, thiourea-bridging will be employed for more extensive studies in cell adhesion and the properties of thiourea-bridged GND will be compared to GND prepared by us previously.[268]

Acknowledgements

S.W., C.S. and A. K. gratefully acknowledge the financial support by the European Commission and the BMBF (contract NanoDiaMed grant no. 13N12255 in EuroNanoMed). C.F., V.C. and T. K. L. are grateful for financial support by the DFG (SFB 677).

5.3 Investigation of P fimbriae mediated bacterial adhesion

The following project is dedicated to the interaction of P fimbriated *E. coli* (cf. chapter 3.1) with the lectin PapG, located at the tips of the fimbriae and synthetic Galα1,4Gal-disaccharides, immobilized on magnetic PEG beads. This project comprises four parts (i) synthesis of the molecules, (ii) functionalization of magnetic PEG beads, (iii) cloning experiments to obtain GFP-expressing, P fimbriated *E. coli* and (iv) analysis of the bacterial adhesion. I performed all work of this project and wrote the manuscript.

5.3.1 Abstract

The inhibition of uropathogenic *E. coli* (UPEC) adhesion is still of high importance to understand molecular mechanisms of the infection process. Here we report the investigation of a new quick and easy assay system to determine P fimbriae-mediated bacterial adhesion. For this, PEG beads were used. With a magnetic core they display certain advantages like long storage possibilities and simple handling. With only one synthetic step they can be addressed with amino-functionalized carbohydrate derivatives. Additionally a new plasmid to obtain only P fimbriated and GFP-expressing *E. coli* bacteria, which can be detected via fluorescence readout, was designed. The adhesion assay showed that the bacteria bind to the glycosylated beads. With low inhibitor concentrations the bacterial adhesion could be diminished.

5.3.2 Introduction

Uropathogenic bacteria still cause severe health problems. Urinary tract infections are among the most common infectious disease in women.[287] Therefore it is crucial to understand the molecular mechanism of this infection process. The most common bacteria here are uropathogenic *E. coli* (UPEC).[137,288] For this species two different types of hair-like protein structures, located on the outer membrane of bacterial cells, are important to generate the first contact between the bacteria and the host. These are type 1 and P fimbriae.[39] Both are very similar in their structure but they differ in their carbohydrate specificity due to different lectins. In case of type 1 fimbriae the lectin is called FimH and binds specifically α-D-mannosides.[108,289] The interactions between FimH and various carbohydrates are well examined and reported.[143,148] An assay is available for an easy investigation of the interaction between live bacteria and different carbohydrates.[77] The lectin PapG which belongs to the P fimbriae shows a specificity for carbohydrates of the globosides series.[66,290] Compared with type 1 fimbriae, the study of the interactions of P fimbriated *E. coli* is not as quick and easy achievable. So far SPR measurements with live bacteria were established to measure the interaction between bacteria and carbohydrates.[291] Therefore, we designed a new assay format based on the functionalization of magnetic PEG beads as previously reported in our group.[80] Additionally, this project includes a molecular cloning part where we introduced a new plasmid in VR123, a bacterial strain which contains the plasmid *p*AP5[292] to obtain solely P fimbriated and GFP-expressing *E. coli*. With this it is possible to use a direct fluorescence readout to determine bacterial adhesion. This type of application is well known and used in our group.[77] For an even faster analysis where less amounts of inhibitor are necessary, PEG beads were introduced. Once

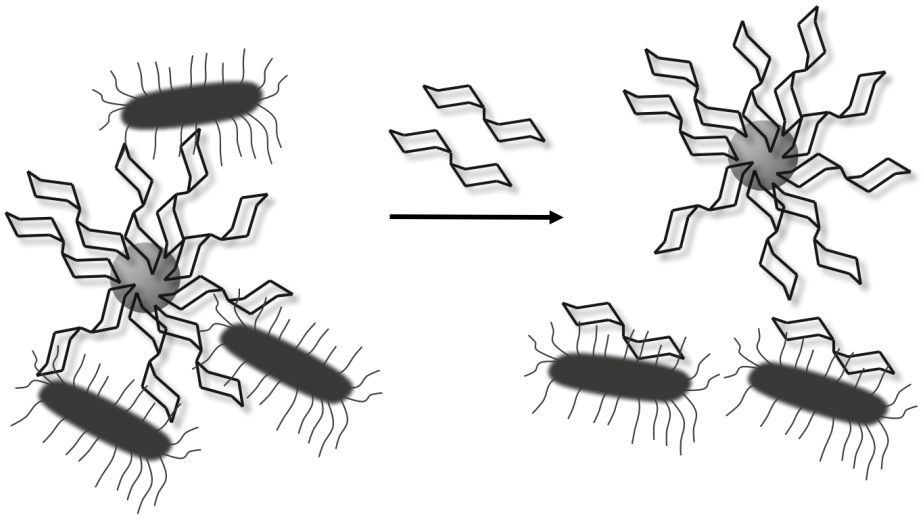

Figure 5.3.1: Schematic illustration of the adhesion process of the P fimbriated *E. coli* to magnetic PEG beads and the inhibition of this adhesion by adding a free inhibitor in solution.

functionalized they can be stored until needed and due to their magnetic core the washing procedures are quick and easy aided by a magnetic separation rack.

5.3.3 Synthesis and PEG bead functionalization

For the beads functionalization a Galα1,4Gal-disaccharide derivative was chosen. The synthesis started with the literature-known glycosyl donor **1** (Figure 5.3.2).[293] All steps were realized according to the published procedure to gain the galactoside **1** in good yields. Analytical data are in accordance with those published.[294] As glycosyl acceptor moiety a 4-OH free galactoside was needed. Starting from either methyl α-D-galactopyranoside or azidoethyl α-D-galactopyranoside a benzylidene protecting group was introduced, followed by Williamson ether synthesis to protect the 2-OH and 3-OH groups.[295–297] Afterwards the benzylidene group was selectively opened to obtain the galactosides **2** and **3**.[297,298] With the glycosyl donor **1** and both glycosyl acceptors **2** and **3**, the glycosylation reaction was carried out with TMSOTf and NIS to obtain the galactosides **4** and **5** respectively in rather good yields.[293] To obtain the unprotected disaccharides **6** and **7**, the benzyl ethers and acetyl protecting groups had to be cleaved. For the benzyl ethers this was only achievable under harsh conditions with Pd/C as catalyst under high H_2 pressure for 120 h. The deacetylation followed with potassium carbonate. The digalactoside **7** was further used for the functionalization of the PEG beads whereas **6** was used as inhibitor in solution.

The PEG beads where prepared according to previously published procedure starting with the carbodiimide activation of the surface carboxyl groups using 1-ethyl-3-(3-dimethylaminopropyl)carbodiimide (EDC) and *N*-hydroxysuccinimide (NHS) in 2-(*N*-morpholino)ethanesulfonic acid (MES) buffer. After subsequent coupling with free amine **7** compound **10** was obtained. The prepared beads suspension in PBS could be stored for several months at 4 °C until use.

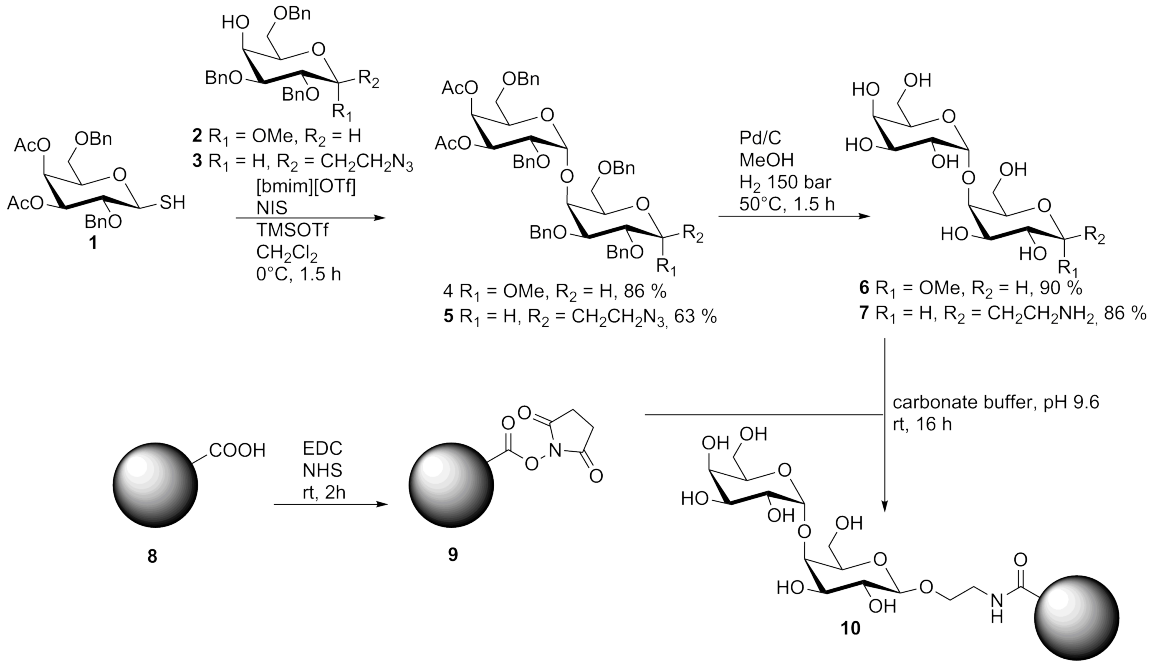

Scheme 5.3.2: Synthesis of the digalactosides **6** and **7** starting from the literature known glycosyl donor **1** and the glycosyl acceptor **2**. The magnetic PEG beads were functionalized according to a previous published method.

5.3.4 Cloning experimenty and bacterial adhesion studies

VR123 (MG1655 delta-fim *p*PAP5) were obtained from the group of F. M Aarestrup (formerly P. Klemm) in Denmark. They already carry the *p*PAP5 plasmid which comprises the whole P fimbriae coding DNA and an ampicillin resistance.[292] For this account we chose *p*ETM-14 vector to build the new plasmid because it provides a kanamycin resistance and a T7 expression system. As insert a green fluorescent protein derived from the jellyfish *Aequorea coerulescens*, *Ac*GFP was used.[299] Both, vector and insert were digested with XhoI and HindIII. With an agarose gel the digested products were purified and extracted. They were applied in a ligation step. The new plasmid was transformed into XL-1 *E. coli* to select the positive clones and after colony PCR (cf. ESI Fig. 7.8.3) and sequencing the plasmid was transformed into VR123 to obtain P fimbriated GFP-expressing *E. coli* (VR123G). After successful functionalization of the magnetic beads and the cloning experiments we analyzed the adhesion of the bacteria to the beads. VR123G were grown in LB media with ampicillin and kanamycin and the GFP expression was induced with IPTG. After harvesting and removal of the media the bacteria were suspended in PBS buffer to obtain a suspension with $OD_{600} = 0.5$. Functionalized beads (**10**) and the bacterial suspension were incubated at room temperature for 45 min and 600 rpm. Non-bounded *E. coli* were removed, the beads washed with PBS twice and transferred to a black microtiter plate for the fluorescence readout. Maximum adhesion (see Figure 5.3.3) was measured and then the inhibitor **6** was added in different concentrations. Again the beads were incubated at room temperature for 45 min and 600 rpm followed by an additional fluorescence readout. The results are depicted in Figure 5.3.3. The adhesion of P fimbriated bacteria to the glycosylated PEG beads can be measured via direct fluorescence read

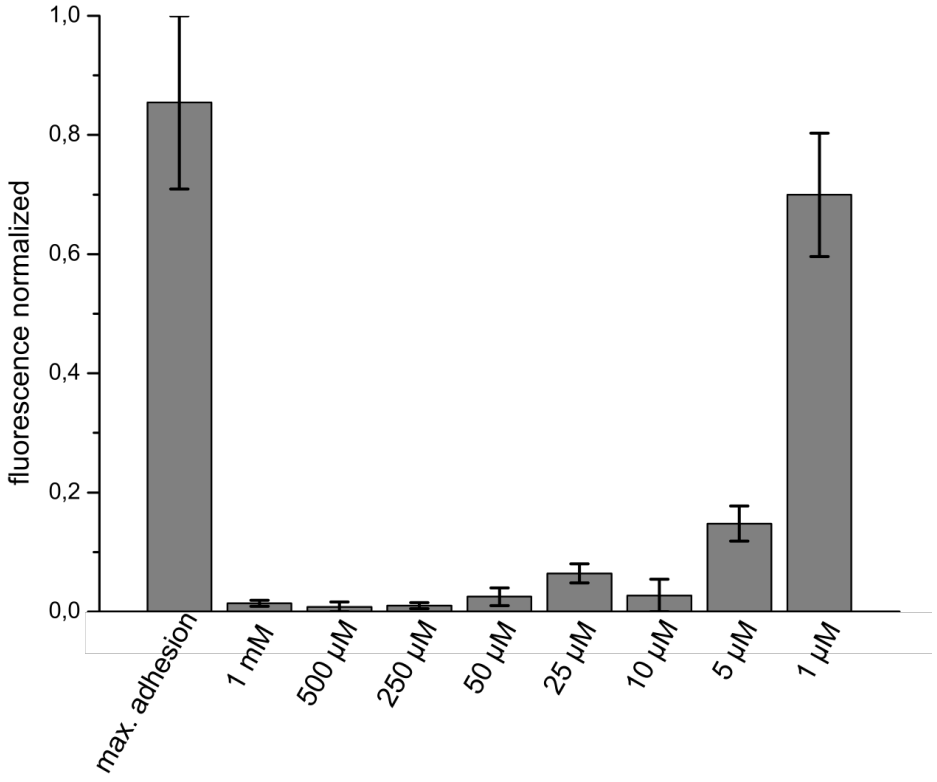

Figure 5.3.3: Results of the bacterial adhesion process to the glycosylated PEG beads. Left the maximal adhesion can be seen compared to different inhibitor concentrations of **6** to inhibit the adhesion to the beads. Error bars result from triplicate results.

out. This results were confirmed during three independent experiments. Disaccharide **6** showed good inhibitor properties at concentrations of 10 µM and above. Inhibitor concentrations were tested starting from 1 mM. Only when inhibitor concentrations of 5 µM were applied, a small increase in the bacterial adhesion to the beads could be seen. When a concentration of 1 µM of **6** was used for the inhibition, the fluorescence measurements exhibited only a slight decrease in fluorescence compared with the maximum adhesion values. Hence, the inhibitor concentration is too small to inhibit all the adhered bacteria.

5.3.5 Conclusion

Here we could show how P fimbriated bacterial adhesion can be investigated in a quick and easy way. The procedure for beads functionalization allows the preparation of magnetic beads which are stable and can be stored at 4 °C over several months. Therefore, the presented assay is very facile and new inhibitors for P fimbriae can be tested quickly and reliable. Another advantage lies in the fact that only a small amount of inhibitors is needed to obtain reliable results.

6 Conclusion

6.1 Bacterial adhesion studies

Since many assays to detect type 1 fimbriae-mediated bacterial adhesion were available, the aim of this project was to test variations of different carbohydrate ligands. In the published manuscript 'Effect of aminophenyl and aminothiahexyl α-D-glycosides of the *manno-, gluco-* and *galacto*-series on type 1 fimbriae-mediated bacterial adhesion of *Escherichia coli'* it was reported that the aglycone as well as the configuration of the carbohydrate has a huge influence on FimH affinity. Three different carbohydrates, mannosides, glucosides and galactosides, varied in the aglycone part were tested. Among these, the best inhibitor was *p*-aminophenyl α-D-mannosides followed by aliphatic mannosides. Additionally, it could be shown that the binding to ligands is improved if they are offered in solution compared to immobilized on a surface. Surprisingly, an inhibitory effect was also detected when glucoside inhibitors were used in solution.

The project continued with variation of the surface. Different carbohydrate inhibitors were tested on artificial polystyrene surfaces under static conditions and also on human cells, both at static and flow conditions. In the published paper 'En route from artificial to natural: Evaluation of inhibitors of mannose-specific adhesion of *E. coli* under flow' it was shown that the potency of six different tested ligands for FimH was influenced by shear stress. Under static conditions on polystyrene inhibitors were able to abolish bacterial adhesion almost completely whereas on cells only some reduction of bacterial adhesion was achieved. When flow was applied, adhesion of *E. coli* was shut down completely even at inhibitor concentrations which could not abolish bacterial adhesion under static conditions.

The next part of this project was the investigation of photoswitching of bacterial adhesion. Azobenzene mannosides were immobilized on glass surfaces and successful switching experiments proved that the adhesivity of this surface can be switched. By the addition of *E. coli* bacteria, the influence of carbohydrate presentation and orientation respectively, on bacterial adhesion could be further verified.

In the last part of the project, the influence of carbohydrate orientation as well as of flow was examined. For this purpose, synthetic mono- and heteroglycocluster were used. In case of the heteroglycoclusters focal point stereoisomers were applied. All glycocluster were immobilized on prefunctionalized glass surfaces and their adhesive properties tested under flow with *E. coli*. For this purpose, a flow assay system had to be established first. The results suggest that the orientation of the carbohydrate within the synthesized glycoclusters plays an important role as well as flow, which is necessary to detect the effect.

6.2 Examination of shear force influence

The previous results revealed a fundamental influence of flow on bacterial adhesion and therefore the influence of shear force was further investigated. Atomic force microscopy was used to examine the binding strength between the lectin FimH and different carbohydrates. For this approach cantilever tips were functionalized with sugar ligands and binding to type 1 fimbriated *E. coli* was investigated by AFM. With this new approach involving AFM it could be revealed that under the influence of shear force, FimH specificity changes from α-D-mannosides to α-D-glucosides.

To improve our understanding of this change in lectin specificity, a model system consisting of the lectin FimH and an attached switchable carbohydrate moiety was designed. For FimH an amino acid exchange was performed to obtain a FimH mutant with a free cysteine on the surface which can be addressed by bioorthogonal ligation chemistry. After this successful mutagenesis, the cysteine residue was addressed with a fluorescent dye as a prove of principal. This project has to be continued and finished involving STD-NMR studies.

6.3 Glyconanoparticles

Finally, glyconanoparticles were investigated as new tools to test bacterial adhesion. In the published paper 'Thiourea-bridged nanodiamond glycoconjugates as inhibitors of bacterial adhesion' glyconanodiamonds were constructed by thiourea-bridging and tested as inhibitors of type 1 fimbriae-mediated bacterial adhesion. Thiourea-bridging proved to be a facile method for nanodiamonds modification and the resulting glyconanodiamonds were suitable as tools to test bacterial adhesion.

Also P fimbriated *E. coli* were tested. For an easy and efficient detection of adhered bacteria, a plasmid containing GFP was constructed and transformed into P fimbriated *E. coli*. Additionally, Galα1,4Gal disaccharide derivatives were synthesized and immobilized on magnetic PEG beads or used as inhibitors in solution, respectively. It was possible to almost completely abolish bacterial adhesion to the glycosylated beads by addition of inhibitor.

Summarizing the described work, it is obvious that new and variable tools to identify and analyze protein-ligand interactions were introduced and successfully tested. Additional to chemical approaches, biochemical and biophysical techniques were employed and led to new insights and improved understanding of bacterial adhesion processes to carbohydrate-covered surfaces.

7 Experimental Part

7.1 Effect of aminophenyl and aminothiahexyl α-glycosides of the *manno-*, *gluco-* and *galacto*-series on type 1 fimbriae-mediated bacterial adhesion of *Escherichia coli*

Glycoside synthesis

All glycosides used for the bacterial adhesion assays (Figure 3.2.2, **1**–**6**) were synthesized according to known procedures. The aminophenyl glycosides, **1**, **3**, and **5**, were obtained by catalytic reduction from the corresponding nitrophenyl glycosides, which are commercially available. The 6-amino-4-thiahexyl glycosides, **2**, **4**, and **6**, where synthesized starting with the respective allyl glycosides by radical addition of cysteamine.[77] All prepared compounds were pure according to NMR and mass spectroscopic analysis, and the analytical data obtained were in accordance with the literature.

Media and buffer solutions

Carbonate buffer solution (pH 9.2): sodium carbonate (1.59 g) and sodium hydrogen carbonate (2.52 g) were dissolved in distilled deionized water. PBS buffer solution (pH 7.2): sodium chloride (8.00 g), potassium chloride (200 mg), sodium hydrogen phosphate dihydrate (1.44 g), and potassium dihydrogen phosphate (200 mg) were dissolved in distilled deionized water (1.00 L). PBST buffer solution: PBS buffer + Tween®20 (0.05 % v/v). Lysogeny broth (LB) medium: tryptone (10.0 g), sodium chloride (10.0 g), and yeast extract (5.00 g) were dissolved in distilled deionized water (1.00 L) and autoclaved, and ampicillin (100 mg) and chloramphenicol (50 mg) were added. Agar plates: tryptone (10.0 g), sodium chloride (10.0 g), yeast extract (5.00 g), and agar (15.0 g) were dissolved in distilled deionized water (1.00 L) and autoclaved, and ampicillin (100 mg) and chloramphenicol (50 mg) were added. All pH values were adjusted with HCl (1 M) and NaOH (1 M).

Bacterial strain, growth Conditions

For testing the GFP-expressing *E. coli* strain PKL1162 was used.[300] This *E. coli* mutant exclusively expresses type 1 fimbriae as well as GFP (green fluorescent protein) allowing for quantification of bacterial adhesion by fluorescence read-out.[77] The *E. coli* strain PKL1162 was constructed by inserting the *p*PKL1174 plasmid into strain SAR18. The *p*PKL1174 plasmid contains the fim gene cluster, which is responsible for the expression of type 1 fimbriae. SAR18 includes the GFP gene on its genome, controlled by a constitutive promoter.[300] The PKL1162 strain was cultured from a frozen stock in LB medium and incubated overnight at 37 °C. After washing twice with PBS buffer

(2.00 mL) the bacteria pellet was resuspended in PBS buffer and the bacterial solution was adjusted to OD_{600} = 0.4 (2 mg/mL) with PBS.

Mannan coating of microtiter plates covalent functionalization

Black 96-well microtiter plates (Nunc, MaxiSorp) were incubated with mannan from *Saccharomyces cerevisiae* (1.2 mg/mL in carbonate buffer, 120 µL/well) and dried overnight at 37 °C. After washing with PBST (3 × 150 µL/well) the wells were blocked with BSA (5% in PBS, 120 µL/well) and incubated at 37 °C for 2 h. Following this, the microtiter plates were washed with PBST (2 × 150 µL/well) and PBS (150 µL/well) [46].

Covalent functionalization of microtiter plates: glycoarray preparation

For glycoarray preparation, black Immobilizer Amino™ F96 MicroWell™ plates (Nunc) were incubated with solutions of the respective glycosides in carbonate buffer (100 µL/well; concentrations of used glycoside solutions are indicated individually, see binding/inhibition curves) at ambient temperature and at 100 rpm overnight. Following washing with PBST (3×150 µL/well), the wells were blocked with ethanolamine (10 mM in carbonate buffer, 120 µL/well) and incubated at ambient temperature and 100 rpm for 2 h. Following this, the microtiter plates were washed with PBST (2×150 µL/well) and PBS (150 µL/well).[77]

Binding assay with GFP-tagged *E. coli*

(a) Variation of bacteria concentration: Glycoarrays were prepared with 10 mM of the respective glycoside in carbonate buffer and to these glycoside-functionalized microtiter plates PBS buffer was added (100 µL/well). Then, the prepared bacterial solution (OD_{600} 0.4) was added to well 1 and 2 and serially diluted (starting with well 2). The plate was incubated for 1 h at 37 °C, at 100 rpm, washed with PBS (3×150 µL/well), and then PBS was added (100 µL/well) and the fluorescence intensity (485 nm/535 nm) determined.[77]
(b) Variation of glycoside concentration: Glycoarrays were prepared using serial dilutions of the respective glycoside (starting with 200 mM glycoside solution in carbonate buffer). Following this, the prepared bacterial solution (OD_{600} 0.4, 100 µL per well) was added and the plate incubated for 1 h at 37 °C at 100 rpm. The plate was washed with PBS (3×150 µL/well), and then PBS was added (100 µL/well) and the fluorescence intensity (485 nm/535 nm) determined.[77]

Adhesion-inhibition assay with GFP-tagged *E. coli*

Solutions of the respective inhibitory glycosides were prepared (200 mM carbonate buffer except for *p*APMan: 10 mM) and serial dilutions of the inhibitor solution added to the mannan-coated microtiter plate wells. The prepared bacterial solution (OD_{600} 0.4, 50 µL/well) was added and the plate incubated for 1 h at 37 °C and 100 rpm. The plates were washed with PBS buffer (3×150 µL/well), and then the wells were filled with PBS (100 µL/well) and the fluorescence intensity (485 nm/535 nm) was determined.[77]

Preincubation-inhibition-adhesion assay with GFP-tagged *E. coli*

Serial dilutions of the respective inhibitory glycoside solution were prepared (starting concentration 200 mM in carbonate buffer except for *p*APMan: 10 mM) and mixed with the prepared bacterial solution (OD_{600} 0.4, 60 µL). /well) for preincubation. These mixtures were incubated for 1 h at 37 °C and 100 rpm and were then transferred to mannan-coated microtiter plates followed by incubation for 1 h at 37 °C and 100 rpm. The plates were washed with PBS buffer (3×150 µL/well), the wells filled with PBS (100 µL/well) and the fluorescence intensity (485 nm/535 nm) was determined.[105]

Bacterial growth tests

Serial dilutions of the respective inhibitory glycoside solutions were prepared (starting concentration 200 mM in carbonate buffer) and mixed with a bacterial solution (OD_{600} 0.4, 50 µL/well). The resulting mixtures were incubated for 1 h at 37 °C and 100 rpm. Following this, 50 µL of each mixture were transferred to an agar plate, which were incubated overnight at 37 °C. Bacterial growth was determined by visual inspection of the agar plates.

7.2 En route from artificial to natural: Evaluation of inhibitors of mannose-specific adhesion of *E. coli* under flow

Bacterial culture

GFP-fluorescent *E. coli* (strain PKL1162)[77] were inoculated in 10 mL LB medium (Sigma-Aldrich, St. Louis, MO) in presence of chloramphenicol (50 mg/L) and ampicillin (100 mg/L) (both Sigma-Aldrich) and grown at 37 °C overnight under constant agitation. For the inhibition on mannan surfaces the bacteria were centrifuged (4000 rpm, 15 min, 4 °C) and washed with PBS two times. Then, a suspension with $OD_{600} = 0.4$ in PBS was prepared for further use. The centrifugation conditions applied here were tested earlier and no influence on bacterial fimbriae (such as breaking) were seen.[77] For the inhibition on HMEC-1 the bacteria were centrifuged and washed two times with DPBS + Ca^{2+}/Mg^{2+} (Life Technologies, Carlsbad, St. Louis, MO) and once with cell medium. Then, the bacteria were suspended in 10 mL cell medium and the optical density at 600 nm was determined. For the experiments under static and under flow condition, a 1:50 dilution of a suspension with $OD_{600} = 0.1$ was used.

Cell culture

HMEC-1 (CDC, Atlanta, GA) were seeded in 96-well microtiter plates (Corning, Corning, NY) or in collagen coated Luer $I^{0.8}$ channels (IBIDI, Martinsried, Germany) and grown to confluency. The cells were cultured in MDCB-131 medium with 1 % glutamax, 10 % FBS, 10 ng/mL hEGF (all Life Technologies), and 1 µg/mL hydrocortisone (Sigma-Aldrich) at 37 °C in 5 % CO_2-atmosphere.

Inhibition of bacterial adhesion

Inhibition on mannan surfaces Mannan coated 96-well microtiter plates (Nunc) were blocked with a solution of PVA (1 % in PBS) for 2 hours with 200 rpm at room temperature. The inhibitors were dissolved in PBS and added in a serial dilution. The bacterial solution was added and the plates were incubated at 37 °C with 100 rpm for 1 hour. The plates were washed with PBS (3 x 300 µL/well) and the fluorescence intensity was determined with a microplate reader.[77]

Inhibition under static conditions on HMEC-1 Cells were grown to confluency in 96-well plates (Corning). A 1:50 dilution of *E. coli* was prepared, inhibitors at the respective concentrations were added, and it was incubated for 20 minutes. The medium was removed from the cells and 200 µL of the bacteria suspension was added. It was incubated for 30 minutes at 37 °C on a shaker (400 rpm). Then, it was washed with 200 µL DPBS +Ca^{2+}/Mg^{2+} (Life Technologies) for 20 minutes (37 °C, 400 rpm). The DPBS was removed and replaced by CO_2-independent medium (Life Technologies).

Inhibition under flow conditions on HMEC-1 Cells were grown to confluency in Luer $I^{0.8}$ channels (IBIDI). For each inhibitor, a single suspension was used. First, bacteria (1:50 dilution of a

suspension with $OD_{600} = 0.1$) were flown over the cells without inhibitor (shear rate = 1.5 dyn/cm^2). Then, the channel was changed and inhibitor was added to the respective concentration. Afterwards, the channel was changed again and inhibitor was added to the next concentration and so on.

Fluorescence microscopy

Confocal fluorescence images of the GFP-fluorescing bacteria were obtained with a commercially available axio cell observer spinning-disk inverted microscope (Zeiss) with an optical section thickness of about 300 nm.

Software

Images were analyzed using ImageJ. For data visualization and analysis, OriginPro 8G was used. Figures were prepared with Corel Draw 12.

Synthesis

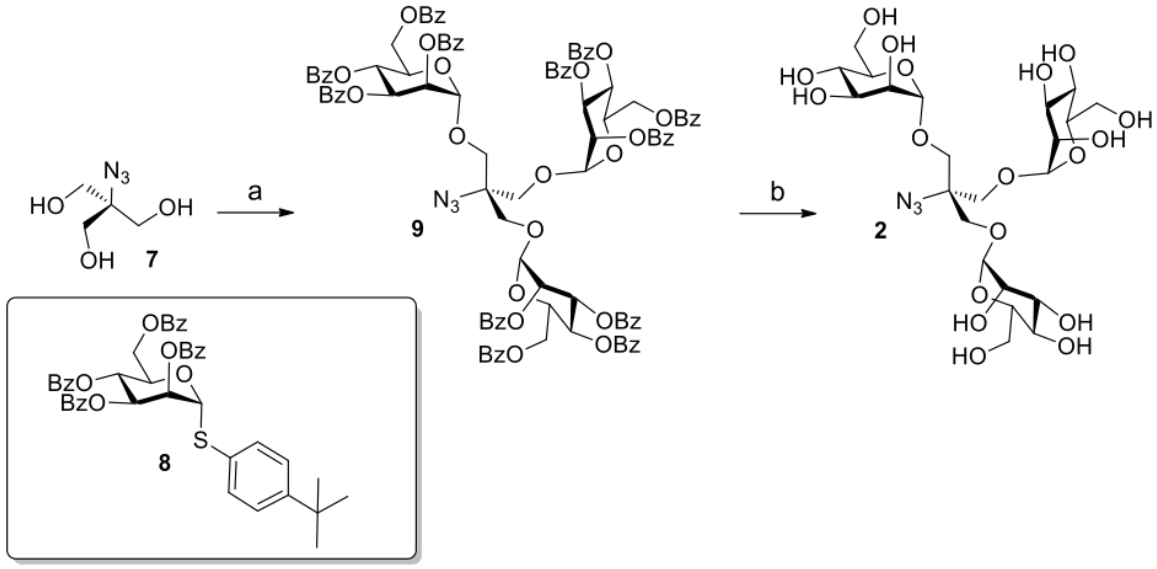

Scheme 7.2.1: Preparation of TRIS-triMan-azido **4**. Reagents and conditions: (a) Donor **2** (3 equiv), NIS (5 equiv), TfOH (0.5 equiv), 3 Å MS, DCM/[bmim][OTf] (9:1), rt, overnight, 47 %; (b) NaOMe, MeOH, rt, overnight, 68 %.

N-(Azido)tris-[(2,3,4,6-tetra-*O*-benzoyl-α-D-mannopyranosyloxy)methyl]methyl (9):

To a solution of **7** (0.102 g, 0.694 mmol) and donor **8** (1.58 g, 2.08 mmol, 3 equiv) in dry CH_2Cl_2/[bmim][OTf] (9:1, 10.0 mL) was added under nitrogen freshly activated 3 Å molecular sieves (1.70 g). The mixture was stirred at room temperature for 15 min then *N*-iodosuccinimide

(0.781 g, 3.47 mmol, 5 equiv) and trifluoromethanesulfonic acid (30 µL, 0.347 mmol, 0.5 equiv) were sequentially added. The mixture was stirred overnight under nitrogen at room temperature then diluted with CH_2Cl_2, filtered over celite. After washing with satd. aq. $NaHCO_3$ and satd. aq. $Na_2S_2O_3$, the aqueous layer was extracted with CH_2Cl_2 then the combined organic layers were dried over magnesium sulfate, filtered and concentrated. The crude residue was purified by flash-column chromatography (cyclohexane/ethyl acetate 9:1 to 7:3) to afford **9** (0.617 g, 47 %) as a white foam. R_f= 0.138 (3:1 cyclohexane/ethyl acetate); ^{1}H NMR (600 MHz, $CDCl_3$) δ = 8.21 – 8.11 (m, 6H, 6H-Ar), 8.03 – 7.96 (m, 6H, 6H-Ar), 7.95 – 7.88 (m, 6H, 6H-Ar), 7.83 – 7.75 (m, 6H, 6H-Ar), 7.56 (q, J = 7.4 Hz, 6H, 6H-Ar), 7.44 – 7.37 (m, 9H, 9H-Ar), 7.34 (t, J = 7.7 Hz, 9H, 9H-Ar), 7.22 (t, J = 7.9 Hz, 6H, 6H-Ar), 7.16 (t, J = 7.9 Hz, 6H, 6H-Ar), 6.23 (dd, $J_{4,3}$ = $J_{4,5}$= 10.0 Hz, 3H, 3H-4), 5.98 (dd, $J_{3,4}$ = 10.2 Hz, $J_{3,2}$ = 3.3 Hz, 3H, 3H-3), 5.81 (dd, $J_{2,3}$ = 3.1 Hz, $J_{2,1}$ = 1.8 Hz, 3H, 3H-2), 5.36 (d, $J_{1,2}$ = 1.4 Hz, 3H, 3H-1), 4.84 (d, $J_{6a,6b}$ = 10.1 Hz, 3H, 3H-6a), 4.69 – 4.55 (m, 6H, 3H-5, 3H-6b), 4.21 (d, J = 10.6 Hz, 3H, (Man-O-CH)$_3$$CN_3$), 4.01 (d, J = 10.6 Hz, 3H, (Man-O-CH)$_3$$CN_3$); ^{13}C NMR (151 MHz, $CDCl_3$) δ = 166.3, 165.6, 165.4 (12C, 12PhC=O), 133.5, 133.4, 133.2, 130.1, 129.9, 129.4, 129.2, 129.0, 128.6, 128.4, (72C, 72C-Ar), 98.7 (3C, 3C-1), 70.3 (3C, 3C-2), 70.1 (3C, 3C-3), 69.9(3C, 3C-5), 67.9 (3C, (Man-O-CH_2)$_3$$CN_3$), 66.6 (3C, 3C-4), 65.0 ((Man-O-CH_2)$_3$$CN_3$), 62.8 (3C, 3C-6); ESI-MS: m/z = 656.2 [M+Na+] (calcd. 656.212 for $C_{22}H_{39}N_3O_{18}$Na+).

N-(Azido)tris-[(α-D-mannopyranosyloxy)methyl]methyl (2):

To a solution of **9** (0.189 g, 0.100 mmol) in dry methanol (3.00 mL) was added under nitrogen methanolic 5.4 M sodium methoxide (three drops). The mixture was stirred overnight under nitrogen at room temperature then neutralized with Amberlite IR120 (H+), diluted with methanol, filtered and concentrated. The residue was taken up into a 1:1 mixture of water and methanol then washed with diethyl ether and the aqueous layer was concentrated. The crude material was purified by size exclusion chromatography on G10 gel (elution with water) to afford **2** (0.043 g, 68 %) as a white amorphous solid after lyophilization. ^{1}H NMR (500 MHz, D_2O) δ = 4.90 (d, $J_{1,2}$ = 1.7 Hz, 3H, 3H-1), 4.02 (dd, $J_{2,3}$ = 3.4 Hz, $J_{2,1}$ = 1.8 Hz, 3H, 3H-2), 3.97 (d, J = 10.5 Hz, 3H, (Man-O-CH)$_3$$CN_3$), 3.92 (dd, $J_{6a,6b}$ = 12.2 Hz, $J_{6a,5}$ = 1.5 Hz, 3H, 3-H6a), 3.87 – 3.83 (m, 3H, 3H-3), 3.80 – 3.77 (m, 3H, 3H-6b), 3.73 (d, J = 10.5 Hz, 3H, (Man-O-CH)$_3$$CN_3$), 3.71 – 3.63 (m, 6H, 3H-4, 3H-5); ^{13}C NMR (126 MHz, D_2O) δ = 100.3 (3C, 3C-1), 73.1 (3C, 3C-4 or 3C-5), 70.5 (3C, 3C-3), 69.8 (3C, 3C-2), 67.3 (3C, (Man-O-CH_2)$_3$$CN_3$), 66.7 (3C, 3C-4 or 3C-5), 64.9 ((Man-O-CH_2)$_3$$CN_3$), 60.9 (3C, 3C-6).

NMR spectra

p-[*N*-(2-Ethoxy-3,4-dioxocyclobut-1-enyl)amino]phenyl α-D-mannopyranoside (1)

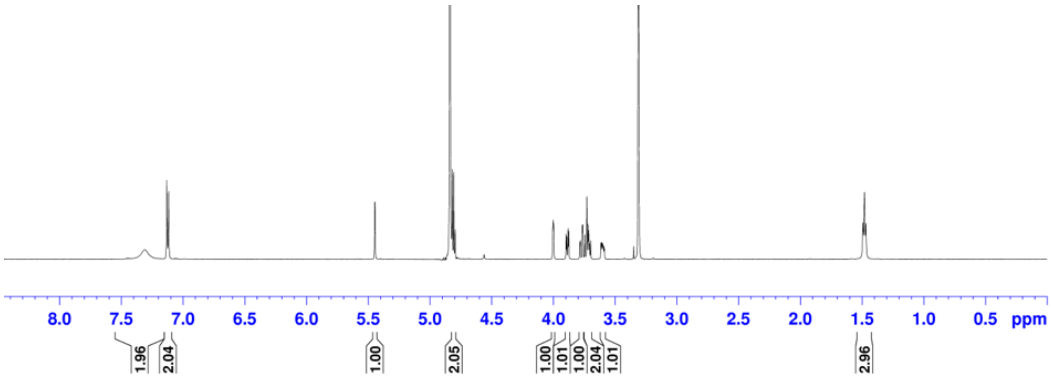

Figure 7.2.2: ^{1}H NMR spectra of **1** (600 MHz, CD_3OD, 300 K)

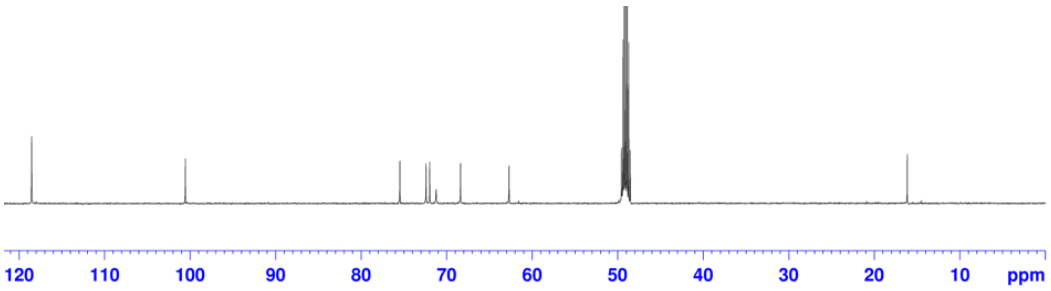

Figure 7.2.3: ^{13}C NMR spectra of **1** (150 MHz, CD_3OD, 300 K)

N-(Azido)tris-[(α-D-mannopyranosyloxy)methyl]methyl (2)

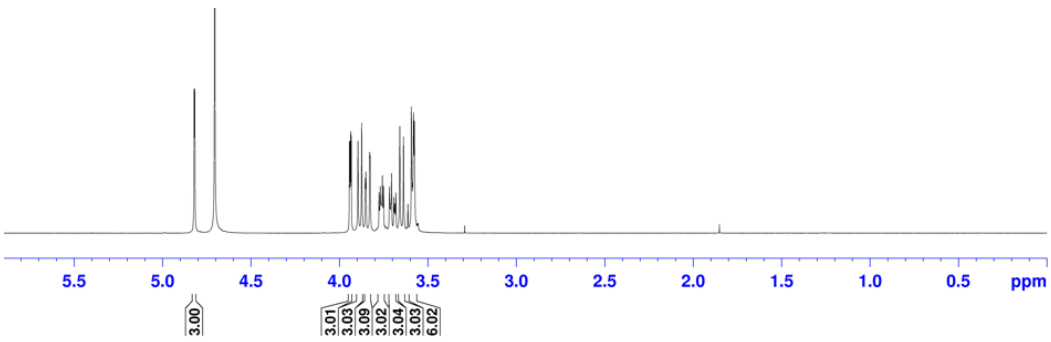

Figure 7.2.4: ^{1}H NMR spectra of **2** (500 MHz, D_2O, 300 K)

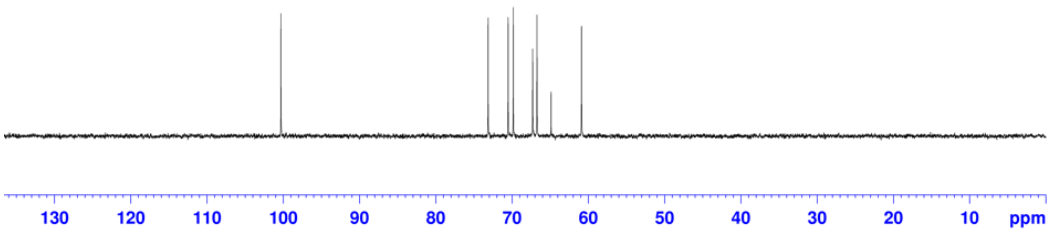

Figure 7.2.5: ^{13}C NMR spectra of **2** (125 MHz, CD_3OD, 300 K)

Heptyl α-D-mannopyranoside (3)

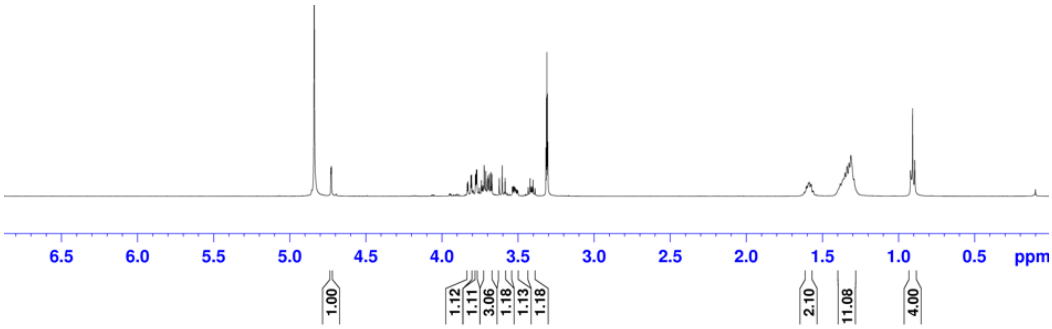

Figure 7.2.6: ^{1}H NMR spectra of **3** (500 MHz, D_2O, 300 K)

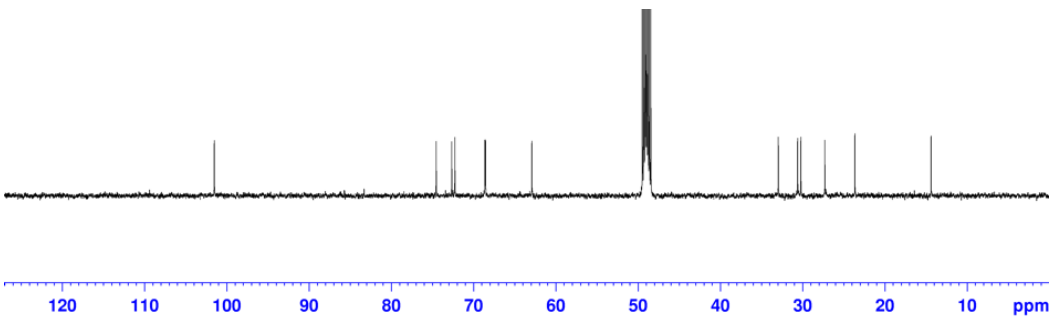

Figure 7.2.7: ^{13}C NMR spectra of **3** (125 MHz, CD_3OD, 300 K)

Octyl α-D-mannopyranoside (4)

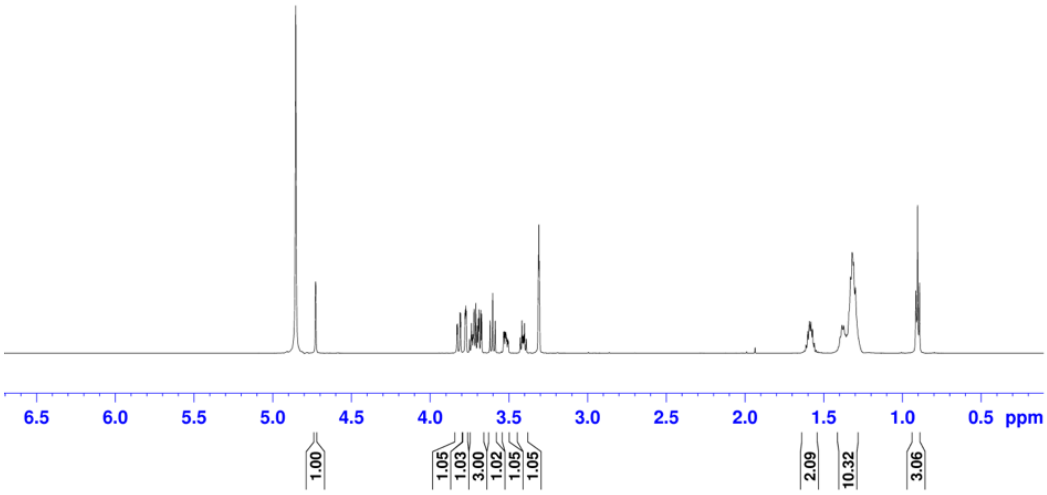

Figure 7.2.8: ^{1}H NMR spectra of **4** (500 MHz, CD_3OD, 300 K)

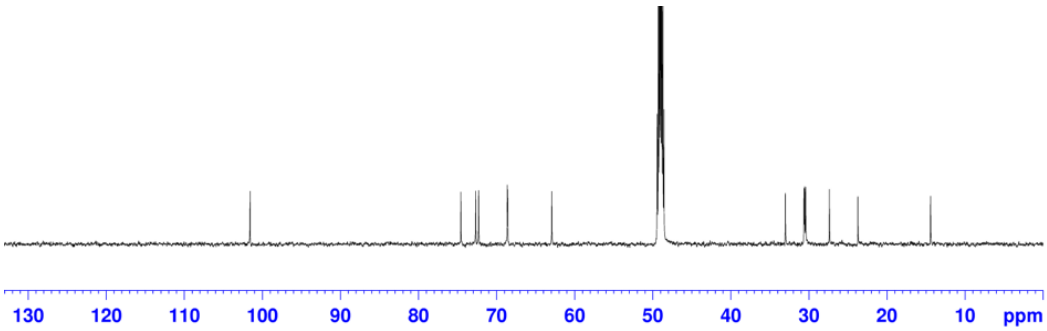

Figure 7.2.9: ^{13}C NMR spectra of **4** (125 MHz, CD_3OD, 300 K)

p-Aminophenyl α-D-mannopyranoside (5)

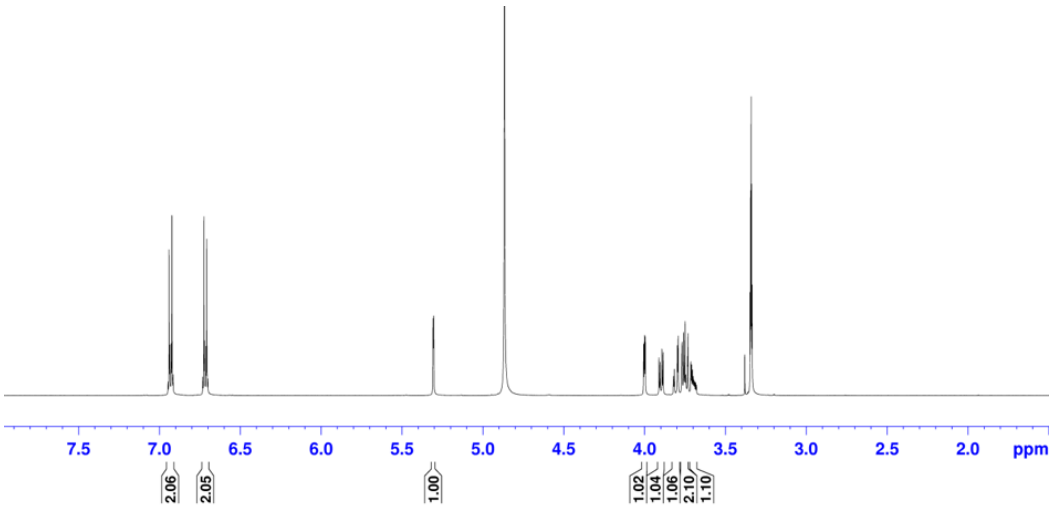

Figure 7.2.10: ^{1}H NMR spectra of **5** (500 MHz, CD_3OD, 300 K)

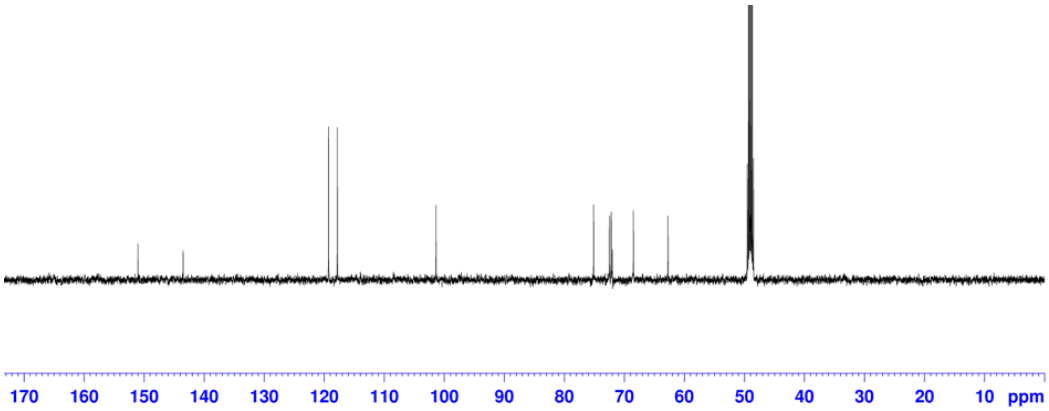

Figure 7.2.11: ^{13}C NMR spectra of **5** (125 MHz, CD_3OD, 300 K)

6-Amino-4-thiahexyl α-D-mannopyranoside (6)

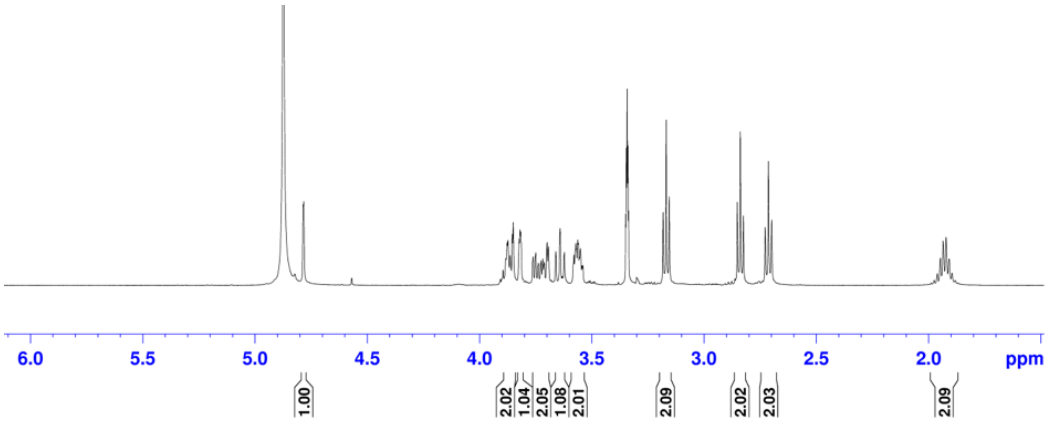

Figure 7.2.12: ^{1}H NMR spectra of **6** (500 MHz, CD_3OD, 300 K)

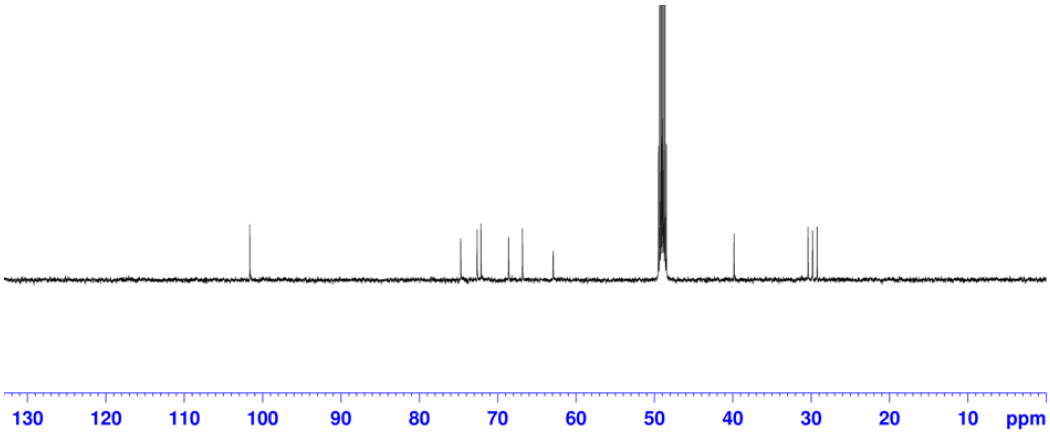

Figure 7.2.13: ^{13}C NMR spectra of **6** (125 MHz, CD_3OD, 300 K)

Bacterial adhesion inhibition assay

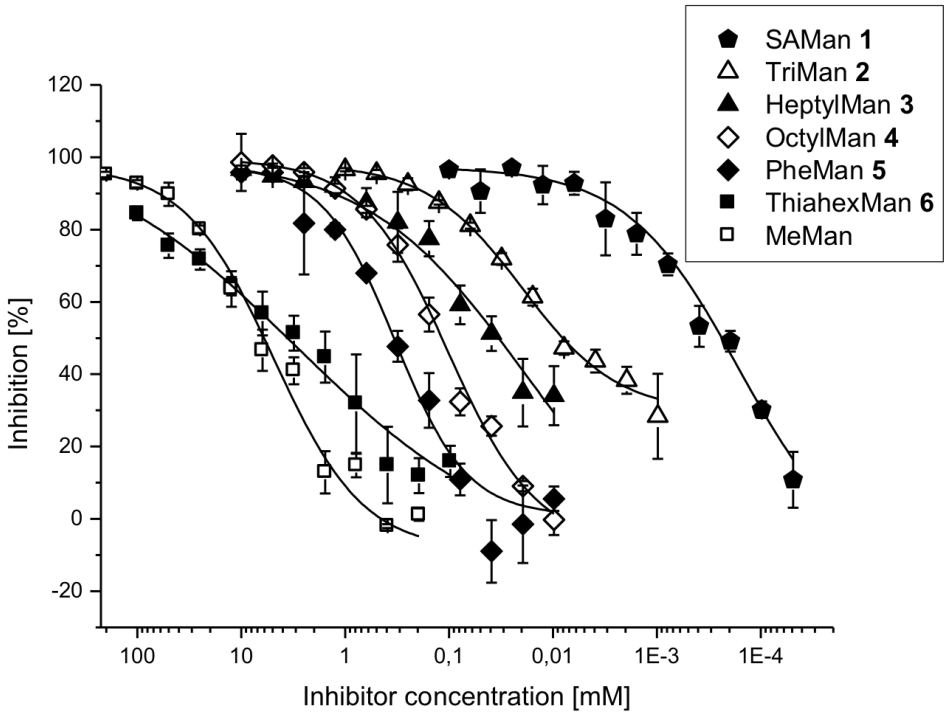

Figure 7.2.14: Inhibition of bacterial adhesion to mannan surfaces under static conditions. Solutions of the respective glycosides were prepared and serial dilutions were added to mannan-coated microtiter plate wells. The prepared bacterial solution (OD_{600} = 0.4) was added and the plate incubated for 1 h at 37 °C and 100 rpm. The plates were washed with PBS buffer and then the wells were filled with PBS for the fluorescence readout (485 nm/535 nm). The depicted binding curves are representative examples from several (>3x) independent experiments. Error bars result from duplicate values on one plate.

Example Images

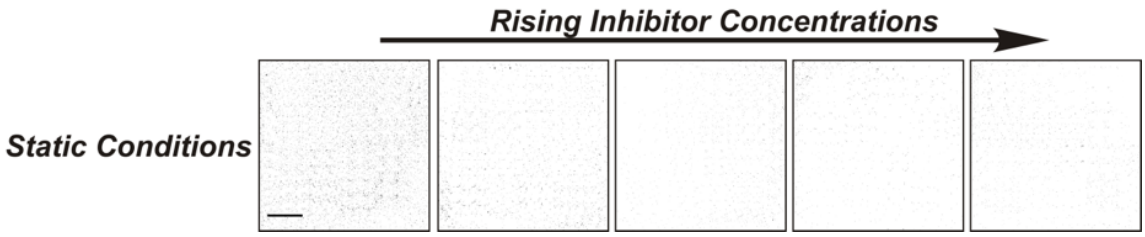

Figure 7.2.15: Example images of bacterial adhesion to HMEC-1 under static conditions using SAMan as inhibitor. The images clearly show that under static conditions, bacteria can adhere up to high inhibitor concentrations (0 / 0.001 / 0.01 / 0.1 / 1 mM). Scale bar = 200 µm. Contrast is inverted for clarity. Contrast settings are equal for all images.

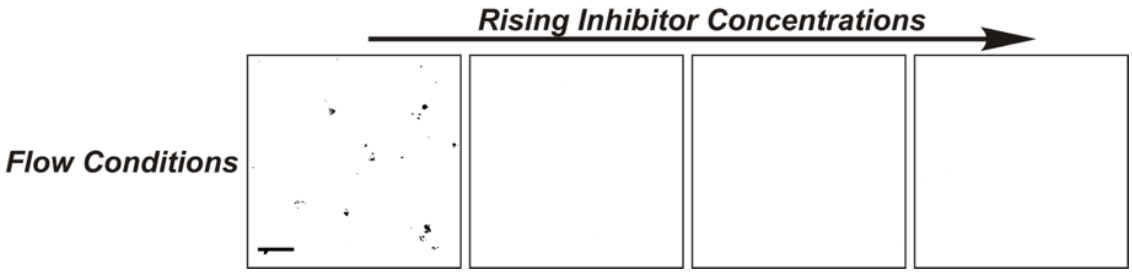

Figure 7.2.16: Example images of bacterial adhesion to HMEC-1 under flow conditions using SAMan as inhibitor. Under flow conditions, no adhesion was detected already at low inhibitor concentrations (0 / 0.1 / 1 / 2 mM). Contrast is inverted for clarity. Contrast settings are equal for all images. Scale bar = 100 µm. Depicted adhesion is after five minutes of bacterial flow.

7.3 Azobenzene glycosides on glass: A tool to investigate photoswitchable cell adhesion

Materials and Methods

11-Aminoundecyltrimethoxysilane (**7**) was purchased from AlfaAesar and used without further purification. Quartz slides were purchased from Plano, GPE Scientific Limited and Chemglass Life Science. Quartz slides have been cut to a size of 2.5 × 1 cm and functionalized in Falcon™ 15 mL Conical centrifuge tubes. Moisture-sensitive reactions were carried out in dry glassware and under a positive pressure of nitrogen. Analytical thin layer chromatography (TLC) was performed on silica gel plates (GF 254, Merck). Visualization was achieved by UV light and/or with 10 % sulfuric acid in ethanol followed by heat treatment at ~180 °C. Flash chromatography was performed on silica gel 60 (Merck, 230-400 mesh, particle size 0.040-0.063 mm) by using distilled solvents. Dry 1,4-dioxane over molecular sieves was purchased from Acros Organics and used without further purification. Melting points (mp) were determined on a Büchi M-56 apparatus. Optical rotations were measured with a Perkin-Elmer 241 polarimeter (sodium D-line: 589 nm, length of cell: 1 dm) in the solvents indicated. Proton (^{1}H) nuclear magnetic resonance spectra and carbon (^{13}C) nuclear magnetic resonance spectra were recorded on a Bruker DRX-500 and AV-600 spectrometer. Chemical shifts are referenced to the residual proton of the NMR solvent. Data are presented as follows: chemical shift, multiplicity (s=singlet, d=doublet, t=triplet, q=quartet, m=multiplet, and br=broad signal), coupling constant in hertz (Hz) and, integration. Full assignment of the peaks was achieved with the aid of 2D NMR techniques (^{1}H/^{1}H COSY and ^{1}H/^{13}C HSQC. All NMR spectra of the *E*-isomers of the azobenzene derivatives were recorded after they were kept for 16 h in the dark at 40 °C. Infrared (IR) spectra were measured with a Perkin Elmer FT-IR Paragon 1000 (ATR) spectrometer and were reported in cm^{-1}. ESI mass spectra were recorded on a LCQ Classic from Thermo Finnigan. UV-Vis absorption spectra were performed on Perkin-Elmer Lambda-241 at a temperature of 20 °C ± 1 °C. For irradiation experiments with 365 nm an apparatus with 10 LEDs (Nichia NCSU276A U365) with a total power of 7500 W was used with 50 % (3750 W). For irradiation with 440 nm a similar apparatus with 10 LEDs (10 x Roithner VL440) with total power of 4500 W was used with 50 % (2250 W). Both apparatus were built from Sahlmann Photochemical Solutions. Fluorescence readout was accomplished with an Infinite® 200 PRO multimode reader from Tecan.

Synthesis

(*E*)-*p*-[*p´*-(*N*-tert-Butoxycarbonyl-aminomethyl)phenylazo]phenyl

α-D-mannopyranoside (3):

Crude **1**[180] (541 mg, 1.55 mmol, calculated via ^{1}H NMR spetroscopy) and *p*-aminophenyl α-D-mannopyranoside[77] (**2**, 420 mg, 1.55 mmol) were dissolved in a mixture of dimethyl sulfoxide and acetic acid (1:1, 14 mL). The reaction mixture was stirred for 16 h at room temperature. The product was precipitated by addition of water, filtered off and washed with water. Purification of the crude product by column chromatography (dichloromethane/methanol, 9:1→8:1) gave **3** as an orange solid

(640 mg, 1.31 mmol, 84 %). R_f = 0.38 (ethyl acetate/methanol, 10:1); m.p. 137 °C; $[\alpha]_D^{23}$ = +114.6 (c = 0.4 in methanol); ^{1}H NMR (600 MHz, MeOH-d_4, 300 K): δ = 7.90-7.83 (m, 4H, Ar-H_{ortho}, Ar $H_{ortho'}$), 7.44-7.42 (m, 2H, Ar-$H_{meta'}$), 7.30-7.27 (m, 2H, Ar-H_{meta}), 5.60 (d, $^3J_{1,2}$ = 1.8 Hz, 1H, H-1), 4.31 (s, 2H, CH_2NHBoc), 4.04 (dd, $^3J_{1,2}$ = 1.8 Hz, $^3J_{2,3}$ = 3.3 Hz, 1H, H-2), 3.93 (dd, $^3J_{2,3}$ = 3.4 Hz, $^3J_{3,4}$ = 9.5 Hz, 1H, H-3), 3.80-3.71 (m, 3H, H-4, H-6, H-6'), 3.59 (ddd, $^3J_{4,5}$ = 9.7 Hz, $^3J_{5,6}$ = 5.4 Hz, $^3J_{5,6'}$ = 2.5 Hz, 1H, H-5), 1.47 (s, 9H, C(CH_3)$_3$) ppm; ^{13}C NMR (126 MHz, MeOH-d_4, 300 K): δ = 160.3 (C-Ar_{para}), 158.6 (C=O_{Boc}), 153.1 (C-$Ar_{ipso'}$), 149.2 (C-Ar_{ipso}), 144.0 (C-$Ar_{para'}$), 128.8 (C-$Ar_{meta'}$), 125.5 (C-Ar_{ortho}), 123.7 (C-$Ar_{ortho'}$), 118.0 (C-Ar_{meta}), 100.1 (C-1), 80.3 (C(CH$_3$)$_3$), 75.7 (C-5), 72.4 (C-3), 71.9 (C-2), 68.3 (C-4), 62.7 (C-6), 44.8 (CH_2NHBoc), 28.8 (C(CH$_3$)$_3$) ppm; IR (ATR): $\tilde{\nu}$ = 3281, 2922, 1683 1600, 1581, 1470, 1363, 1339, 1228, 1098, 1017, 846 cm^{-1}; ESI-MS: *m/z* calcd for $C_{24}H_{31}N_3O_8$: 512.2 [M+Na]+; found 512.2.

(*E*)-*p*-[*p´*-(Aminomethyl)phenylazo]phenyl α-D-mannopyranoside • TFA (4):

To a suspension of the mannosides **3** (832 mg, 1.70 mmol) in dichloromethane (20 mL), trifluoroacetic acid (2 mL) was added. The reaction mixture was stirred for 1.5 h at room temperature. Then the solvent was evaporated and **4** was obtained as an orange solid (850 mg, 1.68 mmol, 99 %). The TFA salt was used in the next step without further purification. R_f = 0.15 (ethyl acetate/methanol, 5:1); m.p. 119 °C; $[\alpha]_D^{23}$ = +148.0 (c = 0.6 in methanol); ^{1}H NMR (500 MHz, MeOH-d_4, 300 K): δ = 7.95-7.91 (m, 4H, Ar-H_{ortho}, Ar $H_{ortho'}$), 7.64-7.61 (m, 2H, Ar-$H_{meta'}$), 7.30-7.27 (m, 2H, Ar-H_{meta}), 5.61 (d, $^3J_{1,2}$ = 1.8 Hz, 1H, H-1), 4.21 (s, 2H, CH_2NH_2), 4.05 (dd, $^3J_{1,2}$ = 1.8 Hz, $^3J_{2,3}$ = 3.5 Hz, 1H, H-2), 3.92 (dd, $^3J_{2,3}$ = 3.5 Hz, $^3J_{3,4}$ = 9.5 Hz, 1H, H-3), 3.80-3.71 (m, 3H, H-4, H-6, H-6'), 3.59 (ddd, $^3J_{4,5}$ = 9.7 Hz, $^3J_{5,6}$ =5.3 Hz, $^3J_{5,6'}$ = 2.6 Hz, 1H, H-5) ppm; ^{13}C NMR (126 MHz, MeOH-d_4, 300 K): δ = 160.7 (C-Ar_{para}), 154.3 (C-$Ar_{ipso'}$), 149.1 (C-Ar_{ipso}), 136.8 (C-$Ar_{para'}$), 130.9 (C-$Ar_{meta'}$), 125.8 (C-Ar_{ortho}), 124.2 (C-$Ar_{ortho'}$), 118.1 (C-Ar_{meta}), 100.1 (C-1), 75.7 (C-5), 72.4 (C-2), 71.8 (C-3), 68.3 (C-4), 62.6 (C-6), 44.0 (CH_2NH_2) ppm; IR (ATR): $\tilde{\nu}$ = 3602, 3184, 2934, 1584, 1492, 1223, 1050, 953, 847 cm^{-1}; ESI-MS: *m/z* calcd for $C_{19}H_{23}N_3O_6$: 412.2 [M+Na]+; found 412.2.

(*E*)-*p*-[*p´*-(Azidomethyl)phenylazo]phenyl α-D-mannopyranoside (5):

To a suspension of the amine **4** (394 mg, 758 µmol), potassium carbonate (210 mg, 1.52 mmol) and $CuSO_4$x5 H_2O (2.00 mg, 7.58 µmol) in methanol (4 mL), imidazole-1-sulfonyl azide hydrochloride (254 mg, 1.21 mmol) was added. The reaction mixture was stirred for 16 h at room temperature. Then the solvent was evaporated and afterwards ethyl acetate (10 mL) and water (10 mL) were added. The phases were separated and the aqueous phase extracted with ethyl acetate (4 × 10 mL). The combined organic phases were dried over $MgSO_4$, it was filtered and the filtrate concentrated under reduced pressure. The crude product was recrystallized from a mixture of methanol and water (1:7) and the azobenzene derivative **5** was obtained as an orange solid (195 mg, 469 µmol, 62 %). R_f = 0.50 (ethyl acetate/methanol, 10:1); m.p. 198 °C; $[\alpha]_D^{23}$ = +135.6 (c = 0.4 in dimethylsulfoxide); ^{1}H NMR (600 MHz, DMSO-d_6, 300 K): δ = 7.90-7.87 (m, 4H, Ar-H_{ortho}, Ar $H_{ortho'}$), 7.58-7.57 (m, 2H, Ar-$H_{meta'}$), 7.29-7.28 (m, 2H, Ar-H_{meta}), 5.53 (d, $^3J_{1,2}$ = 1.4 Hz, 1H, H-1), 5.10 (d, $^3J_{2,OH}$ = 4.4 Hz, 1H, OH_{C-2}), 4.86 (d, $^3J_{4,OH}$ = 5.8 Hz, 1H, OH_{C-4}), 4.79 (d, $^3J_{3,OH}$ = 5.9 Hz, 1H, OH_{C-3}), 4.58

(s, 2H, CH_2N_3), 4.46 (t, $^3J_{6,OH}$ = 5.9 Hz, $^3J_{6',OH}$ = 5.9 Hz, 1H, OH_{C-6}), 3.88-3.86 (m, 1H, H-2), 3.72-3.69 (m, 1H, H-3), 3.61 (ddd, $^2J_{6,6'}$ = 11.7 Hz, $^3J_{5,6}$ = 1.9 Hz, $^3J_{6,OH}$ = 5.9 Hz, 1H, H-6), 3.54-3.46 (m, 2H, H-4, H-6'), 3.41-3.38 (m, 1H, H-5) ppm; ^{13}C NMR (151 MHz, DMSO-d_6, 300 K): δ = 159.1 (C-Ar_{para}), 151.6 (C-$Ar_{ipso'}$), 146.9 (C-Ar_{ipso}), 138.5 (C-$Ar_{para'}$), 129.4 (C-$Ar_{meta'}$), 124.4 (C-Ar_{ortho}), 122.6 (C-$Ar_{ortho'}$), 117.1 (C-Ar_{meta}), 98.7 (C-1), 75.3 (C-5), 70.6 (C-3), 69.9 (C-2), 66.6 (C-4), 61.0 (C-6), 53.1 (CH_2N_3) ppm; IR (ATR): $\tilde{\nu}$ = 3249, 2889, 2165, 2104, 1578, 1493, 1347, 1234, 1119, 1073, 1009, 973, 853 cm^{-1}; ESI-MS: *m/z* calcd for $C_{19}H_{21}N_5O_6$: 438.1 [M+Na]+; found 438.1.

(*E*)-*p*-[*p´*-(Isothiocyanatomethyl)phenylazo]phenyl α-D-mannopyranoside (6):

To a solution of the azide **5** (36.0 mg, 86.7 µmol) in dry dioxane (6.5 mL), first carbon disulfide (100 µL, 1.73 mmol) and then triphenylphosphin (25.0 mg, 95.4 µmol) were added. The reaction mixture was stirred for 16 h at room temperature. Then the solvent was evaporated and purification of the crude product by column chromatography (dichloromethane/methanol, 10:1) gave **6** as an orange solid (33.6 mg, 78.0 µmol, 90 %). R_f = 0.29 (dichloromethane/methanol, 9:1); m.p. 191 °C; $[\alpha]_D^{23}$ = +148.0 (c = 0.6 in dimethylsulfoxide); ^{1}H NMR (500 MHz, MeOH-d_4, 300 K): δ = 7.90-7.82 (m, 4H, Ar-H_{ortho}, Ar-$H_{ortho'}$), 7.48-7.46 (m, 2H, Ar-$H_{meta'}$), 7.29-7.27 (m, 2H, Ar-H_{meta}), 5.60 (d, $^3J_{1,2}$ = 1.8 Hz, 1H, H-1), 4.79 (s, 2H, CH_2NCS), 4.04 (dd, $^3J_{1,2}$ = 1.8 Hz, $^3J_{2,3}$ = 3.5 Hz, 1H, H-2), 3.93 (dd, $^3J_{2,3}$ = 3.5 Hz, $^3J_{3,4}$ = 9.5 Hz, 1H, H-3), 3.80-3.71 (m, 3H, H-4, H-6, H-6'), 3.59 (ddd, $^3J_{4,5}$ = 9.8 Hz, $^3J_{5,6}$ = 5.3 Hz, $^3J_{5,6'}$ = 2.4 Hz, 1H, H-5) ppm; ^{13}C NMR (500 MHz, MeOH-d_4, 300 K): δ = 193.7 (NCS), 160.3 (C-Ar_{para}), 153.2 (C-$Ar_{ipso'}$), 149.2 (C-Ar_{ipso}), 142.4 (C-$Ar_{para'}$), 129.4 (C-$Ar_{meta'}$), 125.5 (C-Ar_{ortho}), 123.8 (C-$Ar_{ortho'}$), 118.0 (C-Ar_{meta}), 100.1 (C-1), 75.7 (C-5), 72.4 (C-3), 71.9 (C-2), 68.3 (C-4), 62.7 (C-6), 49.3 (CH_2NCS) ppm; IR (ATR): $\tilde{\nu}$ = 2972, 2069, 1743, 1597 1496, 1365, 1213, 1126, 1026, 976, 851 cm^{-1}; UV-Vis (MeOH): λmax (ε) = 350 nm (17980 $Lmol^{-1}cm^{-1}$); ESI-MS: *m/z* calcd for $C_{20}H_{21}N_3O_6S$: 454.1 [M+Na]+; found 454.1.

UV-vis studies on azobenzene mannosides 8

For UV-vis spectroscopy, the *E*-configured azobenzene derivative was dissolved in methanol in a UV cuvette, irradiated for 60 s at 365 nm with a distance between LED and cuvette of ~5 cm. UV-vis spectra were recorded immediately afterwards. The absorption spectra (Figure 7.3.1) showed an increase of the absorbance in the n-π* transition and simultaneous decrease in the π-π* transition, indicating the formation of the respective *Z* isomer. Extinction coefficients (ε) were deduced from UV-vis spectra measured at seven different concentrations (5 µM, 10 µM, 20 µM, 40 µM, 60 µM, 70 µM and 80 µM).

Glass slide preparation

The mannosides **6** (43.0 mg, 100 µmol) was dried for 30 min in vacuum and afterwards dissolved in dry dimethylformamide (7 mL). Then molecular sieve 3 Å was added and the reaction mixture was stirred for 15 min at room temperature. Afterwards the silane **7** (30.0 mg, 100 µmol) was added and the reaction was again stirred for 16 h at room temperature. The silane **8** was diluted with dimethylformamide (13 mL) and immediately used for glass immobilization without purification.

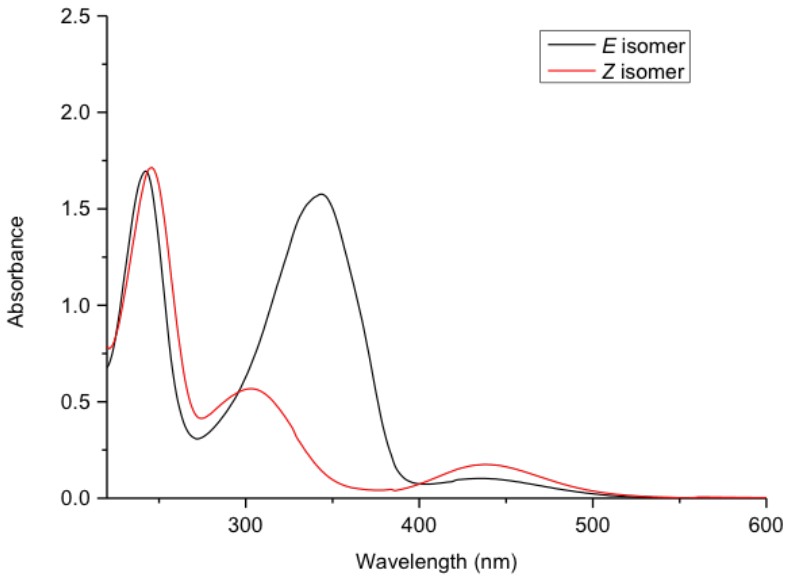

Figure 7.3.1: UV-vis spectra of **6**: *E* isomer in black, *Z* isomer in red; irradiation with 365 nm and 440 nm, respectively, in MeOH at 293 K.

Immobilization on quartz glass surfaces: Quartz glass slides were cleaned using piranha solution (conc. sulfuric acid : 35 % hydrogen peroxide, 3:1) for 16 h at room temperature. The slides were rinsed with water (2×) and methanol (2×) and dried under a nitrogen stream. Cleaned quartz slides were immersed in dimethylformamide (3 mL) and in the azobenzene silane coating solution (1 mL) for 16 h at 37 °C. Afterwards, the quartz slides were rinsed with dimethylformamide (2×) and methanol (2×) and then dried under a nitrogen stream.

UV-vis studies on surface assembly

UV-vis measurements were carried out on dried quartz slides using a slide holder. Irradiations at 365 nm and at 440 nm were carried out in the dark at room temperature and without removing the slides from the holder. For UV-vis spectroscopy, the functionalized glass slides were irradiated for 60 s at 365 nm with a distance between LED and the slide holder of ~5 cm. UV-vis spectra were recorded immediately afterwards. The absorption spectra showed an increase of the absorbance in the n-π* transition and simultaneous decrease in the π-π* transition, indicating the formation of the respective *Z* isomer. The coverslips were irradiated in cycles at $\lambda = 365$ nm and at $\lambda = 440$ nm, respectively for 60 s. Changes in absorbance were measured at 350 nm.

Half-life determination of immobilized azobenzene mannosides **8**: The kinetics of thermal $Z \rightarrow E$ relaxation process was determined using UV-vis spectroscopy at 20 °C in the dark. The half-life $\tau = 1/2$ was determined as $\tau_{1/2} = \ln 2/k$. After irradiation with $\lambda = 365$ nm for 60 s, the UV-Vis spectra of the quartz slide was recorded in regular intervals (30 min) over a period of 2 days. For the

determination of the half-life the changes in absorbance at 350 nm were plotted and an exponential decay of first order fitted to the data.

Contact angle measurements

Contact angle measurements were recorded on a Drop shape analyzer from Krüss GmbH and the contact angle was calculated using a Drop Shape Analysis DSA2 software.

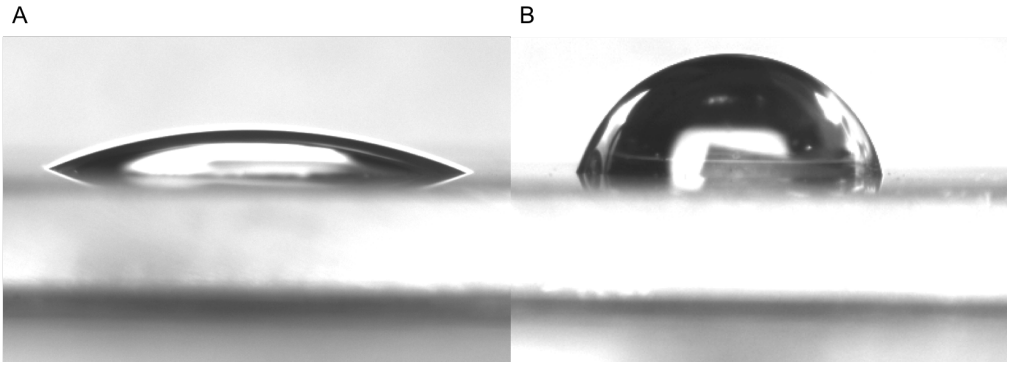

Figure 7.3.2: Contact angle measurements of the unfunctionalized quartz glass slide (A) compared to the azobenzene mannosides functionalized quartz glass slide (B). The contact angle increases from 26 ° up to 86 °.

Bacterial adhesion studies

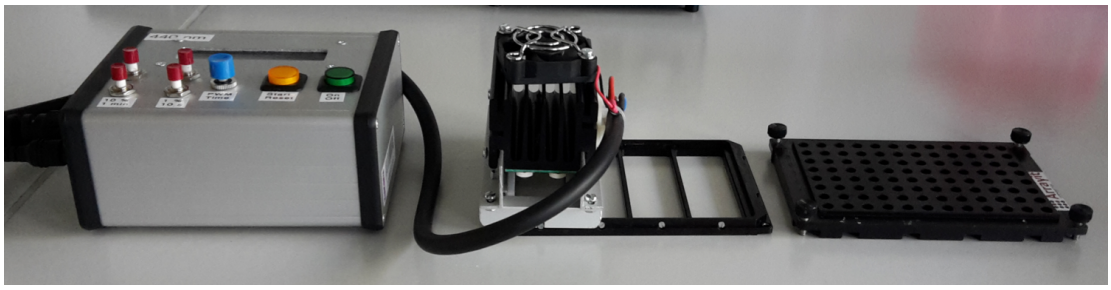

Figure 7.3.3: Setup for irradiation experiments. Glass slides were fixed in the microplate microarray cassette (Arrayit corporation, CA, USA). LEDs were arranged to exposure 1 quarter of the plate uniformly. Distance between glass slides and LED was 1 cm. Top of the plate (right) was added for adhesion of bacteria and the fluorescence readout in a microplate reader.

E. coli (strain PKL1162[77]) was inoculated in LB medium (10 mL) (Carl Roth, Karlsruhe, Germany) in presence of chloramphenicol (50 mg/L) and ampicillin (100 mg/L) (both Sigma-Aldrich) and grown at 37 °C overnight at 175 rpm. Then, the bacteria were centrifuged and washed two times with PBS (Thermo Fisher Scientific, Waltham, MA), suspended in PBS and the optical density at 600 nm was adjusted to 0.45.

The previously prepared glass slides were clamped in a 96-well microarray platform (Arrayit, Sunnyvale, CA) and were exposed in two switching cycles with 365 nm and 440 nm. Every exposure

was carried out for 1 min and 3750 mW (365 nm) or 2225 mW (440 nm). After every exposure one glass slide was taken away for analysis of bacterial adhesion.

The glass slides were incubated with 50 µL/well of the prepared bacterial suspension for 30 min at room temperature. Afterwards the slides were washed with PBS (3 x 100 µL/well) and the fluorescence readout (extinction 485 nm, emission 535 nm) was carried out.

Microscopic pictures of fluorescent *E. coli* bacteria

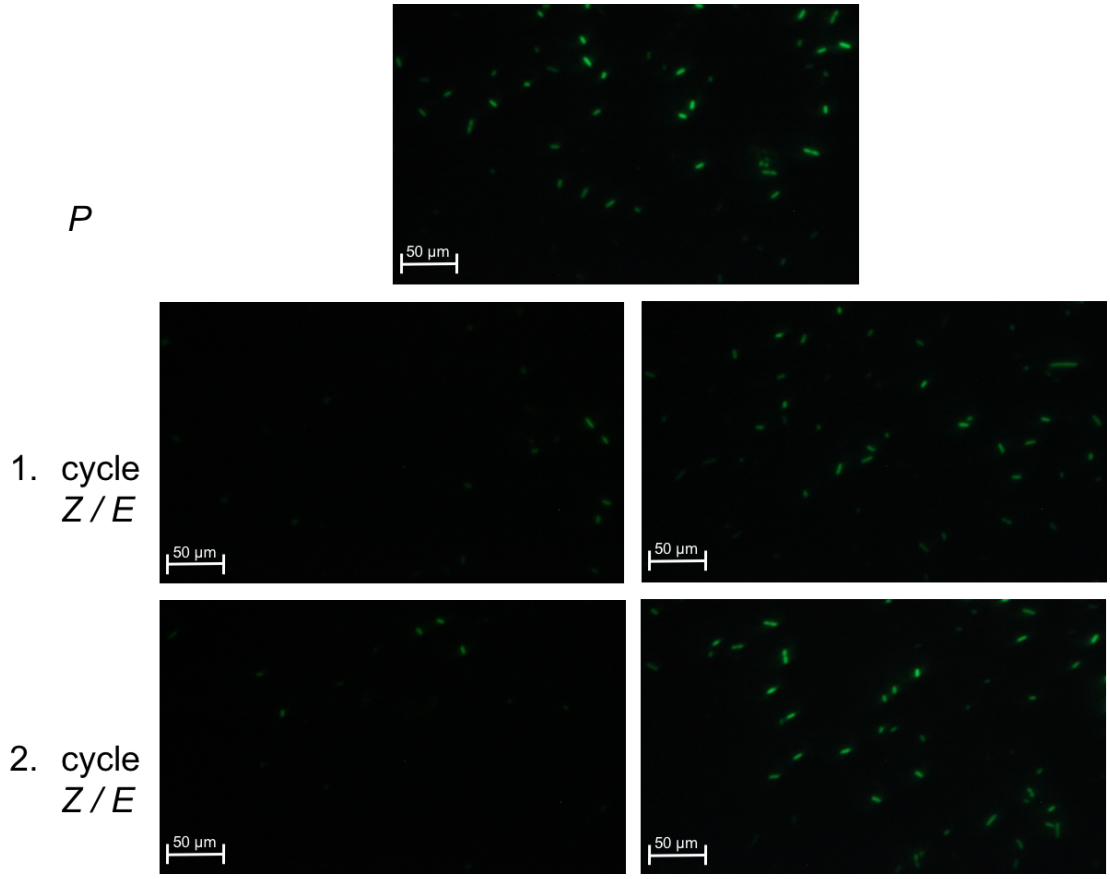

Figure 7.3.4: Adhesion of E. coli to Z and E-configured 8 on glass slides. Bacterial adhesion was additionally verified with fluorescence microscopy. The decrease of adhered E. coli can be seen in the left pictures in both switching cycles. Whereas in the right side the increased adhesion to *E* configured **5** can be seen.

7.4 Biological effects of a small difference: glycocluster chirality

Establishment of a flow assay for Bacterial Adhesion

Buffer solutions

PBS buffer: 140 mM sodium chloride, 2.7 mM potassium chloride, 10 mM sodium dihydrogen phosphate dihydrate, 1.8 mM potassium dihydrogen phosphate, 1 L ddH_2O, pH 7.2; carbonate buffer: sodium carbonate 15 mM, sodium hydrogen carbonate 30 mM, 1 L dd H_2O, pH 9.2; PBST: PBS buffer + 0.05 % v/v Tween®20.

Glass slide preparation

The glass slides (NEXTERION® Slide AL, Schott, Jena, Germany) were clamped in a microarray platform (Arrayit, Sunnyvale, CA) and functionalized with the respective glycosides (5 mM in PBS buffer) with 50 µL/well at room temperature for 1 h. The wells were washed with PBST (3x150 µL) and blocked with ethanolamine (10 mM in PBS) at room temperature for 1 h. Afterwards the wells were washed with PBS buffer (3x150 µL) and dried under nitrogen stream. A sticky-Slide $VI^{0.4}$(IBIDI, Martinsried, Germany) was sticked to the glass slide to receive six single flow chambers.

Bacterial culture

E. coli strain (PKL1167[77]) was incubated in LB medium (Carl Roth, Karlsruhe, Germany) with ampicillin (100 mg/L) and chloramphenicol (50 mg/L, both Sigma-Aldrich) at 37 °C and 175 rpm over night. The bacteria were centrifuged and washed two times with PBS (Thermo Fisher Scientific, Waltham, MA), suspended in PBS and the optical density at 600 nm was adjusted to 0.6.

Flow assay

The previously prepared flow chambers were connected via luer with a syringe pump (HLL Landgraf, Langenhagen, Germany) and the bacterial suspension was channeled through the chambers (100 µL/min, 500 µL). Afterwards the unbound bacteria were removed by washing with PBS (100 µL/min, 100 µL). The flow chamber was clamped again in the microarray platform and a fluorescence readout was performed.

7.5 Applied tensile force determines lectin specificity

General synthetic and analytical methods

Thin layer chromatography was performed on silica gel plates (GF 254, Merck). Detection was effected by charring with sulfuric acid /ethanol solution and ninhydrine solution (300 mg ninhydrine, dissolved in 100 mL butanol and 3 mL conc. acetic acid), both followed by heat treatment. Flash chromatography was performed on a Biotage Isolera™ Flash Purification System with normal-phase (KP-Sil) or reversed-phase (KP-C18-HS) silica gel SNAP cartridges using distilled solvents. Optical rotations were measured with a Perkin–Elmer 241 polarimeter (sodium D-line: 589 nm, length of cell: 1 dm). ^{1}H and ^{13}C NMR spectra were recorded with a Bruker DRX-500 spectrometer. Chemical shifts are reported relative to internal MeOD (δ = 3.31 ppm), D_2O (δ = 4.79 ppm), or $CDCl_3$ (δ = 7.26 ppm). ESI mass spectra were recorded on an Applied Biosystems (Applera) Mariner ESI-TOF system. Commercial reagents were used without purification unless otherwise noted.

Synthesis

General procedure for acetylation

The glycoside to be acetylated was dissolved in pyridine (5-6 mL for 1 g of glycoside), acetic anhydride (10 eq) was added and the mixture was stirred at ambient temperature until the reaction was complete. The mixture was evaporated, co-distilled with toluene twice and the crude product was purified by flash chromatography (ethyl acetate/methanol, 15:1).

General procedure for *O*-deacetylation[286]

The acetylated compound was dissolved in dry methanol (10 mL/g), and freshly prepared sodium methoxide solution (2 mL, 1 M in methanol) was added under nitrogen. The reaction mixture was stirred at ambient temperature until the reaction was complete (minimum 4 h, maximum overnight), then it was neutralized by the addition of Amberlite IR 120 (H+), filtered, and the solution was concentrated under reduced pressure.

General procedure for catalytic hydrogenation of *p*-aminophenyl aglycone

p-Nitrophenyl α-D-pyranoside (500 mg, 1.84 mmol) and a catalytic amount of palladium on charcoal were dissolved in methanol (5.00 mL). The mixture was stirred in a hydrogen atmosphere at ambient temperature for 4 h. The catalyst was removed by filtration over a syringe filter (0.45 µm mesh), solvents were removed in vacuo, and the crude product was purified by filtration over silica gel. The slightly acidic product was neutralized by addition of Dowex 1 anion exchanger and subsequent filtration over a syringe filter (0.45 µm).

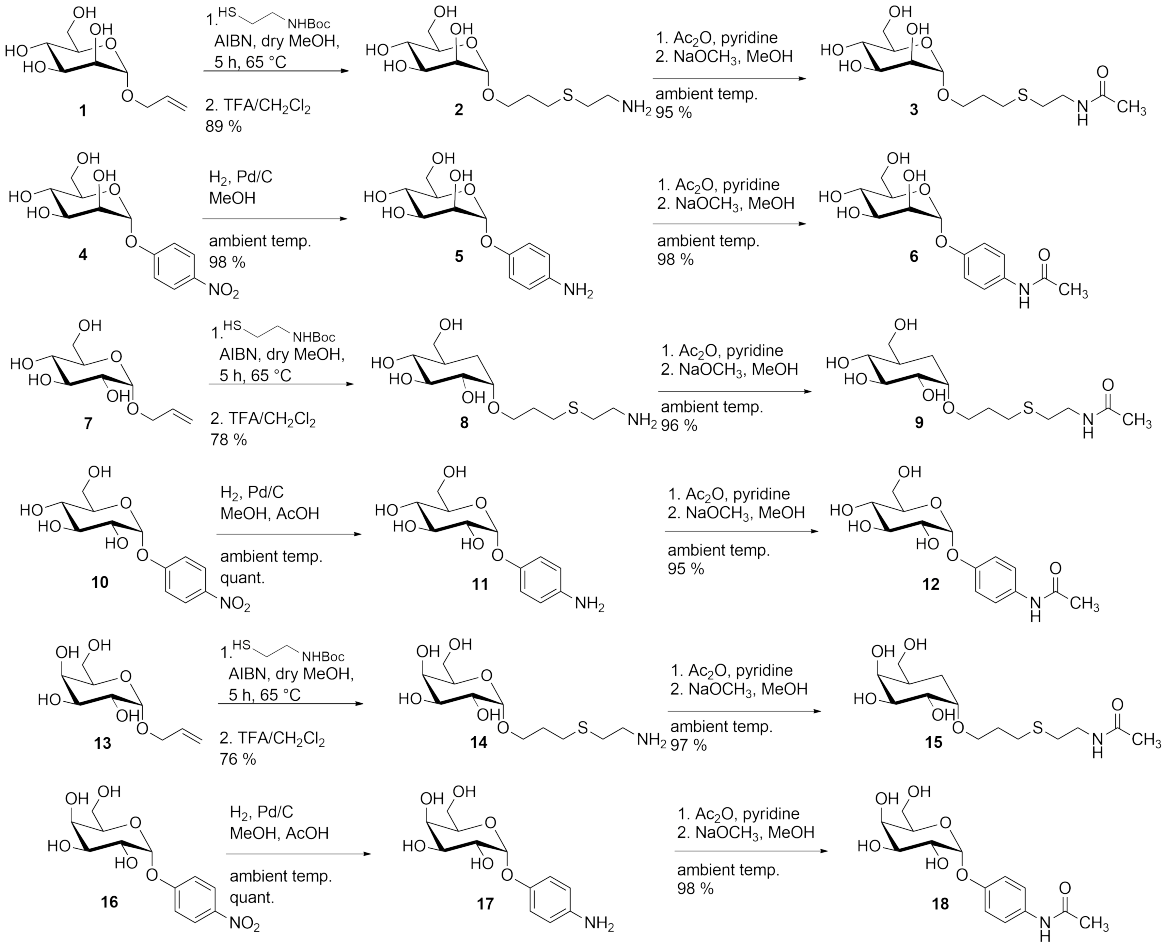

Scheme 7.5.1: Overview of all synthesized molecules. Amino group containing sugars were needed for covalent functionalization of the cantilever tips. Acetylated derivatives were needed for biological assays. Mannosides **5**[301] **6**[302], Glucosides **11**[303], **12**[304] and Galactosides **17**, **18**[305] were synthesized according to known procedures.

***N*-tert-butoxycarbonyl-6-amino-4-thiahexyl-α-D-mannopyranoside:**

Allyl-α-D-mannopyranoside (**1**, 800 mg, 3.63 mmol), *N*-tert-Butoxycarbonyl-cysteamine (2.57 g, 14.52 mmol), and a catalytic amount of 2,2'-azobis(isobutyronitrile) (AIBN) were dissolved in dry methanol (15 mL). The reaction mixture was heated up to 65 °C and stirred at this temperature for 6 h. After removal of the solvent in vacuo the crude product has been purified by column chromatography ($CHCl_3$/methanol, 5:1) and the pure product was obtained as colourless syrup (1.23 g, 3.23 mmol, 89 %). R_f = 0.2 (chloroform/methanol, 6:1); $[\alpha]_D^{23}$ = +16 (c = 0.5, in methanol); ^{1}H NMR (500 MHz, MeOD, 300 K): δ = 4.81 (d, 1H, $^3J_{1,2}$ = 3.7 Hz, H-1), 3.89-3.81 (m, 2H, OC*H*HCH$_2$, H-6), 3.74-3.63 (m, 3H, H-2, H-3, H-6'), 3.62-3.58 (m, 1H, H-4), 3.58-3.54 (m, 1H, OCH*H*CH$_2$), 3.43-3.41 (m, 1H, H-5), 3.25 (t, 2H, ^3J = 7.2 Hz, CH$_2$C*H*$_2$NH), 2.71 (t, 2H, ^3J = 7.1 Hz, OCH$_2$CH$_2$C*H*$_2$S), 2.63 (t, 2H, ^3J = 7.2 Hz, C*H*$_2$CH$_2$NH), 1.89-1.81 (m, 2H, OCH$_2$C*H*$_2$CH$_2$S), 1.47 (s, 9H, C(O)OC(CH$_3$)$_3$) ppm; ^{13}C NMR (125 MHz, MeOD, 300 K): δ = 100.2 (C-1), 80.1 (C(O)O*C*(CH$_3$)$_3$), 75.1 (C-5), 73.7 (C-3), 73.6 (C-2), 71.8 (C-4), 67.4 (O*C*H$_2$CH$_2$), 62.7

(C-6), 41.3 ($CH_2CH_2NH_2$), 32.5 ($CH_2CH_2NH_2$), 30.7 ($OCH_2CH_2CH_2$), 29.3 ($OCH_2CH_2CH_2$), 28.7 ($C(O)OC(CH_3)_3$) ppm; ESI-MS: *m/z* = calcd for $C_{11}H_{23}NO_6S$ [M+H]+: 420.154, found: 420.156.

6-Amino-4-thiahexyl α-D-mannopyranoside (2):

N-tert-Butoxycarbonyl-6-amino-4-thiahexyl-α-D-mannopyranoside (1.20 g, 3.15 mmol) has been dissolved in dichloromethane (30 mL) and trifluoroacetic acid (9 mL) and stirred at ambient temperature for 30 min. After removal of the solvent in vacuo the product was obtained as a slightly yellow syrup (940 mg, 3.15 mmol, quant.). All spectral data were in good accordance with reported data.[77]

6-Acetamido-4-thiahexyl 2,3,4,6-tetra-*O*-acetyl-α-D-mannopyranoside:

6-Amino-4-thiahexyl α-D-mannopyranoside (**2**, 440 mg, 1.48 mmol) was treated according to the general procedure for acetylation. The crude product was purified by flash chromatography (ethyl acetate/methanol, 15:1). The pure product was obtained as yellow oil (730 mg, 1.44 mmol, 97 %). R_f= 0.3 (ethyl acetate/methanol, 7:1); $[\alpha]_D^{23}$ = +125 (c = 0.5, in methanol); ^{1}H NMR (500 MHz, $CDCl_3$): δ = 5.29 (dd, 1H, $^3J_{2,3}$ = 3.4 Hz, $^3J_{3,4}$ = 10.1 Hz, H-3), 5.24 (dd, 1H, $^3J_{3,4}$ = 10.1 Hz, $^3J_{4,5}$ = 10.1 Hz, H-4), 5.19 (dd, 1H, $^3J_{1,2}$ = 1.8 Hz, $^3J_{2,3}$ = 3.4 Hz, H-2), 4.78 (d, 1H, $^3J_{1,2}$ = 1.8 Hz, H-1), 4.23 (dd, 1H, $^3J_{5,6}$ = 5.4 Hz, $^2J_{6,6'}$ = 12.2 Hz, H-6) 4.11-4.06 (m, 1H, H-6'), 3.98-3.94 (m, 1H, H-5), 3.80-3.76 (m, 1H, $OCHHCH_2CH_2$), 3.53-3.49 (m, 1H, $OCHHCH_2CH_2$), 3.42-3.38 (m, 2H, CH_2CH_2NH), 2.64 (t, 2H, $^3J_{CH_2,CH_2}$ = 6.6 Hz, CH_2CH_2NH), 2.60 (t, 2H, $^3J_{CH_2,CH_2}$ = 7.1 Hz, $OCH_2CH_2CH_2S$), 2.12 (s, 3H, $OC(O)CH_3$), 2.07 (s, 3H, $OC(O)CH_3$), 2.01 (s, 3H, $OC(O)CH_3$), 1.93 (s, 6H, $OC(O)CH_3$, $NHC(O)CH_3$), 1.90-1.82 (m, 2H, $OCH_2CH_2CH_2$); ^{13}C NMR (125 MHz, $CDCl_3$): δ = 170.7, 170.4, 170.2, 170.1, 169.8 (5 C, $C(O)CH_3$), 97.6 (C-1), 69.7 (C-2), 69.2 (C-3), 68.7 (C-5), 66.5 ($OCH_2CH_2CH_2S$), 66.3 (C-4), 62.6 (C-6), 38.7 (CH_2CH_2NH), 31.9 (CH_2CH_2NH), 29.1 ($OCH_2CH_2CH_2$), 28.4 ($OCH_2CH_2CH_2$), 23.2 ($NHC(O)CH_3$), 20.9, 20.8, 20.8, 20.8 (4C, $OC(O)CH_3$) ppm; ESI-MS: *m/z* = calcd. for $C_{21}H_{33}NO_{11}S$ [M+Na]+: 530.167, found: 530.165.

6-Acetamido-4-thiahexyl α-D-mannopyranoside (3):

6-Acetamido-4-thiahexyl 2,3,4,6-tetra-O-acetyl-α-D-mannopyranoside (720 mg, 1.42 mmol) was treated according to the general procedure for *O*-deacetylation. The pure product was obtained as colorless syrup (477 mg, 1.41 mmol, 99 %). R_f= 0.2 (ethyl acetate/methanol, 4:1); $[\alpha]_D^{23}$ = +86 (c = 0.5, in methanol); ^{1}H NMR (500 MHz, D_2O, 300 K): δ = 4.89 (d, 1H, $^3J_{1,2}$ = 1.8 Hz, H-1), 3.97 (dd, 1H, $^3J_{1,2}$ = 1.8 Hz, $^3J_{2,3}$ = 3.4 Hz, H-2), 3.92 (dd, 1H, $^3J_{5,6}$ = 1.7 Hz, $^3J_{6,6'}$ = 12.3 Hz, H-6), 3.87-3.77 (m, 3H, H-3, H-6', $OCHHCH_2CH_2$), 3.71-3.61 (m, 3H, H-4, H-5, $OCHHCH_2CH_2$), 3.42 (t, 2H, $^3J_{CH_2,CH_2}$ = 6.6 Hz, CH_2CH_2NH), 2.4 (t, 2H, $^3J_{CH_2,CH_2}$ = 6.6 Hz, CH_2CH_2NH), 2.70 (dt, 2H, $^3J_{CH_2,CH_2}$ = 2.6 Hz, $^2J_{CH,CH'}$ = 7.3 Hz, $OCH_2CH_2CH_2$), 2.03 (s, 3H, $C(O)CH_3$), 2.00-1.87 (m, 2H, $OCH_2CH_2CH_2S$); ^{13}C NMR (125 MHz, D_2O, 300 K): δ = 174.2 ($NHC(O)CH_3$), 99.8 (C-1), 72.8 (C-5), 70.6 (C-3), 70.1 (C-2), 66.7 (C-4), 66.1 ($OCH_2CH_2CH_2$), 60.9 (C-6), 38.7 (CH_2CH_2NH), 30.5 (CH_2CH_2NH), 28.5 ($OCH_2CH_2CH_2$), 27.8 ($OCH_2CH_2CH_2$), 21.9 ($C(O)CH_3$) ppm; ESI-MS: *m/z* = calcd for $C_{13}H_{25}NO_7S$ [M+Na]+: 362.124. Found: 362.124.

_p_-Acetamidophenyl 2,3,4,6-tetra-_O_-acetyl-α-D-mannopyranoside:

_p_-Aminophenyl α-D-mannopyranoside (**5**, 372 mg, 1.37 mmol) was treated according to the general procedure for acetylation. The crude product was obtained as yellow oil (660 mg, 1.37 mmol, quant.). R_f= 0.6 (ethyl acetate/methanol, 5:1); m.p. 149 °C; $[\alpha]_D^{23}$ = +14 (c = 0.5, in methanol); ^{1}H NMR (500 MHz, $CDCl_3$, 300 K): δ = 7.43-7.40 (m, 2H, Aryl-H_{ortho}), 7.02-6.98 (m, 2H, Aryl-H_{meta}), 5.52 (dd, 1H, $^3J_{2,3}$ = 3.5 Hz, $^3J_{3,4}$ = 10.0 Hz, H-3), 5.44 (d, 1H, $^3J_{1,2}$ = 1.8 Hz, H-1), 5.41 (dd, 1H, $^3J_{1,2}$ = 1.8 Hz, $^3J_{2,3}$ = 3.5 Hz, H-2), 5.33 (dd≈t, 1H, $^3J_{3,4}$ = 10.0 Hz, $^3J_{4,5}$ = 10.0 Hz, H-4), 4.25 (dd, 1H, $^3J_{5,6}$ = 5.6 Hz, $^2J_{6,6'}$ = 12.4 Hz, H-6), 4.09-4.04 (m, 2H, H-5, H-6'), 2.17 (s, 3H, OC(O)CH_3), 2.14 (s, 3H, NHC(O)CH_3), 2.03 (s, 3H, OC(O)CH_3), 2.02 (s, 3H, OC(O)CH_3), 2.01 (s, 3H, OC(O)CH_3); ^{13}C NMR (125 MHz, $CDCl_3$, 300 K): δ = 170.8 (NHC(O)CH_3), 170.1, 170.1, 169.9, 168.8 (OC(O)CH_3), 152.2 (Aryl-C_{ipso}), 133.4 (Aryl-C_{para}), 121.7 (Aryl-C_{ortho}), 117.1 (Aryl-C_{meta}), 96.2 (C-1), 69.5 (C-2), 69.2 (C-5), 69.0 (C-3), 66.1 (C-4), 62.3 (C-6), 24.3 (NHC(O)CH$_3$), 20.9, 20.8, 20.8, 20.8 (4C, OC(O)CH$_3$) ppm; ESI-MS: _m/z_ = calcd for $C_{22}H_{27}NO_{11}$ [M+Na]+: 504.148. Found: 504.148.

_N_-Acetyl-_p_-aminophenyl α-D-mannopyranoside (6):

_p_-Acetamidophenyl 2,3,4,6-tetra-_O_-acetyl-α-D-mannopyranoside (600 mg, 1.25 mmol) treated according to the general procedure for _O_-deacetylation. The pure product was obtained after silica gel chromatography (ethyl acetate/methanol, 4:1) as a white lyophilisate (390 mg, 1.25 mmol, quant.). R_f= 0.3 (ethyl acetate/methanol, 5:1); m.p. 78 °C; $[\alpha]_D^{23}$ = +70 (c = 0.5, in methanol); ^{1}H NMR (500 MHz, MeOD, 300 K): δ = 7.46-7.42 (m, 2H, CHC(O)CH), 7.08-7.05 (m, 2H, CHC(NH)CH), 5.42 (d, 1H, $^3J_{1,2}$ = 1.9 Hz, H-1), 3.99 (dd, 1H, $^3J_{1,2}$ = 1.9 Hz, $^3J_{2,3}$ = 3.4 Hz, H-2), 3.89 (dd, 1H, $^3J_{2,3}$ = 3.4 Hz, $^3J_{3,4}$ = 9.4 Hz, H-3) 3.78-3.70 (m, 3H, H-4, H-6, H-6'), 3.63-3.59 (m, 1H, H-5), 2.09 (s, 3H, NHC(O)CH_3); ^{13}C NMR (125 MHz, MeOD, 300 K): δ = 171.4 (NHC(O)CH_3), 154.5 (Aryl-C_{ipso}), 134.5 (Aryl-C_{para}), 122.8 (Aryl-C_{ortho}), 118.1 (Aryl-C_{meta}), 100.5 (C-1), 75.3 (C-5), 72.4 (C-3), 72.0 (C-2), 68.4 (C-4), 62.7 (C-6), 23.6 (C(O)CH$_3$) ppm; ESI-MS: _m/z_ = calcd for $C_{14}H_{19}NO_7$ [M+Na]+: 336.105. Found: 336.102.

_N_-tert-Butoxycarbonyl-6-amino-4-thiahexyl-α-D-glucopyranoside:

Allyl-α-D-glucopyranoside (**7**, 370 mg, 1.72 mmol), _N_-tert-Butoxycarbonyl-cysteamine (1.22 g, 6.89 mmol), and a catalytic amount of 2,2'-azobis(isobutyronitrile) (AIBN) were dissolved in dry methanol (15 mL). The reaction mixture was heated up to 65 °C and stirred at this temperature for 6 h. After removal of the solvent in vacuo the crude product has been purified by column chromatography ($CHCl_3$/methanol, 5:1) and the pure product was obtained as colorless syrup (533 mg, 1.34 mmol, 78 %). R_f= 0.2 (chloroform/methanol, 5:1); $[\alpha]_D^{23}$ = +41 (c = 0.5, in methanol); ^{1}H NMR (500 MHz, MeOD, 300 K): δ = 4.79 (d, 1H, $^3J_{1,2}$ = 3.7 Hz, H-1), 3.87-3.81 (m, 2H, OCHHCH$_2$, H-6), 3.71-3.64 (m, 3H, H-2, H-3, H-6'), 3.63-3.53 (m, 1H, H-4), 3.53-3.45 (m, 1H, OCHHCH$_2$), 3.41-3.40 (m, 1H, H-5), 3.22 (t, 2H, ^3J = 7.1 Hz, CH$_2$CH_2NH), 2.68-2.66 (m, 2H, OCH$_2$CH$_2$CH_2), 2.61 (t, 2H, ^3J = 7.2 Hz, CH_2CH$_2$NH$_2$), 1.97-1.86 (m, 2H, OCH$_2$CH_2CH$_2$), 1.45 (s, 9H, C(O)OC(CH_3)$_3$); ^{13}C NMR (125 MHz, MeOD, 300 K): δ = 100.2 (C-1), 80.1 (C(O)OC(CH$_3$)$_3$),

75.1 (C-5), 73.7 (C-3), 73.6 (C-2), 71.8 (C-4), 67.4 (O*C*H$_2$CH$_2$CH$_2$), 62.7 (C-6), 41.3 (CH$_2$*C*H$_2$NH$_2$), 32.5 (*C*H$_2$CH$_2$NH$_2$), 30.7 (OCH$_2$*C*H$_2$CH$_2$), 29.3 (OCH$_2$CH$_2$*C*H$_2$), 28.8 (C(O)OC(*C*H$_3$)$_3$) ppm; ESI-MS: *m/z* = calcd for $C_{16}H_{30}NO_8S$ [M+Na]+: 420.154. Found: 420.151.

6-Amino-4-thiahexyl α-D-glucopyranoside (8):

N-tert-Butoxycarbonyl-6-amino-4-thiahexyl-α-D-galactopyranoside (520 mg, 1.31 mmol) has been dissolved in dichloromethane (30 mL) and TFA (9 mL) and stirred at ambient temperature for 30 min. After removal of the solvent in vacuo product was obtained as a colorless syrup (390 mg, 1.31 mmol, quant.). All spectral data were in good accordance with reported data.[306]

6-Acetamido-4-thiahexyl 2,3,4,6-tetra-*O*-acetyl-α-D-glucopyranoside:

6-Amino-4-thiahexyl α-D-glucopyranoside (**8**, 340 mg, 1.14 mmol) was treated according to the general procedure for acetylation. The crude product was purified by flash chromatography (ethyl acetate/methanol, 15:1). The pure product was obtained as colorless oil (553 mg, 1.09 mmol, 96 %). R_f= 0.2 (ethyl acetate/methanol, 7:1); $[\alpha]_D^{23}$ = +133 (c = 0.5, in methanol); ^{1}H NMR (500 MHz, $CDCl_3$, 300 K): δ = 5.47 (dd, 1H, $^3J_{3,4}$ = 9.4 Hz, $^3J_{2,3}$ = 10.1 Hz, H-3), 5.07 (d, 1H, $^3J_{1,2}$ = 4.1 Hz, H-1), 5.05 (dd, 1H, $^3J_{3,4}$ = 9.4 Hz, $^3J_{4,5}$ = 10.4 Hz, H-4), 4.87 (dd, 1H, $^3J_{1,2}$ = 4.1 Hz, $^3J_{2,3}$ = 10.1 Hz, H-2), 4.25 (dd, 1H, $^3J_{5,6}$ = 4.6 Hz, $^3J_{6,6'}$ = 12.2 Hz, H-6), 4.12 (dd, 1H, $^3J_{5,6'}$ = 2.4 Hz, $^3J_{6,6'}$ = 12.2 Hz, H-6'), 4.05-4.00 (m, 1H, H-5), 3.84-3.78 (m, 1H, OC*H*HCH$_2$CH$_2$), 3.56-3.49 (m, 1H, OCH*H*CH$_2$CH$_2$), 3.47-3.41 (m, 2H, CH$_2$C*H*$_2$NH), 2.67 (t, 2H, $^3J_{CH_2,CH_2}$ = 6.4 Hz, C*H*$_2$CH$_2$NH) 2.65-2.61 (m, 2H, OCH$_2$CH$_2$C*H*$_2$S), 2.09 (s, 3H, C(O)C*H*$_3$), 2.07 (s, 3H, C(O)C*H*$_3$), 2.03 (s, 3H, C(O)C*H*$_3$), 2.02 (s, 3H, C(O)C*H*$_3$), 2.01 (s, 3H, NHC(O)C*H*$_3$), 1.93-1.87 (m, 2H, OCH$_2$C*H*$_2$CH$_2$); ^{13}C NMR (125 MHz, $CDCl_3$): δ = 170.7, 170.3, 170.2, 170.1, 169.6 (5 C, *C*(O)CH$_3$), 95.8 (C-1), 70.9 (C-2), 70.1 (C-3), 68.6 (C-4), 67.3 (C-5), 66.6 (C-6), 61.92 (O*C*H$_2$CH$_2$CH$_2$S), 38.6 (CH$_2$*C*H$_2$NH), 31.7 (*C*H$_2$CH$_2$NH), 29.0 (OCH$_2$*C*H$_2$CH$_2$), 28.1 (OCH$_2$CH$_2$*C*H$_2$), 23.2 (NHC(O)*C*H$_3$), 20.7, 20.7, 20.7, 20.6 (4C, OC(O)*C*H$_3$) ppm; ESI-MS: *m/z* = calcd for $C_{21}H_{33}NO_{11}S$ [M+Na]+: 530.167. Found: 530.165.

6-Acetamido-4-thiahexyl α-D-glucopyranoside (9):

6-Acetamido-4-thiahexyl 2,3,4,6-tetra-*O*-acetyl-α-D-glucopyranoside (553 mg, 1.09 mmol) was treated according to the general procedure for *O*-deacetylation. The pure product was obtained as colorless syrup (370 mg, 1.09 mmol, quant.). R_f= 0.2 (ethyl acetate/methanol, 4:1); $[\alpha]_D^{23}$ = +94 (c = 0.5, in methanol); ^{1}H NMR (500 MHz, MeOD, 300 K): δ = 4.81 (d, 1H, $^3J_{1,2}$ = 3.74 Hz, H-1), 3.89-3.85 (m, 1H, OC*H*HCH$_2$CH$_2$), 3.84 (dd, 1H, $^3J_{5,6}$ = 2.3 Hz, $^3J_{6,6'}$ = 11.8 Hz, H-6), 3.73-3.64 (m, 2H, H-6', H-3), 3.63-3.53 (m, 2H, H-5, OCH*H*CH$_2$CH$_2$), 3.42 (dd, 1H, $^3J_{1,2}$ = 3.74 Hz, $^3J_{2,3}$ = 9.71 Hz, H-2), 3.39-3.36 (m, 3H, CH$_2$C*H*$_2$NH, H-4), 2.72 (dt, 2H, $^3J_{CH_2,CH_2}$ = 1.8 Hz, $^2J_{CH,CH'}$ = 7.4 Hz, OCH$_2$CH$_2$C*H*$_2$), 2.67 (t, 2H, $^3J_{CH_2,CH_2}$ = 7.1 Hz, C*H*$_2$CH$_2$NH), 1.97 (s, 3H, C(O)C*H*$_3$), 1.96-1.88 (m, 2H, OCH$_2$C*H*$_2$CH$_2$); ^{13}C NMR (125 MHz, MeOD, 300 K): δ = 173.3 (NH*C*(O)CH$_3$), 100.2 (C-1), 75.1 (C-5), 73.7 (C-3), 73.6 (C-2), 71.8 (C-4), 67.4 (O*C*H$_2$CH$_2$CH$_2$), 62.7 (C-6), 40.3 (CH$_2$*C*H$_2$NH), 32.0 (*C*H$_2$CH$_2$NH), 30.7 (OCH$_2$*C*H$_2$CH$_2$), 29.3 (OCH$_2$CH$_2$*C*H$_2$), 22.5 (C(O)*C*H$_3$) ppm; ESI-MS: *m/z* = calcd for $C_{13}H_{25}NO_7S$ [M+Na]+: 362.124. Found: 362.123.

p-Acetamidophenyl 2,3,4,6-tetra-*O*-acetyl-α-D-glucopyranoside:

p-Aminophenyl α-D-glucopyranoside (**11**, 285 mg, 1.05 mmol) was treated according to the general procedure for acetylation. The crude product was obtained as yellow oil (498 mg, 1.04 mmol, 99 %). R_f= 0.7 (ethyl acetate/methanol, 5:1); m.p. 131 °C; $[\alpha]_D^{23}$ = +77 (c = 0.5, in methanol); ^{1}H NMR (500 MHz, $CDCl_3$, 300 K): δ = 7.43-7.41 (d, 2H, Aryl-H$_{ortho}$), 7.05-7.02 (m, 2H, Aryl-H$_{meta}$), 5.68 (dd, 1H, $^3J_{2,3}$ = 9.6 Hz, $^3J_{3,4}$ = 10.0 Hz, H-3), 5.67 (d, 1H, $^3J_{1,2}$ = 3.4 Hz, H-1), 5.15 (dd, 1H, $^3J_{3,4}$ = 10.1 Hz, $^3J_{4,5}$ = 9.8 Hz, H-4), 5.02 (dd, 1H, $^3J_{1,2}$ = 3.6 Hz, $^3J_{2,3}$ = 10.1 Hz, H-2), 4.25 (dd, 1H, $^3J_{5,6}$ = 4.6 Hz, $^2J_{6,6'}$ = 12.3 Hz, H-6), 4.12 (ddd, 1H, $^3J_{4,5}$ = 10.4 Hz, $^3J_{5,6}$ = 4.6 Hz, $^3J_{5,6'}$ = 2.2 Hz, H-5), 4.06 (dd, 1H, $^3J_{5,6'}$ = 2.3 Hz, $^2J_{6,6'}$ = 12.2 Hz, H-6'), 2.16 (s, 3H, C(O)CH_3), 2.07 (s, 3H, C(O)CH_3), 2.06 (s, 3H, C(O)CH_3), 2.05 (s, 3H, C(O)CH_3), 2.03 (s, 3H, C(O)CH_3); ^{13}C NMR (125 MHz, $CDCl_3$, 300 K): δ = 176.7 (NHC(O)CH_3), 170.6 (C(O)CH_3), 170.1 (C(O)CH_3), 169.6 (C(O)CH_3), 168.2 (C(O)CH_3), 152.7 (Aryl-C$_{ipso}$), 133.2 (Aryl-C$_{para}$), 121.7 (Aryl-C$_{ortho}$), 117.1 (Aryl-C$_{meta}$), 94.62 (C-1), 70.5 (C-2), 70.0 (C-4), 68.3 (C-3), 68.0 (C-5), 61.6 (C-6), 24.4 (NHC(O)CH$_3$), 20.7 (C(O)CH$_3$), 20.7 (C(O)CH$_3$), 20.6 (C(O)CH$_3$), 20.6 (C(O)CH$_3$) ppm; ESI-MS: *m/z* = calcd for $C_{22}H_{27}NO_{11}$ [M+Na]+: 504.148. Found: 504.147.

p-Acetamidophenyl α-D-glucopyranoside (12):

p-Acetamidophenyl 2,3,4,6-tetra-*O*-acetyl-α-D-glucopyranoside (480 mg, 1.01 mmol) was treated according to the general procedure for *O*-deacetylation. The pure product was obtained after silica gel chromatography (ethyl acetate/methanol, 4:1) as white lyophilisate (304 mg, 0.97 mmol, 96 %). R_f= 0.3 (ethyl acetate/methanol, 5:1); m.p. 195 °C; $[\alpha]_D^{23}$ = +131 (c = 0.5, in methanol); ^{1}H NMR (500 MHz, MeOD, 300 K): δ = 7.46-7.43 (m, 2H, CHC(O)CH), 7.14-7.11 (m, 2H, CHC(NH)CH), 5.42 (d, 1H, $^3J_{1,2}$ = 3.6 Hz, H-1), 3.84 (dd≈t, 1H, $^3J_{2,3}$ = 9.4 Hz, $^3J_{3,4}$ = 9.4 Hz, H-3), 3.75 (dd, 1H, $^3J_{5,6}$ = 2.6 Hz, $^2J_{6,6'}$ = 14.2 Hz, H-6), 3.71-3.65 (m, 2H, H-5, H-6'), 3.55 (dd, 1H, $^3J_{1,2}$ = 3.6 Hz, $^3J_{2,3}$ = 9.4 Hz, H-2), 3.42 (dd, 1H, $^3J_{4,5}$ = 9.1 Hz, $^3J_{3,4}$ = 9.4 Hz, H-4), 2.10 (s, 3H, NHC(O)CH_3); ^{13}C NMR (125 MHz, MeOD, 300 K): δ = 171.4 (NHC(O)CH_3), 155.2 (Aryl-C$_{ipso}$), 134.5 (Aryl-C$_{para}$), 122.7 (Aryl-C$_{ortho}$), 118.5 (Aryl-C$_{meta}$), 99.7 (C-1), 75.0 (C-3), 74.4 (C-5), 73.3 (C-2), 71.5 (C-4), 62.4 (C-6), 23.6 (C(O)CH$_3$) ppm; ESI-MS: *m/z* = calcd for $C_{22}H_{27}NO_{11}$ [M+Na]+: 336.105. Found: 336.102.

***N*-tert-Butoxycarbonyl-6-amino-4-thiahexyl-α-D-galactopyranoside:**

Allyl-α-D-galactopyranoside (**13**, 500 mg, 2.27 mmol), *N*-tert-Butoxycarbonyl-cysteamine (1.55 g, 8.71 mmol), and a catalytic amount of 2,2'-azobis(isobutyronitrile) (AIBN) were dissolved in dry methanol (25 mL). The reaction mixture was heated up to 65 °C and stirred at this temperature for 6 h. After removal of the solvent in vacuo the crude product has been purified by column chromatography ($CHCl_3$/methanol, 5:1) and the pure product was obtained as colourless syrup (700 mg, 1.77 mmol, 78 %). R_f= 0.2 (chloroform/methanol, 4:1); $[\alpha]_D^{23}$ = +85 (c = 0.5, in methanol); ^{1}H NMR (500 MHz, MeOD, 300 K): δ = 4.82 (d, 1H, $^3J_{1,2}$ = 3.3 Hz, H-1), 3.86-3.81 (m, 2H, OCHHCH_2, H-6), 3.76-3.70 (m, 3H, H-2, H-3, H-6'), 3.57-3.53 (m, 1H, H-4), 3.53-3.45 (m, 1H, OCHHCH2), 3.42-3.40 (m, 1H, H-5), 3.22 (t, 2H, ^3J = 7.2 Hz, CH_2CH_2NH), 2.67 (t, 2H, ^3J = 7.1 Hz,

$OCH_2CH_2CH_2$), 2.61 (t, 2H, ^3J = 7.3 Hz, $CH_2CH_2NH_2$), 1.98-1.85 (m, 2H, $OCH_2CH_2CH_2$), 1.45 (s, 9H, $C(O)OC(CH_3)_3$); ^{13}C NMR (125 MHz, MeOD, 300 K): δ = 100.4 (C-1), 80.1 ($C(O)OC(CH_3)_3$), 76.6 (C-5), 72.6 (C-3), 72.4 (C-2), 71.1 (C-4), 67.6 ($OCH_2CH_2CH_2$), 62.7 (C-6), 41.3 ($CH_2CH_2NH_2$), 32.5 ($CH_2CH_2NH_2$), 30.7 ($OCH_2CH_2CH_2$), 29.4 ($OCH_2CH_2CH_2$), 28.8 ($C(O)OC(CH_3)_3$) ppm; ESI-MS: *m/z* = calcd for $C_{16}H_{30}NO_8S$ [M+Na]+: 420.154. Found: 420.153.

6-Amino-4-thiahexyl α-D-galactopyranoside (14):

N-tert-Butoxycarbonyl-6-amino-4-thiahexyl-α-D-galactopyranoside (600 mg, 1.51 mmol) has been dissolved in dichloromethane (30 mL) and TFA (9 mL) and stirred at ambient temperature for 30 min. After removal of the solvent in vacuo product was obtained as a colourless syrup (450 mg, 1.51 mmol, quant). All spectral data were in good accordance with reported data.[306]

6-Acetamido-4-thiahexyl 2,3,4,6-tetra-*O*-acetyl-α-D-galactopyranoside:

6-Amino-4-thiahexyl α-D-galactopyranoside (**14**, 380 mg, 1.23 mmol) was treated according to the general procedure for acetylation. The crude product was purified by flash chromatography (ethyl acetate/methanol, 15:1). The pure product was obtained as colorless oil (604 mg, 1.19 mmol, 96 %). R_f= 0.3 (ethyl acetate/methanol, 7:1); $[\alpha]_D^{23}$ = +118 (c = 0.5, in methanol); ^{1}H NMR (500 MHz, $CDCl_3$, 300 K): δ = 5.36 (dd, 1H, $^3J_{3,4}$ = 4.42 Hz, $^3J_{2,3}$ = 9.86 Hz, H-3), 5.34 (dd, 1H, $^3J_{1,2}$ = 3.41 Hz, $^3J_{2,3}$ = 9.86 Hz, H-2), 5.14 (d, 1H, $^3J_{1,2}$ = 3.41 Hz, H-1), 4.23 (m, 2H, H-4, H-5), 3.80 (dd, 1H, $^3J_{5,6}$ = 4.8 Hz, $^2J_{6,6'}$ = 12.2 Hz, H-6), 3.53 (dd, 1H, $^3J_{5,6'}$ = 4.7 Hz, $^2J_{6,6'}$ = 12.2 Hz, H-6'), 3.48-3.40 (m, 1H, $OCHCH_2CH_2$), 3.38-3.30 (m, 1H, $OCHCH_2CH_2$), 3.17-3.10 (m, 2H, CH_2CH_2NH), 2.63 (t, 2H, $^3J_{CH_2,CH_2}$ = 6.4 Hz, CH_2CH_2NH) 2.50-2.41 (m, 2H, $OCH_2CH_2CH_2S$), 2.07 (s, 3H, $C(O)CH_3$), 2.05 (s, 3H, $C(O)CH_3$), 2.03 (s, 3H, $C(O)CH_3$), 2.02 (s, 3H, $C(O)CH_3$), 2.01 (s, 3H, $NHC(O)CH_3$), 1.90-1.85 (m, 2H, $OCH_2CH_2CH_2$); ^{13}C NMR (125 MHz, $CDCl_3$, 300 K): δ = 170.5, 170.4, 170.2, 170.1, 169.5 (5 C, $C(O)CH_3$), 96.3 (C-1), 68.2 (C-2), 68.0 (C-3), 67.6 (C-4), 66.3 (C-5), 66.3 (C-6), 61.7 ($OCH_2CH_2CH_2S$),), 38.5 (CH_2CH_2NH), 31.7 (CH_2CH_2NH), 29.0 ($OCH_2CH_2CH_2$), 28.2 ($OCH_2CH_2CH_2$), 23.2 ($NHC(O)CH_3$), 20.8, 20.7, 20.7, 20.6 (4C, $OC(O)CH_3$) ppm; ESI-MS: *m/z* = calcd for $C_{21}H_{33}NO_{11}S$ [M+Na]+: 530.167. Found: 530.166.

6-Acetamido-4-thiahexyl α-D-galactopyranoside (15):

6-Acetamido-4-thiahexyl 2,3,4,6-tetra-*O*-acetyl-α-D-galactopyranoside (600 mg, 1.18 mmol) was treated according to the general procedure for *O*-deacetylation. The pure product was obtained as colorless syrup (400 mg, 1.18 mmol, quant.). R_f= 0.2 (ethyl acetate/methanol, 4:1); $[\alpha]_D^{23}$ = +98 (c = 0.5, in methanol); ^{1}H NMR (500 MHz, MeOD, 300 K): δ = 4.77 (d, 1H, $^3J_{1,2}$ = 1.74 Hz, H-1), 3.89-3.83 (m, 2H, $OCHCH_2CH_2$, H-6), 3.82 (dd, 1H, $^3J_{1,2}$ = 1.74 Hz, $^3J_{2,3}$ = 3.31 Hz, H-2), 3.76-3.70 (m, 2H, H-6', H-3), 3.64 (t, 1H, ^3J = 9.48 Hz, H-5), 3.59-3.52 (m, 2H, $OCHCH_2CH_2$, H-4), 3.39-3.36 (m, 2H, CH_2CH_2NH), 2.69-2.64 (m, 4H, $OCH_2CH_2CH_2$, CH_2CH_2NH), 1.97 (s, 3H, $C(O)CH_3$), 1.93-1.87 (m, 2H, $OCH_2CH_2CH_2$); ^{13}C NMR (125 MHz, MeOD, 300 K): δ = 173.3 ($NHC(O)CH_3$), 101.6 (C-1), 74.7 (C-4), 72.7 (C-3), 72.2 (C-2), 68.6 (C-5), 66.9 ($OCH_2CH_2CH_2$),

62.9 (C-6), 40.3 (CH_2CH_2NH), 32.0 (CH_2CH_2NH), 30.7 ($OCH_2CH_2CH_2$), 29.4 ($OCH_2CH_2CH_2$), 22.5 ($C(O)CH_3$) ppm; ESI-MS: *m/z* = calcd for $C_{13}H_{25}NO_7S$ [M+Na]+: 362.124. Found: 362.124.

p-Acetamidophenyl 2,3,4,6-tetra-*O*-acetyl-α-D-galactopyranoside:

p-Aminophenyl-α-D-galactopyranoside (**17**, 100 mg, 0.369 mmol) was treated according to the general procedure for acetylation. After silica gel chromatography (ethyl acetate/methanol, 10:1) the product was obtained as colourless oil (170 mg, 0.349 mml, 95 %). R_f= 0.6 (ethyl acetate/methanol, 5:1); $[\alpha]_D^{23}$ = +126 (c = 0.5, in methanol); ^{1}H NMR (500 MHz, $CDCl_3$, 300 K): δ = 7.44-7.41 (m, 2H, Aryl-H_{ortho}), 7.06-7.02 (m, 2H, Aryl-H_{meta}), 5.54 (dd, 1H, $^3J_{2,3}$ = 3.5 Hz, $^3J_{3,4}$ = 10.0 Hz, H-3), 5.46 (d, 1H, $^3J_{1,2}$ = 1.7 Hz, H-1), 5.43 (dd, 1H, $^3J_{1,2}$ = 1.8 Hz, $^3J_{2,3}$ = 3.5 Hz, H-2), 5.36 (t, 1H, $^3J_{5,6}$ = 10.1 Hz, $^2J_{6,6'}$ = 12.7 Hz, H-6), 4.27 (ddd, 1H, $^3J_{4,5}$ = 12.4 Hz, $^3J_{5,6'}$ = 5.6 Hz, $^3J_{5,6}$ = 10.3 Hz, H-5), 4.12-4.05 (m, 2H, H-6', H-4), 2.20 (s, 3H, C(O)CH_3), 2.16 (s, 3H, C(O)CH_3), 2.05 (s, 3H, C(O)CH_3), 2.04 (s, 3H, C(O)CH_3), 2.03 (s, 3H, C(O)CH_3); ^{13}C NMR (125 MHz, $CDCl_3$, 300 K): δ = 176.6 (NHC(O)CH_3), 170.5 (C(O)CH_3), 170.0 (C(O)CH_3), 169.9 (C(O)CH_3), 169.7 (C(O)CH_3), 152.2 (Aryl-C_{ipso}), 133.2 (Aryl-C_{para}), 121.5 (Aryl-C_{ortho}), 118.7 (Aryl-C_{meta}), 96.1 (C-1), 70.6 (C-2), 69.4 (C-4), 68.9 (C-3), 65.9 (C-5), 62.1 (C-6), 24.4 (NHC(O)CH_3), 20.8 ($C(O)CH_3$), 20.8 ($C(O)CH_3$), 20.7 ($C(O)CH_3$), 20.6 ($C(O)CH_3$) ppm; ESI-MS: *m/z* = calcd for $C_{22}H_{27}NO_{11}$ [M+Na]+: 504.148. Found: 504.145.

***N*-Acetyl-*p*-aminophenyl α-D-galactopyranoside (18):**

p-Acetamidophenyl 2,3,4,6-tetra-*O*-acteyl-α-D-galactopyranoside (150 mg, 0.316 mmol) was treated according to the general procedure for *O*-deacetylation. The product was obtained as yellow oil (100 mg, 0.316 mmol, quant.). R_f= 0.3 (ethyl acetate/methanol, 5:1); m.p. 78 °C; $[\alpha]_D^{23}$ = +70 (c = 0.5, in methanol); ^{1}H NMR (500 MHz, MeOD, 300 K): δ = 7.46-7.42 (m, 2H, Aryl-H_{ortho}), 7.14-7.10 (m, 2H, Aryl-H_{meta}), 5.43 (d, 1H, $^3J_{1,2}$ = 2.7 Hz, H-1), 3.98 (dd, 1H, $^3J_{1,2}$ = 1.6 Hz, $^3J_{2,3}$ = 2.4 Hz, H-2), 3.95-3.93 (m, 2H, H-3, H-6), 3.72-3.65 (m, 2H, H-6', H-4), 3.31 (ddd, 1H, $^3J_{4,5}$ = 4.9 Hz, $^3J_{5,6}$ = 3.4 Hz, $^3J_{5,6'}$ = 1.6 Hz, H-5), 2.10 (s, 3H, NH(C)OCH_3); ^{13}C NMR (125 MHz, MeOD, 300 K): δ = 171.4 (NHC(O)CH_3), 155.3 (Aryl-C_{ipso}), 134.5 (Aryl-C_{para}), 122.6 (Aryl-C_{ortho}), 118.6 (Aryl-C_{meta}), 100.1 (C-1), 73.0 (C-3), 71.3 (C-5), 70.8 (C-2), 70.0 (C-4), 62.4 (C-6), 23.6 (NHC(O)CH_3) ppm; ESI-MS: *m/*z = calcd for $C_{14}H_{19}NO_7$ [M+Na]+: 336.105. Found: 336.104.

Liquid bacterial culture

GFP expressing *E. coli* strain PKL1162 were grown in LB medium (+ampicillin 100 mg/L, +chloramphenicol 50 mg/L) overnight, washed with PBS buffer (2 mL) and suspended in PBS to a concentration of OD_{600} = 0.4 (OD_{600} = 8x10^8 bacteria cells/mL).

Mannan coating of microtiter plates

Mannan from *Saccharomyces cerevisiae* was dissolved in carbonate buffer (50 mM, pH 9.5) to a concentration of 1.2 mg/mL and transferred to black 96-well microtiter plates (Thermo Fisher

Scientific, Nunc, Maxisorp, 120 µL/well). The plates were dried overnight at 37 °C and then stored at 4 °C until use.

GFP-based bacterial adhesion assay in solution

Mannan-coated black 96-well polystyrene microtiter plates were washed twice with PBST and blocked by incubation with PVA solution (1 % in PBS buffer, 120 µL/well) for 2 h at 4 °C. For all washing steps a Tecan HydroFlex™ was used. The wells were washed three times with PBST. Serial dilutions of the inhibitor glycosides and methyl α-D-mannopyranoside (MeMan) as standard inhibitor (all dissolved in PBS) were added to each well as well as 50 µL of *E. coli* suspension. The plate was agitated at 37 °C for 45 min. The wells were washed three times with PBS. All wells were filled with PBS (100 µL/well) and the surface bound bacteria were detected via fluorescence readout on a TECAN infinite 200 multifunction microplate reader (excitation wavelength, 485 nm, emission wavelength 535 nm). For comparison of results from independent assays, all IC_{50} values were consistently referenced to the inhibitor potency of MeMan (IP MeMan = 1), which was tested in parallel on each plate.

Functionalization of cantilever tips

Cantilevers were amino-functionalized using ethanolamine at 70 °C overnight. After washing twice with dichloromethane, the bis-*N*-hydroxysuccinimidyl-activated linker molecule was coupled under basic conditions using triethylamine at ambient temperature for 4 h to form linker-functionalized cantilever surface. The cantilevers were washed three times with dichloromethane and dried. The batch was divided and the NHS-activated cantilever-bound linkers were reacted with the different amino-functionalized carbohydrates.

Preparation and imaging of dry *E. coli* sample

E. coli PKL1162 were washed with bidest. water and suspended in bidest. water to a concentration of OD_{600} = 0.4. 500 µL of the bacterial suspension were transferred to freshly cleaved mica and the supernatant water was removed with a tissue. The sample was dried under nitrogen flow and then used for AFM measurements. Bacteria were imaged with an atomic force microscope in air using a MFP-3D (Asylum Research, Santa Barbara, CA, USA). Imaging was performed with NSG11-B cantilever (k= 5.5 N/m; NT-MDT, Moscow, Russia) in AC (tapping) mode using frequencies of about 150 kHz. The frequency was chosen to result in an amplitude 10 % lower than the amplitude at the resonance frequency. The set point was always adjusted to guarantee minimum forces applied to the sample. Further image processing (flattening and plane fitting) was done with the MFP-3D software under IGOR Pro (Lake Oswego, OR, USA). Image shown is representative for the samples.

Mannan coating of petri dish lids

Mannan from *Saccharomyces cerevisiae* was dissolved in carbonate buffer (50 mM, pH 9.5) to a concentration of 1.2 mg/mL and 2 mL were transferred to the lid of a polystyrene petri dish (Ø 55

mm). The lid was dried overnight at 37 °C, washed twice with 3 mL water and once with 3 mL PBS. Remaining water was removed using tissue and the lid was applied for immobilization of *E. coli* immediately.

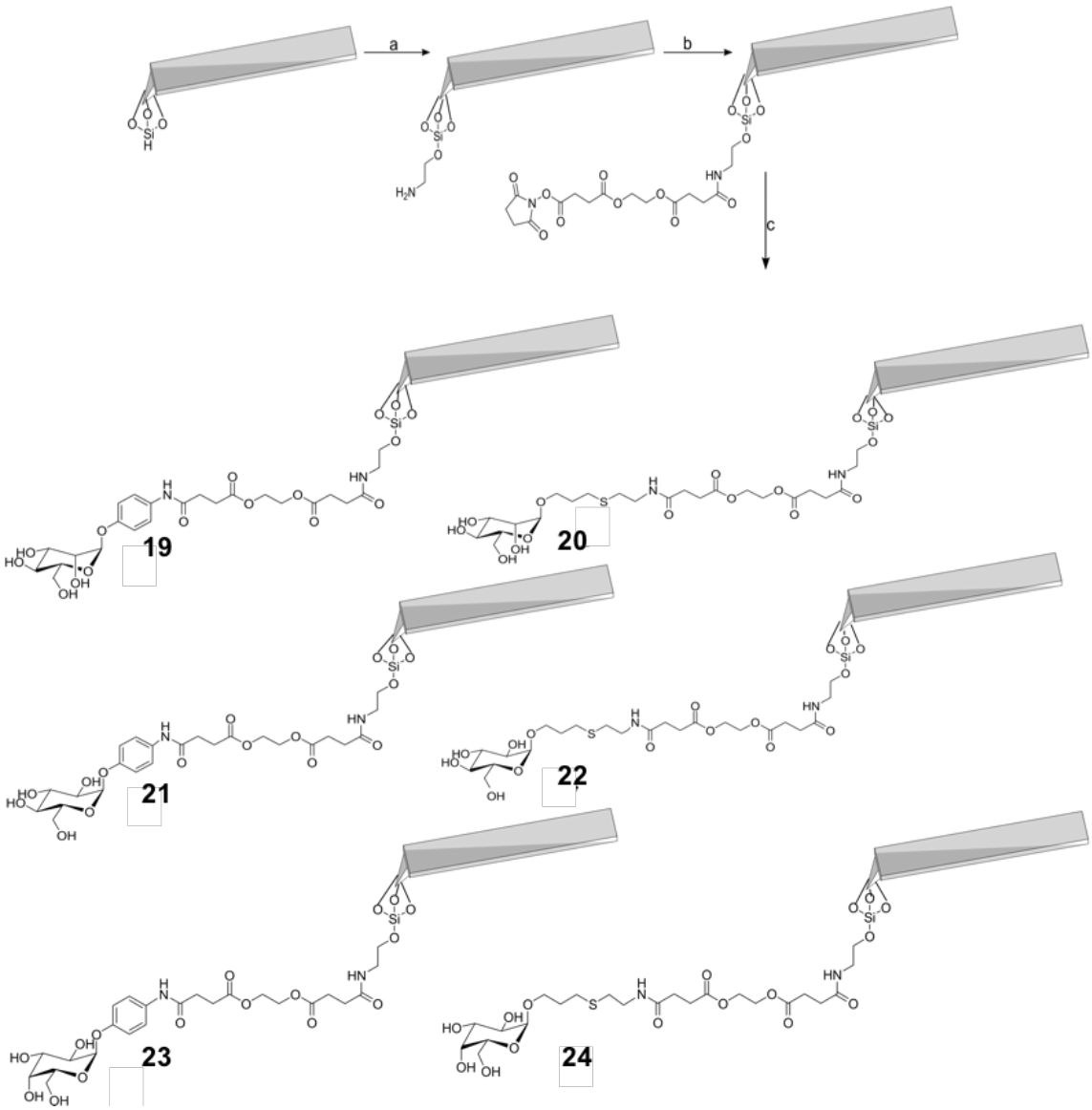

Figure 7.5.2: Functionalization of cantilevers. (a) ethanolamine, MS 3Å, 65 °C, N_2, 16 h, (b) abs. $CHCl_2$, triethylamine, ethyleneglycol-bis(succinic acid *N*-hydroxysuccinimide ester), N_2, 4 h, rt, (c) 10 mM **2**, **5**, **8**, **11**, **14**, **17** in carbonate buffer, pH 9.6, 16 h, rt.

Preparation of *E. coli* sample under buffer

E. coli PKL1162 were washed twice in PBS (2 mL) and suspended in PBS to a concentration of $OD_{600} = 2$. 1.5 mL of *E. coli* suspension were transferred to a mannan-coated petri dish lid and incubated at ambient temperature for 40 min. The lid was washed twice with 2 mL PBS, filled with

2 mL PBS and the sufficient density of immobilized bacteria was checked by fluorescence microscopy before used in force measurements.

Force spectroscopic experiments and force volume mapping

All experiments were performed using a MFP-3D AFM and functionalized OMCL-RC 800PSA-2 cantilever (Olympus, Tokio, Japan). Using the inverted fluorescence microscope, positions with sufficient numbers of bacteria were chosen. The spring constants of the cantilevers were calibrated by the thermal fluctuation method[307] before each experiment. First, a force volume map was recorded with a pulling velocity of 10 µm/s. The height and the adhesion force were calculated. Positions beside bacteria were chosen for individual force curves, which were recorded using pulling velocities between 10 nm/s and 10 µm/s. Higher pulling velocities led to artifacts because of solvent drag and lower because of movement and fluctuations of the bacteria. Experiments were performed in PBS at room temperature of 20 °C. The resolution to detect single rupture events reliably was 30 pN under these conditions. For further analysis the rupture forces of the last two events were determined. A difference between the last and the second last event could not be observed. Histograms were plotted and fitted by a Gausian. The respective values for the pull of forces are given in the figures. The pull of forces were plotted against the loading rate and fitted according to the Bell model.[308,309] The dissociation rate k_{off} and the transition state distance x_B were calculated. A critical velocity, which represents the velocity range in which no binding events above the detection limit of 30 pN could be observed, is given in table 4.2.1. Thus, at the higher limit events could and at the lower limit could not be observed. In case, the critical velocity is above the minimal pulling velocity of 10 nm/s a catch bond mechanism can be postulated.[310] To determine the influence of DMSO on the binding parameter, 200 µL DMSO was added to the 2 mL PBS.

Binding experiments by a surface acoustic wave (SAW) biosensor

Binding experiments under constant flow were performed using a biosensor assay based on surface acoustic waves (K5 Biosensor, SAW Instuments, Bonn, Germany). The technique as well as the used functionalization of the gold surface has been described[S7]. In this case, instead of the functionalization with dextran one of the glycosides was used. The *E. coli* bacteria were injected with a flow of 20 µl/min and the binding to the carbohydrate-functionalized surface was determined. The concentration of the bacteria was $2x10^8$/mL in PBS. The maximum phase shift was measured and all values given in table 4.2.1 are relative to the value using PhαGlc as the functionalization agent. The phase shift is approximately a measure for the mass absorption on the chip surface. Within the possible range for the flow rates (12.5 mL/min - 300 mL/min) no qualitative differences could be observed.

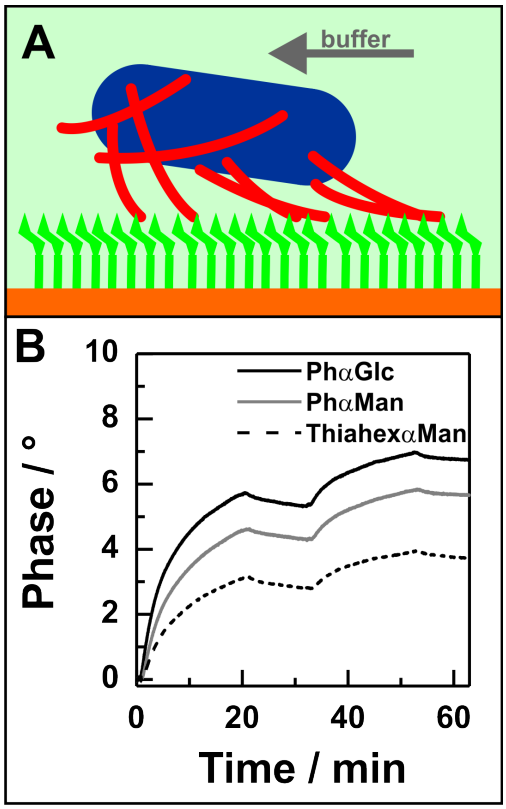

Figure 7.5.3: (A) Schematic illustration of the performed SAW measurements. (B) Results of the SAW measurements of PhαMan, PhαGlc and ThiahexαMan.

7.6 FimH protein engineering

Docking studies

The docking studies were performed with Schrodinger Software. As force field for all of them a OPLS-2005 (Optimized Potentials for Liquid Simulations) was used.[311–313] Both crystal structures of FimH (1KLF[64], 1UWF[65]) were optimized with a PrepWiz. Therefore a single monomer of the structure was taken and the intramolecular binding length and torsions were minimized. With the 2D sketcher of Maestro the ligands were drawn and converted into 3D models minimized with MacroModel. Afterwards different conformations of the minimized ligand were produced with LigPrep. For the docking studies Glide was used.[314,315] Herein the ligand remains flexible whereas the receptor is rigid. After the definition of the carbohydrate binding site the docking started. These calculations resulted in a docking score for each ligand conformation (Tab **4.3.1)**.

Table 7.6.1: Docking scores for ligand **1** and **2** with both structures of FimH.

	open gate 1KLF		*closed gate* 1UWF	
	ligand **1**	ligand **2**	ligand **1**	ligand **2**
1	-11.190	-11.098	-10.119	-10.535
2	-10.775	-10.994	-10.087	-10.531
3	-10.515	-10.990	-9.994	-10.480
4	-10.415	-10.916	-9.890	-10.475
5	-10.389	-10.821	-9.826	-10.471
6	-10.366	-10.774	-9.808	-10.334
7	-10.296	-10.770	-9.806	-10.332
8	-10.214	-10.650	-9.779	-10.327
9	-10.195	-10.637	-9.770	-10.307
10	-10.184	-10.605	-9.770	-10.303
11	-10.175	-10.570	-9.759	-10.231
12	-10.127	-10.565	-9.749	-10.140
13	-10.126	-10.531	-9.739	-10.136
14	-10.091	-10.520	-9.713	-10.116
15	-10.038	-10.515	-9.690	-10.106
16	-9.987	-10.493	-9.686	-10.085
17	-9.951	-10.450	-9.680	-10.080
18	-9.934	-10.447	-9.659	-10.075
19	-9.910	-10.435	-9.651	-10.058
20	-9.887	-10.431	-9.649	-10.052

The docking score consists of different individual terms regarding the ligand receptor interactions. Most important for the calculations here are van der Wals and Couloumb energy potentials which were further optimized regarding water molecules in the binding pocket, hydrophobic interactions and the hydrogen bondage linkage energy.[314] For the depicted pictures Connolly surfaces were used.[316]

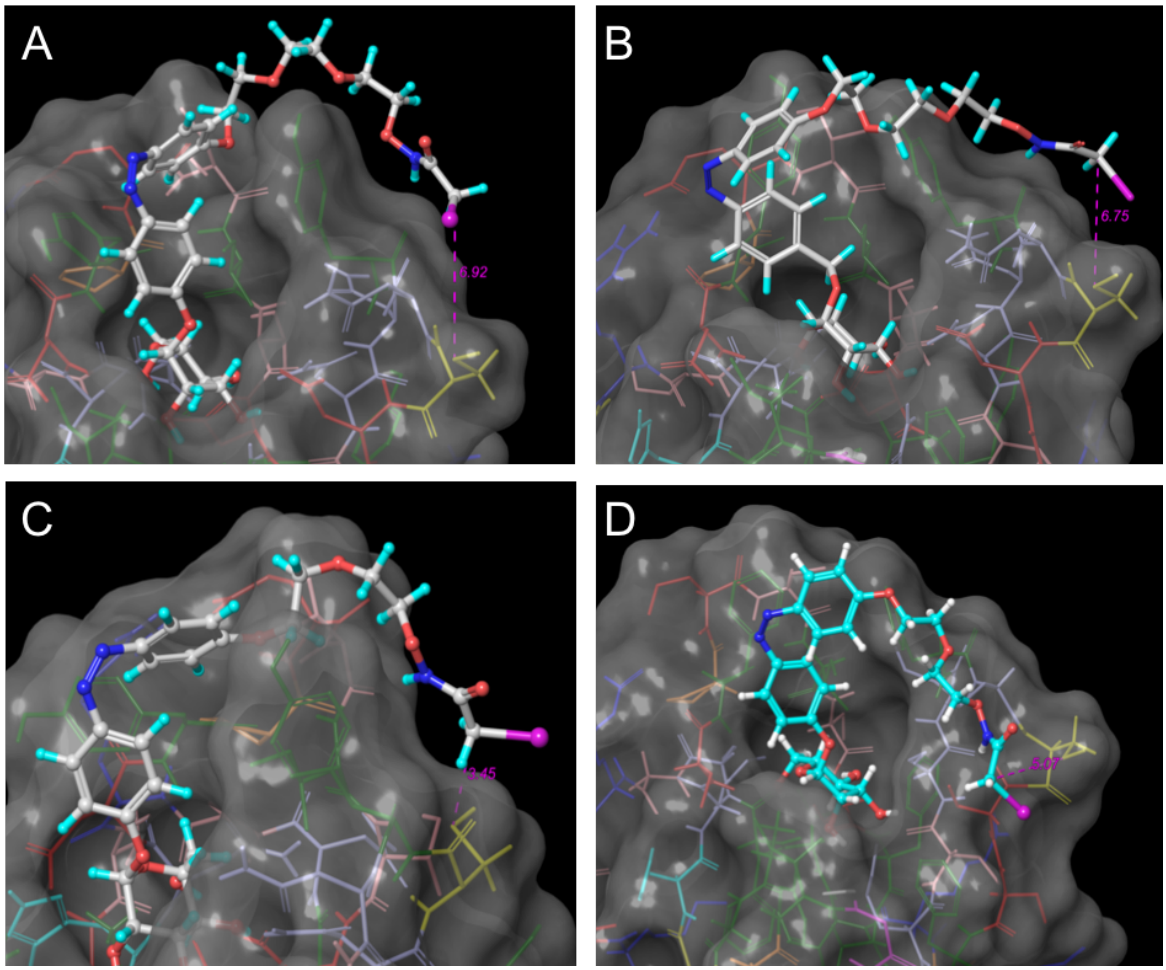

Figure 7.6.1: Additional obtained results of the docking studies. (A) Docking of the *open gate* structure of FimH (1KLF[64])with ligand **2**. S139 was exchanged against cysteine (yellow) and the distance to the iodoacetamido function was measured.. (B) Docking of the *closed gate* structure of FimH (1UWF[65]) with ligand **2**. S139 was exchanged against cysteine (yellow) and the distance to the iodoacetamido function was measured. (C) Docking of the *open gate* structure of FimH (1KLF[64])with ligand **1**. Asparagine 136 was exchanged against cysteine (yellow) and the distance to the iodoacetamido function was measured. (D) Docking of the *closed gate* structure of FimH (1UWF[65]) with ligand **1**. S139 was exchanged against cysteine (yellow) and the distance to the iodoacetamido function was measured.

Protein engineering

Buffer and media

PBS buffer: 140 mM sodium chloride, 2.7 mM potassium chloride, 10 mM sodium dihydrogen phosphate dihydrate, 1.8 mM potassium dihydrogen phosphate, pH 7.4; PBST: PBS buffer+0.05 % v/v Tween®20; binding buffer: 50 mM NaH_2PO_4, 300 mM NaCl, pH 7.4; wash buffer: 50 mM NaH_2PO_4, 300 mM NaCl, 5 mM imidazole, pH 7.4; loading buffer: 0.05 % bromophenol, 40 % sucrose, 0.1 mM EDTA, 0.5 % SDS, pH 8.0; elution buffer: 50 mM NaH_2PO_4, 300 mM NaCl, 150 mM imidazole, pH

7.4; running buffer: LB media: 5.00 g/L yeast extract, 10.0 g/L tryptone, 0.50 g/L NaCl; LB agar: 5.00 g/L yeast extract, 10.0 g/L tryptone, 0.50 g/L NaCl, 15.0 g/L agar.; M9 salts aliquot: 240 mM $Na_2HPOS_4x7H_2O$, 110 mM KH_2PO_4, 43 mM NaCl, 94 mM NH_4Cl; M9 minimal media: 200 mL M9 minimal salts aliquot, 2 mM $MgSO_4$, 2.5 % glucose (w/v), 0.1 µM $CaCl_2$, sucrose buffer: 20 mM TRIS-HCl, 5 mM EDTA, 25 % sucrose, pH 8.0; lysis buffer: 5 mM $MgCl_2$, 50 µM lysozyme; SDS running buffer: 25 mM TRIS, 200 mM glycerol, 0.1 % SDS; fixing/destainer I solution: 10 % glacial acetic acid, 40 % EtOH; stock solution I: 0.2 % SERVA Blue R in 90 % EtOH; stock solution II: 20 % acetic acid; destainer II: 10 % glacial acetic acid, 20 % EtOH.

Site directed mutagenesis

To introduce a point mutation in the plasmid *p*PKL241 [317] a site directed mutagenesis was used. The PKL241 *E. coli* bacteria containing the plasmid were grown in LB media (+ampicillin 100 mg/L) over night at 37 °C and 175 rpm. After plasmid preparation (GeneJet Plasmid Miniprep Kit, Thermo Fisher) a PCR was performed with the following primers (Tab. 7.6.2).

N136C forward: 5´-CGA CAG ACC AAC TGC TAT AAC AGC GAT GAT TTC-3´

reverse: 5´-GAA ATC ATC GCT GTT ATA GCA GTT GGT CTG TCG-3´

S139C forward: 5´-C AAC AAC TAT AAC TGC GAT GAT TTC CAG TTT G-3´

reverse: 5´-C AAA CTG GAA ATC ATC GCA GTT ATA GTT GTT G-3´

Table 7.6.2: PCR attempt for site directed mutagenesis.

	N136C		**S139**	
	1. attempt	2. attempt	1. attempt	2. attempt
dd H_2O	35.5 µL	35.5 µL	35.5 µL	35.5 µL
5x Phusion HF buffer (Stratagene)	10 µL	10 µL	10 µL	10 µL
Phusion DNA polymerase (Stratagene)	0.5 µL	0.5 µL	0.5 µL	0.5 µL
25 mM dNTP	1 µL	1 µL	1 µL	1 µL
template DNA (2.00 ng/µL)	1 µL		1 µL	
template DNA (10.0 ng/µL)		1 µL		1 µL
primer N136C for	1 µL	1 µL		
primer N136C rev	1 µL	1 µL		
primer S139C for			1 µL	1 µL
primer S139C rev			1 µL	1 µL

The PCR was realized with a thermocycler (iCycler, BIO-RAD) after following procedure (Tab 7.6.3).

Table 7.6.3: PCR attempt for site directed mutagenesis.

	temperature	**duration**	**cycles**
hot start	95 °C	120 sec	1
denaturation	95 °C	30 sec	20
hybridization	58 °C	30 sec	20
elongation	72 °C	150 sec	20
final elongation	72 °C	300 sec	1

After the PCR the template DNA was digested with the enzyme DpnI (1 µL; 20 U/µL, Thermo Fisher) which recognizes methylated DNA.

Transformation

The transformation in XL-1 *E. coli* was implemented with the calcium chloride method. The frozen competent cells (100 µL) were defrosted on ice and plasmid DNA was added (2 µL). It was incubated on ice for 30 min followed by an 120 sec heat shock at 42 °C. LB media (600 µL) was admitted and incubated at 37 °C for 1 h. Afterwards 100 µL were plated on a LB agar plate with ampicillin (100 mg/L).

Sequencing

To prove the successful mutagenesis and transformation the plasmid DNA was sequenced (Eurofins Genomics). Figure **7.6.2** display the sequencing results. Both amino acids were exchanged successful.

FimH	1	MKRVITLFAVLLMGWSVNAWSFACKTANGTAIPIGGGSANVYVNLAPVVNVGQNLVVDLS
N136C	1	MKRVITLFAVLLMGWSVNAWSFACKTANGTAIPIGGGSANVYVNLAPVVNVGQNLVVDLS
FimH	61	TQIFCHNDYPETITDYVTLQRGSAYGGVLSNFSGTVKYSGSSYPFPTTSETPRVVYNSRT
N136C	61	TQIFCHNDYPETITDYVTLQRGSAYGGVLSNFSGTVKYSGSSYPFPTTSETPRVVYNSRT
FimH	121	DKPWPVALYLTPVSSAGGVAIKAGSLIAVLILRQTNNYNSDDFQFVWNIYANNDVVVPTG
N136C	121	DKPWPVALYLTPVSSAGGVAIKAGSLIAVLILRQTN**C**YNSDDFQFVWNIYANNDVVVPTG
FimH	181	GHHHHHH
N136C	181	GHHHHHH
FimH	1	MKRVITLFAVLLMGWSVNAWSFACKTANGTAIPIGGGSANVYVNLAPVVNVGQNLVVDLS
S139C	1	MKRVITLFAVLLMGWSVNAWSFACKTANGTAIPIGGGSANVYVNLAPVVNVGQNLVVDLS
FimH	61	TQIFCHNDYPETITDYVTLQRGSAYGGVLSNFSGTVKYSGSSYPFPTTSETPRVVYNSRT
S139C	61	TQIFCHNDYPETITDYVTLQRGSAYGGVLSNFSGTVKYSGSSYPFPTTSETPRVVYNSRT
FimH	121	DKPWPVALYLTPVSSAGGVAIKAGSLIAVLILRQTNNYNSDDFQFVWNIYANNDVVVPTG
S139C	121	DKPWPVALYLTPVSSAGGVAIKAGSLIAVLILRQTNNYN**C**DDFQFVWNIYANNDVVVPTG
FimH	181	GHHHHHH
S139C	181	GHHHHHH

Figure 7.6.2: Sequencing results of the new plasmids. (A) Exchange of N136 against cysteine. (B) Exchange of S139 against cysteine.

Protein expression

For the protein expression *E. coli* were incubated in M9 minimal media with ampicillin (50 mg/L) over night at 37 °C and 175 rpm. In a shaking flask 500 mL M9 minimal media with ampicillin (50 mg/L) were inoculated with the bacteria and at OD_{600} = 0.3 the expression was induced with IPTG (1 mM). After an incubation time of 16 h at 30 °C the bacteria were harvested by centrifugation at 4000 rpm for 20 min.

Protein purification

The bacteria pellet was dissolved in sucrose buffer (4 ml/g) and incubated on ice for 15 min. After centrifugation for 20 min at 4000 rpm the pellet was dissolved in lysis buffer and incubated on ice for 30 min. After a centrifugation (20 min, 4000 rpm) the supernatant was dialyzed with a float-a-lyzer (MWCO: 500 Da, Carl Roth) against binding buffer over night at 4 °C. Due to their His tags all FimH proteins could be purified with His GraviTrap columns (GE Healthcare). Therefore the protein dissolved in binding buffer was applied to the column and afterwards washed with wash buffer. Finally the purified protein was eluted with elution buffer. To improve the purification step we introduced a sephadex mannose column. Therefore Sephadex 6B was functionalized with α-D-mannose.[318] The previous eluted protein fractions were put on the column and after a washing step with wash buffer eluted with elution buffer with α-D-mannose (250 mM). The eluted fractions were united, concentrated with Vivaspin 15R tubes (MWCO: 2000 Da, Sartorius) and lyophilized. To prove the purification a probe from every step was examined in a SDS PAGE.

SDS PAGE

With a SDS PAGE proteins are separated electrophoretically according to their size. By the addition of the anionic detergent SDS proteins were denaturated and negatively charged due to this they move to the positive pole in the electric field. According to their amino acid chain length they were separated in the SDS Gel. The shorter a protein is the faster it moves through the gel. The SDS gel consists of two parts, a running gel and a stacking gel. For the application the protein probes were mixed with loading buffer and incubated at 95 °C for 10 min.[319] The probes (12 µL) were loaded onto the previous prepared gel (Tab 7.6.4). A broad range unstained protein ladder (Thermo Fisher) was used as a marker to compare the size of the proteins. A potential of 200 V was applied for 60 min. The SDS gel was either directly dyed or the fluorescence analyzed with an Odyssey® Fc Imaging System (LI-COR).

Table 7.6.4: Composition of the SDS PAGE.

	running gel 12 %	stacking gel
ddH_2O	1.7 mL	700 µL
30 % acrylamide	2 mL	165 µL
1.5 M TRIS, 0.4 % SDS, pH 8.8	1.25 mL	
0.5 M TRIS, 0.4 % SDS, pH 6.8		125 µL
10 % APS	100 µL	20 µL
TEMED	4 µL	2 µL

For the Coomassie® staining the gel was fixed in fixing solution for 30 min. Prior to use stock solution I was mixed with the same amount of stock solution II and the gel stained for at least 20 min to overnight. For a first rapid destain the gel was incubated in destainer I for a few minutes followed by an incubation in destainer II.

Protein functionalization

FimH S139C and FimH N136C (50 µL, 50 µM) were incubated with TCEP (500 µM) for 30 min and 200 rpm. Texas Red® C2 maleimide (Thermo Fisher) was added (1.25 mM) and incubated for 2.5 h and 200 rpm. The reaction was quenched with DTT (5 mM) and the not reacted dye was separated with Vivaspin 15R tubes (MWCO: 2000 Da, Sartorius).[320]

7.7 Thiourea-bridged nanodiamond glycoconjugates as inhibitors of bacterial adhesion

General Methods

All chemicals were reagent grade and obtained from Acros Organics. Dichloromethane and THF were distilled and dried using standard procedures. Deionized, bidistilled water was used for all diamond syntheses. Acid purified detonation diamond, purchased from Gansu Lingyun Corp. (China), was milled using an attrition mill and 50 µm zirconia beads according to a previously described protocol.[41] ^{1}H and ^{13}C NMR spectra were recorded at 27 °C on a Bruker AVANCE 400 FT-NMR spectrometer, chemical shifts are reported on the δ scale and DMSO-d_6 (δ = 2.50) was used as internal reference. Mass spectrometry (MALDI-TOF) was carried out with a Bruker Daltonics autoflex II. FT-IR spectra were recorded with a Jasco FT/IR-430 equipped with an ATR unit or with a tailor-made vacuum cell for the measurement of KBr pellets, which were dried in vacuum for 2 h. Thermogravimetry (TGA) was carried out with a Perkin Elmer STA 6000 in high purity nitrogen with a heating rate of 4 K min^{-1} (ca. 10 mg of sample were used for an analysis). Elemental analysis (EA) was carried out with an Elementar Vario Micro Element Analyzer. Particle size determination and zeta potential measurements were performed in Millipore water at pH 7 using a Malvern Zetasizer Nanoseries Nano-ZS (dynamic light scattering, backscatter mode). Zetapotentials were measured as single points. Size distributions were obtained using the Marquardt method and are given as volume distributions. For sonification of the particles a Bandelin Sonorex Digitec Typ DT52 (max. 80 W, 35 kHz) and for centrifugation a Thermo Scientific Sorvall MTX 150 was used. For reactions under sonification a Branson Sonifier 450 102C (max. 400 W, 19850 – 20050 Hz) with conical 5 mm titanium-microtip was used.

Synthesis of mannose derivatives

The isothiocyanato-functionalized mannose derivatives **1** [277,278], **2** [279] and **3** [280] that were employed for GND preparation, were synthesized according to the literature. The measured analytical data were in full accordance with the literature.

4-Cyanobenzenediazonium tetrafluoroborate 5

A suspension of 4-aminobenzonitrile (2.37 g, 20.1 mmol) in fluoroboric acid (16 mL, 25% aqueous solution) was cooled to 0 °C. Sodium nitrite (1.41 g, 20.5 mmol) was dissolved in water (4 mL) and this solution added dropwise. The reaction mixture was stirred for 30 min at RT. After cooling to 0 °C, the formed precipitate was filtered off and washed with cold diethyl ether to give **8** as a colourless powder (3.27 g, 75 %). M.p.: 114 °C; ^{1}H NMR (400 MHz, DMSO-d_6): δ = 8.86-8.83 (m, 2 H, N_2CCH), 8.48-8.46 (m, 2 H, $CHCCN$) ppm; ^{13}C NMR (100 MHz, DMSO-d_6): δ = 134.8, 133.0, 121.8, 121.1, 116.4 ppm; MS (MALDI-TOF): calcd. for $C_7H_4N_3$+ [M – BF_{4-}] 130.04, found 130.01; FT-IR (ATR): ῡ = 3119 (CH), 2289 (CN), 1588 (CC_{ar}), 1416 (NN), 1035 (CN), 841 (CH_{ar}) cm^{-1}.

4-Cyanophenyl-functionalized ND 6

4-Cyanobenzenediazonium tetrafluoroborate (**5**, 217 mg, 1 mmol) was added to a dispersion of milled nanodiamond **4** (200 mg) in water (8.5 mL). The mixture was sonicated with an ultrasonic horn for 75 min at RT. The particles were isolated by centrifugation, washed repeatedly with water (until the supernatant became neutral), and then acetone and THF in consecutive washing/centrifugation cycles. Ultrasonic treatment was used in every cycle in order to redisperse the diamond and remove adsorbed impurities. The product nanodiamond **6** was stored as aqueous dispersion. Part of the sample was dried at 70 °C to perform analytical measurements. ND **6** was obtained as a grey powder (179 mg). FT-TR (ATR, KBr): $\tilde{\upsilon}$ = 3427 (OH), 2925 (CH), 2229 (CN), 1717 (CO), 1629 (OH), 845 (CH_{ar}) cm^{-1}; elemental analysis found (%): C 87.24, H 1.44, N 2.55; surface loading (calcd from TGA): 0.12 mmol g^{-1} [Δm (147-445°C) 1.19 %]; fragment: C_7H_4N (102 g mol^{-1}); zeta potential (pH = 7): 36.1 mV; particle size (H_2O): 10 % $\leq$ 38, 50 % $\leq$ 57, 90 % $\leq$ 117 nm.

4-Aminophenyl-functionalized ND 7

4-Cyanophenyl-functionalized nanodiamond **6** (160 mg) was dispersed under nitrogen atmosphere in dry THF (30 mL) and 1 M borane-tetrahydrofurane complex (15 mL) was added at room temperature. The mixture was stirred for 72 h at 80°C, then 2 M HCl (5 mL) was added. The particles were isolated by centrifugation and repeatedly washed with, water (until the supernatant became neutral), and then acetone and an acetone/water mixture (1:1) in consecutive washing/centrifugation cycles. Ultrasonic treatment was used in every cycle in order to redisperse the diamond and remove adsorbed impurities. The product nanodiamond **7** was stored as aqueous dispersion. Part of the sample was dried at 70 °C to perform analytic measurements. ND **7** was obtained as a grey powder (161 mg). FT-TR (ATR, KBr): $\tilde{\upsilon}$ = 3430 (OH), 2925 (CH), 1713 (CO), 1630 (OH) cm^{-1}; elemental analysis found (%): C 87.80, H 1.56, N 2.20; surface loading (calcd. from TGA): 0.09 mmol g^{-1} [Δm (139-435 °C) 0.91 %]; fragment: C_7H_8N (106 g mol^{-1}); zeta potential (pH = 7): 47.7 mV; particle size (H_2O): 10 % $\leq$ 22, 50 % $\leq$ 34, 90 % $\leq$ 61 nm.

General procedure for the synthesis of mannose-conjugated ND (8, 9, 10)

Amino-functionalized nanodiamond **7** was dispersed in dry dichloromethane (40 mL) under nitrogen atmosphere and the respective *O*-acetylated isothiocyanato-functionalized mannose derivative (0.1-0.2 mmol of **1**, **2** or **3**) was added. It was cooled to 0 °C, DIPEA (3 mL) was added and the reaction mixture stirred for 30 min at 0 °C. Stirring was continued at RT for another 90 h. The particles were isolated by centrifugation and repeatedly washed with water (until the supernatant became neutral), and then acetone and methanol in consecutive washing/centrifugation cycles. Ultrasonic treatment was used in every cycle in order to redisperse the diamond and remove adsorbed impurities. The product nanodiamond was stored as aqueous dispersion. Part of the sample was dried at 70 °C to perform analytic measurements.

(Methyl 2,3,4,-tri-*O*-acetyl-α-D-mannoside-6-thioureido)-conjugated ND 8

4-Aminophenyl-functionalized nanodiamond **7** (120 mg) and the protected 6-isothiocyanato functionalized mannosides **1** (60 mg, 0.2 mmol) were reacted according to the general procedure to obtain GND **8** as a grey powder (109 mg). FT-TR (ATR, KBr): $\tilde{\upsilon}$ = 3428 (OH), 2925 (CH), 1712 (CO), 1631 (OH), 1458 (OH), 1236 (CS) cm^{-1}; elemental analysis found (%): C 88.41, H 1.17, N 2.54, S 0.18; surface loading (calcd. from TGA): 0.06 mmol g^{-1} [Δm (127-428 °C) 3.23 %]; fragment: $C_{22}H_{27}N_2O_9S$ (496 g mol^{-1}); zeta potential (pH = 7): 49.0 mV; particle size (H_2O): 10 % ≤ 25, 50 % ≤ 41, 90 % ≤ 154 nm.

(2,3,4,6-Tetra-*O*-acetyl-α-D-mannosyl-thioureido)-conjugated ND 9

4-Aminophenyl-functionalized nanodiamond **7** (101 mg) and the protected mannosyl isothiocyanate **2** (40 mg, 0.10 mmol) were reacted according to the general procedure to obtain GND **9** as a grey powder (83 mg). FT-TR (ATR, KBr): $\tilde{\upsilon}$ = 3425 (OH), 2925 (CH), 1715 (CO), 1642 (OH), 1459 (OH), 1237 (CS) cm^{-1}; elemental analysis found (%): C 88.08, H 1.64, N 2.28, S 0.24; surface loading (calcd. from TGA): 0.08 mmol g^{-1} [Δm (133-437°C) 3.81 %]; fragment: $C_{22}H_{27}N_2O_9S$ (496 g mol^{-1}); zeta potential (pH = 7): 49.8 mV; particle size (H_2O): 10 % ≤ 25, 50 % ≤ 31, 90 % ≤ 201 nm.

(*p*-Thioureidophenyl 2,3,4,6-tetra-*O*-acetyl-α-D-mannoside)-conjugated ND 10

4-Aminophenyl-functionalized nanodiamond **7** (120 mg) and the protected *p*-isothiocyanato-functionalized mannosides **3** (60 mg, 0.10 mmol) were reacted according to the general procedure to obtain GND **10** as a grey powder (101 mg). FT-TR (ATR, KBr): $\tilde{\upsilon}$ = 3423 (OH), 2925 (CH), 1731 (CO), 1631 (OH), 1459 (OH), 1234 (CS) cm^{-1}; elemental analysis found (%): C 87.84, H 1.70, N 2.21, S 0.29; surface loading (calcd. from TGA): 0.09 mmol g^{-1} [Δm (139-438°C) 5.11 %]; fragment: $C_{28}H_{31}N_2O_{10}S$ (588 $gmol^{-1}$); zeta potential (pH = 7): 46.8 mV; particle size (H_2O): 10 % ≤ 26, 50 % ≤ 44, 90 % ≤ 198 nm.

General procedure for the deprotection of mannose-conjugated GND

Nanodiamond conjugated with *O*-acetylated mannose derivatives (**8**, **9**, or **10**) was dispersed in methanol (30 mL) and cooled to 0 °C. Sodium methoxide (5 mg) was added and the mixture was stirred for 18 h at RT. The particles were isolated by centrifugation and repeatedly washed with water (until the supernatant became neutral), and then with acetone and an acetone/water mixture (1:1) in consecutive washing/centrifugation cycles. Ultrasonic treatment was used in every cycle in order to redisperse the diamond and remove adsorbed impurities. The product GND was stored in DMSO as dispersion. Part of the sample was dried at 70 °C to perform analytic measurements.

Deprotected GND 11

According to the general procedure, the protected GND **8** (90 mg) was deprotected to obtain **11** as a grey powder (80 mg). FT-TR (ATR, KBr): $\tilde{\upsilon}$ = 3423 (OH), 2925 (CH), 1709 (CO), 1631 (OH),

1459 (OH), 1241 (CS) cm^{-1}; elemental analysis found (%): C 88.75, H 1.20, N 2.52, S 0.13; surface loading (calcd. from TGA): 0.07 mmol g^{-1} [Δm (139-437°C) 3.37 %]; fragment: $C_{14}H_{19}N_2O_5S$ (327 g mol^{-1}); zeta potential (pH = 7): 44.5 mV; particle size (H_2O): 10 % ≤ 30, 50 % ≤ 44, 90 % ≤ 194 nm.

Deprotected GND 12

According to the general procedure, the protected GND **9** (66 mg) was deprotected to obtain **12** as a grey powder (63 mg). FT-TR (ATR, KBr): ῡ = 3424 (OH), 2925 (CH), 1708 (CO), 1631 (OH) 1457 (OH), 1243 (CS) cm^{-1}; elemental analysis found (%): C 85.70, H 1.62, N 2.48, S 0.17; surface loading (calcd. from TGA): 0.06 mmol g^{-1} [Δm (128-429°C) 2.00 %]; fragment: $C_{14}H_{19}N_2O_5S$ (327 g mol^{-1}); zeta potential (pH = 7): 46.8 mV; particle size (H_2O): 10 % ≤ 38, 50 % ≤ 61, 90 % ≤ 155 nm.

Deprotected GND 13

According to the general procedure, the protected GND **10** (90 mg) was deprotected to obtain **13** as a grey powder (84 mg). FT-TR (ATR, KBr): ῡ = 3423 (OH), 2925 (CH), 1702 (CO), 1631 (OH), 1459 (OH), 1212 (CS) cm^{-1}; elemental analysis found (%): C 88.91, H 1.61, N 2.32, S 0.17; surface loading (calcd. from TGA): 0.09 mmol g^{-1} [Δm (140-430°C) 3.86 %]; fragment: $C_{20}H_{23}N_2O_6S$ (419 g mol^{-1}); zeta potential (pH = 7): 41.6 mV; particle size (H_2O): 10 % ≤ 31, 50 % ≤ 44, 90 % ≤ 160 nm.

Buffers

PBS buffer: 140 mM sodium chloride, 2.7 mM potassium chloride, 10 mM sodium dihydrogen phosphate dihydrate, 1.8 mM potassium dihydrogen phosphate, pH 7.2; carbonate buffer: sodium carbonate 15 mM, sodium hydrogen carbonate 30 mM, pH 9.2; PBST: PBS buffer + 0.05 % v/v Tween®20.

Bacterial culture

The bacterial strain PKL1162[77] was cultured from a frozen stock in LB media (+ampicillin 100 mg/mL and chloramphenicol 50 mg/mL) overnight at 37°C. PKL4 bacteria[77] were cultured under the same conditions in LB media (+ampicillin 100 mg/mL). After washing twice with PBS buffer (2 mL) the bacteria pellet was suspended in PBS buffer and the bacterial solution was adjusted to OD_{600} = 0.4 with PBS.

Sandwich Assay

The sandwich assay was performed according to the literature.[238] Black microtiter plates (Nunc, MaxiSorp) were incubated with mannan from *Saccharomyces cerevisiae* (1.2 mg/mL, 120 µL/well in carbonate buffer) at 37°C overnight. After washing three times with PBST (300 µL/well) non

fluorescent type 1 fimbriated PKL4 *E. coli* bacteria were added (100 µL/well) and incubated for 2 h at 37°C and 100 rpm to form the 'capture layer' (cf. Figure 5.2.4A). The plates were washed with PBS (300 µL/well) three times. The respective glyconanodiamonds were serially diluted in PBS in a separate plate and transferred to the capture layer (50 µL/well) to form the 'adhesive layer' (cf. Figure 5.2.4A) after 1 h incubation time at 37°C. The plates were again three times washed with PBS (300 µL/well) and the fluorescent type 1 fimbriated *E. coli* strain PKL1162 was added (100 µL/well) to build the fluorescent 'detection layer' (cf. Figure 5.2.4A). After 1 h incubation at 37°C and 100 rpm the plates were washed with PBS (300 µL/well) three times and PBS (100 µL/well) was added to determine the fluorescence intensity (excitation wavelength 485 nm, emission wavelength 535 nm).

Kaiser test for the identification of primary amino groups after the reduction of CN groups

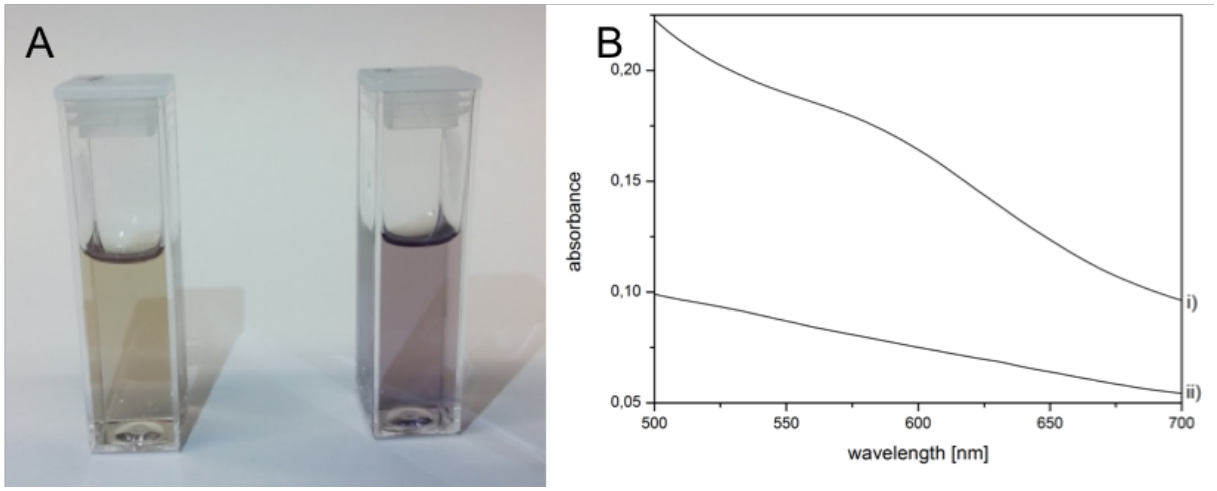

Figure 7.7.1: A) Qualitative Kaiser test showing the absence of amino groups in nitrile-functionalized ND **6** (left) and the presence of the NH_2 groups for ND **7** by the formation of the typical colour of Ruhemanns purple (right); B) UV/Vis spectra of the resulting dye solutions of i) amino-functionalized ND **7**, where the absorption of the dye is visible, ii) ND **6**, where no formation of dye is observed. The spectra have been recorded from the solutions after removal of the diamond by centrifugation and contained the dye generated from 4 mg of the respective nanodiamond in 10 mL solution.

Sandwich Assay to determine bacterial adhesion to (glyco)nanodiamonds

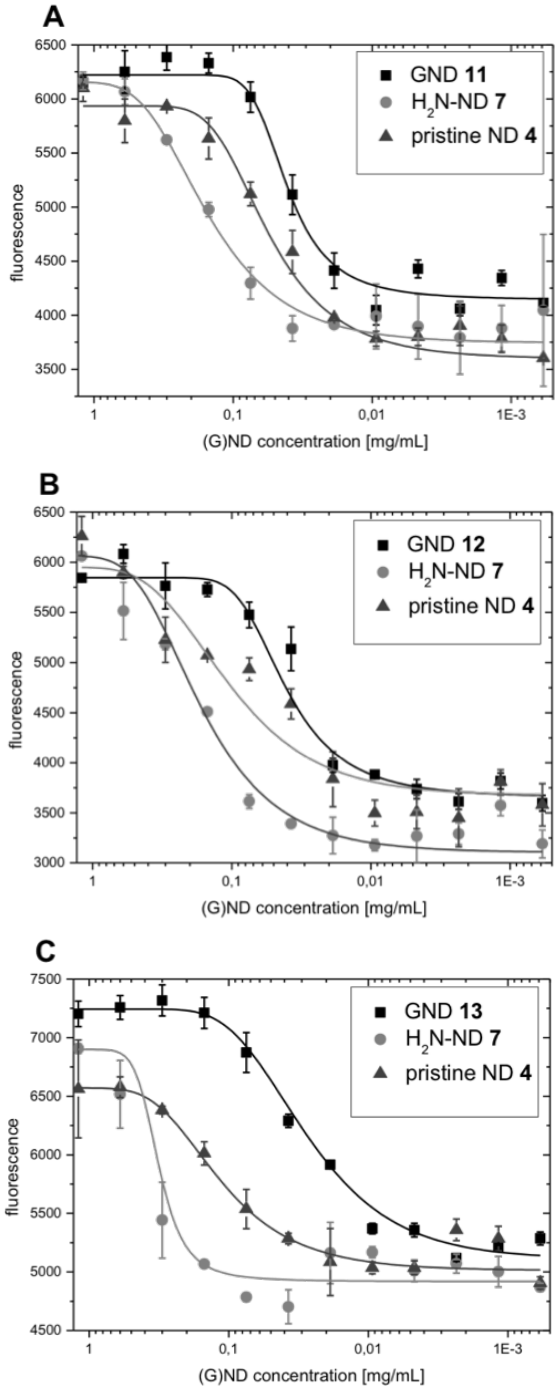

Figure 7.7.2: Bacterial adhesion to glyconanodiamonds **11**-**13** in comparison to pristine ND **4** and amino-prefunctionalized ND **7** as measured with the described sandwich assay (cf. Fig.5.2.4). Given concentrations are based on particle weight. (A) Bacterial adhesion to (methyl α-D-mannoside-6-thioureido)-conjugated-ND **11**; (B) Bacterial adhesion to (α-D-mannosyl-thioureido)-conjugated ND **12**; (C) Bacterial adhesion to (*p*-thioureidophenyl α-D-mannoside)-conjugated ND **13**. Error bars are standard deviations from triplicate values on one plate.

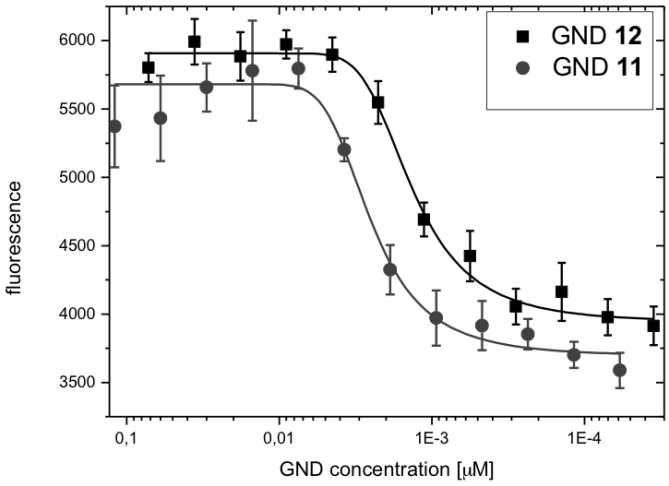

Figure 7.7.3: Bacterial adhesion to glyconanodiamonds **11** and **12** as measured with the described sandwich assay (cf. Fig.5.2.4). Given concentrations are based on surface loading. Bacterial adhesion to (methyl α-D-mannoside-6-thioureido)-conjugated-ND **11** in comparison to (α-D-mannosyl-thioureido)-conjugated ND **12**. Error bars are standard deviations from triplicate values on one plate.

Thermogravimetric data of functionalized nanodiamond

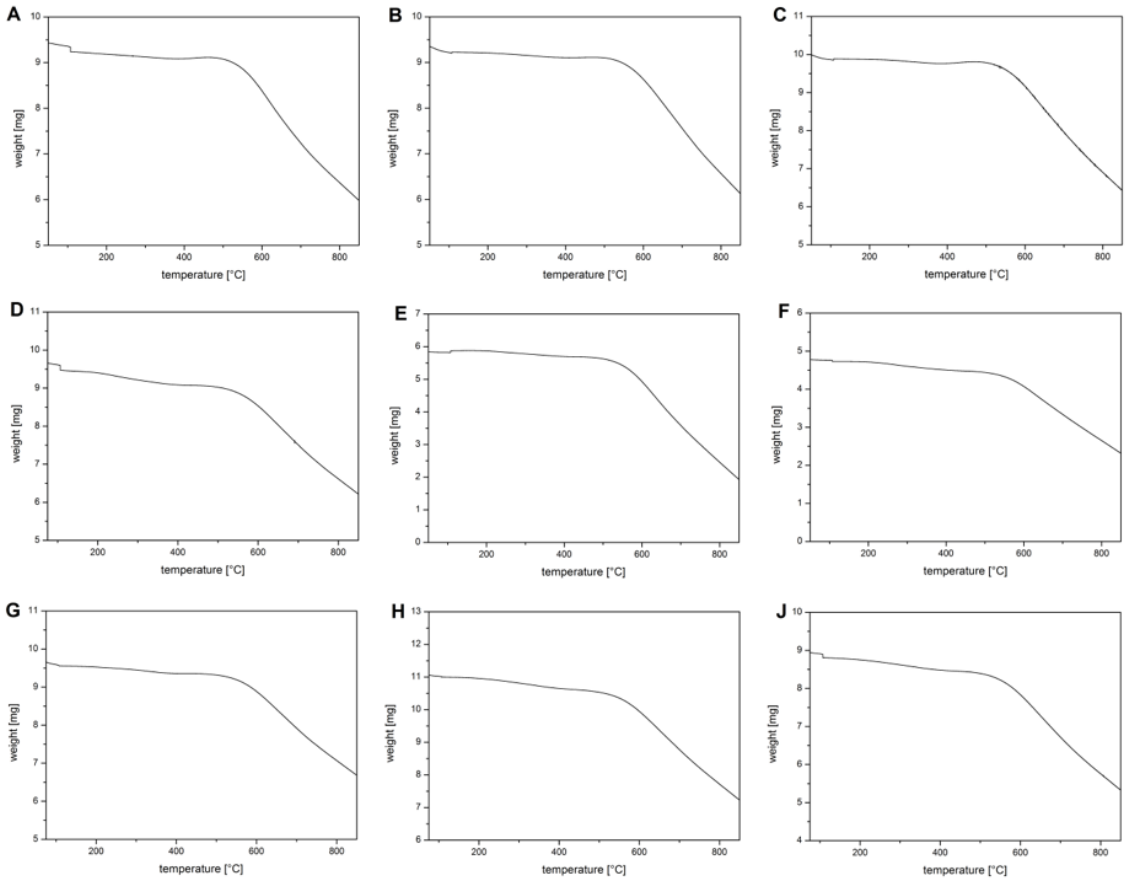

Figure 7.7.4: TGA measurements of A) milled ND **4**; B) 4-cyanophenyl-functionalized ND **6**; C) 4-aminophenyl-functionalized ND **7**; D) (2,3,4,6-tetra-*O*-acetyl-α-D-mannosyl-thioureido)-conjugated ND **9**; E) (methyl 2,3,4,-tri-*O*-acetyl-α-D-mannoside-6-thioureido)-conjugated ND **8**; F) (p-thioureidophenyl 2,3,4,6-tetra-*O*-acetyl-α-D-mannoside)-conjugated ND **10**; G) (α-D-mannosyl-thioureido)-conjugated ND **12**; H) (methyl α-D-mannoside-6-thioureido)-conjugated ND **11**; J) (p-thioureidophenyl α-D-mannoside)-conjugated ND **13**.

^{1}H NMR and ^{13}C NMR Spectra of 5

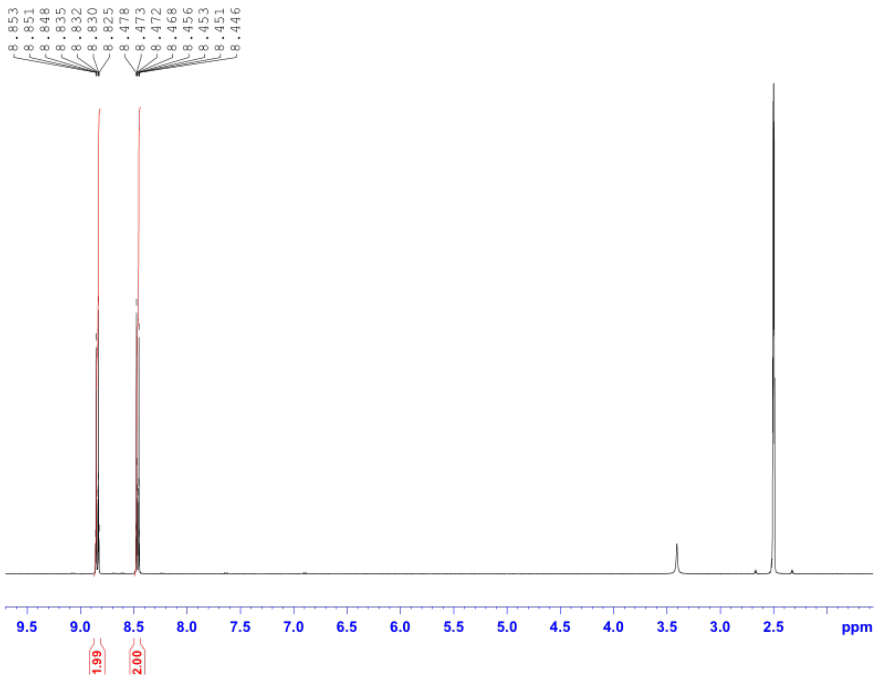

Figure 7.7.5: ^{1}H NMR (DMSO-d$_6$) spectrum of 4-cyanobenzenediazonium tetrafluoroborate (**5**)

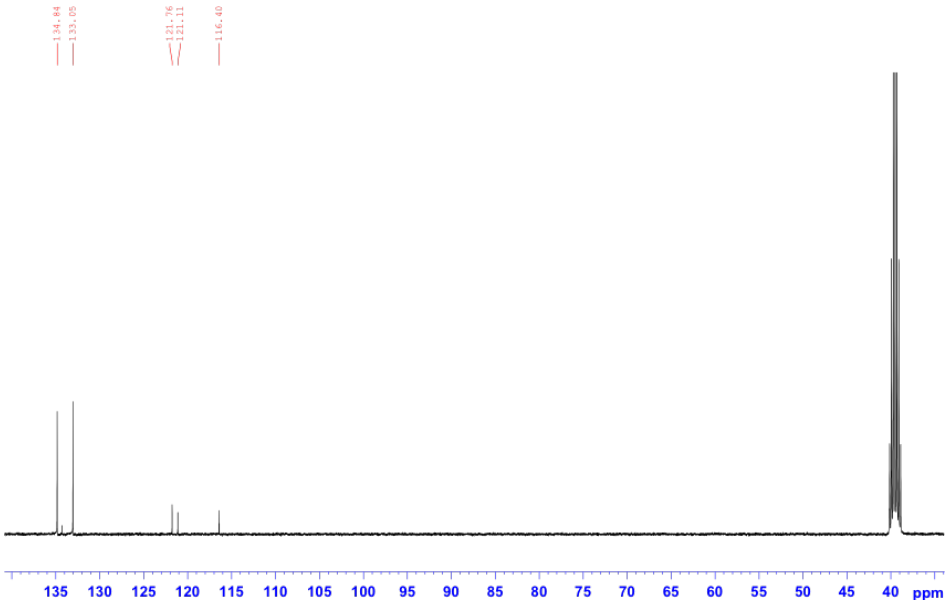

Figure 7.7.6: ^{13}C NMR (DMSO-d$_6$) spectrum of 4-cyanobenzenediazonium tetrafluoroborate (**5**)

7.8 Investigation of P fimbriae mediated bacterial adhesion

General methods

Analytical thin layer chromatography (TLC) was performed on silica gel plates (GF 254, Merck) visualization was achieved by UV light and/or with 10 % sulfuric acid in ethanol followed by heat treatment at ~180 °C. Flash chromatography was performed on silica gel 60 (Merck, 230-400 mesh, particle size 0.040-0.063 mm) by using distilled solvents. Melting points (mp) were determined on a Büchi M-56 apparatus. Optical rotations were measured with a Perkin-Elmer 241 polarimeter (sodium D-line: 589 nm, length of cell: 1 dm) in the solvents indicated. Proton (^{1}H) nuclear magnetic resonance spectra and carbon (^{13}C) nuclear magnetic resonance spectra were recorded on a Bruker DRX-500 and AV-600 spectrometer. Chemical shifts are referenced to the residual proton of the NMR solvent. Data are presented as follows: chemical shift, multiplicity (s=singlet, d=doublet, t=triplet, q=quartet, m=multiplet, and br=broad signal), coupling constant in hertz (Hz) and, integration. Full assignment of the peaks was achieved with the aid of 2D NMR techniques (^{1}H/^{1}H COSY and ^{1}H/^{13}C HSQC). Infrared (IR) spectra were measured with a Perkin Elmer FT-IR Paragon 1000 (ATR) spectrometer and were reported in cm^{-1}. ESI mass spectra were recorded on a LCQ Classic from Thermo Finnigan. Fluorescence readout was accomplished with an Infinite® 200 PRO multimode reader from Tecan.

Synthesis

Methyl (2,6-di-*O*-benzyl-3,4-di-*O*-acetyl-α-D-galactopyranosyl)-(1→4)-2,3,6-tri-O-benzyl-α-D-galactopyranoside (4):

Phenyl 2,6-di-*O*-benzyl-4,5-di-*O*-acetyl-thio-β-D-galactopyranoside (**1**, 560 mg, 1.04 mmol) and methyl 2,3,6-tri-*O*-benzyl-α-D-galactopyranoside (**2**, 483 mg, 1.04 mmol) were dissolved in dry dichloromethane (12 mL) with 5 % [bmim][OTf] and powdered molecular sieves (3 Å). At 0 °C NIS (468 mg, 2.08 mmol) was added and the solution stirred for 30 min. To the ice cold solution TMSOTf (38 µL, 208 µmol) was added dropwise and the reaction stirred for 20 min. The solvent was removed under reduced pressure and the crude product was dissolved in dichloromethane. The organic layer was washed with water (3x25 mL). It was dried over $MgSO_4$, filtered and the filtrate was concentrated under reduced pressure. Purification of the crude product by column chromatography (toluene/ethyl acetate, 7:1) gave **4** as a colorless oil (797 mg, 894 µmol, 86 %). R_f = 0.2 (toluene/ethyl acetate, 7:1); m.p. 134 °C; $[\alpha]_D^{23}$ = +114 (c = 0.5, in methanol); ^{1}H NMR (600 MHz, $CDCl_3$, 300 K, TMS): δ = 7.40-7.11 (m, 25H, Ar-H), 5.55 (dd, 1H, $^3J_{3,4}$ = 3.4 Hz, $^3J_{4,5}$ = 1.1 Hz, H-4), 5.32 (dd, 1H, $^3J_{2,3}$ = 10.3 Hz, $^3J_{3,4}$ = 3.4 Hz, H-3), 5.07 (d, 1H, $^3J_{1,2}$ = 3.6 Hz, H-1), 4.84-4.54 (m, 8H, H-1‘, H-3‘, $(OCH_2)_3$), 4.28-4.20 (m, 2H, OCH_2), 4.08 (m, 1H, H-4‘), 3.99-3.80 (m, 7H, OCH_2, H-2, H-2‘, H-5, H-5, H-6a), 3.44 (dd, 1H, $^3J_{5,6}$ = 5.9 Hz, $^2J_{6a,6b}$ = 9.9 Hz, H-6b), 3.16 (m, 1H, H-6a‘), 3.05 (m, 1H, H-6b‘), 1.95, 1.93 (s, 3H, OCH_3) ppm; ^{13}C NMR (150 MHz, $CDCl_3$, 300 K, TMS): δ = 128.8-127.1 (C-Ar), 100.0 (C-1), 98.5 (C-1‘), 77.5 (C-5), 76.9 (C-2), 75.4 (C-2‘), 74.3 (C-5‘), 73.5, 73.3, 73.1, 73.1, 73.0 (OCH_2), 70.5 (C-3), 69.2 (C-4), 69.0 (C-4‘), 67.8 (C-6), 67.3 (C-3‘), 67.0 (C-6‘) ppm; ESI-MS: *m/z* calcd for $C_{52}H_{58}O_{13}$: 913.4 [M+NA]+; found 913.4.

2-Azidoethyl (2,6-di-*O*-benzyl-3,4-di-*O*-acetyl-α-D-galactopyranosyl)-(1→4)-2,3,6-tri-*O*-benzyl-β-D-galactopyranoside (5):

Phenyl 2,6-di-*O*-benzyl-4,5-di-O-acetyl-thio-β-D-galactopyranoside (**1**, 516 mg, 963 µmol) and 2-azidoethyl 2,3,6-tri-*O*-benzyl-β-D-galactopyranoside (**3**, 500 mg, 963 µmol) were dissolved in dry dichloromethane (12 mL) with 5 % [bmim][OTf] and powdered molecular sieves (3 Å). At 0 °C NIS (434 mg, 1.93 mmol) was added and the solution stirred for 30 min. To the ice cold solution TMSOTf (35 µL, 193 µmol) was added dropwise and the reaction stirred for 20 min. The solvent was removed under reduced pressure and the crude product was dissolved in dichloromethane. The organic layer was washed with water (3x20 mL). It was dried over $MgSO_4$, filtered and the filtrate was concentrated under reduced pressure. Purification of the crude product by column chromatography (cyclohexane/ethyl acetate, 5:1) gave **5** as a colorless oil (574 mg, 607 µmol, 63 %); R_f = 0.3 (toluene/ethyl acetate, 7:1); m.p. 120 °C; $[\alpha]_D^{23}$ = +137 (c = 0.5, in methanol); ^{1}H NMR (600 MHz, $CDCl_3$, 300 K, TMS): δ = 7.40-7.11 (m, 25H, Ar-H), 5.51 (dd, 1H, $^3J_{3,4}$ = 3.6 Hz, $^3J_{4,5}$ = 1.6 Hz, H-4), 5.30 (dd, 1H, $^3J_{2,3}$ = 10.1 Hz, $^3J_{3,4}$ = 3.6 Hz, H-3), 5.01 (d, 1H, $^3J_{1,2}$ = 3.2 Hz, H-1), 4.80-4.52 (m, 8H, H-1‘, H-3‘, $(OCH_2)_3$), 4.28-4.20 (m, 4H, OCH_2, OCH_2CH_2), 4.08 (m, 1H, H-4‘), 3.88-3.79 (m, 9H, OCH_2, H-2, H-2‘, OCH_2CH_2, H-5, H-5, H-6a), 3.41 (m, 1H, H-6b), 3.08 (m, 1H, H-6a‘), 3.02 (m, 1H, H-6b‘), 1.93, 1.91 (s, 3H, OCH_3) ppm; ^{13}C NMR (150 MHz, $CDCl_3$, 300 K, TMS): δ = 128.8-127.1 (C-Ar), 100.2 (C-1), 99.5 (C-1‘), 76.5 (C-5), 75.9 (C-2), 75.4 (C-2‘), 74.1 (C-5‘), 73.5, 73.2, 73.1, 73.0, 73.0 (OCH_2), 70.4 (C-3), 68.2 (C-4), 68.0 (C-4‘), 87.6 (OCH_2CH_2), 66.8 (C-6), 66.3 (C-3‘), 67.0 (C-6‘), 56.4 (OCH_2CH_2) ppm; ESI-MS: *m/z* calcd for $C_{59}H_{53}N_3O_{13}$: 968.4 [M+NA]+; found 968.3.

Methyl (α-d-galactopyranosyl)-(1→4)-α-D-galactopyranoside (6):

Methyl (2,6-di-*O*-benzyl-3,4-di-*O*-acetyl-α-D-galactopyranosyl)-(1→4)-2,3,6-tri-O-benzyl-α-D- galactopyranoside (**4**, 430 mg, 483 µmol) was dissolved in methanol and Pd/C was added. The reaction mixture was stirred at 50 °C under high pressure H_2 (150 bar) for 120 h. After 60 h the catalyst was removed by filtration and new catalyst was added. Finally the catalyst was filtrated and potassium carbonate (13.0 mg, 97.0 µmol) was added and the reaction stirred at ambient temperature for 2 h. Amberlite IR120 (H+) was used for neutralization, filtrated and the solvent was removed under reduced pressure to give **6** as colorless solid (155 mg, 435 µmol, 90 %). R_f = 0.1 (ethyl acetate/methanol, 4:1); m.p. 220 °C; $[\alpha]_D^{23}$ = +186 (c = 0.5, in methanol); ^{1}H NMR (600 MHz, $CDCl_3$, 300 K, TMS): δ = 4.96 (d, $^3J_{1,2}$ = 3.8 Hz, 1H, H-1), 4.73 (d, 1H, $^3J_{1,2}$ = 3.4 Hz, H-1‘), 4.20 (m, 1H, H-3), 4.03 (m, 1H, H-4), 3.91 (dd, 1H, $^3J_{3,4}$ = 1.2 Hz, $^3J_{4,5}$ = 3.2 Hz, H-4‘), 3.88-3.79 (m, 3H, H-3, H-2, H-6a), 3.79-3.72 (m, 5H, H-2´, H-5, H-5´, H-6b, H-6a´), 3.69 (dd, 1H, $^3J_{5,6}$ = 5.2 Hz, $^2J_{6a,6b}$ = 11.3 Hz, H-6b‘), 3.40 (s, 3H, OCH_3) ppm; ^{13}C NMR (150 MHz, $CDCl_3$, 300 K, TMS): δ = 102.9 (C-1), 101.7 (C-1‘), 81.4 (C-4‘), 73.1 (C-3), 71.9 (C-2), 71.3 (C-5), 71.3 (C-4), 71.0 (C-2‘), 70.7 (C-5‘), 70.6 (C-3‘), 62.7 (C-6), 61.6 (C-6‘), 55.8 (OCH_3) ppm; ESI-MS: *m/z* calcd for $C_{13}H_{24}O_{11}$: 379.1 [M+NA]+; found 379.1.

2-Aminoethyl (α-D-galactopyranosyl)-(1→4)-β-D-galactopyranoside (7):

2-Azidoethyl (2,6-di-*O*-benzyl-3,4-di-*O*-acetyl-α-D-galactopyranosyl)-(1→4)-2,3,6-tri-*O*-benzyl-β-D-galactopyranoside (**5**, 350 mg, 370 µmol) was dissolved in methanol and Pd/C was added. The reaction mixture was stirred at 50 °C under high pressure H_2 (150 bar) for 120 h. After 60 h the catalyst was removed by filtration and new catalyst was added. Finally the catalyst was filtrated and potassium carbonate (10.0 mg, 74.0 µmol) was added and the reaction stirred at ambient temperature for 2 h. Amberlite IR120 (H+) was used for neutralization, filtrated and the solvent was removed under reduced pressure to gave **7** as colorless solid (122 mg, 318 µmol, 86 %). R_f = 0.05 (ethyl acetate/methanol, 4:1); m.p. 228 °C; $[\alpha]_D^{23}$ = +161 (c = 0.5, in methanol); ^{1}H NMR (600 MHz, $CDCl_3$, 300 K, TMS): δ = 4.99 (d, $^3J_{1,2}$ = 4.8 Hz, 1H, H-1), 4.76 (d, $^3J_{1,2}$ = 3.6 Hz, 1H, H-1‘), 4.23 (m, 1H, H-3), 4.05 (m, 1H, H-4), 3.94 (m, 1H, H-4‘), 3.90-3.72 (m, 11H, H-2, H-5, H-2‘, H-6, H-3‘, H-5‘,H-6‘, $OCH_2CH_2NH_2$) ppm; ^{13}C NMR (150 MHz, $CDCl_3$, 300 K, TMS): δ = 102.9 (C-1), 101.7 (C-1‘), 81.4 (C-4‘), 73.1 (C-3), 71.9 (C-2), 71.3 (C-5), 71.3 (C-4), 71.0 (C-2‘), 70.7 (C-5‘), 70.6 (C-3‘), 64.3 (OCH_2CH_2), 62.7 (C-6), 61.6 (C-6‘), 52.8 (OCH_2CH_2) ppm; ESI-MS: *m/z* calcd for $C_{14}H_{27}NO_{11}$: 408.2 [M+NA]+; found 408.3.

Buffer solutions

PBS buffer: 140 mM sodium chloride, 2.7 mM potassium chloride, 10 mM sodium dihydrogen phosphate dihydrate, 1.8 mM potassium dihydrogen phosphate, 1 L ddH_2O, pH 7.2; carbonate buffer: sodium carbonate 15 mM, sodium hydrogen carbonate 30 mM, 1 L ddH_2O, pH 9.2; PBST: PBS buffer + 0.05 % v/v Tween®20; MES buffer: 0.5 M MES, 1 L ddH_2O, pH 6.3; TAE buffer: 40 mM TRIS, 20 mM acetic acid, 1 mM EDTA, 1 L ddH_2O, pH 8.3.

Covalent functionalization of magnetic PEG-COOH beads

Magnetic beads (micromer®-M, polystyrol core, surface PEG-COOH, size: 2 µm, 600 µL, 7.2x10^9 particles) were activated as previously reported.[80] The respective glycoside **7** (10 mM in carbonate buffer, 1.00 mL/portion) were incubated with the activated beads (1 portion, 1.8x10^9 particles) at ambient temperature and 600 rpm for 3 h. The beads were washed with PBS buffer (2 × 400 µL), subsequently blocked with ethanolamine (10 mM in carbonate buffer, 1.00 mL/portion) and incubated at ambient temperature and 600 rpm for 1 h. After washing with PBS buffer (2 × 1.00 mL) the functionalized beads were suspended in PBS buffer (1 mL/portion) and stored at 4 °C until use. All steps were carried out in Eppendorf tubes® and a magnetic separation rack (DyneMag-2 magnet, Life technologies) was used for bead extraction synthesis.

Cloning experiments

Restriction The insert *Ac*GFP was cleaved out from a pQE30 plasmid with the restriction enzymes XhOI and HindIII as depicted in table 7.8.1. and incubated at 37 °C for 16 h. The new vector pETM-14 (EMBL-Heidelberg) was treated with the same procedure.

	pETM-14	*Ac*GFP
DNA	21 µL (c = 795 ng/µL)	21 µL (c = 644 ng/µL)
XhoI (Fermentas)	1.5 µL	1.5 µL
HindIII (Fermentas)	1.5 µL	1.5 µL
BSA	3 µL	3 µL
Buffer R (Fermentas)	3 µL	3 µL
total	30 µL	30 µL

Table 7.8.1: Restriction digest of insert *Ac*GFP and vector pETM-14.

The digest was proven with an agarose gel (1.5 % in TAE buffer, cf Figure 7.8.1). The insert was extracted out from the gel (Fermentas) and the concentration was determined (*Ac*GFP c = 35 ng/µL).

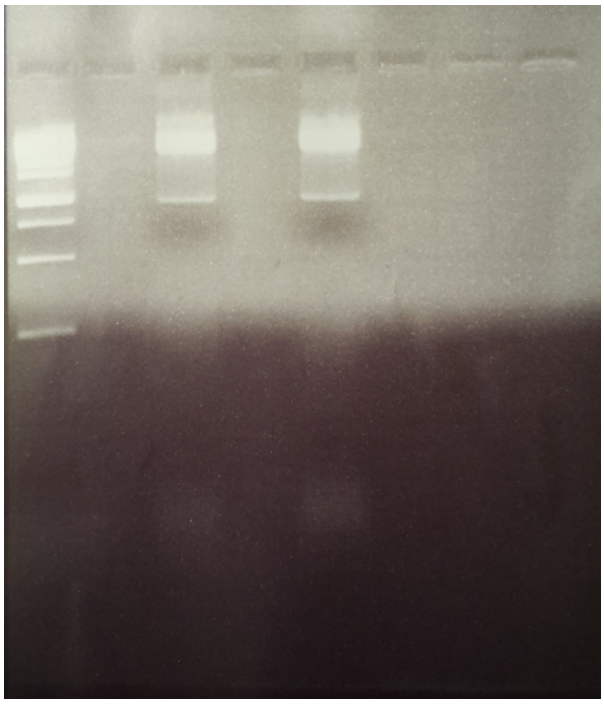

Figure 7.8.1: Agarose gel (1.5 %) with the restricted insert (row 3 and 5).

Ligation The ligation was implemented as depicted in table 7.8.2 and incubated at 18 °C for 16 h.

pETM-14 (c = 188 ng/µL)	3 µL
*Ac*GFP (c = 35 ng/µL)	16 µL
ligase buffer 10x (Fermentas)	2.5 µL
ligase (Fermentas)	2 µL
H_2O	1.5 µL
total	25 µL

Table 7.8.2: Ligation of *Ac*GFP and pETM-14.

The ligation was proven with an additional agarose gel (cf Figure 7.8.2).

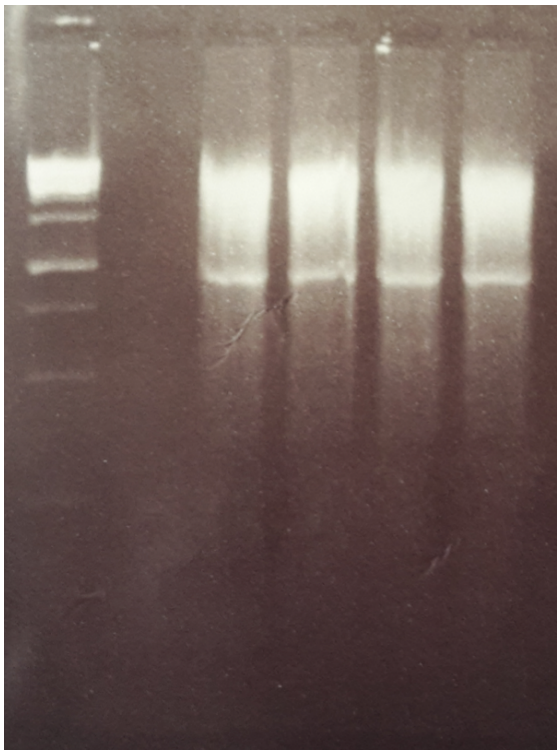

Figure 7.8.2: Agarose gel (1.5 %) after ligation.

Transformation The successful ligated plasmid was transformed via electroporation in competent *E. coli* XL-1. Four aliquots of competent XL-1 were incubated on ice for 10 min with 1 µL of the plasmid DNA. Afterwards they were treated with a heat shock at 42 °C for 120 s and immediately fresh LB media (600 µL) was added and incubated at 37 °C and 800 rpm. After 1 h 100 µL of the bacteria suspension was plated on agar plates with kanamycin (50 mg/L). From the grown colonies a colony PCR was carried out. Therefore single colonies were picked, transferred in PCR tubes, the PCR mix (cf table 7.8.3) was added and the PCR (Thermocycler iCycler, BIO-Rad) was as depicted in table 7.8.4.

PCR Master mix 2x (Fermentas)	5 µL
primer T7 (c = 5 pmol/µL)	1 µL
primer T7 term (c = 5 pmol/µL)	1 µL
H_2O	3 µL
total	10 µL

Table 7.8.3: Colony PCR mix.

	Temperature	Duration	Cycles
Denaturation	95 °C	30 s	20
Annealing	55 °C	30 s	20
Elongation	72 °C	150 s	20
Final Elongation	72 °C	300 s	1

Table 7.8.4: PCR protocol.

Additional the colonies were plated on a new agar plate. The probes from the colony PCR can be seen in an agarose gel (1.5 % in TAE buffer, cf figure 7.8.3).

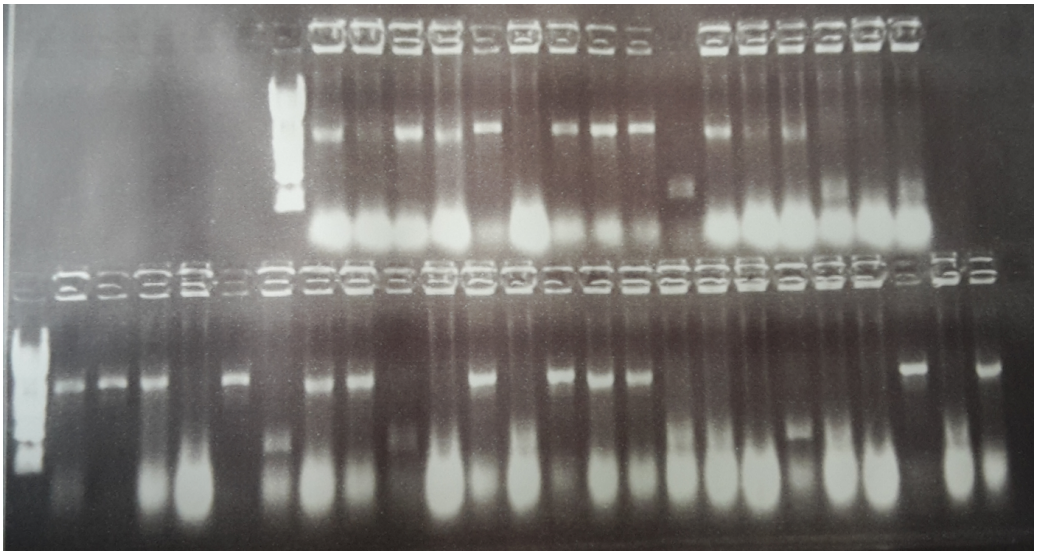

Figure 7.8.3: Agarose gel (1.5 %) after colony PCR.

One successful clone was chosen, grown in LB media for 16 h at 37 °C and 175 rpm and a plasmid preparation (Qiagen) was performed to obtain the new plasmid DNA in a concentration of 62.5 ng/µL.

Sequencing results For verification a DNA sequencing was ordered. A sequence alignment of *Ac*GFP with the new plasmid is displayed in figure 7.8.4. No exchange happend during the plasmid prepararion and therefore the new plasmid was transformed into the P fimbriated VR123 *E. coli* to obtain GFP expressing P fimbriated bacteria.

```
EMBOSS_001         1 ATGGTGAGCAAGGGCGCCGAGCTGTTCACCGGCATCGTGCCCATCCTGAT     50
                     ||||||||||||||||||||||||||||||||||||||||||||||||||
EMBOSS_001         1 ATGGTGAGCAAGGGCGCCGAGCTGTTCACCGGCATCGTGCCCATCCTGAT     50

EMBOSS_001        51 CGAGCTGAATGGCGATGTGAATGGCCACAAGTTCAGCGTGAGCGGCGAGG    100
                     ||||||||||||||||||||||||||||||||||||||||||||||||||||
EMBOSS_001        51 CGAGCTGAATGGCGATGTGAATGGCCACAAGTTCAGCGTGAGCGGCGAGG    100

EMBOSS_001       101 GCGAGGGCGATGCCACCTACGGCAAGCTGACCCTGAAGTTCATCTGCACC    150
                     ||||||||||||||||||||||||||||||||||||||||||||||||||||
EMBOSS_001       101 GCGAGGGCGATGCCACCTACGGCAAGCTGACCCTGAAGTTCATCTGCACC    150

EMBOSS_001       151 ACCGGCAAGCTGCCTGTGCCCTGGCCCACCCTGGTGACCACCCTGAGCTA    200
                     ||||||||||||||||||||||||||||||||||||||||||||||||||||
EMBOSS_001       151 ACCGGCAAGCTGCCTGTGCCCTGGCCCACCCTGGTGACCACCCTGAGCTA    200

EMBOSS_001       201 CGGCGTGCAGTGCTTCTCACGCTACCCCGATCACATGAAGCAGCACGACT    250
                     ||||||||||||||||||||||||||||||||||||||||||||||||||||
EMBOSS_001       201 CGGCGTGCAGTGCTTCTCACGCTACCCCGATCACATGAAGCAGCACGACT    250

EMBOSS_001       251 TCTTCAAGAGCGCCATGCCTGAGGGCTACATCCAGGAGCGCACCATCTTC    300
                     ||||||||||||||||||||||||||||||||||||||||||||||||||||
EMBOSS_001       251 TCTTCAAGAGCGCCATGCCTGAGGGCTACATCCAGGAGCGCACCATCTTC    300

EMBOSS_001       301 TTCGAGGATGACGGCAACTACAAGTCGCGCGCCGAGGTGAAGTTCGAGGG    350
                     ||||||||||||||||||||||||||||||||||||||||||||||||||||
EMBOSS_001       301 TTCGAGGATGACGGCAACTACAAGTCGCGCGCCGAGGTGAAGTTCGAGGG    350

EMBOSS_001       351 CGATACCCTGGTGAATCGCATCGAGCTGACCGGCACCGATTTCAAGGAGG    400
                     ||||||||||||||||||||||||||||||||||||||||||||||||||||
EMBOSS_001       351 CGATACCCTGGTGAATCGCATCGAGCTGACCGGCACCGATTTCAAGGAGG    400

EMBOSS_001       401 ATGGCAACATCCTGGGCAATAAGATGGAGTACAACTACAACGCCCACAAT    450
                     ||||||||||||||||||||||||||||||||||||||||||||||||||||
EMBOSS_001       401 ATGGCAACATCCTGGGCAATAAGATGGAGTACAACTACAACGCCCACAAT    450

EMBOSS_001       451 GTGTACATCATGACCGACAAGGCCAAGAATGGCATCAAGGTGAACTTCAA    500
                     ||||||||||||||||||||||||||||||||||||||||||||||||||||
EMBOSS_001       451 GTGTACATCATGACCGACAAGGCCAAGAATGGCATCAAGGTGAACTTCAA    500

EMBOSS_001       501 GATCCGCCACAACATCGAGGATGGCAGCGTGCAGCTGGCCGACCACTACC    550
                     ||||||||||||||||||||||||||||||||||||||||||||||||||||
EMBOSS_001       501 GATCCGCCACAACATCGAGGATGGCAGCGTGCAGCTGGCCGACCACTACC    550

EMBOSS_001       551 AGCAGAATACCCCCATCGGCGATGGCCCTGTGCTGCTGCCCGATAACCAC    600
                     ||||||||||||||||||||||||||||||||||||||||||||||||||||
EMBOSS_001       551 AGCAGAATACCCCCATCGGCGATGGCCCTGTGCTGCTGCCCGATAACCAC    600

EMBOSS_001       601 TACCTGTCCACCCAGAGCGCCCTGTCCAAGGACCCCAACGAGAAGCGCGA    650
                     ||||||||||||||||||||||||||||||||||||||||||||||||||||
EMBOSS_001       601 TACCTGTCCACCCAGAGCGCCCTGTCCAAGGACCCCAACGAGAAGCGCGA    650

EMBOSS_001       651 TCACATGATCTACTTCGGCTTCGTGACCGCCGCCGCCATCACCCACGGCA    700
                     ||||||||||||||||||||||||||||||||||||||||||||||||||||
EMBOSS_001       651 TCACATGATCTACTTCGGCTTCGTGACCGCCGCCGCCATCACCCACGGCA    700

EMBOSS_001       701 TGGATGAGCTGTACAAGTGA    720
                     ||||||||||||||||||||
EMBOSS_001       701 TGGATGAGCTGTACAAGTGA    720
```

Figure 7.8.4: Sequence alignment between the known *Ac*GFP sequence and the insert DNA.

Bacterial adhesion experiments

GFP expressing P fimbriated *E. coli* were incubated in LB media with kanamycin (50 mg/L) and ampicillin (100 mg/L) at 37 °C over night. At OD_{600} = 0.5 the GFP expression was induced with 1 mM IPTG. After 4 h the bacteria were harvested (4000 rpm, 20 min) and washed with PBS (2 mL) twice. A bacterial suspension with PBS OD_{600} = 0.5 was adjusted. From the previous prepared beads 50 µL were washed with PBS (400 µL and resuspended in 150 µL PBS. 50 µL bacteria suspension was added and at room temperature and 600 rpm incubated for 45 min. Afterwards the magnetic beads were washed twice with PBS (400 µL), suspended in 100 µL PBS and the fluorescence was readout. Inhibitor solutions in the respective concentrations were added (50 µL) and again incubated at room temperature and 600 rpm for 45 min. After washing twice with PBS (400 µL) another fluorescence readout was performed.

Bibliography

[1] R. B. Welbourn, *Gesnerus* **1992**, *49 Pt 2*, 137–50.

[2] K. Landsteiner, *Circ. Res.* **1969**, *25*, 500.

[3] W. T. Morgan, W. M. Watkins, *Br. Med. Bull.* **1969**, *25*, 30–4.

[4] W. E. Pricer, Jr, R. L. Hudgin, G. Ashwell, R. J. Stockert, A. G. Morell, *Methods Enzymol.* **1974**, *34*, 688–91.

[5] E. Garman, G. Laver, *The Structure, Function, and Inhibition of Influenza Virus Neuraminidase*, Springer US, Boston, MA **2005**, 247–267.

[6] A. Dell, H. R. Morris, *Science* **2001**, *291*, 2351–6.

[7] H. van Haalbeck, *Curr. Opin. Struct. Biol.* **1994**, *4*, 697–709.

[8] M. Sawa, T.-L. Hsu, T. Itoh, M. Sugiyama, S. R. Hanson, P. K. Vogt, C.-H. Wong, *Proc. Natl. Acad. Sci.* **2006**, *103*, 12371–6.

[9] X. Song, J. Heimburg-Molinaro, R. D. Cummings, D. F. Smith, *Curr. Opin. Chem. Biol.* **2014**, *18*, 70–7.

[10] A.Varki, R. D. Cummings, J. D. Esko, H. H. Freeze, P. Stanley, C. R. Bertozzi, G. W. Hart, M. E. Etzler, *Essentials of Glycobiology*, 2nd Edition, Cold Spring Harbor Laboratory Press **2009**.

[11] B. G.A., *Toxicology* **1974**, *2*, 77–102.

[12] M. C. Z. Meneghetti, A. J. Hughes, T. R. Rudd, H. B. Nader, A. K. Powell, E. A. Yates, M. A. Lima, *J. R. Soc. Interface* **2015**, *12*, 0589.

[13] L. M. Hiebert, J. Han, A. K. Mandal, *Antioxid. Redox Signal.* **2014**, *21*, 1032–43.

[14] Basappa, K. S. Rangappa, K. Sugahara, *Glycoconj. J.* **2014**, *31*, 461–7.

[15] L. Jin, J. P. Abrahams, R. Skinner, M. Petitou, R. N. Pike, R. W. Carrell, *Proc. Natl. Acad. Sci.* **1997**, *94*, 14683–8.

[16] Z. Fujimoto, H. Tateno, J. Hirabayashi, *Methods Mol. Biol.* **2014**, *1200*, 579–606.

[17] N. Sharon, *Protein Sci.* **1998**, *7*, 2042–2048.

[18] N. Sharon, H. Lis, *Glycobiology* **2004**, *14*, 53R–62R.

[19] G. D. Griffiths, *Toxins* **2011**, *3*, 1373–92.

[20] J. B. Sumner, S. F. Howell, *J. Bacteriol.* **1936**, *32*, 227–37.

[21] T. K. Chowdhury, *Adv. Exp. Med. Biol.* **1975**, *55*, 1–12.

[22] A. Williams, D. R. Westhead, *Protein Eng.* **2002**, *15*, 771–4.

[23] N. M. Dahms, M. K. Hancock, *Biochim. Biophys. Acta* **2002**, *1572*, 317–40.

[24] K. Drickamer, M. E. Taylor, *Curr. Opin. Struct. Biol.* **2015**, *34*, 26–34.

[25] J. C. Hoving, G. J. Wilson, G. D. Brown, *Cell. Microbiol.* **2014**, *16*, 185–94.

[26] J. W. Becker, G. N. Reeke, Jr, J. L. Wang, B. A. Cunningham, G. M. Edelman, *J. Biol. Chem.* **1975**, *250*, 1513–24.

[27] I. R. Nabi, J. Shankar, J. W. Dennis, *J. Cell Sci.* **2015**, *128*, 2213–9.

[28] T. Advedissian, F. Deshayes, F. Poirier, C. Grandjean, M. Viguier, *Med. Sci.* **2015**, *31*, 499–505.

[29] D. I. Liao, G. Kapadia, H. Ahmed, G. R. Vasta, O. Herzberg, *Proc. Natl. Acad. Sci.* **1994**, *91*, 1428–32.

[30] B. S. Bochner, N. Zimmermann, *J. Allergy Clin. Immunol.* **2015**, *135*, 598–608.

[31] P. R. Crocker, *Curr. Opin. Struct. Biol.* **2002**, *12*, 609–15.

[32] S. Magesh, H. Ando, T. Tsubata, H. Ishida, M. Kiso, *Curr. Med. Chem.* **2011**, *18*, 3537–50.

[33] W. Van Breedam, S. Pöhlmann, H. W. Favoreel, R. J. de Groot, H. J. Nauwynck, *FEMS Microbiol. Rev.* **2014**, *38*, 598–632.

[34] F. Li, C. Ma, J. Wang, *Curr. Med. Chem.* **2015**, *22*, 1361–82.

[35] M. D. Esona, R. Gautam, *Clin. Lab. Med.* **2015**, *35*, 363–91.

[36] E. J. Kremer, G. R. Nemerow, *PLoS Pathog.* **2015**, *11*, e1004821.

[37] N. Sharon, *FEBS Lett.* **1987**, *217*, 145–57.

[38] G. Waksman, S. J. Hultgren, *Nat. Rev. Microbiol.* **2009**, *7*, 765–74.

[39] J. Lillington, S. Geibel, G. Waksman, *Biochim. Biophys. Acta* **2014**, *1840*, 2783–93.

[40] D. Chappell, M. Jacob, K. Hofmann-Kiefer, M. Rehm, U. Welsch, P. Conzen, B. F. Becker, *Cardiovasc. Res.* **2009**, *83*, 388–96.

[41] S. Weinbaum, J. M. Tarbell, E. R. Damiano, *Annu. Rev. Biomed. Eng.* **2007**, *9*, 121–67.

[42] K. W. Moremen, M. Tiemeyer, A. V. Nairn, *Nat. Rev. Mol. Cell Biol.* **2012**, *13*, 448–62.

[43] H. Schachter, *Glycoconj. J.* **2000**, *17*, 465–83.

[44] E. Mohorko, R. Glockshuber, M. Aebi, *J. Inherit. Metab. Dis.* **2011**, *34*, 869–78.

[45] A. D. Humphries, S. M. Townsend, R. A. Kingsley, T. L. Nicholson, R. M. Tsolis, A. J. Bäumler, *FEMS Microbiol. Lett.* **2001**, *201*, 121–5.

[46] T. P. V. Madhavan, H. Sakellaris, *Adv. Appl. Microbiol.* **2015**, *90*, 155–97.

[47] P. Lüthje, A. Brauner, *Adv. Microb. Physiol.* **2014**, *65*, 337–72.

[48] M. Erhardt, K. Namba, K. Hughes, *CSH Persp. Biol.* **2010**, *2*, 299.

[49] R. Fronzes, H. Remaut, G. Waksman, *EMBO J.* **2008**, *27*, 2271–2280.

[50] M. Achtmann, G. Morelli, S. Schwuchow, *J. Bacteriol.* **1978**, *3*, 1053–1061.

[51] D. Mangan, I. Snyder, *Infect. Immun.* **1979**, *2*, 520–527.

[52] J. S. Mattick, *Annu. Rev. Microbiol.* **2002**, *56*, 289–314.

[53] O. Schneewind, D. Missiakas, *Biochim. Biophys. Acta* **2014**, *1843*, 1687–97.

[54] W. J. Allen, G. Phan, G. Waksman, *Curr. Opin. Struct. Biol.* **2012**, *22*, 500–506.

[55] I. Ofek, D. L. Hasty, R. J. .Doyle, *Bacterial Adhesion to Animal Cells and Tissues*, ASM Press Washington **2003**.

[56] M. A. Schembri, K. Kjaergaard, E. V. Sokurenko, P. Klemm, *J. Infect. Dis.* **2001**, *1*, 28–31.

[57] G. E. Soto, S. J. Hultgren, *J. Bacteriol.* **1999**, *181*, 1059–1071.

[58] K. W. Dodson, J. S. Pinkner, T. Rose, G. Magnusson, S. J. Hultgren, G. Waksman, *Cell* **2001**, *105*, 733–743.

[59] J. Morschhäuser, H. Hoschützky, K. Jann, J. Hacker, *Infect. Immun.* **1990**, *58*, 2133–8.

[60] J. Parkkinen, G. N. Rogers, T. Korhonen, W. Dahr, J. Finne, *Infect. Immun.* **1986**, *54*, 37–42.

[61] D. I. Kisiela, S. Chattopadhyay, V. Tchesnokova, S. Paul, S. J. Weissman, I. Medenica, S. Clegg, E. V. Sokurenko, *MBio* **2013**, *4*.

[62] *Mol. Microbiol.* **2005**, *55*, 441–455.

[63] S. D. Knight, J. Bouckaert, *Top. Curr. Chem.* **2009**, *288*, 67–107.

[64] C.-S. Hung, J. Bouckaert, D. Hung, J. Pinkner, C. Widberg, A. DeFusco, C. G. Auguste, R. Strouse, S. Langermann, G. Waksman, S. J. Hultgren, *Mol. Microbiol.* **2002**, *44*, 903–15.

[65] J. Bouckaert, J. Berglund, M. Schembri, E. De Genst, L. Cools, M. Wuhrer, C.-S. Hung, J. Pinkner, R. Slättegård, A. Zavialov, D. Choudhury, S. Langermann, S. J. Hultgren, L. Wyns, P. Klemm, S. Oscarson, S. D. Knight, H. De Greve, *Mol. Microbiol.* **2005**, *55*, 441–55.

[66] N. Strömberg, B. I. Marklund, B. Lund, D. Ilver, A. Hamers, W. Gaastra, K. A. Karlsson, S. Normark, *EMBO J.* **1990**, *9*, 2001–10.

[67] S. J. Hultgren, F. Lindberg, G. Magnusson, J. Kihlberg, J. M. Tennent, S. Normark, *Proc. Natl. Acad. Sci.* **1989**, *86*, 4357–61.

[68] K.-A. Karlsson, *Mol. Microbiol.* **1998**, *29*, 1–11.

[69] N. Sharon, *Biochem. Soc. Trans.* **2008**, *36*, 1457–60.

[70] C. Beloin, A. Roux, J. M. Ghigo, *Curr. Top. Microbiol. Immunol.* **2008**, *322*, 249–89.

[71] A. Penesyan, M. Gillings, I. T. Paulsen, *Molecules* **2015**, *20*, 5286–98.

[72] Y. Ma, I. Sobkiv, V. Gruzdys, H. Zhang, X.-L. Sun, *Anal. Bioanal. Chem.* **2012**, *404*, 51–8.

[73] S. N. Narla, H. Nie, Y. Li, X.-L. Sun, *Glycoconj. J.* **2015**, *32*, 483–95.

[74] K. Yamamoto, *Methods Mol. Biol.* **2014**, *1200*, 319–26.

[75] T. K. Lindhorst, C. Kieburg, U. Krallmann-Wenzel, *Glycoconj. J.* **1998**, *15*, 605–13.

[76] A. K. Horst, S. Kötter, T. K. Lindhorst, A. Ludwig, E. Brandt, C. Wagener, *Med. Microbiol. Immunol.* **2001**, *190*, 145–9.

[77] M. Hartmann, A. K. Horst, P. Klemm, T. K. Lindhorst, *Chem. Commun.* **2010**, *46*, 330–332.

[78] L. Möckl, C. Fessele, G. Despras, C. Bräuchle, T. K. Lindhorst, *Biochim. Biophys. Acta* **2016**, *1860*, 2031–6.

[79] P. Aprikian, G. Interlandi, B. A. Kidd, I. Le Trong, V. Tchesnokova, O. Yakovenko, M. J. Whitfield, E. Bullitt, R. E. Stenkamp, W. E. Thomas, E. V. Sokurenko, *PLoS Biol.* **2011**, *9*, e1000617.

[80] A. Müller, K. Kolbe, D. Pussack, L. Hartmann, T. K. Lindhorst, *ChemBioChem* **2016**, *manuscript in preparation.*

[81] M. Hartmann, T. K. Lindhorst, *Eur. J. Org. Chem.* **2011**, *2011*, 3583–3609.

[82] A. R. Brumbaugh, H. L. T. Mobley, *Expert Rev. Vaccines* **2012**, *11*, 663–76.

[83] K. Melican, R. M. Sandoval, A. Kader, L. Josefsson, G. A. Tanner, B. A. Molitoris, A. Richter-Dahlfors, *PLoS Pathog.* **2011**, *7*, e1001298.

[84] P. Klemm, M. A. Schembri, *Int. J. Med. Microbiol.* **2000**, *290*, 27–35.

[85] K. Ohlsen, T. A. Oelschlaeger, J. Hacker, A. S. Khan, *Top. Curr. Chem.* **2009**, *288*, 17–65.

[86] A. L. Kau, D. A. Hunstad, S. J. Hultgren, *Curr. Opin. Microbiol.* **2005**, *8*, 54–9.

[87] K. S. Kim, *Curr. Opin. Infect. Dis.* **2012**, *25*, 273–8.

[88] B. Chassaing, A. Darfeuille-Michaud, *J. Bacteriol.* **2013**, *195*, 76–84.

[89] I. Ofek, E. H. Beachey, *Infect. Immun.* **1978**, *22*, 247–54.

[90] N. Firon, I. Ofek, N. Sharon, *Carbohydr. Res.* **1983**, *120*, 235–49.

[91] N. Firon, S. Ashkenazi, D. Mirelman, I. Ofek, N. Sharon, *Infect. Immun.* **1987**, *55*, 472–6.

[92] J. R. Neeser, B. Koellreutter, P. Wuersch, *Infect. Immun.* **1986**, *52*, 428–36.

[93] P. R. Crocker, T. Feizi, *Curr. Opin. Struct. Biol.* **1996**, *6*, 679–91.

[94] N. Nagahori, R. T. Lee, S.-I. Nishimura, D. Pagé, R. Roy, Y. C. Lee, *ChemBioChem* **2002**, *3*, 836–44.

[95] M. Dubber, O. Sperling, T. K. Lindhorst, *Org. Biomol. Chem* **2006**, *4*, 3901–12.

[96] M. Touaibia, A. Wellens, T. C. Shiao, Q. Wang, S. Sirois, J. Bouckaert, R. Roy, *ChemMedChem* **2007**, *2*, 1190–201.

[97] C. D. Heidecke, T. K. Lindhorst, *Chemistry* **2007**, *13*, 9056–67.

[98] M. Touaibia, R. Roy, *Mini Rev. Med. Chem.* **2007**, *7*, 1270–83.

[99] R. J. Pieters, *Med. Res. Rev.* **2007**, *27*, 796–816.

[100] S. G. Gouin, A. Wellens, J. Bouckaert, J. Kovensky, *ChemMedChem* **2009**, *4*, 749–55.

[101] Y. M. Chabre, R. Roy, *Adv. Carbohydr. Chem. Biochem.* **2010**, *63*, 165–393.

[102] R. J. Pieters, *Adv. Exp. Med. Biol.* **2011**, *715*, 227–40.

[103] A. Papadopoulos, T. C. Shiao, R. Roy, *Mol. Pharm.* **2012**, *9*, 394–403.

[104] T. Klein, D. Abgottspon, M. Wittwer, S. Rabbani, J. Herold, X. Jiang, S. Kleeb, C. Lüthi, M. Scharenberg, J. Bezençon, E. Gubler, L. Pang, M. Smiesko, B. Cutting, O. Schwardt, B. Ernst, *J. Med. Chem.* **2010**, *53*, 8627–41.

[105] C. Grabosch, M. Hartmann, J. Schmidt-Lassen, T. K. Lindhorst, *ChemBioChem* **2011**, *12*, 1066–74.

[106] H. Zuilhof, J. S. Pinkner, B. Ford, E. Chorell, J. M. Crowley, C. K. Cusumano, S. Campbell, J. P. Henderson, S. J. Hultgren, J. W. Janetka, *J. Med. Chem.* **2012**, *55*, 3945–3959.

[107] X. Jiang, D. Abgottspon, S. Kleeb, S. Rabbani, M. Scharenberg, M. Wittwer, M. Haug, O. Schwardt, B. Ernst, *J. Med. Chem.* **2012**, *55*, 4700–13.

[108] D. Abgottspon, B. Ernst, *Chimia (Aarau)* **2012**, *66*, 166–9.

[109] A. Bernardi, J. Jiménez-Barbero, A. Casnati, C. De Castro, T. Darbre, F. Fieschi, J. Finne, H. Funken, K.-E. Jaeger, M. Lahmann, T. K. Lindhorst, M. Marradi, P. Messner, A. Molinaro, P. V. Murphy, C. Nativi, S. Oscarson, S. Penadés, F. Peri, R. J. Pieters, O. Renaudet, J.-L. Reymond, B. Richichi, J. Rojo, F. Sansone, C. Schäffer, W. B. Turnbull, T. Velasco-Torrijos, S. Vidal, S. Vincent, T. Wennekes, H. Zuilhof, A. Imberty, *Chem. Soc. Rev.* **2013**, *42*, 4709–27.

[110] A. Wellens, C. Garofalo, H. Nguyen, N. Van Gerven, R. Slättegård, J.-P. Hernalsteens, L. Wyns, S. Oscarson, H. De Greve, S. Hultgren, J. Bouckaert, *PLoS One* **2008**, *3*, e2040.

[111] A. Wellens, M. Lahmann, M. Touaibia, J. Vaucher, S. Oscarson, R. Roy, H. Remaut, J. Bouckaert, *Biochemistry* **2012**, *51*, 4790–9.

[112] O. Sperling, A. Fuchs, T. K. Lindhorst, *Org. Biomol. Chem.* **2006**, *4*, 3913–22.

[113] B. Ernst, J. L. Magnani, *Nat. Rev. Drug Discov.* **2009**, *8*, 661–77.

[114] I. Ofek, D. L. Hasty, N. Sharon, *FEMS Immunol. Med. Microbiol.* **2003**, *38*, 181–91.

[115] N. Sharon, *Biochim. Biophys. Acta* **2006**, *1760*, 527–37.

[116] M. Totsika, M. Kostakioti, T. J. Hannan, M. Upton, S. A. Beatson, J. W. Janetka, S. J. Hultgren, M. A. Schembri, *J. Infect. Dis.* **2013**, *208*, 921–8.

[117] W. Thomas, *Annu. Rev. Biomed. Eng.* **2008**, *10*, 39–57.

[118] I. Le Trong, P. Aprikian, B. A. Kidd, M. Forero-Shelton, V. Tchesnokova, P. Rajagopal, V. Rodriguez, G. Interlandi, R. Klevit, V. Vogel, R. E. Stenkamp, E. V. Sokurenko, W. E. Thomas, *Cell* **2010**, *141*, 645–55.

[119] M. Ambrosi, N. R. Cameron, B. G. Davis, *Org. Biomol. Chem.* **2005**, *3*, 1593–608.

[120] J. E. Turnbull, R. A. Field, *Nat. Chem. Biol.* **2007**, *3*, 74–7.

[121] T. Horlacher, P. H. Seeberger, *Chem. Soc. Rev.* **2008**, *37*, 1414–22.

[122] Y. Liu, A. S. Palma, T. Feizi, *Biol. Chem.* **2009**, *390*, 647–56.

[123] C. Grabosch, K. Kolbe, T. K. Lindhorst, *ChemBioChem* **2012**, *13*, 1874–9.

[124] J. W. Wehner, M. J. Weissenborn, M. Hartmann, C. J. Gray, R. Šardzík, C. E. Eyers, S. L. Flitsch, T. K. Lindhorst, *Org. Biomol. Chem.* **2012**, *10*, 8919–26.

[125] S. N. Narla, X.-L. Sun, *Org. Biomol. Chem.* **2011**, *9*, 845–50.

[126] K. Larsen, M. B. Thygesen, F. Guillaumie, W. G. T. Willats, K. J. Jensen, *Carbohydr. Res.* **2006**, *341*, 1209–34.

[127] C. Siebold, K. Flükiger, R. Beutler, B. Erni, *FEBS Lett.* **2001**, *504*, 104–11.

[128] M. Hartmann, H. Papavlassopoulos, V. Chandrasekaran, C. Grabosch, F. Beiroth, T. K. Lindhorst, C. Röhl, *FEBS Lett.* **2012**, *586*, 1459–65.

[129] M. Sato, M. Takemura, S. Atarashi, K. Higashi, T. Nagahara, M. Furukawa, T. Ikeuchi, Y. Osada, *J. Antibiot.* **1987**, *40*, 1292–302.

[130] G. N. Tew, D. Liu, B. Chen, R. J. Doerksen, J. Kaplan, P. J. Carroll, M. L. Klein, W. F. DeGrado, *Proc. Natl. Acad. Sci.* **2002**, *99*, 5110–4.

[131] J. Choi, J. Kim, K. Kim, S.-T. Yang, J.-I. Kim, S. Jon, *Chem. Commun.* **2007**, 1151–3.

[132] V. Koteswara Rao, A. Janardhan Rao, S. Subba Reddy, C. Naga Raju, P. Visweswara Rao, S. K. Ghosh, *Eur. J. Med. Chem.* **2010**, *45*, 203–9.

[133] A. Dondoni, A. Massi, P. Nanni, A. Roda, *Chemistry* **2009**, *15*, 11444–9.

[134] G. Estrada-Gutierrez, N. Gomez-Lopez, V. Zaga-Clavellina, S. Giono-Cerezo, A. Espejel-Nuñez, M. A. Gonzalez-Jimenez, S. Espino y Sosa, D. M. Olson, F. Vadillo-Ortega, *Infect. Immun.* **2010**, *78*, 4792–9.

[135] D. L. LaRock, A. Chaudhary, S. I. Miller, *Nat. Rev. Microbiol.* **2015**, *13*, 191–205.

[136] A. Persat, C. D. Nadell, M. K. Kim, F. Ingremeau, A. Siryaporn, K. Drescher, N. S. Wingreen, B. L. Bassler, Z. Gitai, H. A. Stone, *Cell* **2015**, *161*, 988–97.

[137] M. Totsika, D. G. Moriel, A. Idris, B. A. Rogers, D. J. Wurpel, M.-D. Phan, D. L. Paterson, M. A. Schembri, *Curr. Drug Targets* **2012**, *13*, 1386–99.

[138] T. R. D. Costa, C. Felisberto-Rodrigues, A. Meir, M. S. Prevost, A. Redzej, M. Trokter, G. Waksman, *Nat. Rev. Microbiol.* **2015**, *13*, 343–59.

[139] A. J. Mathers, G. Peirano, J. D. D. Pitout, *Clin. Microbiol. Rev.* **2015**, *28*, 565–91.

[140] M. Otto, *FEMS Microbiol. Rev.* **2014**, *38*, 1250–70.

[141] S. Kleeb, L. Pang, K. Mayer, D. Eris, A. Sigl, R. C. Preston, P. Zihlmann, T. Sharpe, R. P. Jakob, D. Abgottspon, A. S. Hutter, M. Scharenberg, X. Jiang, G. Navarra, S. Rabbani, M. Smiesko, N. Lüdin, J. Bezençon, O. Schwardt, T. Maier, B. Ernst, *J. Med. Chem.* **2015**, *58*, 2221–39.

[142] J. Zakrisson, K. Wiklund, O. Axner, M. Andersson, *Biophys. J.* **2013**, *104*, 2137–48.

[143] V. B. Rodriguez, B. A. Kidd, G. Interlandi, V. Tchesnokova, E. V. Sokurenko, W. E. Thomas, *J. Biol. Chem.* **2013**, *288*, 24128–39.

[144] J. Claes, T. Vanassche, M. Peetermans, L. Liesenborghs, C. Vandenbriele, K. Vanhoorelbeke, D. Missiakas, O. Schneewind, M. F. Hoylaerts, R. Heying, P. Verhamme, *Blood* **2014**, *124*, 1669–76.

[145] S. E. W. Grubb, C. Murdoch, P. E. Sudbery, S. P. Saville, J. L. Lopez-Ribot, M. H. Thornhill, *Infect. Immun.* **2009**, *77*, 3872–8.

[146] D. Freebairn, D. Linton, E. Harkin-Jones, D. S. Jones, B. F. Gilmore, S. P. Gorman, *Expert Rev. Med. Devices* **2013**, *10*, 85–103.

[147] L. M. Nilsson, W. E. Thomas, E. V. Sokurenko, V. Vogel, *Appl. Environ. Microbiol.* **2006**, *72*, 3005–10.

[148] B. Fiege, S. Rabbani, R. C. Preston, R. P. Jakob, P. Zihlmann, O. Schwardt, X. Jiang, T. Maier, B. Ernst, *ChemBioChem* **2015**, *16*, 1235–46.

[149] J. Schmidt-Lassen, T. K. Lindhorst, *Med. Chem. Commun.* **2014**, *5*, 1218–1226.

[150] M. Collot, J. Savreux, J.-M. Mallet, *Tetrahedron* **2008**, *64*, 1523 – 1535.

[151] A. Titz, Z. Radic, O. Schwardt, B. Ernst, *Tetrahedron Lett.* **2006**, *47*, 2383 – 2385.

[152] C. Fessele, T. K. Lindhorst, *Biology (Basel)* **2013**, *2*, 1135–49.

[153] R. Roy, F. D. Tropper, T. Morrison, J. Boratynski, *J. Chem. Soc., Chem. Commun.* **1991**, 536–538.

[154] Y. Kikuchi, H. Toi, Y. Aoyama, *Bull. Chem. Soc. Jpn.* **1993**, *66*, 1856–1858.

[155] M. Dubber, T. K. Lindhorst, *Carbohydr. Res.* **1998**, *310*, 35 – 41.

[156] M. Scharenberg, X. Jiang, L. Pang, G. Navarra, S. Rabbani, F. Binder, O. Schwardt, B. Ernst, *ChemMedChem* **2014**, *9*, 78–83.

[157] Z. Han, J. S. Pinkner, B. Ford, E. Chorell, J. M. Crowley, C. K. Cusumano, S. Campbell, J. P. Henderson, S. J. Hultgren, J. W. Janetka, *J. Med. Chem.* **2012**, *55*, 3945–59.

[158] W. E. Thomas, E. Trintchina, M. Forero, V. Vogel, E. V. Sokurenko, *Cell* **2002**, *109*, 913–23.

[159] M. Virji, *Top. Curr. Chem.* **2009**, *288*, 139–56.

[160] M. Essig, G. Friedlander, *J. Am. Soc. Nephrol.* **2003**, *14 Suppl 1*, S33–5.

[161] P. Cadieux, G. Wignall, R. Carriveau, In J. Denstedt, A. Atala, Hg., *Biomaterials and Tissue Engineering in Urology*, Woodhead Publishing Series in Biomaterials. Woodhead Publishing **2009**, 3 – 41.

[162] V. Kumar, J. V. Dhabalia, G. G. Nelivigi, M. S. Punia, M. Suryavanshi, *Indian J. Urol.* **2009**, *25*, 461–6.

[163] A. Kouki, R. J. Pieters, U. J. Nilsson, V. Loimaranta, J. Finne, S. Haataja, *Biology* **2013**, *2*, 918–35.

[164] T. Weber, V. Chandrasekaran, I. Stamer, M. B. Thygesen, A. Terfort, T. K. Lindhorst, *Angew. Chem. Int. Ed.* **2014**, *53*, 14583–6.

[165] J.-L. Reymond, M. Bergmann, T. Darbre, *Chem. Soc. Rev.* **2013**, *42*, 4814–22.

[166] P. D. Olson, D. A. Hunstad, *Pathogens* **2016**, *5*.

[167] J. M. Rini, *Annu. Rev. Biophys. Biomol. Struct.* **1995**, *24*, 551–77.

[168] C. R. Bertozzi, L. L. Kiessling, *Science* **2001**, *291*, 2357–64.

[169] N. Laurent, J. Voglmeir, S. L. Flitsch, *Chem. Commun.* **2008**, 4400–12.

[170] M. Kleinert, T. Winkler, A. Terfort, T. K. Lindhorst, *Org. Biomol. Chem.* **2008**, *6*, 2118–32.

[171] M. A. Wolfert, G.-J. Boons, *Nat. Chem. Biol.* **2013**, *9*, 776–784.

[172] H.-J. Gabius, S. André, J. Jiménez-Barbero, A. Romero, D. Solís, *Trends Biochem. Sci.* **2011**, *36*, 298–313.

[173] V. Chandrasekaran, H. Jacob, F. Petersen, K. Kathirvel, F. Tuczek, T. K. Lindhorst, *Chemistry* **2014**, *20*, 8744–52.

[174] J. Auernheimer, C. Dahmen, U. Hersel, A. Bausch, H. Kessler, *J. Am. Chem. Soc.* **2005**, *127*, 16107–10.

[175] P. M. Mendes, *Chem. Soc. Rev.* **2013**, *42*, 9207–18.

[176] W. R. Browne, B. L. Feringa, *Annu. Rev. Phys. Chem.* **2009**, *60*, 407–28.

[177] M.-M. Russew, S. Hecht, *Adv. Mater.* **2010**, *22*, 3348–60.

[178] C. Poloni, W. Szymanski, B. L. Feringa, *Chem. Commun.* **2014**, *50*, 12645–8.

[179] L. Möckl, A. Müller, C. Bräuchle, T. K. Lindhorst, *Chem. Commun.* **2016**, *52*, 1254–7.

[180] B. Priewisch, K. Rück-Braun, *J. Org. Chem.* **2005**, *70*, 2350–2.

[181] E. D. Goddard-Borger, R. V. Stick, *Org. Lett.* **2007**, *9*, 3797–3800, PMID: 17713918.

[182] M. S. Shive, S. M. Hasan, J. Anderson, *J. Biomed. Mater Res.* **1999**, *46*, 511–519.

[183] V. F. Fiore, L. Ju, Y. Chen, C. Zhu, T. H. Barker, *Nat. Commun.* **2014**, *5*, 4886.

[184] B. T. Marshall, M. Long, J. W. Piper, T. Yago, R. P. McEver, C. Zhu, *Nature* **2003**, *423*, 190–3.

[185] E. Evans, A. Leung, V. Heinrich, C. Zhu, *Proc. Natl. Acad. Sci.* **2004**, *101*, 11281–6.

[186] D. K. Das, Y. Feng, R. J. Mallis, X. Li, D. B. Keskin, R. E. Hussey, S. K. Brady, J.-H. Wang, G. Wagner, E. L. Reinherz, M. J. Lang, *Proc. Natl. Acad. Sci.* **2015**, *112*, 1517–22.

[187] B. Liu, W. Chen, B. D. Evavold, C. Zhu, *Cell* **2014**, *157*, 357–68.

[188] A. Ronald, *Am. J. Med.* **2002**, *113 Suppl 1A*, 14S–19S.

[189] M. M. Sauer, R. P. Jakob, J. Eras, S. Baday, D. Eriş, G. Navarra, S. Bernèche, B. Ernst, T. Maier, R. Glockshuber, *Nat. Commun.* **2016**, *7*, 10738.

[190] M. Zaborowski, P. Grabiec, T. Gotszalk, E. Romanowska, I. W. Rangelow, *Microelectron. Eng.* **2001**, *57*, 787–792.

[191] T. Sulchek, R. Hsieh, S. C. Minne, C. F. Quate, S. R. Manalis, *Nanotechnol.* **2001**, 562–566.

[192] R. Berger, C. Gerber, H. P. Lang, J. K. Gimzewski, *Microelectron. Eng.* **1997**, *35*, 373–379.

[193] B. N. Johnson, R. Mutharasan, *Biosens. Bioelectron.* **2012**, *32*, 1–18.

[194] C. D. Spicer, B. G. Davis, *Nat. Commun.* **2014**, *5*, 4740.

[195] O. Boutureira, G. J. L. Bernardes, *Chem. Rev.* **2015**, *115*, 2174–95.

[196] H. Staudinger, J. Meyer, *Hel. Chim. Acta* **1919**, *2*, 635–646.

[197] S. I. van Kasteren, H. B. Kramer, H. H. Jensen, S. J. Campbell, J. Kirkpatrick, N. J. Oldham, D. C. Anthony, B. G. Davis, *Nature* **2007**, *446*, 1105–9.

[198] B. L. Nilsson, L. L. Kiessling, R. T. Raines, *Org. Lett.* **2000**, *2*, 1939–41.

[199] E. Saxon, J. I. Armstrong, C. R. Bertozzi, *Org. Lett.* **2000**, *2*, 2141–3.

[200] G. A. Lemieux, C. L. De Graffenried, C. R. Bertozzi, *J. Am. Chem. Soc.* **2003**, *125*, 4708–9.

[201] W. Szymański, B. Wu, C. Poloni, D. B. Janssen, B. L. Feringa, *Angew. Chem. Int. Ed.* **2013**, *52*, 2068–72.

[202] S. Naganathan, S. Ye, T. P. Sakmar, T. Huber, *Biochemistry* **2013**, *52*, 1028–36.

[203] K. L. Kiick, E. Saxon, D. A. Tirrell, C. R. Bertozzi, *Proc. Natl. Acad. Sci.* **2002**, *99*, 19–24.

[204] M.-L. Tsao, F. Tian, P. G. Schultz, *ChemBioChem* **2005**, *6*, 2147–9.

[205] V. V. Rostovtsev, L. G. Green, V. V. Fokin, K. B. Sharpless, *Angew. Chem. Int. Ed.* **2002**, *41*, 2596–9.

[206] M. L. Blackman, M. Royzen, J. M. Fox, *J. Am. Chem. Soc.* **2008**, *130*, 13518–9.

[207] W. Song, Y. Wang, J. Qu, Q. Lin, *J. Am. Chem. Soc.* **2008**, *130*, 9654–5.

[208] E. M. Sletten, C. R. Bertozzi, *Angew. Chem. Int. Ed.* **2009**, *48*, 6974–98.

[209] M. L. Smith, J. A. Lindbo, S. Dillard-Telm, P. M. Brosio, A. B. Lasnik, A. A. McCormick, L. V. Nguyen, K. E. Palmer, *Virology* **2006**, *348*, 475–88.

[210] J. M. Chalker, G. J. L. Bernardes, Y. A. Lin, B. G. Davis, *Chem. Asian J.* **2009**, *4*, 630–40.

[211] N. Lundell, T. Schreitmüller, *Anal. Biochem.* **1999**, *266*, 31–47.

[212] R. Kundu, Z. T. Ball, *Chem. Commun.* **2013**, *49*, 4166–8.

[213] M. D. Simon, F. Chu, L. R. Racki, C. C. de la Cruz, A. L. Burlingame, B. Panning, G. J. Narlikar, K. M. Shokat, *Cell* **2007**, *128*, 1003–12.

[214] C. Chatterjee, T. W. Muir, *J. Biol. Chem.* **2010**, *285*, 11045–50.

[215] D. P. Gamblin, S. van Kasteren, G. J. L. Bernardes, J. M. Chalker, N. J. Oldham, A. J. Fairbanks, B. G. Davis, *Mol Biosyst* **2008**, *4*, 558–61.

[216] M. E. B. Smith, F. F. Schumacher, C. P. Ryan, L. M. Tedaldi, D. Papaioannou, G. Waksman, S. Caddick, J. R. Baker, *J. Am. Chem. Soc.* **2010**, *132*, 1960–5.

[217] J. M. Chalker, S. B. Gunnoo, O. Boutureira, S. C. Gerstberger, M. Fernandez-Gonzalez, G. J. L. Bernardes, L. Griffin, H. Hailu, C. J. Schofield, B. G. Davis, *Chem. Sci.* **2011**, *2*, 1666–1676.

[218] J. M. Chalker, L. Lercher, N. R. Rose, C. J. Schofield, B. G. Davis, *Angew. Chem. Int. Ed.* **2012**, *51*, 1835–9.

[219] M. C. Good, J. G. Zalatan, W. A. Lim, *Science* **2011**, *332*, 680–6.

[220] S. Pokutta, W. I. Weis, *Annu. Rev. Cell Dev. Biol.* **2007**, *23*, 237–61.

[221] A. Imberty, *Bacterial Lectins and Adhesins: Structures, Ligands and Functions*, Bentham eBooks **2011**, 3–11.

[222] M. Forero, O. Yakovenko, E. V. Sokurenko, W. E. Thomas, V. Vogel, *PLoS Biol.* **2006**, *4*, e298.

[223] D. C. Klein, C. M. Stroh, H. Jensenius, M. van Es, A. S. Kamruzzahan, A. Stamouli, H. J. Gruber, T. H. Oosterkamp, P. Hinterdorfer, *ChemPhysChem* **2003**, *4*, 1367–71.

[224] O. Björnham, O. Axner, *Biophys. J.* **2010**, *99*, 1331–41.

[225] C. Bustamante, J. F. Marko, E. D. Siggia, S. Smith, *Science* **1994**, *265*, 1599–600.

[226] L. Laprell, E. Repak, V. Franckevicius, F. Hartrampf, J. Terhag, M. Hollmann, M. Sumser, N. Rebola, D. A. DiGregorio, D. Trauner, *Nat. Commun.* **2015**, *6*.

[227] C. V. Smythe, *J. Biol. Chem.* **1936**, *114*, 601–612.

[228] C. A. Hutchinson, S. Phillips, M. H. Edgell, S. Gillam, P. Jahnke, M. Smith, *J. Biol. Chem.* **1978**, *253*, 6551–6560.

[229] A. Surendiran, S. Sandhiya, S. C. Pradhan, C. Adithan, *Indian. J. Med. Res.* **2009**, *130*, 689–701.

[230] R. P. Allaker, K. Memarzadeh, *Int. J. Antimicrob. Agents* **2014**, *43*, 95–104.

[231] S. Chernousova, M. Epple, *Angew. Chem. Int. Ed.* **2013**, *52*, 1636–53.

[232] I. Francolini, G. Donelli, *FEMS Immunol. Med. Microbiol.* **2010**, *59*, 227–38.

[233] E. Taylor, T. J. Webster, *Int. J. Nanomed.* **2011**, *6*, 1463–73.

[234] S. M. Dizaj, F. Lotfipour, M. Barzegar-Jalali, M. H. Zarrintan, K. Adibkia, *Mater. Sci. Eng. Mater. Biol. Appl.* **2014**, *44*, 278–84.

[235] J. Conde, G. Doria, P. Baptista, *J. Drug. Deliv.* **2012**, *2012*, 751075.

[236] G. Doria, J. Conde, B. Veigas, L. Giestas, C. Almeida, M. Assunção, J. Rosa, P. V. Baptista, *Sensors (Basel)* **2012**, *12*, 1657–87.

[237] S. Szunerits, A. Barras, R. Boukherroub, *Int. J. Environ. Res. Public Health* **2016**, *13*.

[238] M. Hartmann, P. Betz, Y. Sun, S. N. Gorb, T. K. Lindhorst, A. Krueger, *Chemistry* **2012**, *18*, 6485–92.

[239] J. M. de la Fuente, S. Penadés, *Biochim. Biophys. Acta* **2006**, *1760*, 636–51.

[240] A. G. Barrientos, J. M. de la Fuente, T. C. Rojas, A. Fernández, S. Penadés, *Chemistry* **2003**, *9*, 1909–21.

[241] J. Rojo, V. Díaz, J. M. de la Fuente, I. Segura, A. G. Barrientos, H. H. Riese, A. Bernad, S. Penadés, *ChemBioChem* **2004**, *5*, 291–7.

[242] M. Reynolds, M. Marradi, A. Imberty, S. Penadés, S. Pérez, *Chemistry* **2012**, *18*, 4264–73.

[243] S. Szunerits, R. Boukherroub, *Chem. Commun.* **2012**, *48*, 8999–9010.

[244] M. Veerapandian, S. K. Lim, H. M. Nam, G. Kuppannan, K. S. Yun, *Anal. Bioanal. Chem.* **2010**, *398*, 867–876.

[245] Reed, Randall, Aggarwal, Matyi, Moore, Wetsel, *Phys. Rev. Lett.* **1988**, *60*, 535–537.

[246] P. Bojarová, V. Křen, *Biomater. Sci.* **2016**, *4*, 1142–60.

[247] S. Cecioni, V. Oerthel, J. Iehl, M. Holler, D. Goyard, J.-P. Praly, A. Imberty, J.-F. Nierengarten, S. Vidal, *Chemistry* **2011**, *17*, 3252–61.

[248] M. Durka, K. Buffet, J. Iehl, M. Holler, J.-F. Nierengarten, J. Taganna, J. Bouckaert, S. P. Vincent, *Chem. Commun.* **2011**, *47*, 1321–3.

[249] M. J. Chmielewski, E. Buhler, J. Candau, J.-M. Lehn, *Chemistry* **2014**, *20*, 6960–77.

[250] S. Zhang, R.-O. Moussodia, H.-J. Sun, P. Leowanawat, A. Muncan, C. D. Nusbaum, K. M. Chelling, P. A. Heiney, M. L. Klein, S. André, R. Roy, H.-J. Gabius, V. Percec, *Angew. Chem. Int. Ed.* **2014**, *53*, 10899–903.

[251] S. Bernardi, P. Fezzardi, G. Rispoli, S. E. Sestito, F. Peri, F. Sansone, A. Casnati, *Beilstein J. Org. Chem.* **2014**, *10*, 1672–80.

[252] M. Gómez-García, J. M. Benito, A. P. Butera, C. Ortiz Mellet, J. M. García Fernández, J. L. Jiménez Blanco, *J. Org. Chem.* **2012**, *77*, 1273–88.

[253] A. Barras, F. A. Martin, O. Bande, J.-S. Baumann, J.-M. Ghigo, R. Boukherroub, C. Beloin, A. Siriwardena, S. Szunerits, *Nanoscale* **2013**, *5*, 2307–16.

[254] M. Khanal, F. Larsonneur, V. Raks, A. Barras, J.-S. Baumann, F. A. Martin, R. Boukherroub, J.-M. Ghigo, C. Ortiz Mellet, V. Zaitsev, J. M. Garcia Fernandez, C. Beloin, A. Siriwardena, S. Szunerits, *Nanoscale* **2015**, *7*, 2325–35.

[255] N. P. Pera, A. Kouki, S. Haataja, H. M. Branderhorst, R. M. J. Liskamp, G. M. Visser, J. Finne, R. J. Pieters, *Org. Biomol. Chem.* **2010**, *8*, 2425–9.

[256] Z. Krpetić, S. Anguissola, D. Garry, P. M. Kelly, K. A. Dawson, *Adv. Exp. Med. Biol.* **2014**, *811*, 135–56.

[257] M. Behra, N. Azzouz, S. Schmidt, D. V. Volodkin, S. Mosca, M. Chanana, P. H. Seeberger, L. Hartmann, *Biomacromolecules* **2013**, *14*, 1927–35.

[258] D. Arosio, F. Chiodo, J. J. Reina, M. Marelli, S. Penadés, Y. van Kooyk, J. J. Garcia-Vallejo, A. Bernardi, *Bioconjug. Chem.* **2014**, *25*, 2244–51.

[259] M. Marradi, M. Martín-Lomas, S. Penadés, *Adv. Carbohydr. Chem. Biochem.* **2010**, *64*, 211–90.

[260] V. N. Mochalin, O. Shenderova, D. Ho, Y. Gogotsi, *Nat. Nanotechnol.* **2012**, *7*, 11–23.

[261] E. Osawa, *Pure Appl. Chem.* **2008**, *80*, 1365–1379.

[262] A. M. Schrand, S. A. C. Hens, O. A. Shenderova, *Crit. Rev. Solid State Mat. Sci.* **2009**, *34*, 18–74.

[263] A. Krueger, *J. Mater. Chem.* **2011**, *21*, 12571–12578.

[264] A. Y. Vul, A. T. Dideikin, A. E. Aleksenskii, M. V. Baidakova, *J. Nanosci. Nanotechnol.* **2014**, *31*, 27–48.

[265] H. Man, J. Sasine, E. K. Chow, D. Ho, In *Nanodiamond*. The Royal Society of Chemistry **2014**, 151–169.

[266] E. Perevedentseva, Y.-C. Lin, M. Jani, C.-L. Cheng, *Nanomedicine* **2013**, *8*, 2041–60.

[267] Y. Zhu, J. Li, W. Li, Y. Zhang, X. Yang, N. Chen, Y. Sun, Y. Zhao, C. Fan, Q. Huang, *Theranostics* **2012**, *2*, 302–12.

[268] A. Krueger, D. Lang, *Adv. Funct. Mat.* **2012**, *22*, 890–906.

[269] X. Li, J. Shao, Y. Qin, C. Shao, T. Zheng, L. Ye, *J. Mater. Chem.* **2011**, *21*, 7966–7973.

[270] E. V. Basiuk, A. Santamaría-Bonfil, V. Meza-Laguna, T. Y. Gromovoy, E. Alvares-Zauco, F. F. Contreras-Torres, J. Rizo, G. Zavala, V. A. Basiuk, *Appl. Surf. Sci.* **2013**, *275*, 324 – 334.

[271] H. C. Kolb, M. G. Finn, K. B. Sharpless, *Angew. Chem. Int. Ed.* **2001**, *40*, 2004–2021.

[272] V. N. Mochalin, I. Neitzel, B. J. M. Etzold, A. Peterson, G. Palmese, Y. Gogotsi, *ACS Nano* **2011**, *5*, 7494–502.

[273] T. Meinhardt, D. Lang, H. Dill, A. Krueger, *Adv. Funct. Mat.* **2011**, *21*, 494–500.

[274] G. Dördelmann, T. Meinhardt, T. Sowik, A. Krueger, U. Schatzschneider, *Chem. Commun.* **2012**, *48*, 11528–30.

[275] K. V. Purtov, A. I. Petunin, A. E. Burov, A. P. Puzyr, V. S. Bondar, *Nanoscale Res. Lett.* **2010**, *5*, 631–636.

[276] Y. Sun, A. Finne-Wistrand, T. Waag, Z. Xing, M. Yassin, A. Yamamoto, K. Mustafa, D. Steinmüller-Nethl, A. Krueger, A.-C. Albertsson, *Macromol. Mat. and Eng.* **2015**, *300*, 436–447.

[277] M. Walter, K. T. Lindhorst, *Monatshefte für Chemie / Chemical Monthly 133*, 473–483.

[278] M. I. García-Moreno, P. Díaz-Pérez, J. M. Benito, C. Ortiz Mellet, J. Defaye, J. M. García Fernández, *Carbohydr. Res.* **2002**, *337*, 2329–34.

[279] C. Kieburg, T. K. Lindhorst, *Tetrahedron Lett.* **1997**, *38*, 3885 – 3888.

[280] D. Pagé, R. Roy, *Glycoconj. J.* **1997**, *14*, 345–56.

[281] M. Kühne, Z. Györgydeák, T. K. Lindhorst, *Synthesis* **2006**, *2006*, 949–951.

[282] Y. Liang, T. Meinhardt, G. Jarre, M. Ozawa, P. Vrdoljak, A. Schöll, F. Reinert, A. Krueger, *J. Colloid. Interface Sci.* **2011**, *354*, 23–30.

[283] M. Ozawa, M. Inaguma, M. Takahashi, F. Kataoka, A. Krüger, E. Ōsawa, *Adv. Mat.* **2007**, *19*, 1201–1206.

[284] M. Gruner, D. Pfeifer, H. G. O. Becker, R. Radeglia, J. Epperlein, *J. Prak. Chem.* **1985**, *327*, 63–79.

[285] G. Jarre, S. Heyer, E. Memmel, T. Meinhardt, A. Krueger, *Beilstein J. Org. Chem.* **2014**, *10*, 2729–37.

[286] G. Zemplén, E. Pascu, *Ber. Dtsch. Chem. Ges.* **1929**, *62*, 1614–1623.

[287] R. Rossi, S. Porta, B. Canovi, *J. Clin. Gastroenterol.* **2010**, *44 Suppl 1*, S61–2.

[288] G. R. Nielubowicz, H. L. T. Mobley, *Nat. Rev. Urol.* **2010**, *7*, 430–41.

[289] S. Sattin, A. Bernardi, *Trends Biotechnol.* **2016**.

[290] M. C. Lane, H. L. T. Mobley, *Kidney Int.* **2007**, *72*, 19–25.

[291] A. Salminen, V. Loimaranta, J. A. F. Joosten, A. S. Khan, J. Hacker, R. J. Pieters, J. Finne, *J. Antimicrob. Chemother.* **2007**, *60*, 495–501.

[292] F. P. Lindberg, B. Lund, S. Normark, *EMBO J.* **1984**, *3*, 1167–1173.

[293] Z. Li, L. Zhu, J. Kalikanda, *Tetrahedron Lett.* **2011**, *52*, 5629 – 5632.

[294] Z. Li, J. C. Gildersleeve, *J. Am. Chem. Soc.* **2006**, *128*, 11612–9.

[295] S. J. Angyal, Y. Kondo, *Carbohydr. Res.* **1980**, *81*, 35–48.

[296] R. Hevey, A. Morland, C.-C. Ling, *J. Org. Chem.* **2012**, *77*, 6760–72.

[297] M. Alpe, S. Oscarson, *Carbohydr. Res.* **2002**, *337*, 1715–22.

[298] E. Attolino, G. Catelani, F. D'Andrea, *Eur. J. Org. Chem.* **2006**, *2006*, 5279–5292.

[299] N. G. Gurskaya, A. F. Fradkov, N. I. Pounkova, D. B. Staroverov, M. E. Bulina, Y. G. Yanushevich, Y. A.Labas, S. Lukyanov, K. A. Lukyanov, *Biochem. J.* **2003**, *373*, 403–408.

[300] A. Reisner, J. A. Haagensen, M. A. Schembri, E. L. Zechner, S. Molin, *Mol. Microbiol.* **2003**, *48*, 933–946.

[301] M. Amaike, H. Kobayashi, S. Shinkai, *Bull. Chem. Soc. Jpn.* **2000**, *73*, 2553–2558.

[302] Z. Han, J. S. Pinkner, B. Ford, R. Obermann, W. Nolan, S. A. Wildman, D. Hobbs, T. Ellenberger, C. K. Cusumano, S. J. Hultgren, J. W. Janetka, *J. Med. Chem.* **2010**, *53*, 4779–92.

[303] K. Kobayashi, N. Kakishita, M. Okada, T. Akaike, T. Usui, *J. Carbohydr. Chem.* **1994**, *13*, 753–766.

[304] S. Park, S. Hyun, S.-i. Do, J. Yu, *Bioorg. Med. Chem. Lett.* **2011**, *21*, 2441–4.

[305] G. Boschi, M. Desiles, A. LÂŽHelgoualcÂŽh, R. Rips, *Eur. J. Med. Chem.* **1981**, *16*, 125–130.

[306] R. T. Lee, Y. C. Lee, *Carbohydr. Res.* **1974**, *37*, 193–201.

[307] J. L. Hutter, J. Bechhoefer, *Rev. Sci. Instrum.* **1993**, *64*, 1868–1873.

[308] G. Bell, *Science* **1978**, *200*, 618–627.

[309] D. F. Tees, R. E. Waugh, D. A. Hammer, *Biophys. J.* **2001**, *80*, 668–82.

[310] E. A. Evans, D. A. Calderwood, *Science* **2007**, *316*, 1148–53.

[311] W. L. Jorgensen, D. S. Maxwell, , J. Tirado-Rives, *J. Am. Chem. Soc.* **1996**, *118*, 11225–11236.

[312] W. L. Jorgensen, J. Tirado-Rives, *J. Am. Chem. Soc.* **1988**, *110*, 1657–1666.

[313] D. Shivakumar, J. Williams, Y. Wu, W. Damm, J. Shelley, W. Sherman, *J. Chem. Theory Comput.* **2010**, *6*, 1509–1519, PMID: 26615687.

[314] R. A. Friesner, J. L. Banks, R. B. Murphy, T. A. Halgren, J. J. Klicic, D. T. Mainz, M. P. Repasky, E. H. Knoll, M. Shelley, J. K. Perry, D. E. Shaw, P. Francis, P. S. Shenkin, *J. Med. Chem.* **2004**, *47*, 1739–1749.

[315] T. A. Halgren, R. B. Murphy, R. A. Friesner, H. S. Beard, L. L. Frye, W. T. Pollard, J. L. Banks, *J. Med. Chem.* **2004**, *47*, 1750–1759.

[316] M. Connolly, *Science* **1983**, *221*, 709–713.

[317] M. A. Schembri, H. Hasman, P. Klemm, *FEMS Microbiol. Lett.* **2000**, *188*, 147–151.

[318] N. Fornstedt, J. Porath, *FEBS Lett.* **1975**, *57*, 187–91.

[319] U. K. Laemmli, *Nature* **1970**, *227*, 680–5.

[320] K. Tyagarajan, E. Pretzer, J. E. Wiktorowicz, *Electrophoresis* **2003**, *24*, 2348–58.

List of Abbreviations

E. coli	*Escherichia coli*
*p*APGal	*p*-aminophenyl α-D-galctopyranoside
*p*APGlc	*p*-aminophenyl α-D-glucopyranoside
*p*APMan	*p*-aminophenyl α-D-mannopyranoside
m	*meta*
o	*ortho*
p	*para*
aa	amino acid
AFM	atomic force microscopy
AIBN	2,2'-azobis(isobutyronitrile)
aq.	aqueous
Asn	asparagine
BAI	bacterial adhesion inhibition
Boc	*tert*-butyloxycarbonyl
ConA	Concanavalin A
COSY	correlation spectroycopy
CRD	carbohydrate recgonition domain
CuAAC	copper-promoted azide-alkyne cycloaddition
D	aspartic acid
DMF	*N,N*-dimethylformamide
DMSO	dimethyl sulfoxide
DNA	deoxyribonucleic acid
EDC	1-ethyl-3-(3-dimethylaminopropyl)carbodiimide
ELISA	enzyme-linked immunosorbent assay
ER	endoplasmatic reticulum
F	phenylalanine
Fuc	fucose
Gal	galactose

GalNAc	*N*-acetylgalactosamine
GBP	glycan-binding protein
GFP	green fluorescent protein
Glc	glucose
GlcA	glucoronic acid
GlcNAc	*N*-acetylglucosamine
GND	glyconanodiamond
GNP	glyconanoparticle
HeptMan	heptyl α-D-mannopyranoside
HMEC	human microvascular endothelial cells
IC	inhibitory concentration
IdoA	iduronic acid
IEDDA	inverse-electron demand diels-alder
Ig	immunoglobulin
IP	inhibitory potency
IR	infrared spectroscopy
ITC	isothermal titration calorimetry
LB	lysogeny broth
m	multiplet (NMR)
Man	mannose
MeMan	methyl α-D-mannopyranoside
MES	2-(*N*-morpholino)ethanesulfonic acid
MHC	major histocompatibility complex
mp	melting point
N	asparagine
NCS	isothiocyanate
ND	nanodiamond
Neu5Ac	*N*-acetylneuraminic acid
NHS	*N*-hydroxysuccinimide
NMR	nuclear magnetic resonance spectroscopy
NP	nanoparticle
OctMan	octyl α-D-mannopyranoside
OD	opical density

OST	oligosaccharyltransferase
PBS	phosphate-buffered saline
PCR	polymerase chain reaction
PDB	protein data base
PEG	polyethylene glycol
PhαGal	*p*-aminophenyl α-D-galctopyranoside
PhαGlc	*p*-aminophenyl α-D-glucopyranoside
PhαMan	*p*-aminophenyl α-D-mannopyranoside
PI	phosphoinositol
PS	polystyrene
PVA	polyvinyl alcohol
Q	glutamine
RIP	relative inhibitory potencies
RNA	ribonucleic acid
rt	room temperature
S	serine
s	singlet (NMR)
SAM	self-assembled monolayer
SAMan	squaric acid α-D-mannopyranoside
SAW	surface acoustic wave
SDS PAGE	sodium dodecyl sulfate polyacrylamide gel electrophoresis
Ser	serine
Siglecs	sialic acid-binding immunoglobulin-type lectins
SPR	surface plasmon resonance
STD-NMR	saturation transfer difference NMR
t	triplet (NMR)
TFA	trifluoroacetic acid
ThiahexGal	thiahexyl α-D-galactopyranoside
ThiahexGal	thiahexyl α-D-galactopyranoside
ThiahexGlc	thiahexyl α-D-glucopyranoside
ThiahexMan	thiahexyl α-D-mannopyranoside
Thr	threonine
TLC	thin layer chromatography

TMS-SCN	trimethylsilyl isothiocyanate
TriMan	*N*-azido tris α-D-mannopyranoside
UAA	unnatural amino acid
UPEC	uropathogenic *Escherichia coli*
UTI	urinary tract infection
UV	ultraviolet
vis	visible
WLC	worm-like-chain
Xyl	xylose

List of Figures

Acknowledgement

An dieser Stelle möchte ich mich bei allen nachfolgenden Personen bedanken, die maßgeblich zur Entstehung dieser Promotionsschrift beigetragen haben:

Ein großer Dank gilt meiner Doktormutter Frau Prof. Dr Thisbe K. Lindhorst für die Bereitstellung des spannenden Themas und die Betreuung meiner Arbeit. Die mir gewährten Freiräume und ihr mir entgegengebrachtes Vertrauen und stete Unterstützung haben maßgeblich zum Gelingen dieser Arbeit beigetragen.

Prof. Dr. Axel Scheidig danke ich für all die Unterstützung seit Beginn meines Masterstudiums in Kiel. Besonders danke ich ihm für seine wissenschaftliche Betreuung bei unseren Kooperationsprojekten und die Übernahme der Aufgabe des Zweitgutachters.

Auch meinen zahlreichen weiteren Kooperationspartnern: Prof. Dr. Thomas Gutsmann, Prof. Dr. Anke Krüger, Stefan Wachtler, Dr. Leonhard Möckl, Dr. Guillaume Despras und Anne Müller gebührt ein großer Dank für all die spannenden Diskussionen und die stets freundliche und produktive Zusammenarbeit.

Außerdem möchte ich mich bei allen technischen und wissenschaftlichen Mitarbeitern unseres Instituts bedanken: Holger Franzen, Gitta Kohlmeyer-Yilmaz, Marion Höftmann, Dirk Meyer, Silke Rühl, Rolf Schmied, Andreas Wilms und Rüdiger Kargoll.

Ein besonderer Dank geht an Christine Haug und Elwira Klima-Barczak, die mit ihrer freundlichen und hilfsbereiten Art mich jederzeit und bei allen Anliegen unterstützt haben.

Ein Danke auch an meine Bachelorstudenten und F3-Praktikanten Annika Carstens, Fabian Kruse, Hauke Themer und Nina Seestädt.

Bei allen aktuellen und ehemaligen Mitglieder des Arbeitskreises Lindhorst möchte ich mich für die schöne Zeit, die lustigen Kaffeepausen, Frühstücksrunden, gemeinsame Ausflüge und alle chemischen und nicht-chemischen Diskussionen bedanken. Danke für all die schönen Erinnerungen und Erlebnisse!

Meiner Laborpartnerin Franziska Reise danke ich für die letzten gemeinsamen Jahre in unserem Labor. Anne Müller und Franziska Reise danke ich besonders für ihre Freundschaft, die schöne und lustige Zusammenarbeit und alle gemeinsamen Diskussionen und Gespräche.

Zuletzt möchte ich mich bei den wichtigsten Menschen in meinem Leben: meiner ganzen Familie, besonders bei meinem Vater, meinen Brüdern und meinem Mann bedanken. Danke, dass ihr immer für mich da seid und mich bei all meinen Plänen unterstützt. Ohne eure Hilfe wäre diese Arbeit nie zustande gekommen.